INTERPRETATION OF THE FROZEN SOILS BEHAVIOR EXTENDING THE MECHANICS OF UNSATURATED SOILS

JUNPING REN

Thesis submitted in partial fulfillment
of the requirements for the
Doctorate in Philosophy degree in Civil Engineering

Department of Civil Engineering
Faculty of Engineering
University of Ottawa

Dedicated to my grandparents and parents,

and to my wife Cuizhen.

Preface

The studies presented in this Ph.D. thesis were conducted at the Department of Civil Engineering, University of Ottawa by myself, under the supervision of Prof. Sai K. Vanapalli. The thesis is gathered as a collection of several manuscripts, which were written by myself and edited by Prof. Sai K. Vanapalli. The presented studies are the results of original and rigorous investigation and analysis by myself under the supervision of Prof. Sai K. Vanapalli. The literature review, experimental tests, data analysis, and discussions were done by myself. The manuscripts that are published or under peer review are listed in Section 1.4.

The extensive experimental studies presented in this thesis are time- and labor-consuming. I received assistance from two master students (Mr. Omenogor, K.O., and Mr. Bai, Y.), mainly for dry soils preparation. I also received help from Dr. Zhong Han for the measurement of soil physical properties and the equipment setup for soil resilient modulus test under room temperature, and useful discussions. They are listed as co-authors of one of the manuscripts, which is written by myself.

Abstract

Soil is the most widely used material in the construction of various civil infrastructure. Various types of soils are extensively used in its natural or compacted form in the construction of dams, canals, road and railway subgrades, and waste containment structures such as soil covers and liners. These infrastructure and foundation soils are exposed to the influence of environmental factors. In the permafrost and seasonally frozen regions, soils can be in different states (e.g., saturated or unsaturated, frozen or thawed, or combinations of them) due to the variations in moisture content and temperature. The soil-water characteristic curve (SWCC), which is the relationship between soil water content and suction, is used in the interpretation and prediction of unsaturated soils behavior. Similarly, the soil-freezing characteristic curve (SFCC), which is the relationship between unfrozen water content and subzero temperature, is used in the prediction and interpretation of frozen soils behavior. In this thesis, the SWCC and SFCC of two Canadian soils (i.e. Toronto silty clay (TSC) and Toronto lean clay (TLC)) were extensively investigated for better understanding the fundamental relationship between SWCC and SFCC.

The soil resilient modulus (M_R) is a key material property used in the rational design of pavements. Experimental investigations were undertaken to determine the M_R of five Canadian soils (i.e., TSC, TLC, Kincardine lean clay (KLC), Ottawa Leda clay (OLC), and Indian Head till (IHT)), considering the influence of moisture and temperature, with the aid of an advanced triaxial testing equipment. Two simple models were proposed for estimating the M_R of frozen soils, in this thesis. In addition, an artificial neural network (ANN) model was developed for estimating the M_R of the five Canadian soils considering various influencing factors.

The conclusions from the various studies in this thesis are succinctly summarized below.

(1) Four expressions (i.e. power relationship, exponential relationship, van Genuchten equation, and Fredlund and Xing equation) that are widely used for representing the SFCC were selected for providing comparisons between the measured and fitted SFCCs for different soils. The results suggest that the exponential relationship and van Genuchten equation are suitable for sandy soils. The power relationship reasonably fits the SFCC for soils with different particle

sizes, but not for saline silts. The Fredlund and Xing equation is flexible and provides good fits for all the soils.

(2) The SFCC and SWCC of TSC and TLC were experimentally determined, analyzed, and compared. Many factors influence the reliable measurement of SFCC, which include sensors' resolution and stability, sensor calibration for each soil, and thermodynamic equilibrium condition. The hysteresis of SFCC for the two soils is mainly attributed to the supercooling of pore water. The quantitative dissimilarity in the measured SFCC and SWCC may be attributed to specimen structure variations during compaction and saturation, and during freezing / thawing processes, and cracks formation due to sensors insertion. In addition, some fundamental differences may exist between the drying / wetting and freezing / thawing processes, resulting in dissimilarity.

(3) Two novel models were proposed for the estimation of M_R of frozen soils. The semi-empirical model extends the mechanics of unsaturated soils and employs SFCC for prediction. Several coarse- and fine-grained saturated soils were used to validate this model. The empirical hyperbolic model was proposed considering that the frozen M_R versus subzero temperature relationship resembles hyperbola. This model was validated on coarse- and fine-grained soils under saturated / unsaturated conditions. The hyperbolic model has wider application since it can be used for both saturated and unsaturated frozen soils. Both the models are simple and promising.

(4) The M_R of five Canadian soils subjected to wetting and freezing was determined by using the GDS ELDyn triaxial testing system. A freezing system was established for controlling the desired testing temperatures within the soil specimens. The results suggest: (i) The effect of subzero temperature on the M_R is significant. (ii) For TLC, KLC, OLC, and IHT, the frozen M_R versus subzero temperature relationship of the saturated specimen typically has steeper slope than specimen at the optimum water content, for the temperature range from 0 to -5 °C. (iii) The effect of stress levels on the frozen M_R depends on soil type, water content, and subzero temperature. Lastly, (iv) Loading frequency does not show a significant influence on the frozen

M_R.

(5) The M_R of the five Canadian soils was determined considering wetting and freeze-thaw (F-T) conditions. The results suggest: (i) The F-T cycles result in weak soil structure due to reduction in suction, particles movement, loss of cohesion, and formation of cracks / channels. (ii) The critical numbers of F-T cycles were determined as 1, 1, 2, and 1 for TLC, KLC, OLC, and IHT at the optimum water content, respectively. (iii) The percentage of reduction in M_R after the critical number of F-T cycles was strongly related to the plasticity index for specimens tested at the optimum water content. (iv) The wetting process results in the decrease in suction and enlargement of soil pores. Consequently, relatively low M_R values were measured at high water contents, and the effect of F-T cycles becomes insignificant. Finally, (v) The effect of stress levels on the M_R was dependent on the initial water content of the specimen and soil type.

Acknowledgements

The studies presented in this Ph.D. thesis were conducted at the Department of Civil Engineering, University of Ottawa under the supervision of Prof. Sai K. Vanapalli. I would like to express my deepest appreciation to him for his continuous motivation, patience, and encouragement throughout my doctoral study. Prof. Vanapalli is a nice and tough professor, who tackles the difficulties in life with a smile while those in research with a rigorous attitude. Prof. Vanapalli is always there to provide as much support as he can to his students. His philosophy and approach towards life and research will be always guiding and encouraging me to enjoy life as well as to overcome hard times in the future.

The financial supports received from the China Scholarship Council (CSC) - University of Ottawa joint scholarship, the Natural Sciences and Engineering Research Council of Canada (NSERC), and the Ministry of Transportation of Ontario (MTO) are gratefully acknowledged.

I am grateful to Prof. Xiong Bill Yu (Case Western Reserve University, USA), Prof. Mamadou Fall (University of Ottawa), Prof. Julio Angel Infante Sedano (University of Ottawa), and Prof. Shawn Kenny (Carleton University), for serving as committee members and providing insightful criticism and guidance on my Ph.D. thesis.

My appreciations extend to my colleagues at the University of Ottawa for their friendship, company, and support. They are: Luc, Jean-Claude, Paula, Zhong, Shunchao, Yunlong, Huade, Ping, Mohammed, Penghai, Guanlong, Hongyu, Xiuhan, Kun, Xiaokun, Shilong, Faria, Mingshu, Xingyi, Yu, Kenneth, Wenjun, Xinting, Mengxi, Ahmed, Maha, Frederick, Moussa, and Sada.

Special thanks to my wife, Cuizhen. Thank her for always loving me, supporting me, and encouraging me to pursue my dreams.

Table of Contents

List of Figures

List of Tables

Chapter 1 Introduction

1.1 Background

The most widely used material in the construction of engineered infrastructure is soil, in its natural or modified form. For example, soils are compacted to form dams, canals, roads and railway subgrades, and waste containment structures such as soil covers and liners. The infrastructure constructed is typically in a state of unsaturated condition during their service life. The soil below the natural groundwater table is in a state of saturated condition; however, the soil above it is typically in a state of unsaturated condition. There has been significant interest in understanding the unsaturated soils behavior for geotechnical engineering applications after Bishop (1959) put forward the now well-known effective stress equation for unsaturated soils. Rational interpretation of unsaturated soils behavior is important because unsaturated soils are found in all continents, particularly in the arid and semiarid regions that cover about 33% of the earth's surface (Fredlund et al., 2012). These regions are scattered in more than 60% of countries in the world. In addition, unsaturated soils are also found in tropical countries such as Brazil, which have extended periods of dry seasons (Feuerharmel et al., 2006).

The zone above the groundwater table is widely referred to as the vadose zone in the literature, as shown in **Figure 1.1**. The vadose zone can be divided into three sub-zones based on the degree of saturation (S), which is defined as the ratio of the volume of water to the total volume of void space in a soil. There exists a certain depth of soil in the vadose zone, immediately above the groundwater table, which is referred to as the capillary fringe zone. Water from the groundwater table migrates into the capillary fringe zone. The soil in this zone can be considered to be closely in a state of saturation as most or all of the soil pore spaces are occupied by water; except for the presence of some occluded air bubbles. The degree of saturation is typically greater than 90%. The depth of the capillary fringe zone depends largely on soil type and particle size distribution. On the contrary, the surface soil is much drier due to the evaporation and evapotranspiration effects of the environment. The soil in this dry zone has low degree of saturation (i.e. $S < 15\%$), and typically has continuous air phase but discontinuous

liquid water phase (Fredlund et al., 2012). The limited amount of water that is present in this zone is mainly adsorbed by and tightly held by the soil particles. Between these two zones is a two-phase transition zone, in which certain amount of air and water co-exist. Both the air phase and water phase can be continuous in this zone. The soil in the two-phase transition zone has a degree of saturation typically in the range between 15 to 90%.

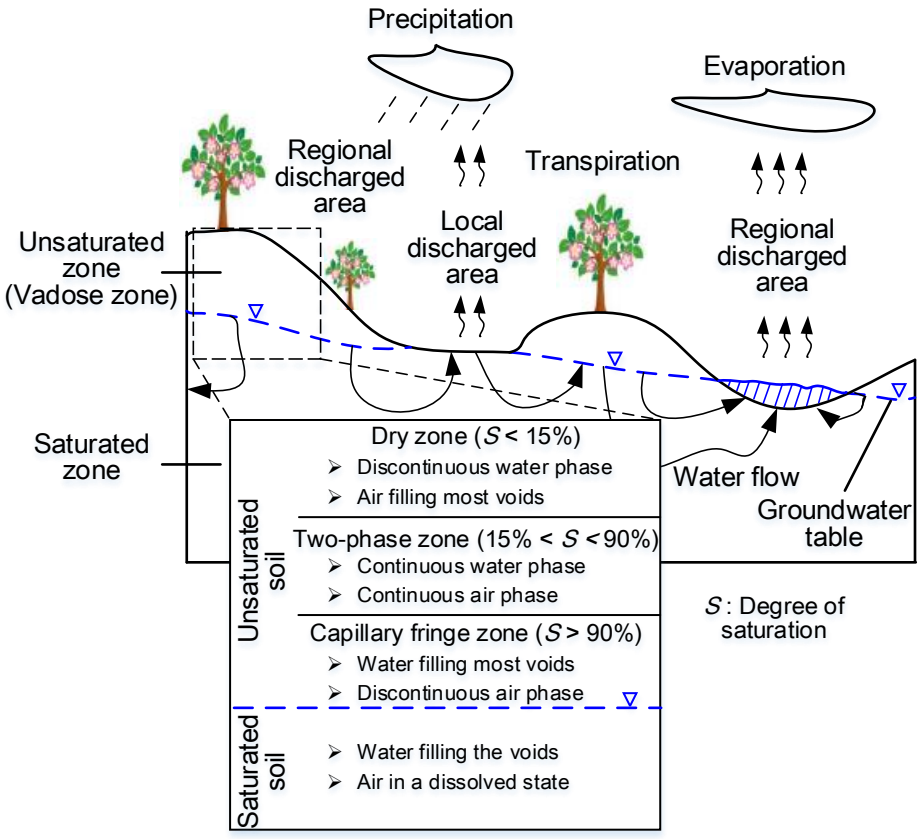

Figure 1.1 Subdivisions of vadose zone (unsaturated zone) on local and regional basis (modified after Fredlund et al., 2012)

The soil pore water has lower free energy compared to free water due to the interactions between soil particles, pore water and pore air in unsaturated soils. The soil-water characteristic curve (SWCC) defines the relationship between the free energy of pore water (or pore water potential, or soil suction) and the amount of pore water in the unsaturated soil. The quantity of

pore water can be represented by either the gravimetric water content, or volumetric water content, or degree of saturation (e.g., Qi, 2017). The SWCC is a conceptual and interpretative tool by which the behavior of unsaturated soils can be understood (Vanapalli et al., 1999; Elkeshky, 2011). For example, the SWCC has been used for predicting the hydraulic and mechanical properties of unsaturated soils, such as hydraulic conductivity (e.g., Fredlund et al., 1994), shear strength (e.g., Vanapalli et al., 1996), and modulus of elasticity (e.g., Oh et al., 2009).

The SWCC has been used in the mechanistic-empirical design of pavement structures, such as in the *Guide for Mechanistic-Empirical Design of New and Rehabilitated Pavement Structures* that is well known as the *Mechanistic-Empirical Pavement Design Guide* or MEPDG (ARA, Inc., 2004). In pavement design, the unbound base / subbase and subgrade soils are typically compacted at their optimum moisture contents. In other words, these compacted soils are in a state of unsaturated condition. The deformation at the surface of the subgrade soils has a significant influence on the pavement performance. Large uneven deformation of the subgrade soils can lead to fracture of concrete slabs and non-uniform deformation of surface layers of asphalt pavement.

The concept of resilient modulus (M_R) was introduced in California, USA during the 1950s in view of the differences between the real and idealized behavior of pavement materials, since conventionally pavement layers were characterized by Young's modulus (Brown, 1996). Professor Harry Seed and his colleagues at the University of California, Berkeley, were the pioneers who carried out repeated load triaxial tests on compacted soils and defined the M_R as the ratio of cyclic deviator stress (which simulates the repeated traffic loading) to the recoverable (resilient) axial strain, as shown in **Figure 1.2**. In other words, M_R is equivalent to a resilient Young's modulus (Brown, 1996), or M_R is analogous to the Young's modulus in statically loaded strength test (Culley, 1971). A similar definition was applied when testing compacted granular materials (Hicks and Monismith, 1971). The M_R was recommended as per the AASHTO (1986) pavement design guide, and has been widely used since then as the key property in the

mechanistic pavement design methods to rationally characterize the resilient behavior of unbound base / subbase and subgrade soils under repeated traffic loading (Han and Vanapalli, 2016).

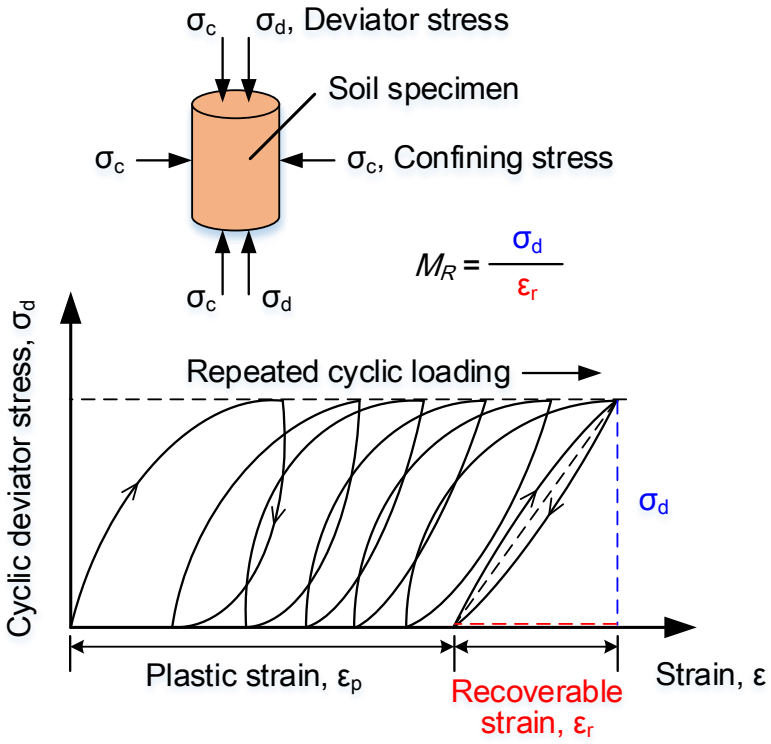

Figure 1.2 The definition of soil resilient modulus

Several types of laboratory testing equipment, which include triaxial shear, simple shear, resonant column, torsional shear, hollow cylinder test and true triaxial equipment, have been used for determining soil resilient behavior (e.g., Kim and Stokoe II, 1992; Brown, 2003; Wang et al., 2005; Puppala, 2008; Han and Vanapalli, 2016). However, these laboratory tests are costly and time-consuming, as they require large number of samples to be collected and tested for obtaining representative and reliable results. It is difficult to obtain a large quantity of undisturbed samples from field in many scenarios; and it is equally difficult to reproduce in-situ conditions with reconstituted / compacted samples. For this reason, approximate, empirical or semi-empirical methods are preferred to estimate or predict the soil M_R. During the past several

decades, many prediction models related to M_R have been proposed (e.g., Heukelom and Klomp, 1962; Drumm et al., 1990; Uzan, 1992; Lekarp et al., 2000; Vogrig et al., 2003; ARA, Inc., 2004; Christopher et al., 2006; Ikechukwu et al., 2018). Recently, Caicedo (2018) have provided a comprehensive summary of these models for the design of pavements. These include simple empirical relationships between the M_R and the California Bearing Ratio (CBR) and R-value, and relationships incorporating soil physical properties and soil stresses. However, these relationships do not consider the influence of environmental factors on the M_R of pavement materials.

The compacted unbound base / subbase and subgrade soils typically stay in an unsaturated condition during their service life (although both saturated and unsaturated conditions can occur (Brown, 1996)) and are subjected to environmental influences (e.g., Oloo et al., 1997; Zhang et al., 2014; Ikechukwu et al., 2018; Kodikara et al., 2018). For example, environmental factors contribute to moisture regime and soil suction variations within the pavement structure which, in turn, influence the strength and stiffness of these unbound soils (e.g., Hicks, 1970; Zhang et al., 2014; Han and Vanapalli, 2016). During the past two decades, many researchers demonstrated the strong correlations between the M_R and soil suction (or moisture condition) as well as established models to predict the M_R by incorporating the soil suction (e.g., Johnson et al., 1986; Heath et al., 2004; Sawangsuriya et al., 2009; Sahin et al., 2013; Han and Vanapalli, 2015). The variation of soil moisture in the base / subbase and subgrade layers is important to the pavement design process, because the change in soil stiffness or modulus due to moisture variation is the direct cause of the deformation and distress of pavements. In the MEPDG, the influence of the variation of moisture content on the M_R of unbound soils is predicted with the aid of SWCC.

The environmental impacts on the M_R of unbound soils would not be fully considered by only incorporating the influence of moisture variation into the prediction models. This is because the phase change of soil pore water (from liquid to solid or vice versa), which is the result of freezing and thawing of soils located in cold regions, will have a significant impact on various soil properties including the M_R. This soil behavior should be well understood since a vast area

on our earth is categorized as the permafrost or seasonally frozen regions. For example, the permafrost regions occupy about 24.91×10^6 km^2, i.e. 25.6% of the land surface in the northern hemisphere (Zhang et al, 2003; Gens, 2010) (as shown in **Figure 1.3**). The maximum extent of seasonally frozen ground is much larger, which is approximately 48.12×10^6 km^2 or 50.5% of the exposed lands in the northern hemisphere.

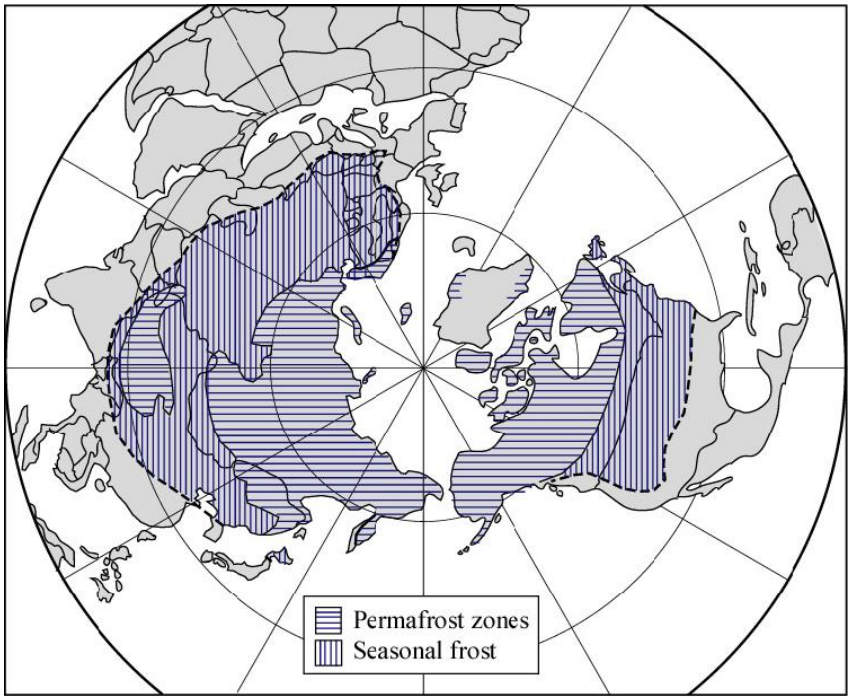

Figure 1.3 Distribution of permafrost and seasonally frozen regions in the northern hemisphere (Doré and Zubeck, 2009)

In cold regions, soils are exposed to freezing and thawing processes. **Figure 1.4** shows the soil freezing process in an open-system (i.e. with external water supply). When the air temperature is lower than the soil temperature, heat is extracted from the soil to the environment, which results in a temperature profile as presented in **Figure 1.4**(a). If the air temperature is below 0 °C, a freezing front (i.e. 0 °C isotherm) will penetrate downward into the soil. For example, the frost penetration in northern Ontario, Canada can be deeper than 3 m; while it is typically around 1 to 2 m in southern Ontario (MTO, 2013). The freezing front progresses as a

function of the imbalance associated with heat supplied to the heat removed as the pore water freezes in situ (Konrad and Morgenstern, 1980). As the freezing front advances, the upper portion of the soil becomes frozen while the lower portion remains unfrozen. A partially frozen layer, namely the frozen fringe, exists between the frozen and unfrozen soil layers (**Figure 1.4**(b)) (Marion, 1995). Thermodynamic processes in the frozen fringe contribute to the generation of negative pore water pressure (Williams, 1966; Konrad and Morgenstern, 1980), as presented in **Figure 1.4**(c). As a result, hydraulic gradient develops and water migrates from the unfrozen soil mass to the frozen soil (Van Vliet-Lanoë, 1985; White, 1999). Migration of water to the frozen soil is manifested as vertical shrinkage cracks below the freezing front (**Figure 1.4**(b)).

Water that migrates into the soil freezes behind the freezing front. Ice lenses may form if a sufficient amount of water is accumulated behind the freezing front, resulting in soil mass heave (**Figure 1.4**(b)). The thickness and spacing of the ice lenses depend on the relative magnitudes of the rate of freezing and water availability (Penner, 1961). The rate of freezing near soil surface is high because the temperature gradient is large. However, the pore water does not have enough time to form thick ice lenses. Instead, thin ice lenses form with a relatively close spacing for this situation. As the freezing front penetrates deeper soil layers, the rate of freezing is relatively low due to lower temperature gradient. For such a scenario, there is enough time for water to migrate towards the freezing front from the lower unfrozen zone and to freeze. Therefore, thick ice lenses develop. The formation of ice lenses in Fujinomori clay and glass beads was directly observed by Watanabe et al. (1997) and Mutou et al. (1998), with the aid of a microscope. The non-uniform distribution of ice lenses in the soil mass contributes to the development of cracks, which occur more frequently near the soil surface and decrease in frequency with increasing depth (Benson and Othman, 1993). These cracks pose a significant influence on the performance of different infrastructure constructed in frozen soil regions.

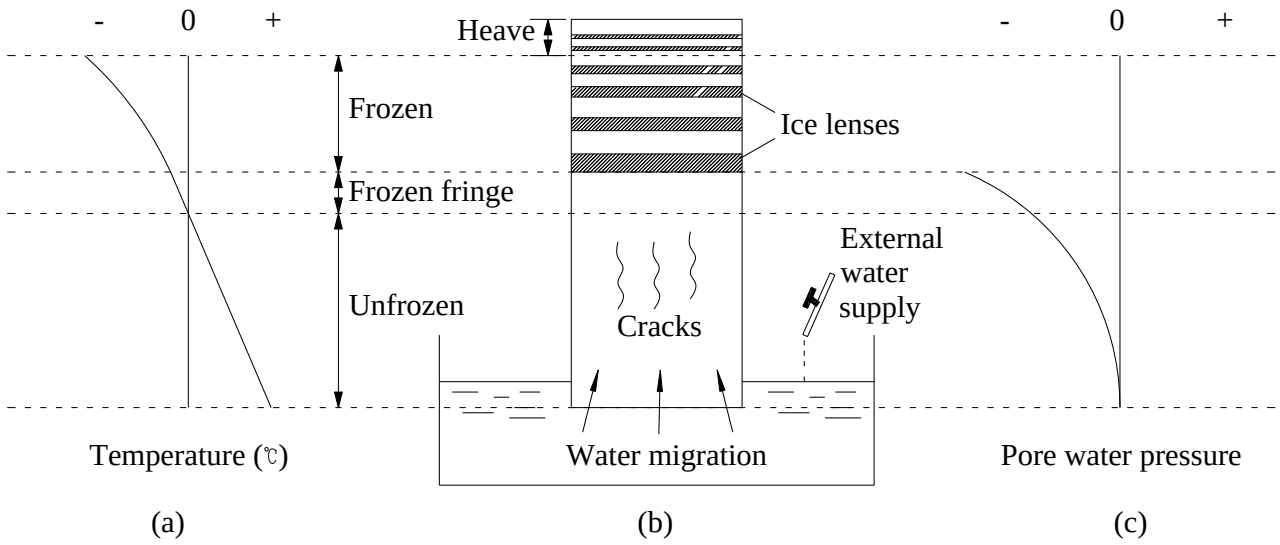

Figure 1.4 Soil freezing in an open-system: (a) temperature profile; (b) soil profile, water migration and ice lenses formation; and (c) negative pore water pressure profile (modified after Benson and Othman, 1993)

The unfrozen water and pore ice typically coexist within a frozen soil (He et al., 2016). The unfrozen water exists in small pore spaces and as thin films adsorbed on the surfaces of soil particles in equilibrium with the pore ice at subzero temperatures (i.e. temperatures below 0 °C) (Harlan, 1973). The relationship between unfrozen water content and subzero temperature in a frozen soil is defined as the soil-freezing characteristic curve, i.e. SFCC (Koopmans and Miller, 1966; Patterson and Smith, 1981; Fu and Dash, 1993; Spaans and Baker, 1996; Azmatch et al., 2012a; Azmatch et al., 2012b; Liu et al., 2012; Carnero-Guzman et al., 2019). Several researchers during the past five decades have shown the similarity between SWCC and SFCC (e.g., Koopmans and Miller, 1966; Spaans and Baker, 1996; Grant and Sletten, 2002; Liu et al., 2012; Schafer and Beier, 2017). This background lays the foundation for a significant part of the research presented in this thesis for using the SFCC as a tool for cold regions engineering practice applications by extending the mechanics of unsaturated soils.

Figure 1.5 shows the typical soil thawing process. As the air temperature goes up above 0 °C, there is a temperature gradient between the air and the soil surface since the upper soil

temperature is below 0 °C. The soil continues to absorb heat from the environment as long as the temperature of air is higher than that of the upper soil mass. With the thawing front (which is the 0 °C isotherm) penetrating downward, pore ice and ice lenses melt. However, the melt water from the ice phase is trapped in the thawed layer by the impermeable frozen layer below (Shoop et al., 2008), resulting in high moisture content or even saturation in the upper portion of the soil mass. Additional moisture may be added to the surface soils by snow melting and precipitation, as shown in **Figure 1.5**. The increased ability to absorb solar radiation at the soil surface would contribute to a rise in soil temperature due to the higher moisture content and lower albedo of the thawed soil. Such a phenomenon favors the evaporation of the soil moisture to a certain extent (Yang et al., 2003).

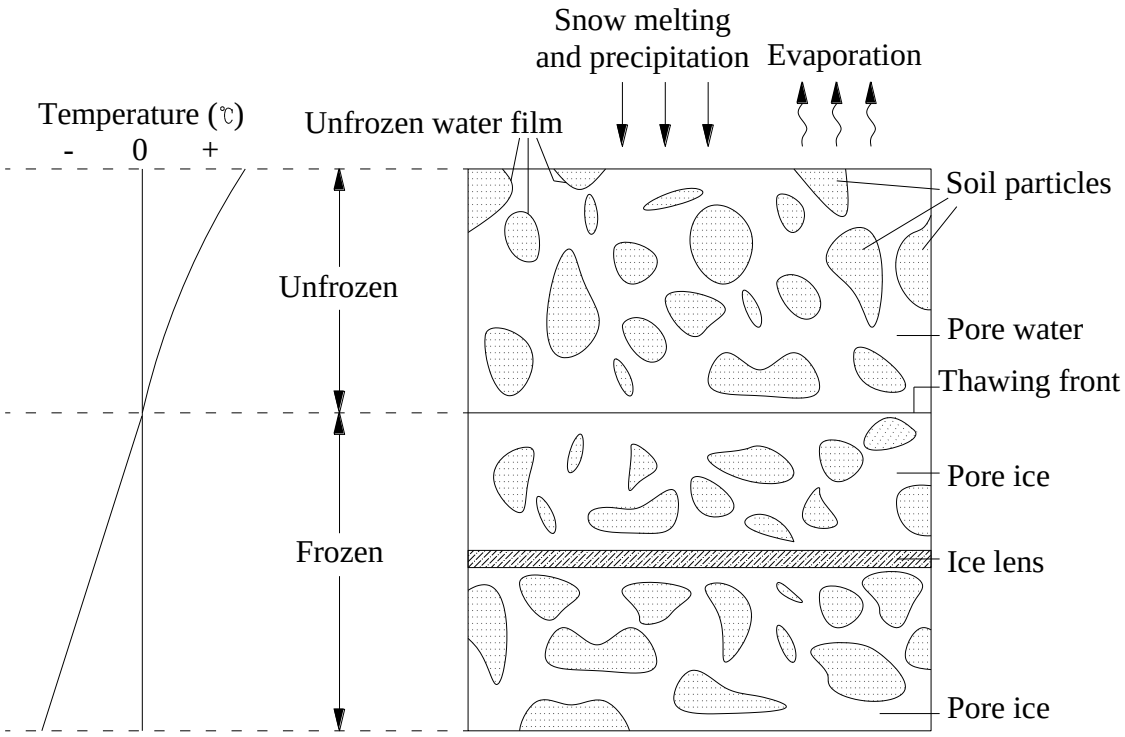

Figure 1.5 Typical soil thawing process

The described freezing-thawing process is a weathering process, which has a significant effect on many engineering applications such as the pavements, railroads, pipelines, and building

constructions (Zaimoglu, 2010). The number of freeze-thaw (F-T) cycles is dependent on the local climate conditions (e.g., Fraser, 1959; Hayhoe et al., 1992; Ho and Gough, 2006). In regions where the temperature varies significantly, many cycles of F-T can be typically expected. Alternatively, if the temperature remains below freezing for a significant period of the winter season, soil will be subjected to fewer F-T cycles (Othman et al., 1994). The number of F-T cycles also depends on the location of the soils. Soils that locate near the ground surface, such as subgrade soils, are more sensitive to change in air temperature and hence are subjected to more cycles of F-T. On the other hand, deeper foundation soils that have relatively limited or no fluctuations in temperature are subjected to only a few F-T cycles (e.g., Hayhoe et al., 1992).

The F-T cycles considerably change the physical and mechanical properties of unbound soils, such as their density, hydraulic conductivity, strength, and stiffness. In general, as the soil temperature drops below 0 °C, ice crystals start nucleating in large soil pores, fissures, and cracks. When pore water changes phase to ice, its volume increases by 9% due to the opening of the lattice of its hexagonal crystal structures. As pore water keeps phase changing, the ice crystals increase in sizes, and they interfere with each other as well as the surrounding soil particles (Andersland and Anderson, 1978). The formed pore ice exerts pressure and contributes to the movement and rearrangement of the surrounding soil particles (Fraser, 1959; Chamberlain and Blouin, 1977). However, the soil particles are not able to move back to their original positions; due to this reason, the cohesion between soil particles is weakened after the soil thaws. In addition, the F-T cycles typically weaken the soil structure, resulting in more cracks and fissures as well as reduction in the fine content in the pores of the coarse fraction. This leads to higher hydraulic conductivity and lower mechanical strengths, such as shear strength and tensile strength (e.g., Fredlund et al., 1975; Chamberlain and Gow, 1979; Lerouil et al., 1991; Othman and Benson, 1992; Simonsen et al., 2002; Wang et al., 2007; Kamei et al., 2012; Li et al., 2012).

1.2 Key objectives and novelty of the thesis

The permafrost and seasonally frozen regions spread out across our earth and occupy a vast

area. The fundamental behavior of frozen soils and the associated mechanisms should be well understood for developing sound engineering practices in these regions. Frozen soil typically consists of four components; namely, soil particles, air, unfrozen water, and ice phases. The most important parameter in a frozen soil is the amount of unfrozen water and / or ice. The relative amount of unfrozen water and ice is predominantly controlled by subzero temperature. Since the SFCC links the degree of phase transition to the subzero temperature in a frozen soil, it is a fundamental feature of frozen soils. Many other important soil properties in cold regions engineering practice, such as the hydraulic conductivity, thermal conductivity, strength and stiffness, are functions of unfrozen water content. In addition, the constitutive relationships for hydraulic, thermal, and mechanical properties of frozen soils are functions of the quantity of unfrozen water. Therefore, the SFCC is essential for modeling the transport mechanism of water, heat, and solutes in frozen soils (e.g., Black and Miller, 1985; Spaans and Baker, 1996; Lai et al., 2014; Zhang et al., 2016; Lu et al., 2019). The SFCC has also been used to analyze the F-T behavior of frozen soils (Liu et al. 2012).

The similarity between SFCC and SWCC has been investigated by many researchers (e.g., Koopmans and Miller, 1966; Spaans and Baker, 1996; Liu et al., 2012; Schafer and Beier, 2017). This similarity can be associated with the free energy of pore water in both the unsaturated unfrozen soil and frozen soil (either saturated or unsaturated) is lowered by the confinement of soil pores and the interaction by soil particles. The decrease in the quantity of pore water, which is replaced either by air in unsaturated unfrozen soil or by ice in frozen soil, is related to the decrease in the free energy of pore water. This physical similarity provides the basis for many studies using the SFCC in a similar manner as the SWCC for extending the mechanics of unsaturated soils.

Currently, there are limited experimental studies in the literature related to the M_R of typical Canadian soils. For example, subgrade soils are typically subjected to moisture variation, freezing / thawing, and F-T cycles in many areas in Canada, which are seasonally frozen or permafrost regions. The measured M_R data considering the influence of environmental factors

can provide a better understanding of soil behavior for the rational design of pavement structures in these regions. In addition, this information can contribute to the development of simple and reliable models for estimating the M_R and for using them in the rational design of pavements. Furthermore, the soil resilient behavior under cyclic loading can promote the understanding of the mechanical response of soils subjected to other types of long-term low-level dynamic loadings, such as those induced by train, earthquake, ocean wave, wind, and construction work (e.g., pile driving, tunneling or blasting) (e.g., Ishikawa et al., 2011; Ling et al., 2013; Ishikawa and Miura, 2015).

The key objectives and associated novelty of this thesis are summarized below:

(1) Comprehensive review on SFCC and its similarity to SWCC, and on some commonly used SFCC models.

The basic concepts of SWCC and SFCC are reviewed. In addition, a comprehensive review related to the similarity between SFCC and SWCC is derived from relevant studies in the literature. The possible reasons for the hysteretic behavior of SFCC are summarized. In light of the physical similarity between drying and freezing processes, and wetting and thawing processes of a soil, the conceptual behavior of SFCC and its similarity to SWCC are derived. Based on these discussions, SFCC has been conceptually divided into three different zones, which is consistent to SWCC.

The reliable determination of SFCC is the primary step to employ SFCC as a tool in engineering practice where frozen soils are encountered. Two different approaches are commonly used for determining the SFCC. The first approach focuses on the direct measurement of SFCC. The second approach focuses on estimating SFCC using the soil physical properties, the similarity between SFCC and SWCC and / or physical and theoretical mechanisms. Some commonly used methods belonging to these two approaches are reviewed.

The widely used four SFCC expressions are selected and compared to facilitate the use of these expressions in engineering practice.

(2) Investigation on the fundamental behavior of SFCC for two Canadian soils.

The SFCC and SWCC of two soils from Toronto, Ontario, Canada (i.e. Toronto silty clay (TSC) and Toronto lean clay (TLC)) are measured, compared, and analyzed. The freezing and thawing branches of SFCC were determined to understand the hysteretic characteristics of these two soils. Experimental results are critically interpreted to understand the fundamental behavior of the SFCC. The comparison between the measured SFCC and SWCC gives insight to the similarity and dissimilarity of these two types of water retention curves. The possible reasons for the dissimilarities between SFCC and SWCC are discussed. The experimental procedures used in the present study could be followed by future studies for investigating the SFCC behavior of soils. The need for reliable determination and rational interpretation of SFCC to facilitate its use for cold region engineering applications is highlighted.

(3) Two models for the estimation of the M_R of frozen soils, and extending the mechanics of unsaturated soils to frozen soil engineering by using SFCC as a tool.

Two novel models are proposed for the estimation of the M_R of frozen soils. The first one is a semi-empirical model, which is established specifically for frozen saturated soils. This model extends the mechanics of unsaturated soils by using SFCC as a tool in a similar manner as SWCC. The soil cryogenic suction (depending on subzero temperature) and degree of unfrozen water saturation are two parameters used in this model. The second one is an empirical hyperbolic model, which is established for both saturated and unsaturated frozen soils. This model exploits the hyperbolic shape of the frozen M_R - subzero temperature relationship. The two models address the shortcomings in the MEPDG that the frozen M_R of unbound soils was set to constant values (depending on soil types) rather than taking account of the variation associated with the decrease in soil temperature.

(4) Experimental investigation of the environmental influence (i.e. moisture and temperature) on the M_R of five Canadian soils.

The M_R of five Canadian soils (i.e., TSC, TLC, Kincardine lean clay (KLC), Ottawa Leda clay (OLC), and Indian Head till (IHT)) considering environmental influences (i.e. moisture and

temperature) is experimentally determined, with the aid of an advanced cyclic loading triaxial testing system. The effect of freezing, wetting, and F-T cycles on the M_R of the five soils is comprehensively investigated. The wetting process simulates the increase in moisture content of in-situ subgrade soils after compaction and during their service life. The freezing and F-T cycles simulate the weathering process caused by temperature variation in seasonally frozen regions. The critical number of F-T cycles determined from the experimental results for the five soils can be used as a basis for engineering structure design in relevant regions.

The above experimental program contributes to our understanding of the resilient behavior of typical Canadian soils. It provides first-hand data and promotes the rational implementation of the MEPDG for the design of pavements in Canada. In addition, the experimental data can be used for the validation of the two novel models that were proposed and for understanding the behavior of soils subjected to various types of dynamic loading.

An artificial neural network (ANN) model is established based on the large amount of experimental data for the estimation of the M_R of the five Canadian soils subjected to variation in water content, different number of F-T cycles and various stress levels. This novel approach, first of its kind for the estimation of the M_R considering various influencing factors in cold regions, can be incorporated into the MEPDG.

1.3 Thesis layout

This thesis is organized in a format of "a collection of manuscripts". The thesis consists of nine chapters. **Chapter 1** introduces the thesis while **Chapter 9** provides overall summary for the presented studies as well as suggestions for future research. The main contents of the other seven chapters are succinctly described below.

Chapter 2 presents a comprehensive review on the important concepts related to the research work addressed in this thesis. The SWCC that is used as a tool in the interpretation and prediction of unsaturated soils behavior is first reviewed. Along similar lines, the SFCC of frozen soils is reviewed. The similarity between the SWCC of an unfrozen unsaturated soil and SFCC

of a frozen saturated soil are critically discussed. In addition, the possible reasons for the hysteretic behavior of SFCC are summarized. Two approaches in the literature for determining SFCC (i.e. direct measurement and estimation) are reviewed. Finally, the effects of freezing / thawing processes and F-T cycles on soil physical and mechanical properties, with a focus on soil modulus, are critically discussed.

Chapter 3 mainly presents discussions on several widely used SFCC expressions from the literature. These expressions are categorized into two groups. The first group is based on empirical relationships between unfrozen water content and subzero temperature. The second group is developed by exploiting the similarity between SFCC and SWCC, with the aid of the Clapeyron equation that correlates subzero temperature to cryogenic suction. Four of these SFCC expressions (two from each category) are selected and used to best-fit the measured SFCCs of four soils collected from the literature. The results are compared and discussed. Recently, a more advanced void ratio-dependent SFCC model was proposed by Mu et al. (2018). Some discussions regarding this SFCC model and its parameters are provided in this thesis. In addition, a simpler and more straightforward SFCC model, which directly uses subzero temperature (rather than using cryogenic suction as in the original model) as an independent variable, is proposed in this thesis. This part of work is summarized in Appendix A.

Chapter 4 presents a comprehensive experimental study on the measurement of both the SFCC and SWCC of TSC and TLC. The SFCC is measured under a set of subzero temperatures by using moisture content sensor and temperature sensor, and the SWCC is measured by using three different methods that covering a wide range of soil suction values, i.e. pressure plate method, WP4-T dew point method, and vapor equilibrium method. Two freezing methods; namely, direct freezing and step freezing were used for determining the freezing and thawing branches of SFCC of the two soils. The experimental results were used to provide comparisons between SFCC and SWCC. In addition, these results are critically interpreted to understand the fundamental behavior of the SFCC. Finally, the possible reasons for the dissimilarities between SFCC and SWCC are critically discussed.

In **Chapter 5**, a semi-empirical model, which uses SFCC as a tool, is proposed for predicting the variation of M_R of saturated frozen soils with subzero temperature (and the associated cryogenic suction). Experimental data on seven different unbound road materials (including both coarse- and fine-grained soils) from the literature are used to validate the proposed model. This semi-empirical model extends the mechanics of unsaturated soils and employs SFCC in a manner similar to SWCC for pavement design in cold regions.

In **Chapter 6**, a model with two-constants is proposed for estimating the variation of soil M_R with subzero temperature exploiting the hyperbolic shape of the frozen M_R - subzero temperature relationship. Experimental data on eighteen different unbound materials from the literature, which include both coarse- and fine-grained soils that were tested under saturated / unsaturated conditions, are used to validate the proposed model. The proposed model is simple and is capable of reasonably predicting the M_R of the investigated soils that are in a state of frozen condition.

Chapter 7 presents an experimental investigation on the frozen M_R of five Canadian soils (i.e., TSC, TLC, KLC, OLC, and IHT). A freezing system is designed for freezing and maintaining the soil specimens under the desired testing temperatures. The freezing system mainly consists of an isotemp bath circulator filled with antifreeze liquid, a wrapped copper coil that is placed around the soil specimen, and insulation materials for minimizing thermal exchange between the soil specimen and surrounding environment. The M_R tests are performed by using a GDS Entry Level Dynamic (ELDyn) triaxial testing system following the AASHTO standard T307-99 (AASHTO, 2007) with some necessary modifications. The effects of water content, subzero temperature, stress level, and loading frequency on the frozen M_R are investigated.

In **Chapter 8**, the M_R of the above five Canadian soils subjected to different wetting and F-T conditions are experimentally determined and analyzed. The wetting process simulates the increase in moisture content of in-situ subgrade soils after compaction and during their service life. The F-T cycles simulate the weathering process caused by temperature variation in

seasonally frozen regions. The same triaxial testing system is used and the testing program is undertaken following AASHTO T307-99 with some modifications. Based on the extensive experimental data, an artificial neural network (ANN) model is developed for estimating the M_R of the five soils considering the influence of water content, number of F-T cycles and stress level.

1.4 Publications

Under review

1. **Ren, J.P.**, and Vanapalli, S.K. 2019. Experimental study on the resilient moduli of five Canadian soils subjected to freezing. Under peer review with a Journal.
2. **Ren, J.P.**, Vanapalli, S.K., Han, Z., Omenogor, K.O., and Bai, Y. 2018. The resilient moduli of five Canadian soils under wetting and freeze-thaw conditions and their estimation by using an Artificial Neural Network model. Under peer review with a Journal.

Journal publications

3. **Ren, J.P.**, and Vanapalli, S.K. 2019. Comparison of soil-freezing and soil-water characteristic curves of two Canadian soils. *Vadose Zone Journal*, 18:180185. DOI: 10.2136/vzj2018.10.0185
4. **Ren, J.P.**, and Vanapalli, S.K. 2018. Discussion on "A new model for capturing void ratio-dependent unfrozen water characteristics curves" by Q.Y. Mu, C.W.W. Ng, C. Zhou, G.G.D. Zhou, and H.J. Liao. *Computers and Geotechnics*, 103: 82-85. DOI: 10.1016/j.compgeo.2018.07.017
5. **Ren, J.P.**, and Vanapalli, S.K. 2018. Model for predicting the resilient modulus of frozen unbound road materials using a hyperbolic function. *Transportation Geotechnics*, 17: 66-74. DOI: 10.1016/j.trgeo.2018.09.011
6. Han, Z., Vanapalli, S.K., **Ren, J.P.**, and Zou, W.L. 2018. Characterizing cyclic and static modulus and strength of compacted pavement subgrade soils considering moisture variation. *Soils and Foundations*, 58(5): 1187-1199.

DOI: 10.1016/j.sandf.2018.06.003

7. **Ren, J.P.**, and Vanapalli, S.K. 2017. Prediction of the resilient modulus of frozen unbound road materials using the soil-freezing characteristic curve. *Canadian Geotechnical Journal*, 1-8.

   DOI: 10.1139/cgj-2017-0153

8. **Ren, J.P.**, Vanapalli, S.K., and Han Z. 2017. Soil freezing process and different expressions for the soil-freezing characteristic curve. *Sciences in Cold and Arid Regions*, 9(3): 0221–0228.

   DOI: 10.3724/SP.J.1226.2017.00221

Conference publications

9. Wu, X.Y., **Ren, J.P.**, and Vanapalli, S.K. 2019. The influence of temperature and moisture on the behavior of fine-grained soils. The 9th International Conference on Geotechnique, Construction Materials and Environment, Tokyo, Japan.
10. Han, Z., Vanapalli, S.K., **Ren, J.P.**, and Zou, W.L. 2018. Empirical relationships for predicting the resilient modulus of Ontario subgrade soils. Transportation Research Board 97th Annual Meeting Transportation Research Board, (No. 18-00494).
11. **Ren, J.P.**, and Vanapalli, S.K. 2017. Soil-freezing characteristic curve of Toronto Silty Clay. In Proceedings of the 70th Canadian Geotechnical Conference, Ottawa, Canada.
12. Ahmed, F., Han, Z., Vanapalli, S.K., and **Ren, J.P.** 2017. Estimating the variation of resilient modulus with moisture content for a compacted subgrade soil from pocket penetrometer results. In Proceedings of the 70th Canadian Geotechnical Conference, Ottawa, Canada.
13. **Ren, J.P.**, Han, Z., and Vanapalli, S.K. 2017. Predicting resilient modulus of frozen subgrade soils. Transportation Research Board 96th Annual Meeting Transportation Research Board, (No. 17-03396).
14. Han, Z., **Ren, J.P.**, Ahmed, F., and Vanapalli, S.K. 2016. Modelling the resilient modulus of Ontario subgrade soils considering the environmental influences. In Proceedings of the 69th Canadian Geotechnical Conference, Vancouver, Canada.

1.5 References

AASHTO, 1986. Standard method of test for resilient modulus of subgrade soils. T272-82, Washington, DC.

Andersland, O.B. and Anderson, D.M. 1978. Geotechnical engineering for cold regions. McGraw-Hill Book Co., Inc., New York, N.Y.

ARA, Inc., ERES Consultants Division. 2004. Guide for mechanistic–empirical design of new and rehabilitated pavement structures. Final report, NCHRP Project 1-37A. Transportation Research Board of the National Academies, Washington, D.C.

Azmatch, T.F., Sego, D.C., Arenson, L.U. and Biggar, K.W., 2012a. Using soil freezing characteristic curve to estimate the hydraulic conductivity function of partially frozen soils. Cold Regions Science and Technology, 83, pp.103-109.

Azmatch, T.F., Sego, D.C., Arenson, L.U. and Biggar, K.W., 2012b. New ice lens initiation condition for frost heave in fine-grained soils. Cold Regions Science and Technology, 82, pp.8-13.

Benson, C.H., Othman, M.A., 1993. Hydraulic conductivity of compacted clay frozen and thawed in situ. Journal of Geotechnical Engineering, 119(2): 276-294.

Bishop, A. W. 1959. The principle of effective stress, Teknisk Ukeblad, Norwegian Geotechnical Institute, Vol. 106, No. 39, pp. 859–863.

Black, P.B. and R.D. Miller (1985) A continuum approach to modeling of frost heaving. In Freezing and Thawing of Soil-Water Systems (D.M. Anderson and P.J. Williams, Ed.). Technical Council on Cold Regions Engineering Monograph. ASCE, p. 36-45.

Brown, S.F., 1996. Soil mechanics in pavement engineering. Géotechnique, 46(3), pp.383-426.

Brown, S.F., 2003. Keynote lecture: Soil mechanics for pavement engineers. In The Symposium Transportation Geotechnics Institution of Civil Engineers.

Caicedo, B., 2018. Geotechnics of Roads: Fundamentals. CRC Press, Boca Raton, Florida, USA.

Carnero-Guzman, G.G., Bouazza, A., Gates, W.P. and Rowe, R.K., 2018, October. A Review of Experimental and Prediction Methods for Assessing the Freezing Characteristic Curve of GCLs. In the International Congress on Environmental Geotechnics (pp. 616-623). Springer, Singapore.

Chamberlain, E.J. and Blouin, S.E., 1977. Freeze-thaw enhancement of the drainage and consolidation of fine-grained dredged material in confined disposal areas. Department of Defense, Department of the Army, Corps of Engineers, Waterways Experiment Station, Environmental Effects Laboratory.

Chamberlain, E.J. and Gow, A.J., 1979. Effect of freezing and thawing on the permeability and structure of soils. Engineering Geology, 13, pp. 73-92.

Christopher, B.R., Schwartz, C.W. and Boudreau, R.L., 2006. Geotechnical aspects of pavements: Reference manual. US Department of Transportation, Federal Highway Administration.

Culley, R.W., 1971. Effect of freeze–thaw cycling on stress–strain characteristics and volume change of a till subjected to repetitive loading. Canadian Geotechnical Journal, 8(3), pp.359-371.

Doré. G., and Zubeck, H.K. 2009. Cold Regions Pavement Engineering, ASCE Press, McGraw

Hill, New York, USA.
Drumm, E.C., Boateng-Poku, Y. and Johnson Pierce, T. 1990. Estimation of subgrade resilient modulus from standard tests. Journal of Geotechnical Engineering, 116(5): 774-789.
Elkeshky, M.M., 2011. Temperature effect on the soil water retention characteristic. Master thesis, Arizona State University, Tempe, USA.
Feuerharmel, C., Pereira, A., Gehling, W.Y.Y. and Bica, A.V.D., 2006. Determination of the shear strength parameters of two unsaturated colluvium soils using the direct shear test. In Unsaturated Soils 2006 (pp. 1181-1190).
Fraser, J.K., 1959. Freeze-thaw frequencies and mechanical weathering in Canada. Arctic, 12(1), pp.40-53.
Fredlund, D.G., Bergan, A.T. and Sauer, E.K. 1975. Deformation characterization of subgrade soils for highways and runways in northern environments. Canadian Geotechnical Journal, 12(2): 213-223.
Fredlund, D.G., Rahardjo, H., and Fredlund, M.D. 2012. Unsaturated Soil Mechanics in Engineering Practice. John Wiley & Sons, Inc., Hoboken, New Jersey, USA.
Fredlund, D.G., Xing, A. and Huang, S., 1994. Predicting the permeability function for unsaturated soils using the soil-water characteristic curve. Canadian Geotechnical Journal, 31(4), pp.533-546.
Fu, H. and Dash, J.G., 1993. Characterization of frost susceptibility of soils by mercury porosimetry. Journal of colloid and interface science, 159(2), pp.343-348.
Gens, A., 2010. Soil-environment interactions in geotechnical engineering. Géotechnique, 60(1), p.3.
Grant, S.A. and Sletten, R.S., 2002. Calculating capillary pressures in frozen and ice-free soils below the melting temperature. Environmental geology, 42(2-3), pp.130-136.
Han, Z. and Vanapalli, S.K., 2015. Model for predicting resilient modulus of unsaturated subgrade soil using soil-water characteristic curve. Canadian Geotechnical Journal, 52(10): 1605-1619.
Han, Z. and Vanapalli, S.K. 2016. State-of-the-Art: Prediction of Resilient Modulus of Unsaturated Subgrade Soils. International Journal of Geomechanics, 1-15.
Harlan, R.L. 1973. Analysis of coupled heat‐fluid transport in partially frozen soil. Water Resources Research, 9(5): 1314-1323.
Hayhoe, H.N., Pelletier, R.G. and Moggridge, S., 1992. Analysis of freeze-thaw cycles and rainfall on frozen soil at 7 Canadian locations. Canadian Agricultural Engineering, 34(2), pp.135-142.
He, H., Dyck, M., Zhao, Y., Si, B., Jin, H., Zhang, T., Lv, J. and Wang, J., 2016. Evaluation of five composite dielectric mixing models for understanding relationships between effective permittivity and unfrozen water content. Cold Regions Science and Technology, 130, pp.33-42.
Heath, A.C., Pestana, J.M., Harvey, J.T., et al. 2004. Normalizing behavior of unsaturated granular pavement materials. Journal of Geotechnical and Geoenvironmental Engineering, 130(9): 896-904.

Heukelom, W. and Klomp, A. 1962. Dynamic testing as a means of controlling pavements during and after construction. In International conference on the structural design of asphalt pavements, 203: (1).

Hicks, R.G., 1970. Factors influencing the resilient properties of granular materials. Doctoral dissertation, University of California, Berkeley, California, USA.

Hicks, R. G. and Monismith, C. L. 1971. Factors influencing the resilient response of granular materials, Highway Res. Record No. 345, Highway Research Board, Washington, DC, 15-31.

Ho, E. and Gough, W.A., 2006. Freeze thaw cycles in Toronto, Canada in a changing climate. Theoretical and Applied Climatology, 83(1-4), pp.203-210.

Ikechukwu, A.F., Hassan, M.M. and Moubarak, A., 2018, November. Evaluation of Subgrade Resilient Modulus from Unsaturated CBR Test. In International Congress and Exhibition " Sustainable Civil Infrastructures: Innovative Infrastructure Geotechnology" (pp. 60-81). Springer, Cham.

Ishikawa, T. and Miura, S., 2015. Influence of moving wheel loads on mechanical behavior of submerged granular roadbed. Soils and Foundations, 55(2), pp.242-257.

Ishikawa, T., Sekine, E. and Miura, S., 2011. Cyclic deformation of granular material subjected to moving-wheel loads. Canadian Geotechnical Journal, 48(5), pp.691-703.

Johnson, T.C., Berg, R.L., Chamberlain, E.L., et al. 1986. Frost action predictive techniques for roads and airfields. A comprehensive survey of research findings. CRREL-86–18. U.S, Army Cold Regions Research and Engineering Laboratory, Hanover, N.H.

Kamei, T., Ahmed, A. and Shibi, T. 2012. Effect of freeze–thaw cycles on durability and strength of very soft clay soil stabilised with recycled Bassanite. Cold Regions Science and Technology, 82: 124-129.

Kim, D.S., Stokoe II, K.H., 1992. Characterization of resilient modulus of compacted subgrade soils using resonant column and torsional shear tests (No. 1369), 83-91.

Kodikara, J., Islam, T. and Shounthrarajah, A., 2018. Review of soil compaction: History and recent developments. Transportation Geotechnics, 17, pp.24-34.

Konrad, J.M. and Morgenstern, N.R. 1980. A mechanistic theory of ice lens formation in fine-grained soils. Canadian Geotechnical Journal, 17(4): 473-486.

Koopmans, R.W.R. and Miller, R.D. 1966. Soil freezing and soil water characteristic curves. Soil Science Society of America Journal, 30(6), 680-685.

Lai, Y., Pei, W., Zhang, M. and Zhou, J., 2014. Study on theory model of hydro-thermal–mechanical interaction process in saturated freezing silty soil. International Journal of Heat and Mass Transfer, 78, pp.805-819.

Lekarp, F., Isacsson, U. and Dawson, A., 2000. State of the art. I: Resilient response of unbound aggregates. Journal of transportation engineering, 126(1), pp.66-75.

Leroueil, S., Tardif, J., Roy, M., et al. 1991. Effects of frost on the mechanical behaviour of Champlain Sea clays. Canadian Geotechnical Journal, 28(5): 690-697.

Li, G., Ma, W., Zhao, S., et al. 2012. Effect of freeze-thaw cycles on mechanical behavior of compacted fine-grained soil. In Cold Regions Engineering 2012: Sustainable Infrastructure

Development in a Changing Cold Environment, 72-81. ASCE Publications.
Ling, X., Li, Q., Wang, L., Zhang, F., An, L. and Xu, P., 2013. Stiffness and damping radio evolution of frozen clays under long-term low-level repeated cyclic loading: experimental evidence and evolution model. Cold Regions Science and Technology, 86, pp.45-54.
Liu, Z., Zhang, B., (Bill) Yu, X., and Tao, J., 2012. A new method for soil water characteristic curve measurement based on similarities between soil freezing and drying. Geotechnical Testing Journal, 35(1): 2-10.
Lu, J., Pei, W., Zhang, X., Bi, J. and Zhao, T., 2019. Evaluating of calculation models for the unfrozen water content of freezing soils. Journal of Hydrology. (in press)
Marion, G.M., 1995. Freeze-Thaw Processes and Soil Chemistry (No. CRREL-SR-95-12). Cold Regions Research and Engineering Lab Hanover, NH., USA.
MTO, 2013. Pavement design and rehabilitation manual, Second Edition. The Ministry of Transportation of Ontario, Ontario, Canada.
Mu, Q.Y., Ng, C.W.W., Zhou, C., Zhou, G.G.D. and Liao, H.J., 2018. A new model for capturing void ratio-dependent unfrozen water characteristics curves. Computers and Geotechnics, 101, pp.95-99.
Mutou, Y., Watanabe, K., Ishizaki, T., Mizoguchi, M., Lewkowicz, A.G. and Allard, M., 1998, June. Microscopic observation of ice lensing and frost heave in glass beads. In Proc. Seventh Intl. Conf. on Permafrost, June (Vol. 2327, No. 1998, p. 283287).
Oh, W.T., Vanapalli, S.K., and Puppala, A.J. 2009. Semi-empirical model for the prediction of modulus of elasticity for unsaturated soils. Canadian Geotechnical Journal, 46(8): 903–914.
Oloo, S.Y., Fredlund, D.G. and Gan, J.K., 1997. Bearing capacity of unpaved roads. Canadian Geotechnical Journal, 34(3), pp.398-407.
Othman, M.A. and Benson, C.H. 1992. Effect of freeze-thaw on the hydraulic conductivity of three compacted clays from Wisconsin, 1369: 118-125.
Othman, M.A., Benson, C.H., Chamberlain, E.J. and Zimmie, T.F., 1994. Laboratory testing to evaluate changes in hydraulic conductivity of compacted clays caused by freeze-thaw: state-of-the-art. In Hydraulic conductivity and waste contaminant transport in soil. ASTM International, 227-254.
Patterson, D.E. and Smith, M.W., 1981. The measurement of unfrozen water content by time domain reflectometry: Results from laboratory tests. Canadian Geotechnical Journal, 18(1), pp.131-144.
Penner E, 1961. The importance of freezing rate in frost action in soils. Proceedings of the American Society for Testing and Materials, 60: 1151–1165.
Puppala, A.J., 2008. Estimating stiffness of subgrade and unbound materials for pavement design. NCHRP synthesis 382, National Cooperative Highway Research Program. Transportation Research Board, Washington, D.C., USA.
Qi, S., 2017. Numerical investigation for slope stability of expansive soils and large strain consolidation of soft soils. Doctoral thesis, University of Ottawa, Ottawa, Canada.
Sahin, H., Gu, F., Tong, Y., et al. 2013. Unsaturated soil mechanics in the design and performance of pavements. Keynote Address, Proc. 1st Pan-Am. Conf. on Unsaturated Soils,

CRC Press/ Balkema, Rotterdam, the Netherlands.

Sawangsuriya, A., Edil, T.B. and Benson, C.H. 2009. Effect of suction on resilient modulus of compacted fine-grained subgrade soils. Transportation Research Record. 2101, Transportation Research Board, Washington, D.C., 82-87.

Schafer, H.L. and Beier, N.A., 2017. Development of soil freezing characteristic curves for fluid fine tailings using TDR. In Proceedings of the 70th Canadian Geotechnical Conference, Ottawa, Canada, 1-8.

Shoop, S., Affleck, R., Haehnel, R., et al. 2008. Mechanical behavior modeling of thaw-weakened soil. Cold Regions Science and Technology, 52(2): 191-206.

Simonsen, E., Janoo, V.C. and Isacsson, U. 2002. Resilient properties of unbound road materials during seasonal frost conditions. Journal of Cold Regions Engineering, 16(1): 28-50.

Spaans, E.J. and Baker, J.M. 1996. The soil freezing characteristic: its measurement and similarity to the soil moisture characteristic. Soil Science Society of America Journal, 60: 13–19.

Uzan, J. 1992. Resilient characterization of pavement materials. International Journal for Numerical and Analytical Methods in Geomechanics, 16(6): 453-459.

Vanapalli, S.K., Fredlund, D.G. and Pufahl, D.E. 1999. The influence of soil structure and stress history on the soil-water characteristics of a compacted till. Géotechnique, 49(2): 143-159.

Vanapalli, S.K., Fredlund, D.G., Pufahl, D.E. and Clifton, A.W., 1996. Model for the prediction of shear strength with respect to soil suction. Canadian Geotechnical Journal, 33(3), pp.379-392.

Van Vliet-Lanoë, B., 1985. Frost effects in soils. Soils and quaternary landscape evolution, pp.117-158.

Vogrig, M., McDonald, A., Vanapalli, S.K., Siekmeier, J., Roberson, R. and Garven, E., 2003. A laboratory technique for estimating the resilient modulus of unsaturated soil specimens from CBR and unconfined compression test. In Proc. 56th Canadian Geotechnical Conference, Winnipeg, Manitoba, Canada.

Wang, D.Y., Ma, W., Niu, Y.H., et al. 2007. Effects of cyclic freezing and thawing on mechanical properties of Qinghai–Tibet clay. Cold regions science and technology, 48(1): 34-43.

Wang, L., Hoyos, L.R., Mohammad, L. and Abadie, C., 2005. Characterization of asphalt concrete by multi-stage true triaxial testing. Journal of ASTM International, 2(10), pp.1-10.

Watanabe, K., Mizoguchi, M., and Ishizaki, T., 1997. Experimental study on microstructure near freezing front during soil freezing. Transactions-Japanese Society of Irrigation Drainage and Reclamation Engineering, pp.53-58.

White, T.L., 1999. Soil microstructure and the thermodynamic behaviour of permafrost affected soils. In Advances in Cold-Region Thermal Engineering and Sciences (pp. 519-532). Springer, Berlin, Heidelberg.

Williams, P.J. 1966. Pore pressures at a penetrating frost line and their prediction. Géotechnique, 16(3): 187-208.

Yang, M., Yao, T., Gou, X., et al. 2003. The soil moisture distribution, thawing–freezing processes and their effects on the seasonal transition on the Qinghai–Xizang (Tibetan)

plateau. Journal of Asian Earth Sciences, 21(5): 457-465.
Zaimoglu, A.S. 2010. Freezing–thawing behavior of fine-grained soils reinforced with polypropylene fibers. Cold regions science and technology, 60(1): 63-65.
Zhang, S., Teng, J., He, Z., Liu, Y., Liang, S., Yao, Y. and Sheng, D., 2016. Canopy effect caused by vapour transfer in covered freezing soils. Géotechnique, 66(11): 927-940.
Zhang, T., Barry, R.G., Knowles, K., et al. 2003. Distribution of seasonally and perennially frozen ground in the Northern Hemisphere. In Proceedings of the 8th International Conference on Permafrost, 2: 1289-1294.
Zhang, Y., Ishikawa, T., Tokoro, T. and Nishimura, T., 2014. Influences of degree of saturation and strain rate on strength characteristics of unsaturated granular subbase course material. Transportation Geotechnics, 1(2), pp.74-89.

Chapter 2 Literature review

2.1 Introduction

In this chapter, the basic concepts of SWCC and SFCC are reviewed. A comprehensive review on the similarity between SFCC and SWCC is derived from relevant studies in the literature. The possible reasons for the hysteretic behavior of SFCC are summarized. The commonly used methods for the determination of SFCC (direct measurement and estimation) are reviewed. In addition, the effect of freeze-thaw (F-T) cycles and freezing / thawing on the physical and mechanical properties of soils are reviewed.

2.2 Soil-water characteristic curve (SWCC)

The energy status, which is also termed as soil water potential or pressure, is defined as the energy (per unit mass, volume, or weight of water) that must be applied to withdraw an infinitesimal amount of water from the soil to a reference reservoir containing free water (Spaans and Baker, 1996). The soil water has lower energy than the free water because soil water is confined by soil pore spaces and influenced by the adsorption of soil particles. The energy of soil water can be measured in terms of its partial vapor pressure (Fredlund and Rahardjo, 1993).

The pore spaces in an initially saturated soil are occupied by water along with possibly some occluded air bubbles as shown in **Figure 2.1**(a). The water phase is continuous at this stage, which is referred to as the boundary effect stage. When the saturated soil is subjected to drying, water drains from the pore spaces, and the energy of the remaining pore water decreases (or soil suction increases). The soil suction (ψ) is defined as the pressure difference between the pore air and pore water phases (i.e. $\psi = p_a - p_w$) along an air-water interface in an unsaturated soil. At a certain value of soil suction, air phase starts to enter into large pore spaces. This suction value is generally referred to as the air-entry value (AEV). During this stage (i.e. the primary transition stage), the air phase is typically not continuous, but the water phase is still continuous, as shown in **Figure 2.1**(b).

The soil suction keeps increasing as the drying process continues. During this process, more and more water will be replaced by air with an increase in the soil suction. The air bubbles increase in size and penetrate smaller pore spaces. During this stage (referred to as the secondary transition stage), both the air and water phases can be continuous, as shown in **Figure 2.1**(c). The remainder of pore water is found in increasingly narrower spaces, with decreasing radii of curvature of the air-water interface. At a certain value of suction, most of the pore water is replaced by air and only a small amount of water is available in the soil. This water is adsorbed and is available on the surfaces of soil particles as thin films and confined in small pore spaces that air phase cannot penetrate under the current suction value (**Figure 2.1**(d)). This soil water content is in the residual stage and is widely referred to as the residual water content. Since adsorptive forces increase with distance close to the soil particle's surface, and capillary forces are inversely proportional to the radius of curvature, more energy is needed to remove a subsequent amount of pore water (Spaans and Baker, 1996).

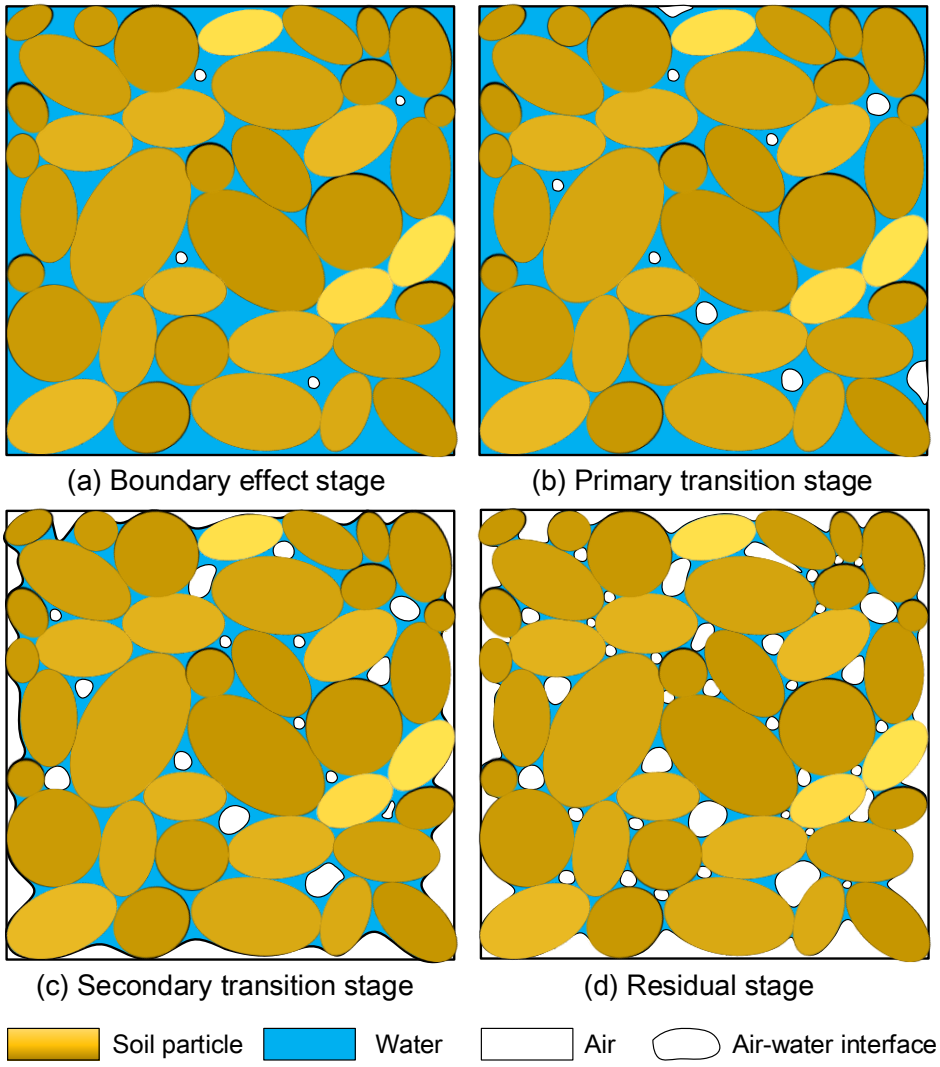

Figure 2.1 Probable variations of water and air phases in a saturated soil subjected to drying (modified after Vanapalli et al., 1996; Yin and Vanapalli, 2018)

The soil-water characteristic curve (SWCC) defines the relationship between suction (or water potential, or energy) and the gravimetric water content, or volumetric water content, or degree of saturation of an unsaturated soil. It can be used as a conceptual tool to both interpret and predict the physical and mechanical behavior of unsaturated soils (Vanapalli et al., 1999). **Figure 2.2** shows a typical plot of SWCC (degree of saturation vs. suction) for a silty soil highlighting some key features. The SWCC is hysteretic under drying (desorption) and wetting

(adsorption) conditions. However, it is usually sufficient to only consider the desorption curve. The AEV and the residual water content (or the residual state of saturation) is shown in **Figure 2.2**. Use these two distinct points, the SWCC can be divided into three different zones, i.e. boundary effect zone, transition zone, and residual zone of unsaturation. This is in agreement with the variations of water and air phases shown in **Figure 2.1**. The three zones have also been described as the capillary regime, funicular regime, and pendular regime respectively (e.g., Lu and Likos, 2004; Yin and Vanapalli, 2018). In addition, two more description methods have been used to represent the three different zones (Zhang et al., 2014). Thermodynamic considerations show that the suction value corresponding to zero water content is approximately one million kPa (Fredlund, 1996). Many expressions have been proposed in the literature for best-fitting the measured SWCC. The descriptions, advantages and limitations of these expressions can be found in studies and textbooks such as Leong and Rahardjo (1997), Lu and Likos (2004), and Fredlund et al. (2012).

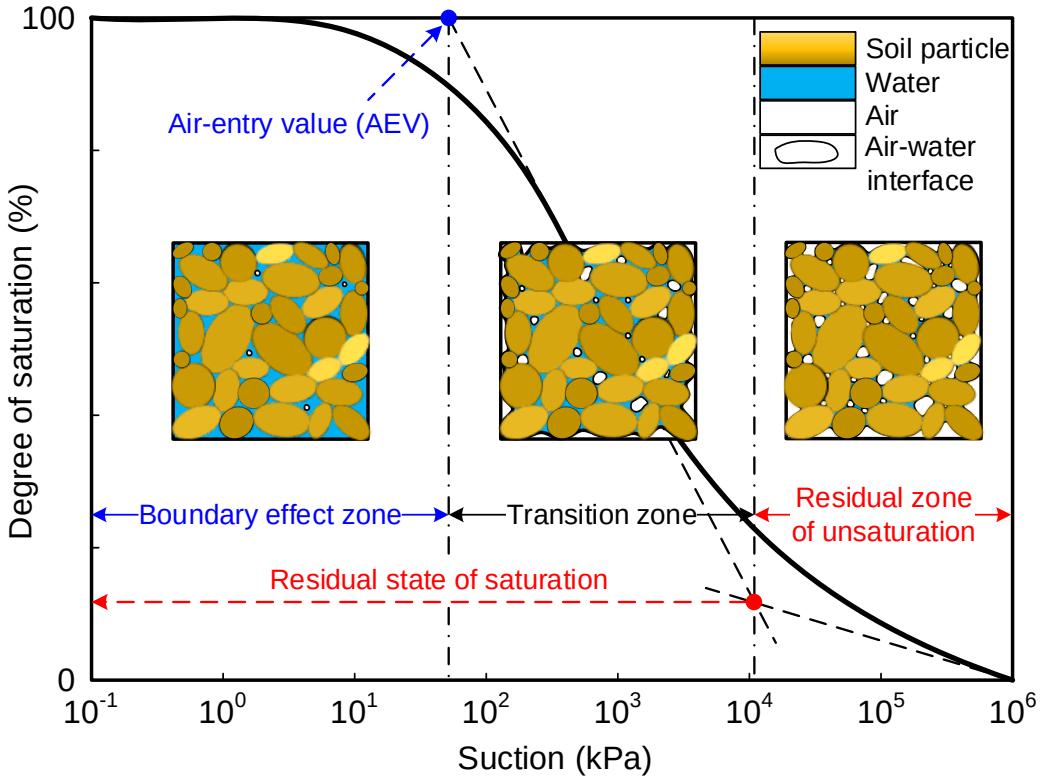

Figure 2.2 Typical plot of SWCC for a silty soil (modified after Vanapalli et al., 1999; Yin and Vanapalli, 2018)

The physical and mechanical properties of unsaturated soils such as the hydraulic conductivity, thermal conductivity, shear strength, stiffness, and volume change are difficult to measure directly since it requires cumbersome equipment that can be operated only by skilled technicians, and requires a long time. Many studies in the literature have shown that the behavior of unsaturated soils could be predicted by using the SWCC (e.g., Fredlund and Rahardjo, 1993; Vanapalli et al., 1999). As the soil moves from a saturated state to drier conditions, the distribution of water and air phases changes, influencing the properties of unsaturated soils. Since the SWCC represents the amount of water phase as well as air phase in a soil, it can be used as a tool to predict the engineering behavior of unsaturated soils. For example, in some cases the behavior may be primarily related to the volume of the separate phases (e.g., water content), or the continuity and tortuosity of the water phase (e.g., hydraulic conductivity and

molecular diffusion) or the air phase (e.g., coefficient of vapor or oxygen diffusion). In other cases, it is the nature of the interphase contact area controlling stress transfers (e.g., shear strength and volume change) or interphase mass transfers (e.g., chemical adsorption and volatilization) which controls behavior. These interphase relationships can be derived using the SWCC and can then be used for estimating or predicting unsaturated soil properties (Barbour, 1998; Vanapalli et al., 1999).

2.3 Soil-freezing characteristic curve (SFCC)

In a frozen soil, liquid water and pore ice coexist (e.g., Edwards and Cresser, 1992; Ishizaki et al., 1994; Dash et al., 1995). Bouyoucos (1917) first demonstrated the existence of liquid water in a frozen soil-water system by use of a dilatometer. The principal factor determining the quantity of water remaining unfrozen is subzero temperature (Nersesova and Tsytovich, 1963). Pressure is less important than temperature; however, it is a reasonably significant factor. An increase in pressure increases the unfrozen water content at a given temperature. Besides the external influences (i.e. temperature and pressure), solute concentration can also exert an effect. In addition, the manner in which freezing was accomplished, the soil microstructure and specific surface area of soil particles, the chemical and mineralogical nature of the soil matrix, and physicochemical characteristics, especially the nature of the exchangeable cations may also be important (e.g., Nersesova and Tsytovich, 1963; Anderson and Tice, 1973; Chai et al., 2018).

For an initially unfrozen saturated soil, all its pore spaces are occupied by liquid water, as shown in **Figure 2.3**(a). When the soil is subjected to freezing, the temperature of pore water decreases. Since pore water is confined and influenced by soil particles, the freezing point of pore water is lower than that of free water, which typically freezes at 0 °C. This means that pore water will not freeze when soil temperature decreases to 0 °C. Therefore, at this time, the pore spaces are completely filled with liquid water. With a further decrease in temperature, however, small ice crystals will form (nucleate) in large pores and replace some water, as shown in **Figure**

2.3(b). This specific subzero temperature can be referred to as the ice-entry value (IEV), which is analogous to the AEV in the SWCC. There remains a significant quantity of liquid water and the water phase is continuous at this stage. The ice crystals will increase in size and penetrate smaller pore spaces. As a result, more and more water will be replaced by ice as soil temperature decreases (see **Figure 2.3**(c)). Both the ice and water phases can be continuous during this stage. Finally, when a certain value of subzero temperature is achieved, most of the pore water become ice and only a small amount of liquid water is left. This amount of unfrozen water is tightly adsorbed on the surfaces of soil particles as thin films and confined in small pore spaces, as shown in **Figure 2.3**(d). This particular water content can be referred to as the residual unfrozen water content. At this stage, the ice phase is continuous while the water phase is not.

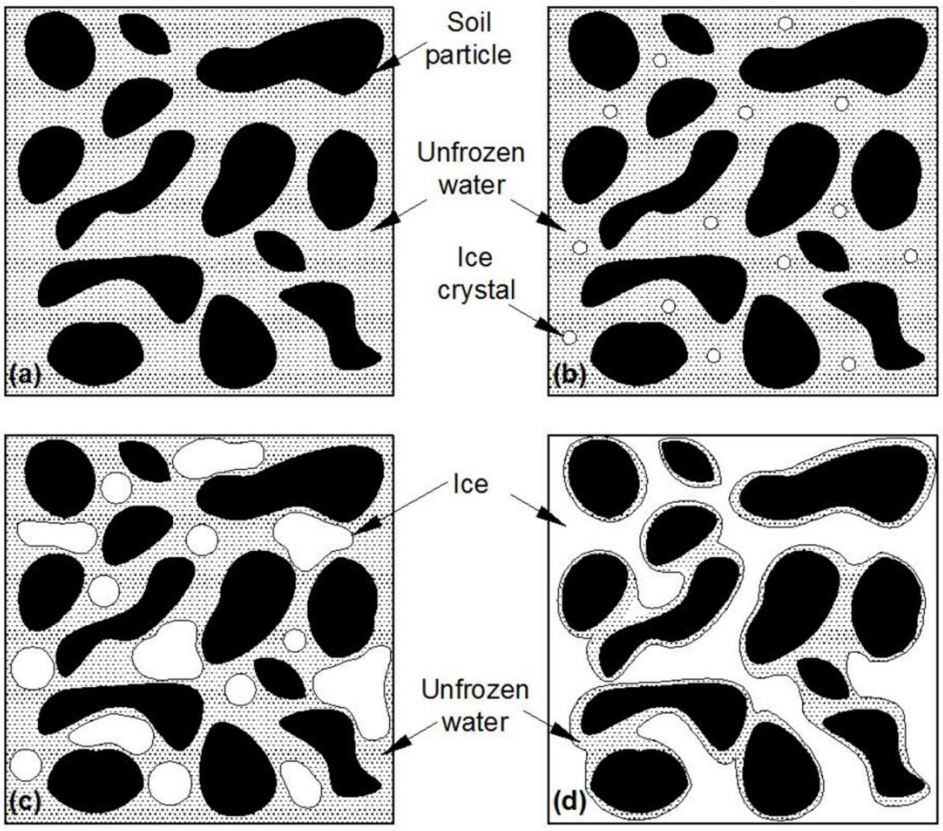

Figure 2.3 Probable variations of unfrozen water and ice phases in a saturated soil subjected to freezing: (a) no ice has formed; (b) formation of ice crystals; (c) increase of ice crystals; (d) residual stage

The soil-freezing characteristic curve (SFCC) describes the relationship between the amount of unfrozen water and subzero temperature in a frozen soil (Koopmans and Miller, 1966; Spaans and Baker, 1996; Flerchinger et al., 2006; Azmatch et al., 2012a; Azmatch et al., 2012b; Liu et al., 2012a; Wu et al., 2015; Watanabe and Osada, 2016; Schafer, 2018). Similar to the case in unsaturated soils, the quantity of unfrozen water can be represented by either the gravimetric water content, or volumetric water content, or degree of (unfrozen water) saturation. The relationship between unfrozen water content and temperature has also been referred to as the phase composition curve (PCC) (e.g., Anderson and Tice, 1972; Anderson et al., 1973; Liu and Yu, 2014), unfrozen water characteristic curve (UWCC) (Mu et al., 2018), freezing temperature equation or equilibrium equation (Kurylyk and Watanabe, 2013), soil freezing curve (SFC) (Grant and Sletten, 2002), and soil freezing retention curve (SFRC) (Mao et al., 2018). In order to have similar expression as the SWCC, the abbreviation SFCC is used through the remainder of this thesis except for Appendix A.

The SFCC links the degree of phase transition to the subzero temperature in a frozen soil. Therefore, many important soil properties in cold regions engineering practice, such as the hydraulic conductivity (Azmatch et al., 2012a), segregation potential for frost heave (Konrad, 2001), resilient modulus (Bigl and Berg, 1996b), and strength (Akagawa and Nishisato, 2009; Agergaard and Ingeman-Nielsen, 2012), can be estimated using SFCC. In addition, the constitutive relationships for hydraulic, thermal, and mechanical properties of frozen soils are functions of the quantity of unfrozen water, the SFCC is therefore essential to modeling the transport mechanism of water, heat, and solutes in frozen soils (e.g., Black and Miller, 1985; Spaans and Baker, 1996; Zhang et al., 2016; Yu et al., 2018). The SFCC has also been used to analyze the F-T behavior of frozen soils, for example as recently presented by Liu et al. (2012b).

The cryogenic suction (or cryosuction), which is associated with the potential that develops between pore ice and pore water (or the pressure difference between the ice and water phases along curved ice-water interface, i.e. $\psi_{cryo} = p_i - p_w$) in frozen soils, is conceptually similar to the suction developed between the air and water phases in unfrozen unsaturated soils (Gens, 2010;

Caicedo, 2017; Na, 2018). The cryogenic suction is of fundamental importance when considering the mechanical and other properties of frozen soils, and contributes to the increase of shear strength, apparent pre-consolidation pressure, and stiffness of frozen soils (Shastri and Sanchez, 2012).

The Clapeyron equation can be used to convert the subzero temperature to cryogenic suction or vice versa. The original form of the Clapeyron equation, which was derived from the thermodynamic concept of Gibbs free energy, can be generalized for multiple phases by first writing the Gibbs-Duhem relationship for each phase and then combining the resulting terms (Kurylyk and Watanabe, 2013). In a solute-free saturated frozen soil, the relation between changes in chemical potential for the unfrozen water and ice phases, is given by the Gibbs-Duhem equation as below (Grant et al., 1999; Lebeau and Konrad, 2012),

$$\mathrm{d}\mu_w = -s_w \mathrm{d}T_w + v_w \mathrm{d}p_w \tag{2.1}$$

$$\mathrm{d}\mu_i = -s_i \mathrm{d}T_i + v_i \mathrm{d}p_i \tag{2.2}$$

where μ_w and μ_i are the chemical potential of unfrozen water and ice phases respectively; s_w and s_i are the specific entropy of unfrozen water and ice phases respectively; T_w and T_i are the temperature of unfrozen water and ice phases respectively; v_w and v_i are the specific volume (v) of unfrozen water and ice phases respectively ($v = 1 / \rho$, ρ is the density). At thermodynamic equilibrium condition, the changes in chemical potential and temperature of the unfrozen water and ice phases are equal (i.e., $\mathrm{d}\mu_w = \mathrm{d}\mu_i$; $T_w = T_i = T$), this results in,

$$v_w \mathrm{d}p_w - v_i \mathrm{d}p_i = (s_w - s_i)\mathrm{d}T = \frac{L}{T}\mathrm{d}T \tag{2.3}$$

which can be rearranged and integrated to give,

$$-\mathrm{d}p_i + \frac{v_w}{v_i}\mathrm{d}p_w = \frac{1}{v_i}\frac{L}{T}\mathrm{d}T \tag{2.4}$$

$$\int_{p_0}^{p_i} \mathrm{d}p_i - \frac{v_w}{v_i}\int_{p_0}^{p_w} \mathrm{d}p_w = -\frac{1}{v_i}\int_{T_0}^{T} \frac{L}{T}\mathrm{d}T \tag{2.5}$$

$$p_i - p_0 - \frac{v_w}{v_i}(p_w - p_0) = -\frac{1}{v_i}\int_{T_0}^{T}\frac{L}{T}\mathrm{d}T \tag{2.6}$$

$$p_i - p_w + (1-\frac{v_w}{v_i})(p_w - p_0) = -\frac{1}{v_i}\int_{T_0}^{T}\frac{L}{T}\mathrm{d}T \tag{2.7}$$

where L is the latent heat of fusion of water (L = 334 kJ/kg); T_0 is the normal freezing temperature of water (T_0 = 0 °C); T is the subzero temperature in °C (when expressed in K, T (K) = T (°C) + 273.15); and p_0 is the reference pressure which is usually taken as the atmospheric pressure.

Extending the assumption that p_i is constant and equal to the atmospheric pressure, and that the density difference between water and ice phases is negligible (i.e. $\rho_w = \rho_i$, and $v_w = v_i$), the above equation (i.e. Eq. (2.7)) can be simplified as,

$$\psi_{cryo} = p_i - p_w = -L\rho_w \ln\frac{T+273.15}{T_0+273.15} = -334000 * \ln\frac{T+273.15}{273.15} \tag{2.8}$$

where ψ_{cryo} is the cryogenic suction in kPa; ρ_w is the density of water (ρ_w = 1000 kg/m^3). The calculated cryogenic suction versus subzero temperature relationship by Eq. (2.8) is approximately linear with a slope of about 1225 kPa/°C when the subzero temperature is not too low, as shown in **Figure 2.4**. This value is in agreement with other values provided by different researchers (e.g., Williams and Smith, 1989; Grant, 1994; Konrad, 1994; Ma et al. 2015; Caicedo, 2018). The theoretical limit of suction in a soil (i.e. 10^6 kPa) can be converted to a subzero temperature of -259.47 °C, by using Eq. (2.8).

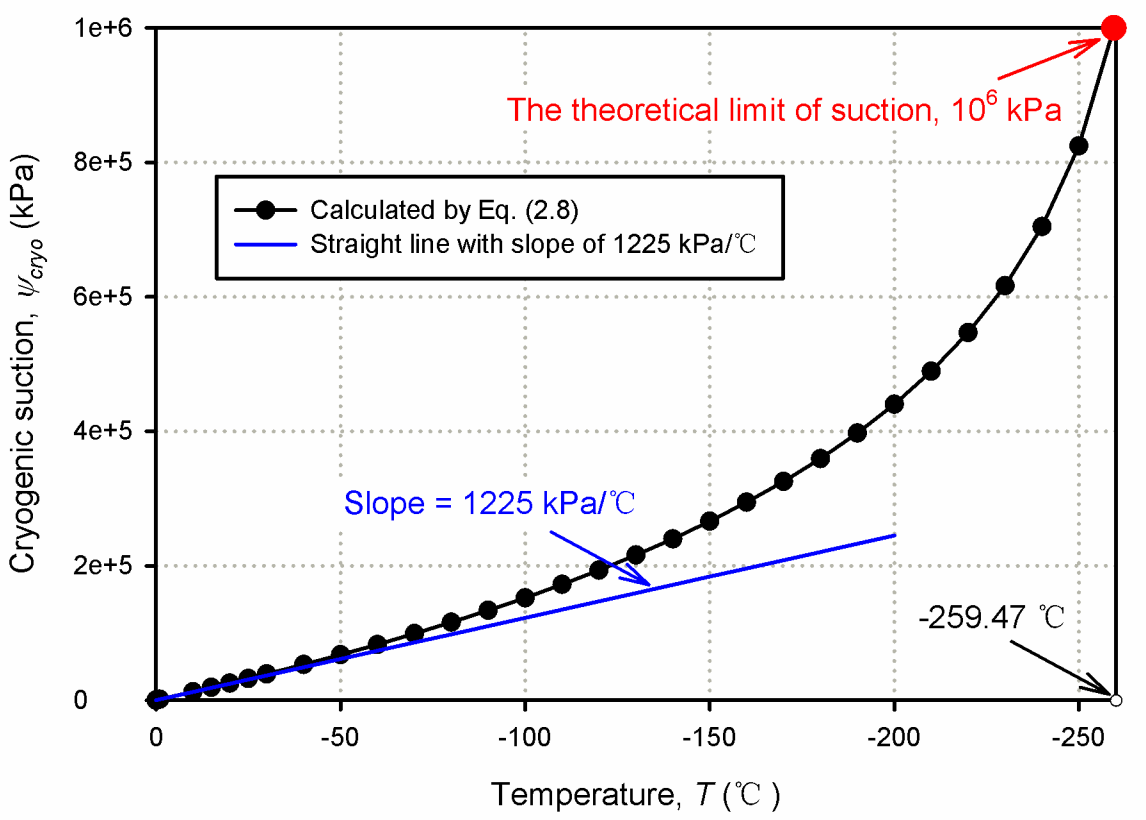

Figure 2.4 The Clapeyron equation

Several researchers have summarized various forms of the Clapeyron equations that are available in the literature (e.g., Spaans, 1994; Black, 1995; Dall'Amico, 2010; Kurylyk and Watanabe, 2013). A comprehensive review on these various forms of the Clapeyron equation is out of the scope of this thesis. It is interesting to note that many researhers refer to Eq. (2.8) as the Clausius-Clapeyron equation. This is, however, not fully valid. As stated by Black (1995): "*This is not correct; the Clausius-Clapeyron equation applies to liquid-vapor equilibrium, whereas the Clapeyron equation refers to any equilibrium phase composition*." This point of view is also supported by Hansson et al. (2004), who expressed that the Clausius-Clapeyron equation is a simplified version of the Clapeyron equation.

The shape of the SFCC depends on the intial void ratio, the cooling rate, and the F-T cycle (e.g., Konrad, 1989; Azmatch et al., 2012b; Mu et al., 2018). A typical SFCC of Devon silt specimen measured by Azmatch et al. (2012b) is shown in **Figure 2.5**. The soil slurry was

prepared at a moisture content of 60% and then de-aired prior to being consolidated under 100 kPa. The unfrozen water conent was measured using the time domain reflectometry (TDR) technique. The cryogenic suction value was calculated from the corresponding subzero temperature by using the Clapeyron equation. As mentioned above, an important point when a soil is subjected to freezing is the IEV, defined as the subzero temperature or cryogenic suction at which ice first begins to enter the largest soil pores. The procedure for determining the IEV is shown in **Figure 2.5**. The initial straight-line portion of the SFCC is extended to intersect a linear extension of the transition zone (where there is a sharp drop in the unfrozen water content) of the SFCC. The intersection of the two straight lines gives the IEV (Azmatch et al., 2012b).

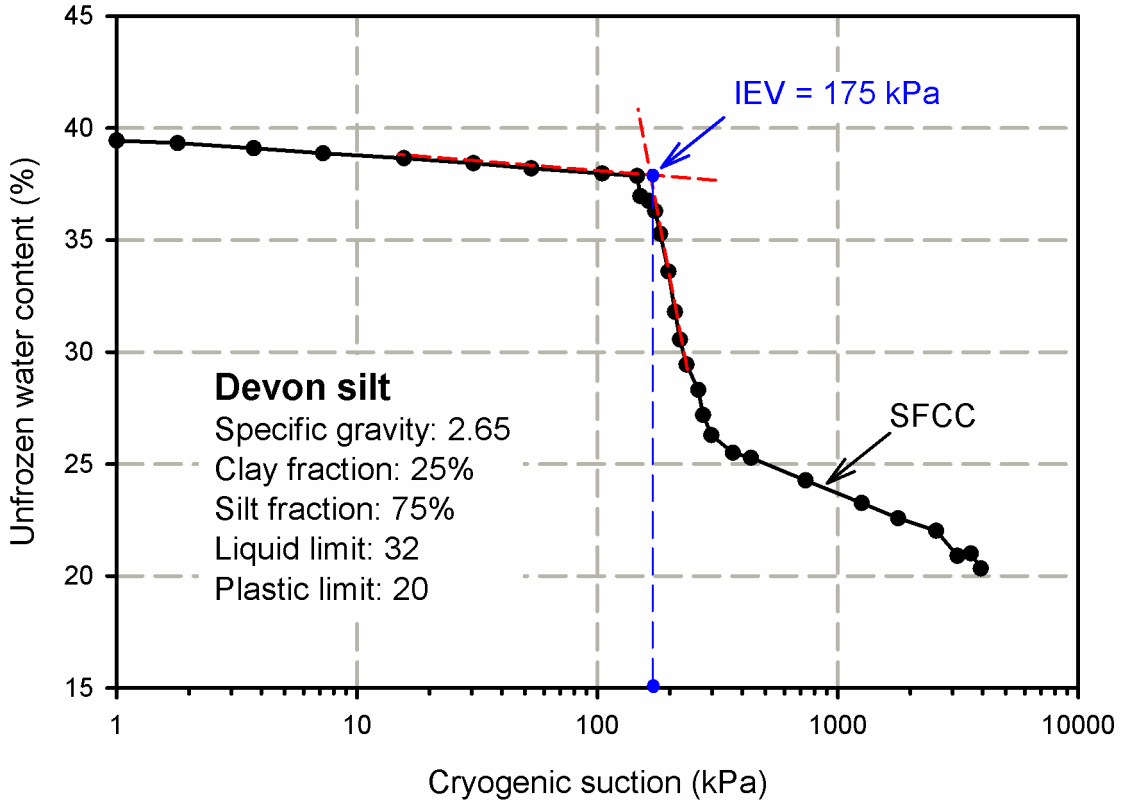

Figure 2.5 The SFCC of Devon silt specimen consolidated to 100 kPa and determination of IEV (modified after Azmatch et al., 2012b)

2.4 Similarity between SFCC and SWCC

As can be seen from the above two sections, the physical process that a soil undergoes during drying (and wetting) cycles under unfrozen condition has similar features to that when the soil is subjected to freezing (and thawing) cycles. When an initially saturated soil is subjected to drying, water is gradually removed and replaced by air, leaving the remainder water at an increasingly lower matric potential. In a similar fashion, liquid water in the soil changes phase and gradually becomes ice when it is subjected to freezing. Two different mechanisms contribute to matric potential; namely, the adsorptive force and capillary force (e.g., Bittelli et al., 2003; Lu and Khorshidi, 2015). The adsorptive force acts on the mineral-water interface. Water is adsorbed by soil particles as thin films. Therefore, it is considered immaterial whether ice or air is present on the other side of the water film; for this reason, reductions of soil matric potential in frozen and unfrozen conditions due to adsorptive force can be considered identical (Spaans and Baker, 1996; Na, 2018). The capillary force at the interface of different phases, such as air-water, ice-water, and air-ice interfaces, is proportional to the surface energy of the interface. The surface energy of air-water interface is higher than that of ice-water interface (Spaans, 1994). For this reason, reductions of soil matric potential associated with capillary force are different in a soil that is at frozen and unfrozen conditions.

The similarity between drying / wetting and freezing / thawing processes was observed long time ago but has not received sufficient attention (Liu et al., 2012a). Buckingham (1907) noticed the analogy between the flow of capillary water and flow of heat, which are the result of water pressure difference and temperature gradient respectively. He also defined the capillary potential as the measure of the attraction of soil for water. Beskow (1935) initially proposed the concept that soil freezing is related to soil drying and that water flow to the freezing front in freezing soils is similar to water flow to the evaporative front in drying soils (Kurylyk and Watanabe, 2013). Schofield (1935) introduced the pF scale to indicate the energy status or suction of soil water in the unit of cm H_2O. The pF is the logarithm of the Buckingham's potential. The free energy difference between soil water and bulk free water (and hence the pF)

can be directly related to the freezing point depression. The proposed relationship between the pF and freezing point depression by him is a simplified form of the Clapeyron equation.

Koopmans and Miller (1966) were the pioneers who measured both the SFCC and SWCC for three different types of soils (i.e. SS, SLS, and SSLS). The SS soil is free of colloidal materials and represents soils such as sand, silt, or coarse clay fractions that have direct solid-to-solid (SS) contacts between particles. In SS type soils, each particle is wedged with the other adjacent particles and the pore geometry is fixed. A change in water content causes a displacement of the air-water interface within the pore system; however, there will be no change in the bulk volume of the soil. The other extreme scenario relates to the soil particles are always separated by liquid water (i.e. solid-liquid-solid), designated as the SLS soil. A change in water content is accompanied by corresponding changes in particle spacing and in the bulk volume. Macroscopic cracks may open or close due to changes in water content; however, the air phase does not penetrate the spaces between particles. The schematic representation of the SS and SLS soils and their basic features are shown in **Figure 2.6**. In reality, the behavior of a majority of natural soils lies in between the SS and SLS; for this reason, they are designated as SSLS soil.

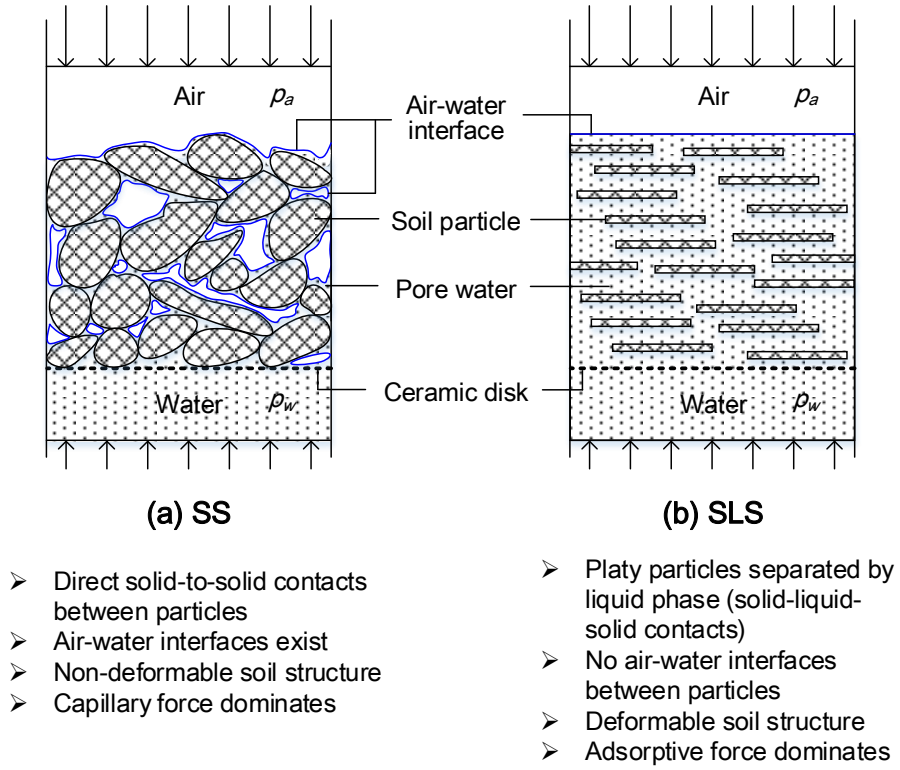

Figure 2.6 Schematic representation of (a) SS and (b) SLS soils (figures are modified after Miller, 1980)

It is reasonable to assume that adsorptive force dominates the water retention behavior in the SLS soil. The SFCC and SWCC are expected to be identical and do not require any adjustment if soil water is at similar state in the frozen and unfrozen SLS soil. However, because of the difference between the surface energy of air-water and ice-water interfaces in a SS soil, an adjustment factor is required to relate its SWCC to SFCC (Koopmans and Miller, 1966; Miller, 1980). **Figure 2.7** shows the measured SFCC and SWCC of these three different types of soils. As can be seen, by using an adjustment factor of 2.2 for the SS and SSLS soils and with no adjustment for the SLS soil, good agreement was achieved between the SFCC and SWCC (Miller, 1973). It is of interest to note that a value of 2.2 would lead to erroneous result for the SSLS soil from a theoretical point of view. Investigators were also inspired to find an adjustment factor that is dependent on temperature since most soils behave as SSLS soils, which cannot be categorized as dominated by either capillary or adsorptive force (Kurylyk and Watanabe, 2013).

Soil pore water freezes gradually and the governing force (capillary or adsorptive) may switch with a decrease in temperature. At higher subzero temperature, pore water is mainly present as the result of capillary force since the curvature of ice-water interface is significant in this situation. However, when there is a further decrease in temperature, most pore water becomes ice and only thin adsorbed film of water is available. Hence at this stage, adsorptive force dominates and no capillary force is considered (Lebeau and Konrad, 2012; Kurylyk and Watanabe, 2013).

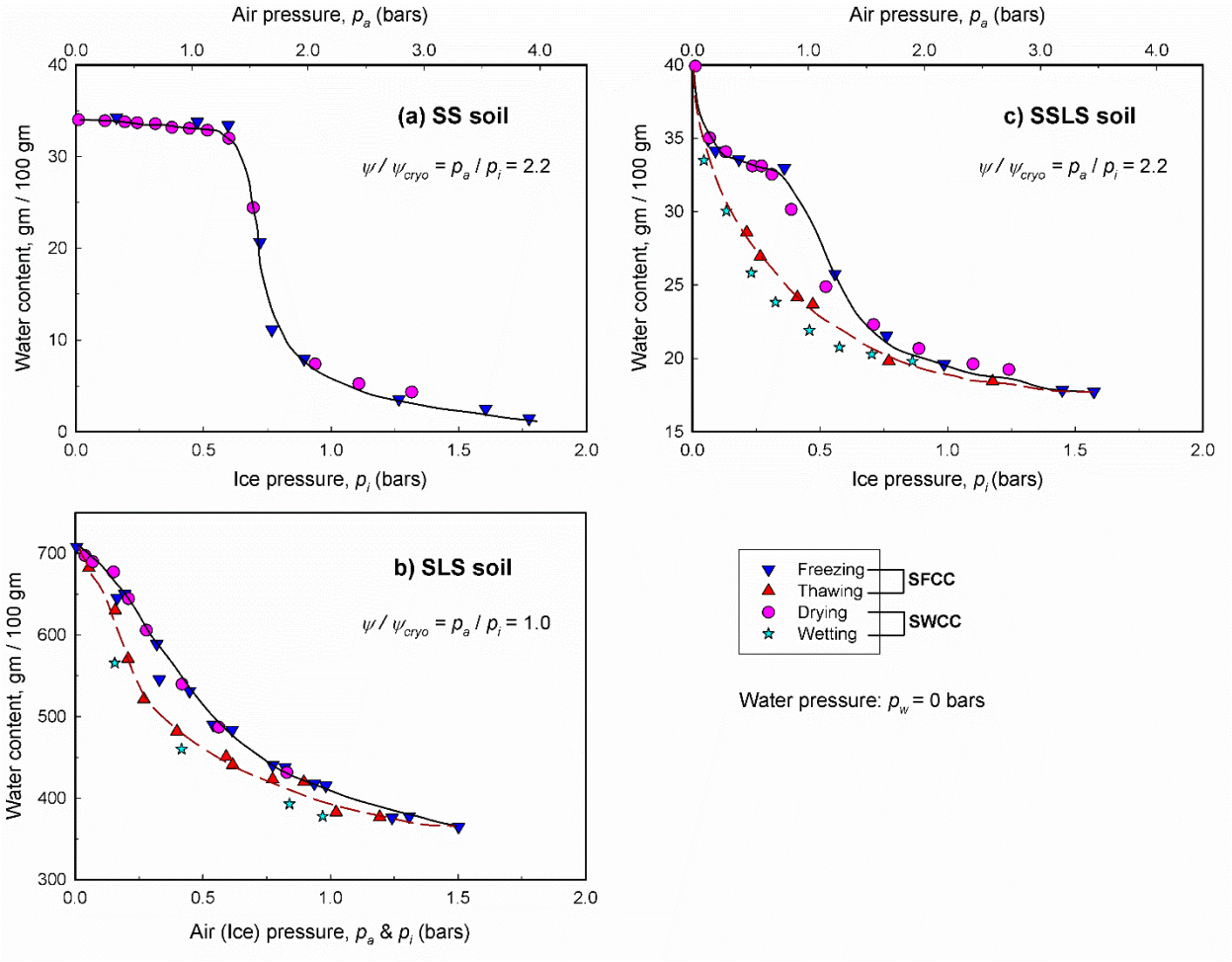

Figure 2.7 (a) SFCC for second freezing and SWCC for drying for SS soil; (b) SFCC and SWCC for SLS soil; and (c) SFCC for third F-T cycle and SWCC for dry-wet cycle for SSLS soil (data from Koopmans and Miller, 1966)

Figure 2.8 highlights the characteristics similar in both the SFCC and SWCC. In a SWCC, the soil is in a state of saturated condition until soil suction reaches to the AEV. The soil water content drops significantly with the continuous increase of soil suction beyond the AEV point, until most of the pore water drains away and only a small amount of water is left as thin adsorbed films on soil particles. This particular water content is known as the residual water content. It is generally acknowledged that further increase in soil suction does not contribute to a significant reduction in water content as the residual condition is achieved. The SWCC can thus be divided into three zones with the aid of the two key definitions (i.e. the AEV and residual water content): boundary effect zone, transition zone, and residual zone (as summarized in Section 2.2). In a SFCC, with a decrease in subzero temperature (which corresponds to an increase in cryogenic suction), ice crystals start to form in large soil pores which were originally filled with unfrozen water. The corresponding subzero temperature (or cryogenic suction) at this stage is referred to as the IEV. Both the AEV and IEV can be described by the Young-Laplace equation, through the surface energy of air-water interface and ice-water interface, respectively. The unfrozen water content continues to decrease at a relatively faster rate as soil temperature decreases. At certain subzero temperature, most pore water turns into ice and beyond which extremely low temperature (i.e. high cryogenic suction) would be required to reduce the quantity of unfrozen water. This critical point is the residual unfrozen water content (as shown in **Figure 2.8**(b)), which is similar to the residual water content of SWCC. At this point, unfrozen water is firmly held by and close to the soil particles (as summarized in Section 2.3). The SFCC could then be divided into three zones similar to SWCC, as shown in **Figure 2.8**. In addition, scanning curves exist for both SWCC and SFCC (e.g., Patterson and Smith, 1981; Spaans and Baker, 1996; Pham et al., 2005; Parkin et al., 2013). The SFCC also shows hysteretic behavior (Williams, 1967; Homshaw, 1980; Patterson and Smith, 1981; Overduin et al., 2006; Azmatch, 2013; Yu et al., 2018).

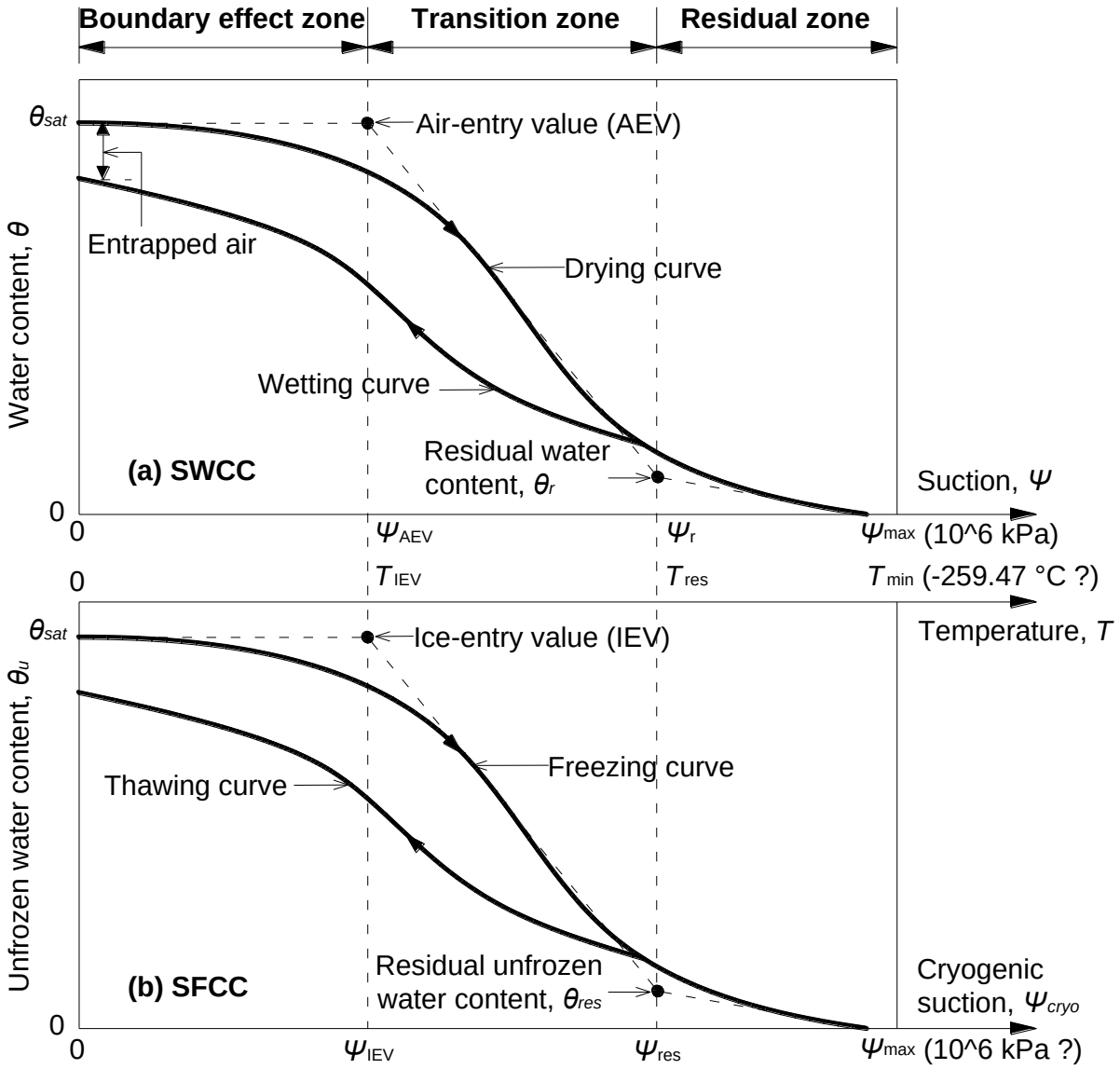

Figure 2.8 Conceptual sketch for the similarity between SWCC and SFCC

Figure 2.9 displays the typical SWCC and SFCC of sand, silt, and Regina clay using the data collected from different studies (Smith and Tice, 1988; Vanapalli et al., 1999; Bronfenbrener and Bronfenbrener, 2012). It should be noted that the SWCC and SFCC of each soil were not necessarily obtained from identical specimens (the respective soil physical properties are shown in **Figure 2.9**). The figure serves for illustrating basic features of SWCC and SFCC of the same type of soil. For SFCC, the originally measured subzero temperature is converted to cryogenic suction through the Clapeyron equation (i.e. Eq. (2.8)). As can be seen from **Figure 2.9**, the

SWCC and SFCC show similar trends in variation with an increase in soil suction. The desorption rate of coarser soils is relatively fast; due to this reason, the water content of sand and silt drops significantly (pore water is replaced by either air or ice) in a relatively small range of soil suction, and then levels off. The water content of Regina clay, on the other hand, decreases at a much slower rate and continues decreasing even when soil suction is relatively high. The reason for such a behavior is that fine-grained soils consist of small size platy particles, which have a capacity to retain large amount of water by strong adsorptive forces.

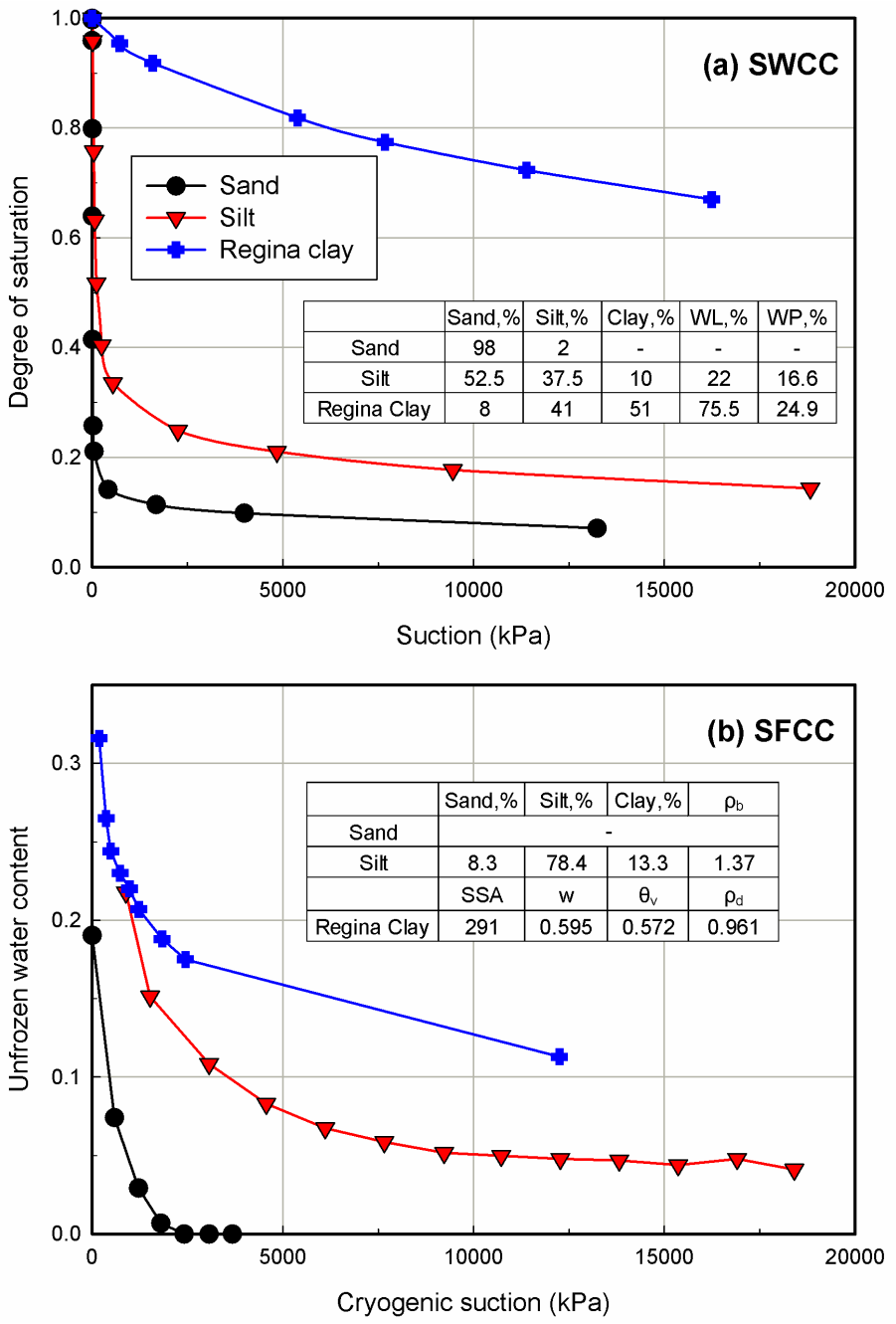

Figure 2.9 Typical (a) SWCC and (b) SFCC of sand, silt, and Regina clay

Note: SWCC data were collected from Vanapalli et al. (1999); SFCC data of Regina clay was collected from Smith and Tice (1988) and those of sand and silt were collected from Bronfenbrener and Bronfenbrener (2012). (WL: Liquid limit; WP: Plastic limit; ρ_b: Bulk density, g/cm^3; SSA: Specific surface area, m^2/g; w: Gravimetric water content; θ_v: Volumetric water content; ρ_d: Dry density, g/cm^3)

2.5 Hysteresis of SFCC

As shown in **Figure 2.8**, the SFCC exhibits hysteretic behavior similar to SWCC. This can be attributed to several possible mechanisms: (1) *Supercooling of pore water* (Bittelli et al., 2003; He and Dyck, 2013; Tian et al., 2014; He et al., 2015). Soil pore water does not necessarily freeze when its freezing temperature is reached. Instead, pore water remains in a liquid phase and is supercooled to a lower temperature, until freezing is induced by ice nucleation. (2) The *effect of electrolytes* (Bittelli et al., 2003; He and Dyck, 2013; Tian et al., 2014; He et al., 2015). Since electrolytes will be excluded from ice when soil is subjected to freezing, the solute concentration in the remainder of pore water becomes larger, which contributes to freezing point depression of pore water and yields hysteresis. (3) *Pore geometry* (Homshaw, 1980; Anderson et al., 2009). Hysteresis may be attributed to differences in ice-water interface curvatures during crystallization (freezing) and melting (thawing), especially in soil that contains a notable component of pores that are cylindrical. (4) *Pore blocking* (Bittelli et al., 2003; Anderson et al., 2009). Bottle neck effect (originating from large pores with narrow necks), which is considered as a primary cause of the hysteresis commonly observed for air-water phase transition in soil with a wide distribution of interconnected pores of different radii, may similarly lead to the hysteresis for ice-water phase transition in the soil. (5) The *effect of contact angle* (Liu and Yu, 2013; Zhou et al., 2019). The advancing contact angle during soil freezing is different from the receding contact angle during soil thawing. (6) The *change in pore structure*. The thixotropic property and aging effects that influence pore size distribution, may contribute to hysteresis (Liu and Yu, 2013).

In addition, soil particles typically move from their original positions as soil pores are enlarged due to ice expansion during the freezing process. Therefore, there would be more large pores than prior to soil freezing. When soil is subjected to thawing, pore ice melting initiates in small pores first and then progresses successively to larger pores (Tan et al., 2015). Due to this reason, for the same unfrozen water content, temperature on the thawing branch is higher than that on the freezing branch. In other words, the thawing branch is below the freezing branch (i.e.

hysteresis). Nevertheless, the reasons for hysteresis in porous media such as soils are still not well understood. This may be associated with the complexity of pore structure, which may likely comprise of various heterogeneous (at the pore scale) pore geometries, a wide range of pore diameters and varying degrees of interconnectivity (Anderson et al., 2009).

2.6 Determination of SFCC (or unfrozen water content)

The reliable determination of SFCC is the primary step to employ SFCC as a tool in the prediction of the physical and mechanical properties of frozen soils. Two different approaches are commonly used for determining the SFCC. The first approach focuses on the direct measurement of SFCC, with the aid of convenient and / or advanced testing equipment. Several methods have been used in laboratory and in situ during the past few decades. A significant amount of data is published in the literature following these methods. The widely used methods and their principles, advantages and / or limitations are summarized in **Table 2.1**. The second approach focuses on the estimation of SFCC using soil physical properties, the similarity between SFCC and SWCC and / or physical and theoretical mechanisms. **Table 2.2** provides a summary of these details for the estimation of SFCC. This summary is aimed to provide information on several representative estimation methods rather than including all the models that have been proposed in the literature, avoiding tedious contents.

Table 2.1 Conventional methods for measuring the unfrozen water content

Method	Principle in brief	Advantages and / or limitations
Dilatometry[1,2]	Soil sample is placed in the dilatometer under an immiscible liquid that would not freeze until -10 °C. The sample is then undercooled to a desired temperature and ice nucleation is induced by, for example, a gentle tap. The volume of expansion during freezing can be calculated from the position of the meniscus of the immiscible liquid in the capillary extension of the dilatometer before and after freezing. The volume of expansion is an indicator of an equivalent quantity of water that changed phase to ice. The quantity of unfrozen water can be estimated by comparing to the total water content.	The state, distribution and properties of the unfrozen water are not known. This method usually overestimates the unfrozen water content[10]. It is most suitable for the temperature range of 0 to about -2 °C. This method cannot be used on natural soils, since samples must be slurried and completely de-aired[11].
Adiabatic calorimetry[2]	A frozen soil sample is brought to thermal equilibrium at a desired subzero temperature and then quickly transferred to an adiabatic calorimeter filled with liquid at temperature above 0 °C. Heat exchange occurs between the sample and liquid until there is an equilibrium condition with temperature. The energy gained by the sample is equal to the energy yielded by the liquid, which can be calculated from temperature change, heat capacity and weight of the calorimeter liquid. By subtracting the portion of energy absorbed by the sample constituents, the energy expended in melting ice present in the frozen sample is then simply determined. The ice content is then computed as this amount of energy divided by the latent heat of freezing.	In general, the lower the initial sample temperature, the less reliable the result. The state, distribution and properties of the unfrozen water could not be known. The operation and calculation are complicated[10].
Differential thermal analysis (DTA) [1,2]	This method is closely related to calorimetry. When properly calibrated, it is called differential scanning calorimetry (DSC, which has also been used for measuring unfrozen water content[3]). In DTA, the temperature of a sample is compared by means of an electrical thermometer with that of an inert reference substance while both are exposed symmetrically to a uniformly changing temperature. The sample temperature either lags behind or precedes that of the reference substance depending on whether heat is being released or absorbed during a phase change. When a moist soil is frozen during a low temperature DTA run, an exotherm corresponding to liberation of the latent heat of freezing is observed. This can be used to estimate the quantity of ice formed and is the basis for the estimation of the unfrozen water content.	Some other important aspects (e.g., nucleation temperatures, nucleation sites, and the existence of one or more low temperature phases of the interfacial water) are clarified. Limited to detect the amount of unfrozen water that is able to undergo phase change[13]. It is useful primarily as a method for determining unfrozen water content at low temperatures where the dilatometer and adiabatic calorimeter are most questioned. Thermodynamic equilibrium and a complete SFCC are difficult to achieve.

Table 2.1 Conventional methods for measuring the unfrozen water content (Cont'd)

Method	Principle in brief	Advantages and / or limitations
Isothermal calorimetry[1,2]	This method was developed to circumvent the limitations of the DTA method. Soil samples with different water contents are put in the isothermal calorimeter, and then a constant subzero temperature is applied inside the apparatus. As each sample freezes (freezing is induced manually), the electrical signal proportional to the energy released within the sample is recorded. Not all the samples will have nucleated if the water content range has been properly selected. Thus, a plot of exotherm intensity versus water content, yields the minimum water content at which ice exists (this is taken as the unfrozen water content at the controlled subzero temperature). A number of measurements at different subzero temperatures, which are sufficient to construct a SFCC, can be obtained by repeating these steps.	This method is limited to temperatures above about -10 °C.
X-ray diffraction (XRD) [1,2]	In this method, the average distance between mineral grains (individual lamella) in a frozen sample of a platy clay is determined at various temperatures. It is assumed that during freezing, segregated ice crystals and polycrystalline ice masses grow at the expense of the unfrozen water surrounding the soil grains. Hence, by knowing the total surface area of a 2:1 lattice-expanding clay and the average distance between adjacent mineral surfaces, the amount of unfrozen water contained between adjacent lamella can be estimated.	This method does not have wide applicability (probably only the expanding lattice clays can be used as samples). It requires expensive apparatus and is time-consuming to perform the test. It does not account for the unfrozen water bounding external surfaces.
Frequency domain reflectometry (FDR, aka capacitance technique) [4,7]	The capacitance based techniques have an oscillating circuit and a sensing part which is embedded in the soil. This technique determines the apparent dielectric constant, K_a, of a soil by measuring the charge time of a capacitor which uses the soil as a dielectric. This capacitor works with the oscillator to form a tuned circuit, and changes in soil water content are detected by the changes occurring in the operating frequency. The K_a of the soil is more sensitive to relatively small changes in the proportion of free water in the soil than to changes in the proportions of the other soil components. Empirical relationship between K_a and the volumetric water content can be used to estimate soil water content.	Low initial cost; fast acquisition; portable. It is suitable for both laboratory and field use. There is a great dependence of FDR sensors on the salt content and on the soil type. Air gaps around the sensor can profoundly influence the readings. Low FDR frequencies are problematic.
Time domain transmissometry (TDT) [4]	In TDT, an electrical signal is sent along a transmission line and the evanescent field around the transmission line interacts with the surrounding soil. The pulse speed and wave shape of these signals are affected by the dielectric constant (K_a) of the soil. Empirical relationship between K_a and the volumetric water content can be used to estimate soil water content.	May be subjected to circuit board (semiconductor) problems at temperatures below -40 °C.

Table 2.1 Conventional methods for measuring the unfrozen water content (Cont'd)

Method	Principle in brief	Advantages and / or limitations
Nuclear magnetic resonance (NMR)[4,5]	The nuclei of hydrogen atoms resemble miniature bar magnets that will align along a strong magnetic field. When radio frequencies are applied, atoms absorb a certain amount of energy to realign to another stable position within the magnetic field. If a soil sample is placed in a pulsed NMR analyzer and a single radio frequency pulse is applied, a voltage is induced in a receiver coil that surrounds the sample. The magnitude of this voltage is directly proportional to the amount of water in the sample. A drop in signal intensity is observed as soil water freezes if the NMR is tuned to the hydrogen proton associated with unfrozen water only. Such that the unfrozen water content can be obtained.	Accurate and fast measurement; high cost. Its use is restricted to the laboratory. Water distribution in the soil sample can be inferred[9]. Sampling is difficult due to the size limitation, and the results are sensitive to organic matter content[10]. Cannot measure the variation of unfrozen water content dynamically[15]. It requires separate calibration for each sample, and the method is sensitive to temperature[11]. Its reliability still needs to be studied[14].
Time domain reflectometry (TDR)[4,6,7]	TDR is a form of pulse-reflection measurement, which can determine the propagation velocity and reflection of electromagnetic waves in a transmission line. A pulse travels down and will remain unaltered as long as the characteristic of the transmission line stay the same. However, any discontinuity in the transmission line will give rise to partial reflection and partial transmission of the pulse. The apparent dielectric constant (K_a) of soil sample can be determined from the TDR trace (K_a is a function of the transmission line length, the velocity of electromagnetic radiation in free space, and travel time). Empirical relationship between K_a and the volumetric water content can be established[8]. Specific calibration may be required when measuring unfrozen water content. A combined TDR-dilatometer was also used for simultaneously measuring K_a and unfrozen water content[11, 12].	High temporal resolution; fast acquisition; good repeatability. High initial cost; loss of reflection in highly saline soil; increase in conductivity with wetting of the soil mass. It is suitable for both laboratory and field use.

[1]Anderson and Morgenstern, 1973; [2]Anderson and Tice, 1973; [3]Kozlowski, 2003; [4]Yoshikawa and Overduin, 2005; [5]Smith and Tice, 1988; [6]Patterson and Smith, 1980; [7]SU et al., 2014; [8]Topp et al., 1980; [9]Tian et al., 2014; [10]Li et al., 2018; [11]Patterson and Smith, 1981; [12]Patterson and Smith, 1985; [13]Carnero-Guzman et al., 2018; [14]Kozlowski, 2016; [15]Lu et al., 2019a.

Table 2.2 Various methods used for estimating unfrozen water content

No.	Author(s)	Key information	Advantages and / or limitations
1	Dillon and Andersland, 1966	Proposed an equation for predicting unfrozen water content by incorporating temperature and certain soil properties, which include specific surface area, activity ratio, and the expandable clay lattice.	Empirical, simple, but hard to guarantee satisfactory predictions under various conditions. Incapable of fitting complete SFCC, especially at higher subzero temperatures.
2	Anderson and Tice, 1972	Unfrozen water content can be conveniently expressed as a function of subzero temperature by a simple power curve with two constants, which can be estimated from soil specific surface area. They further plotted a family of SFCC for the range of specific surface areas encompassing various natural soils.	Empirical, simple, and theoretically tenable. Hard to guarantee satisfactory predictions under different conditions.
3	Xu et al., 1985	The two-constants power relationship proposed above can be represented as a linear relationship on log-log coordinate. The slope of the linear relationship is mainly influenced by soil types and salinity. For a particular soil, the slope value can be estimated by measuring the freezing points of the soil under two different initial water contents (i.e. two-point method). A simpler method (i.e. one-point method) can also be used to estimate the slope value. Once the slope of the linear relationship is known, the unfrozen water content can be estimated with the aid of the initial (total) water content and initial freezing point.	Empirical and simple, requires less measurements. The difficulty in accurately measuring the freezing point when the soil has low initial water content may introduce errors. Not widely used in the literature.
4	Liu and Yu, 2013	The bundle of cylindrical capillary (BCC) model was present to give physical description of SFCC. Incorporated the Clapeyron equation into the van Genuchten (1980) SWCC equation, and proposed a closed-form relationship between temperature and saturation in frozen soils, which can be either saturated or unsaturated under unfrozen conditions. The parameters in the SFCC equation were determined by curve-fitting.	Soil physical property parameters are no longer needed. Wide application. Can be used when the saturation of the soil under unfrozen conditions is unknown. The fitting results will indicate whether the soil specimen is saturated before freezing occurs and indicate this water saturation. The whole range of SFCC can be reproduced by using measured data at a relatively small temperature range.

Table 2.2 Various methods used for estimating unfrozen water content (Cont'd)

No.	Author(s)	Key information	Advantages and / or limitations
5	Liu and Yu, 2014	Based on the same physical mechanisms as in Liu and Yu (2013), but instead of using the van Genuchten (1980) equation, the Fredlund and Xing (1994) SWCC equation was used to establish SFCC equation. The four parameters (a, b, c, ψ_r) in the SFCC equation were first determined from soil index properties. Then, (b, ψ_r) were fixed and (a, c) were adjusted by curve-fitting using the measured data point. (a, b, c, ψ_r are the four parameters used in Liu and Yu model)	Can accurately predict the SFCC with only one measured data point (i.e., without resorting to extensive sophisticated experiments), thus facilitate the use of SFCC in engineering practice.
6	Wang et al., 2017	Considered the total amount of unfrozen water in a soil as the sum of unfrozen water in unfrozen pores and unfrozen water in freezing pores. They determined the amount of these two types of unfrozen water based on pore size distribution of the soil and equilibrium thickness of unfrozen water film respectively, extending a theoretical framework. Specifically, the relationship between the unfrozen water content in unfrozen pores and subzero temperature was established through the Gibbs-Thomson equation and pore size distribution. With the aid of the Clapeyron equation, the pore water potential (which is a function of subzero temperature) was obtained by assuming zero pore ice potential. The unfrozen water content in freezing pores was estimated through the equilibrium thickness of unfrozen water film, which can be calculated from the pore water potential. Therefore, the total unfrozen water content in a soil can be represented by subzero temperature.	It is more convenient than the empirical formulas in numerical modeling, and it can overcome the shortcoming that the empirical formulas are not derivative at the temperatures near the freezing point. It directly expresses the relationship between residual unfrozen water content and temperature under extremely low temperature conditions.
7	Amiri et al., 2018	A stochastic-conceptual approach was employed to generate SFCC, by averaging the calculated results of water saturation and temperature of a set of heterogeneous soil columns, through 1-D modelling. The study specifically investigated the effect of local sub-grid/sub-REV (Representative Elementary Volume) heterogeneity of soil thermal conductivity and freezing temperature depression on the SFCC.	Suggests that pore water phase change can be partly attributed to soil heterogeneities besides the capillary and adsorptive forces. Different sources of heterogeneity can be incorporated.

Table 2.2 Various methods used for estimating unfrozen water content (Cont'd)

No.	Author(s)	Key information	Advantages and / or limitations
8	Bai et al., 2018	The integral form for a SFCC was derived from the perspective of soil pore structure. According to the assumption that unfrozen water content can be integrated from pore volumes, and the relationship between pore radius and freezing temperature (the Gibbs-Thomson equation), the unfrozen water content can be expressed as a function of temperature (i.e. SFCC), though the so-called distribution function (which is a function of temperature). An exponential function was employed as the distribution function, and finally, the theoretical expression of SFCC was obtained.	The parameters of the proposed SFCC equation have clear physical meanings, and the equation is continuous at the initial freezing temperature. Only one parameter (i.e. the shape factor of the distribution function) is needed to be determined by curve fitting.
9	Mu et al., 2018	The proposed void ratio-dependent SFCC model separates the freezing of capillary and adsorbed water. The Gallipoli et al. (2003) SWCC model was modified for modelling the freezing of capillary water at different void ratios; the cryogenic suction obtained through Clapeyron equation was used as an independent variable. A new exponential equation was proposed for the freezing of adsorbed water, by taking temperature as the independent variable. The proposed model has been used to predict the SFCC of silt at different initial void ratios and clay over a wide range of subzero temperatures.	This model explicitly considers both capillarity and adsorption. It incorporates the influence of void ratio on unfrozen water content. More discussions related to this model are summarized in Appendix A.

1, 2, 3: based on soil physical properties. 4: based on similarity between SFCC and SWCC, and on physical mechanisms. 5: based on similarity between SFCC and SWCC, and on physical mechanisms and soil physical indices. 6: based on pore size distribution and theoretical mechanisms. 7: based on theoretical mechanisms. 8: based on physical mechanisms. 9: partially based on similarity between SFCC and SWCC.

2.7 Effect of freeze-thaw cycles and freezing / thawing

The effects of the harsh climate found in regions such as north America, north Europe, and northeast Asia on civil engineering structures should not be neglected by designers and contractors (Bronfenbrener and Bronfenbrener, 2012). For example, in the Province of Quebec, Canada, with freezing indices ranging from 800 to over 2000 degree-days, the freezing front penetrates to depths between 1.2 and 2.0 m, and frost action mainly develops in frost-susceptible soils, leading to ice lens formation, surface heave, and eventual distress of pavement structures (Konrad, 2005). In some seasonally frozen areas in northeast China, the frost penetration ranges between 1.6 to 1.9 m (Liu et al., 2003). In much colder climate regions such as Siberia in the Russian Federation, freezing indices of 4000 to 6000 degree-days are found with frost penetration to depths greater than 2.5 m (Feldman, 1988). For construction involving newly exposed soils in cold regions, care must be taken with respect to F-T cycling. For instance, in Quebec, newly constructed highway embankments are left unpaved for a few years, which to some extent is an accommodation relating to F-T action (Eigenbrod, 1996).

The effects of continuous redistribution of water and ice, and displacement associated with freezing and thawing cause significant alterations in the microstructure of soil fabric (Hohmann-Porebska, 2002). Several investigations were undertaken to study the effect of freezing / thawing and F-T cycles on the physical and mechanical properties of soils, such as volume change (e.g., Hamilton, 1966; Dagesse, 2010; Dagesse, 2016), void ratio (e.g., Chamberlain and Gow, 1979; Viklander, 1998), hydraulic conductivity (e.g., Burt and Williams, 1976; Chamberlain and Gow, 1979; Chamberlain et al., 1990; Benson and Othman, 1993; Eigenbrod, 1996; Viklander, 1998; Viklander and Eigenbrod, 2000; Hohmann-Porebska, 2002; Ishikawa et al., 2010; Ishikawa and Tokoro, 2013), thermal conductivity (e.g., Tucker, 1985; Mizoguchi, 1990; Overduin et al., 2006), stress-strain relationship (e.g., Simonsen, et al., 2002; Ishikawa et al., 2010; Li et al., 2012; Li et al., 2015; Lu et al., 2019b), water retention characteristic (e.g., Ishikawa et al., 2010; Ishikawa and Tokoro, 2013), shear / compressive strength (e.g., Czurda and Hohmann, 1997; Qi et al., 2008; Li et al., 2012; Ghazavi and Roustaei,

2013; Xie et al., 2015; Liu et al., 2016; De Guzman et al., 2018; Xu et al., 2018; Lu et al., 2019b; Xu et al., 2019), rheological and viscous properties (e.g., Zhou et al., 2018), and modulus / stiffness (e.g., Johnson et al., 1979; Skaggs, 1992; Li et al., 2012; Ghazavi and Roustaei, 2013; Liu et al., 2016; Lin et al., 2017; Lu et al., 2019b; Tian et al., 2019). Several review papers have provided comprehensive summaries regarding the physical and mechanical properties, and constitutive models of soils in cold regions (e.g., Jessberger, 1981; Qi et al., 2006; Ma and Wang, 2012; Lai et al., 2013; Qi et al., 2016). This section is aimed to provide a critical review on the influence of freezing / thawing and F-T cycles on soil properties, especially on soil modulus.

2.7.1 Effect of freeze-thaw cycles

Fine-grained soils, when exposed to F-T cycles, will generally experience volume changes, loss in shear strength and increased compressibility (Graham and Au, 1985), and frequently alterations in their hydraulic conductivity (Eigenbrod, 1996).

For example, most studies demonstrated that F-T cycles generate micro-fissures within the soils and correspondingly change their hydraulic conductivity. Chamberlain and Gow (1979) performed unidirectional open-system freezing and thawing on four fine-grained soils. The slurry samples were prepared at a water content twice the liquid limit and were consolidated in a specially designed F-T consolidation apparatus (Chamberlain and Blouin, 1977). **Figure 2.10** illustrates the void ratio change of the slurry sample during the freezing and thawing processes. The slurry sample is fully consolidated to point ***a*** (where pore water pressure is zero) on the virgin compression curve. When the sample is frozen under one-dimensional open-system freezing, the sample undergoes a net increase in void ratio to point ***b*** in terms of total stress analysis, due to the expansion of water to ice and water migration from the external source. However, since large cryogenic suction (i.e. negative pore water pressure) forms below the freezing front during the freezing process, the effective stress at this location increases. Therefore, the clay layer just below the warmest ice lens is over-consolidated to point ***b'*** (the void ratio decreases). Upon thawing, the effective stress path within the clay layers (between two adjacent

ice lenses) is depicted along line ***b'-c*** to point ***c***, where the pore water pressures are in equilibrium with the applied load. The slurry sample has undergone a net decrease in void ratio from point ***a*** to ***c*** (Chamberlain and Blouin, 1977).

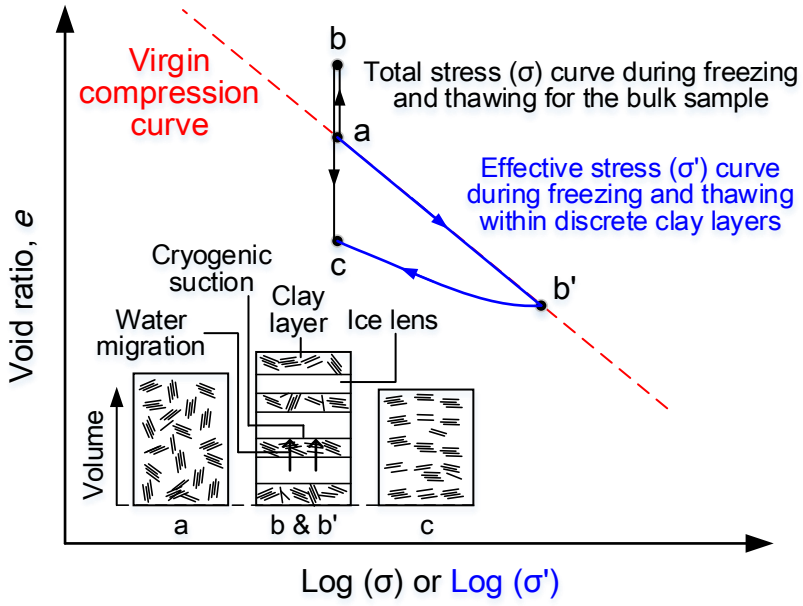

Figure 2.10 Theorized thaw consolidation process (modified after Chamberlain and Gow, 1979)

The hydraulic conductivity test indicated that there was an increase in vertical hydraulic conductivity of different types of fine-grained soils (Chamberlain and Gow, 1979). The increase in the hydraulic conductivity was attributed to the formation of polygonal shrinkage cracks and / or the reduction in the fine content in the pores of the coarse fraction, the mechanism controlling the process depending on soil type. While cracks and other structural changes may not be visible to the naked eye after thawing, they have been observed under scanning electron microscope (SEM) (Hunsicker, 1987). At low magnification, distinct cracks spaced at 0.5 mm were observed in Fort Edwards Clay specimens. However, at higher magnifications, voids as large as 0.005 mm were observed within the aggregates formed during the freezing process (Othman et al., 1994). Therefore, freezing and thawing processes cause changes in both the macro- and

micro-structures of soils.

Previous studies show that F-T has a dual influence on soil density, i.e. loose soils tend to densify and dense soils become looser after F-T cycles (Qi et al., 2008). According to this phenomenon, Viklander (1998) proposed a residual void ratio with respect to F-T cycles. This phenomenon has been confirmed by other studies (Qi and Ma, 2006; Qi et al., 2008). Viklander (1998) observed void ratio change of a fine-grained non-plastic till subjected to F-T cycles. The void ratios of different specimens show significant change after one F-T cycle, after which the change is less substantial. **Figure 2.11** is a schematic illustration of the freezing-thawing process for initially loose and dense soils. The initially loose soil experiences volume increase during freezing (due to ice-lensing) and decrease during thawing (due to consolidation of soil matrix). Therefore, the density will increase and larger soil particles will come closer. On the other hand, the void ratio of an initially dense soil might increase due to F-T, since soil particles cannot fall back to exactly the same position after thawing, resulting in a net volume increase of the soil. Therefore, the soil structure is slightly looser than prior to freezing. The void ratios of the two soils reach a residual value after a certain number of F-T cycles.

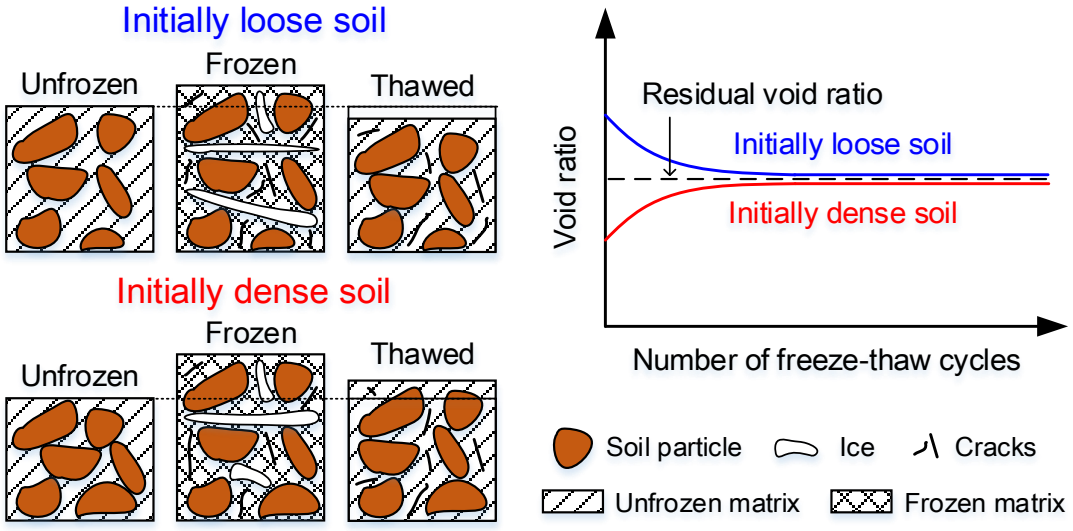

Figure 2.11 Microstructural changes of a fine-grained till due to freezing and thawing (modified after Viklander, 1998)

The resilient response of compacted soils under cyclic loading is controlled by soil fabric (or soil structure) (e.g., Lee et al., 1995; Simonsen and Isacsson, 2001). Generally, soil resilient modulus will decrease as F-T cycles weaken the soil structure. Culley (1971) investigated the resilient stains and resilient moduli of till specimens under the effect of one-dimensional closed-system F-T cycling. The specimens were compacted to various densities and water contents. At water contents lower than the optimum water content, the decrease in resilient modulus resulting from F-T cycling decreased as density increased; at water contents of optimum and higher, the detrimental F-T effect increased as density increased. The water content at which the maximum F-T effect occurred increased as density increased, ranging from 1.5% less than optimum at 93% density to 1.5% greater than optimum at 100% density. These trends followed those for resilient strain.

Weimer (1972) measured the suction of the compacted glacial till specimens after five F-T cycles. The results indicated that there was dramatic reduction in suction below the optimum water content and insignificant above the optimum water content. Fredlund et al. (1975) also found a remarkable reduction in the matric suction of soil specimens subjected to F-T cycles, which resulted in the reduction in soil resilient modulus.

Based on the resilient modulus tests performed on five cohesive soils sampled from the subgrades of in-service pavements, Lee et al. (1995) concluded that the stress at 1% strain in the unconfined compression test ($S_{u1.0\%}$) was a good indicator of the resilient modulus, and an empirical relationship between the resilient modulus and $S_{u1.0\%}$ was obtained. The proposed relationship is applicable to both as-compacted and in-service subgrade soils. There was a negligible effect of F-T on resilient modulus, when there was no ice lens formation, for soils having values of $S_{u1.0\%}$ less than 8 psi (approximately 55 kPa). The effect of F-T increased as the value of $S_{u1.0\%}$ increased. It was observed that a single cycle of F-T caused a 30% - 50% reduction in resilient modulus. The resilient moduli of various coarse- and fine-grained subgrade soils subjected to F-T cycles were presented by Simonsen et al. (2002), the results indicated that all the soils exhibited a substantial reduction in resilient modulus (approximately 20% - 60%

depending on the types of soils) after F-T cycles.

Skaggs (1992) performed resilient modulus test on four soils subjected to one-dimensional open-system F-T cycles. The four soils represent different soil types which include clayey sand (labeled as A-2-6(1) and A-6(2)), silt (labeled as A-7-6(14)), and lean clay (labeled as A-4(5)). A significant reduction in resilient modulus was observed for all the four soils with F-T cycles. The first F-T cycle reduced the resilient modulus as much as 80% for the A-6(2) soil. For the soils investigated to eight F-T cycles, little reduction in resilient modulus was observed after the fourth cycle. In addition, the influence of moisture imbibition on the specimens with no F-T cycling was investigated. The moisture imbibed specimen had low resilient modulus in comparison with specimen that was not subjected to imbibition; the trend in results was approximately similar to that of the specimens subjected to F-T cycles.

Wang et al. (2007) investigated the physical and mechanical properties of Qinghai-Tibet clay subjected to a maximum of 21 closed-system freezing and thawing cycles. The results suggest a strong relationship between the failure strength and the number of F-T cycles; however, the shape of the stress-strain behavior curves showed less variation. The authors also reported that the magnitude of the resilient modulus decreased by 18% - 27% of unfrozen soil depending on confining pressure applied during the triaxial compression tests. The greatest changes in resilient modulus in all of the four different confining pressure conditions (i.e., 200, 400, 600, and 800 kPa) were obtained after the first F-T cycle (as shown in **Figure 2.12**), suggesting that a significant disturbance took place during the first F-T cycle.

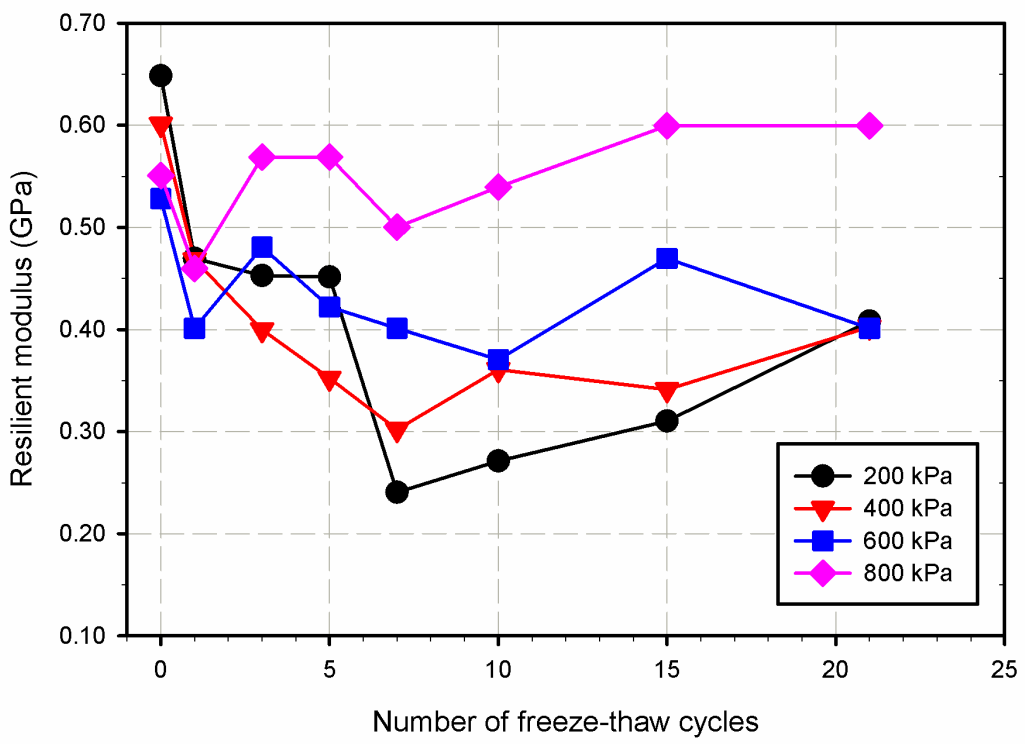

Figure 2.12 Resilient modulus of soils versus the number of F-T cycles (data from Wang et al., 2007)

In seasonally frozen regions, subgrade soils are not only subjected to environmental influences such as F-T cycles, but also to large number of repeated cyclic loading at a stress level lower than their shear strength. This makes the long-term resilient behavior of subgrade soils as important as those of the short-term determined by standard test procedures (Lin et al., 2017). Lin et al. (2017) investigated the evolution of the resilient modulus of thawed saturated silty clay during the long-term repeated cyclic loading, considering the effects of F-T cycles, stress amplitude (both deviator and confining stresses) and loading frequency. The results suggested that the resilient modulus typically decreases with an increase in the number of F-T cycles and in the deviator stress, and increases with the increase in the confining stress and loading frequency. A long-term resilient modulus model was also proposed, which considers the above influencing factors together with the number of loading cycles.

Lu et al. (2019c) considered the case of shallow groundwater level in seasonally frozen

regions. Because water will migrate to upper soil layers such as subgrade soils, the water content of the soils will increase due to freezing and thawing. They conducted one-dimensional open-system F-T cycles on a clay with low liquid limit. The effects of the number of F-T cycles, initial water content, initial dry density, freezing temperature, and confining stress on the failure strength and elastic (Young's) modulus (E, defined below) of the compacted soil specimens were studied. The results indicated that the failure strength and elastic modulus decreased dramatically (the reduction rates of both the two indices were more than 60%) after just one F-T cycle, and stabilized after three F-T cycles. It is also interesting to note that the failure strength and elastic modulus increased with an increase in the initial water content of the specimens, which were with an initial dry density of 1.57 g/cm^3 and subjected to three F-T cycles. The authors concluded that when the initial water content of the specimen was high, the frost heave was low due to larger heat capacity of the specimen and limited frost penetration. Therefore, fewer parts of the specimens were involved in F-T cycles. The mechanical properties were enhanced to a certain extent.

The elastic modulus (E) is conventionally calculated from the straight portion of the stress-strain curve; however, in most cases, the stress-strain curves of many soils are not straight for any appreciable distance (Kumar and Singh, 2008; Li et al., 2015). Therefore, it is calculated as the ratio of the increment of deviator stress to the increment of axial strain when the axial strain reaches 1.0% (Li et al., 2015; Lu et al., 2019c). The equation is shown below,

$$E = \frac{\Delta\sigma}{\Delta\varepsilon} = \frac{\sigma_{1.0\%} - \sigma_0}{\varepsilon_{1.0\%} - \varepsilon_0} \tag{2.9}$$

where $\Delta\sigma$ and $\Delta\varepsilon$ are the increments of deviator stress and axial strain respectively, $\sigma_{1.0\%}$ is the corresponding deviator stress at the axial strain of 1.0% (i.e. $\varepsilon_{1.0\%}$), and σ_0 and ε_0 are the initial stress and strain, respectively.

Frost heave unusually occurs in seasonally frozen region soils. Several studies suggest that silty soils are much more susceptible to frost heave than sands and clays. The susceptibility of soils to ice lens formation and frost heave is related to the amount of water that the soil is able to

supply from below (e.g., Chamberlain, 1981). Sands have a limited capillary zone and the water in the unsaturated zone will quickly drain from the pores under small negative pressures (i.e. relatively low suction values). Although clays can sustain high negative pore pressures (i.e. high suction values), they cannot supply water to the ice lenses quickly enough due to their low hydraulic conductivity. However, silty soils have relatively large permeability and can sustain high negative pore pressures to induce water migration to ice lenses. Therefore, for subgrade soils with relatively high silt content, water in the lower portion of the subgrade or foundation soils can gradually migrate to the upper portion of the subgrade to facilitate the formation of ice lenses. During the freezing process, different freezing temperatures can provide different freezing rates, which cause different frost heaves of subgrade soils, and then thawing settlement occurs because of the melt of pore ice and ice lenses. The void ratio changes and connections between soil particles experience breaking and rebuilding during the freezing and thawing processes. Compared to frozen-thawed soil, the unfrozen soil has a more stable structure to resist the applied cyclic loading. The freezing-thawing processes weaken the original soil stability (Li et al., 2015). Destruction of soil structure invariably occurs in the form of larger pores created by the wedging and splitting action at the specific location of the growing crystals. Therefore, the effects of freezing on a larger scale are destructive for the subgrade soils (Dagesse, 2006).

2.7.2 Effect of freezing / thawing

As summarized in earlier sections, soil structure is generally weakened after F-T cycles. However, the variation in soil stiffness (or modulus) during the freezing and thawing processes can be significantly different due to the phase change of pore water. For example, a pavement structure located in seasonally frozen region (as shown in **Figure 2.13**) will be subjected to at least one cycle of F-T annually. As stated in Section 1.1, the freezing front (0 °C isotherm) progresses into the pavement structure as a function of the imbalance of the heat supplied to the heat removed, and pore water in pavement materials and foundation soils freeze. During the thawing period, the 0 °C isotherm (i.e. thawing front) will go up from inside foundation soils and

penetrate downward from pavement surface. Therefore, pore ice and ice lenses absorb large amount of heat and melts, especially when the surface layer is asphalt mixture, which has high solar absorptivity.

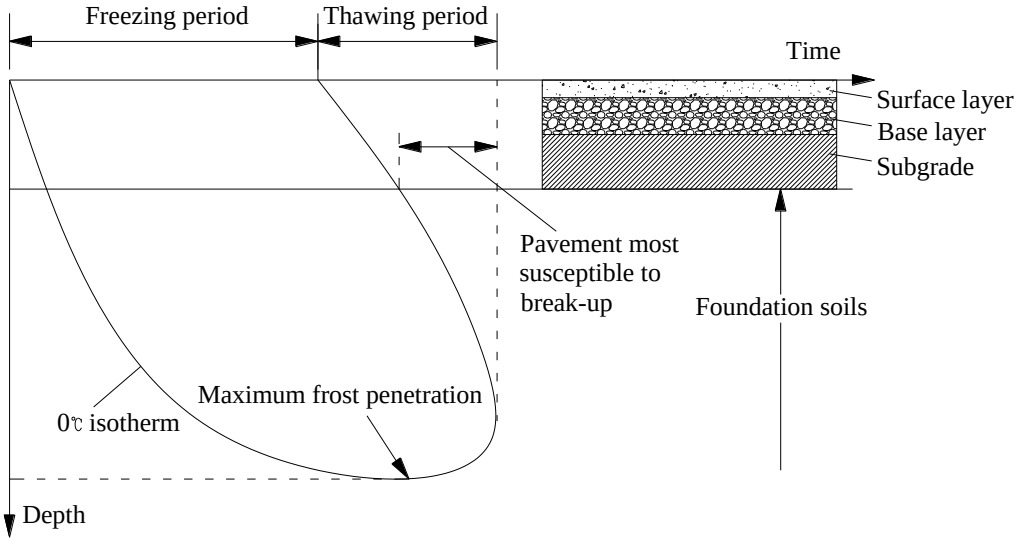

Figure 2.13 Seasonal ground freezing and thawing beneath a pavement structure (modified after Andersland and Ladanyi, 1994)

The phase change of pore water has significant impact on the resilient moduli of base, subbase, subgrade and foundation soils. When pore water freezes, ice bonds adjacent soil particles together (Andersland and Ladanyi, 2004), which causes a dramatic increase in the resilient modulus (Jong et al., 1998). For example, Bigl and Berg (1996a) show that the resilient modulus of subbase and subgrade soils can increase two orders of magnitude when the soil freezes. Bosscher and Nelson (1987) report a 20-fold increase in modulus of Ottawa sand after frozen. Similar increases in moduli for frozen granular base soils were observed by Cole et al. (1987). Therefore, freezing has been used temporarily to stabilize soils during the construction of retaining walls, foundations, tunnels, and other projects where weak soils are encountered (Chamberlain and Gow, 1979; Aukenthaler, 2016).

On the other hand, when the pore water freezes it generates cryogenic suction in the frozen

soils, which contributes to water migration from the lower portion of subgrade or foundation soils to upper frozen subgrade soils, causing desiccation and cracks. Thawing of pavement is accompanied by the loss of inter-particle ice bonds and increase in water content as ice melts in subgrade soils during warm period. Thawing contributes to a significant decrease in soil suction; in some scenarios, pore water pressures may even become positive. As a result, the subgrade has a low resilient modulus and therefore is susceptible to deformation under cyclic traffic loading during this period. For example, Bigl and Berg (1996a) show that the post-thawing resilient modulus can be 10 times lower than the resilient modulus of the same soil that was never frozen. Mahoney et al. (1985) found that the average modulus of the base and subgrade decreased by 52% and 23%, during thawing period. However, after the thawing process, the resilient modulus will gradually recover to its pre-freezing value with the gradual dissipation of excess pore water pressure and the consolidation of soil mass (Cole et al., 1986; Berg et al., 1996).

Figure 2.14 shows the typical variation in the stiffness of pavement structure subjected to freezing and thawing during one-year period. During the freezing process and at the frozen state, the pavement structure has a relatively high stiffness and bearing capacity; due to this reason, it is typically capable to carry higher loads than its design value. Overloading of the pavement structure is allowable with little or no damage to it. On the contrary, during the thaw-weakening period, the stiffness and bearing capacity of the pavement structure reduces significantly in comparison with its pre-freezing value. Therefore, to minimize the damage to the pavement structure during spring thaw, many highway agencies impose load restrictions on their pavements (e.g., Janoo and Cortez, 2002; Baïz, 2007; Asefzadeh et al., 2016).

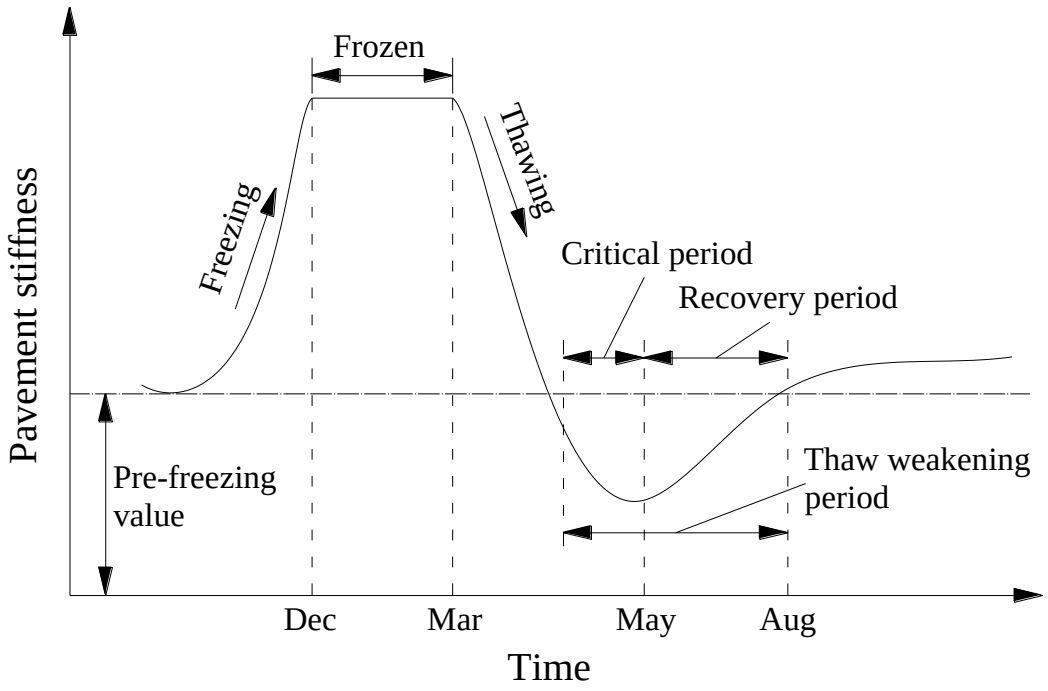

Figure 2.14 Variation in pavement stiffness under freezing and thawing conditions (modified after Janoo and Cortez, 2002)

2.8 References

Agergaard, F., Ingeman-Nielsen, T., 2012. Development of bearing capacity of fine grained permafrost deposits in western Greenland urban areas subject to soil temperature changes. Cold Reg. Eng. 82–92.

Akagawa, S. and Nishisato, K. 2009. Tensile strength of frozen soil in the temperature range of the frozen fringe. Cold regions science and technology, 57(1): 13-22.

Amiri, E.A., Craig, J.R. and Kurylyk, B.L., 2018. A theoretical extension of the soil freezing curve paradigm. Advances in Water Resources, 111: 319-328.

Andersland, O.B. and Ladanyi, B. 1994. An introduction to frozen ground engineering, New York: ASCE & John Wiley & Sons.

Andersland, O.B. and Ladanyi, B. 2004. Frozen ground engineering (Second Edition), New York: ASCE & John Wiley & Sons.

Anderson, D.M. and Morgenstern, N.R., 1973. Physics, chemistry and mechanics of frozen ground: A review. In Permafrost: The North American Contribution to the Second International Conference, National Academy of Sciences, Washington, DC (pp. 257-288).

Anderson, D.M. and Tice, A.R., 1972. Predicting unfrozen water contents in frozen soils from surface area measurements. Highway research record, 393: 12-18.

Anderson, D.M. and Tice, A.R. 1973. The unfrozen interfacial phase in frozen soil water systems. Springer Berlin Heidelberg, 107-124.s.

Anderson, D.M., Tice, A.R. and McKim, H.L. 1973. The unfrozen water and the apparent specific heat capacity of frozen soils. In Proceedings of the Second International Conference on Permafrost, 289-295.

Anderson, R., Tohidi, B. and Webber, J.B.W., 2009. Gas hydrate growth and dissociation in narrow pore networks: capillary inhibition and hysteresis phenomena. Geological Society, London, Special Publications, 319(1): 145-159.

Asefzadeh, A., Hashemian, L., Haghi, N.T. and Bayat, A., 2016. Evaluation of spring load restrictions and winter weight premium duration prediction methods in cold regions according to field data. Canadian Journal of Civil Engineering, 43(7), pp.667-674.

Aukenthaler, M., 2016. The frozen & unfrozen Barcelona Basic Model: A verification and validation of a new constitutive model. MSc. thesis, Delft University of Technology.

Azmatch, T.F., 2013. Frost heave: new ice lens initiation condition and hydraulic conductivity prediction. Doctoral thesis, University of Alberta, Edmonton, Canada.

Azmatch, T.F., Sego, D.C., Arenson, L.U. and Biggar, K.W., 2012a. Using soil freezing characteristic curve to estimate the hydraulic conductivity function of partially frozen soils. Cold Regions Science and Technology, 83, pp.103-109.

Azmatch, T.F., Sego, D.C., Arenson, L.U. and Biggar, K.W., 2012b. New ice lens initiation condition for frost heave in fine-grained soils. Cold Regions Science and Technology, 82, pp.8-13.

Bai, R., Lai, Y., Zhang, M. and Yu, F., 2018. Theory and application of a novel soil freezing characteristic curve. Applied Thermal Engineering, 129: 1106-1114.

Baïz, S., 2007. Using Road Weather Information Systems (RWIS) to Optimize the Scheduling of Load Restrictions on Northern Ontario's Low-volume Highways. Master's thesis, University of Waterloo, Ontario, Canada.

Barbour, S.L., 1998. Nineteenth Canadian Geotechnical Colloquium: The soil-water characteristic curve: a historical perspective. Canadian Geotechnical Journal, 35(5), pp.873-894.

Benson, C.H. and Othman, M.A. 1993. Hydraulic conductivity of compacted clay frozen and thawed in situ. Journal of Geotechnical Engineering, 119(2): 276-294.

Berg, R.L., S.R. Bigl, J. Stark and G. Durrell. 1996. Resilient modulus testing of materials from Mn/ROAD, Phase 1. USA Cold Regions Research and Engineering Laboratory, Special Report 96- 19, Mn/DOT Report 96-21.

Beskow G., 1935. Soil freezing and frost heaving with special applications to roads and railroads: with special supplement for the English translation of progress from 1935 to 1946. Swed Geol Soc; 26:145.

Bigl, S.R., and Berg. R.L. 1996a. Material Testing and Initial Pavement Design Modeling: Minnesota Road Research Project. CRREL Report 96-14, USACE Cold Regions Research and Engineering Laboratory, Hanover, N.H.

Bigl, S.R. and Berg, R.L. 1996b. Modeling of Mn/ROAD Test Sections with the CRREL Mechanistic Pavement Design Procedure (No. CRREL-SR-96-21). Cold Regions Research and Engineering Laboratory, Hanover, N.H.

Bittelli, M., Flury, M. and Campbell, G.S., 2003. A thermodielectric analyzer to measure the freezing and moisture characteristic of porous media. Water Resources Research, 39(2): 1-10.

Black, P.B., 1995. Applications of the Clapeyron equation to water and ice in porous media (No. CRREL-95-6). Cold Regions Research and Engineering Laboratory, Hanover, N.H.

Black, P.B. and R.D. Miller (1985) A continuum approach to modeling of frost heaving. In Freezing and Thawing of Soil-Water Systems (D.M. Anderson and P.J. Williams, Ed.). Technical Council on Cold Regions Engineering Monograph. ASCE, p. 36-45.

Bosscher, P. J., and D. L. Nelson. 1987. Resonant Column Testing of Frozen Ottawa Sand. Geotechnical Testing Journal, 10(3), 123–134.

Bouyoucos, G.J., 1917. Measurement of the inactive or unfree moisture in the soil by means of the dilatometer method. Jour. Agr. Res, 8(6), pp.195-217.

Bronfenbrener, L. and Bronfenbrener, R., 2012. A temperature behavior of frozen soils: Field experiments and numerical solution. Cold Regions Science and Technology, 79: 84-91.

Buckingham, E., 1907, Studies of the Movement of Soil Moisture, U.S. Depart. of Agriculture, Bureau of Soils Bulletin, Washington, D.C., Vol. 38.

Burt, T.P. and Williams, P.J., 1976. Hydraulic conductivity in frozen soils. Earth Surface Processes, 1(4), pp.349-360.

Caicedo, B., 2017. Physical modelling of freezing and thawing of unsaturated soils. Géotechnique, 67(2), pp.106-126.

Caicedo, B., 2018. Geotechnics of Roads: Fundamentals. CRC Press, Boca Raton, Florida, USA.

Carnero-Guzman, G.G., Bouazza, A., Gates, W.P. and Rowe, R.K., 2018, October. A Review of Experimental and Prediction Methods for Assessing the Freezing Characteristic Curve of GCLs. In the International Congress on Environmental Geotechnics (pp. 616-623). Springer, Singapore.

Chai, M., Zhang, J., Zhang, H., Mu, Y., Sun, G. and Yin, Z., 2018. A method for calculating unfrozen water content of silty clay with consideration of freezing point. Applied Clay Science, 161, pp.474-481.

Chamberlain, E.J., 1981. Frost susceptibility of soil, review of index tests (No. CRREL-81-2). Cold Regions Research and Engineering Laboratory, Hanover, N.H.

Chamberlain, E.J. and Blouin, S.E., 1977. Freeze-thaw enhancement of the drainage and consolidation of fine-grained dredged material in confined disposal areas. Department of Defense, Department of the Army, Corps of Engineers, Waterways Experiment Station, Environmental Effects Laboratory.

Chamberlain, E.J. and Gow, A.J. 1979. Effect of freezing and thawing on the permeability and structure of soils. Engineering Geology, 13(1): 73-92.

Chamberlain, E.J., Iskander, I., and Hunsiker, S. 1990. Effect of freeze–thaw on the permeability and macrostructure of soils. In Proceedings, International Symposium on Frozen Soil Impacts on Agriculture, Range and Forest Lands, Spokane, Wash., 145–155.

Cole, D.M., Bentley, D.L., Durell, G.D. and Johnson, T.C., 1986. Resilient Modulus of Freeze-Thaw Affected Granular Soils for Pavement Design and Evaluation. Part 1.

Laboratory Tests on Soils from Winchendon, Massachusetts, Test Sections (No. CRREL-86-4). Cold Regions Research and Engineering Laboratory, Hanover, N.H.

Cole, D.M., Bentley, D.L., Durell, G.D. and Johnson, T.C., 1987. Resilient Modulus of Freeze-Thaw Affected Granular Soils for Pavement Design and Evaluation. Part 3. Laboratory Tests on Soils from Albany County Airport (No. CRREL-87-2). Cold Regions Research and Engineering Laboratory, Hanover, N.H.

Culley, R.W., 1971. Effect of freeze–thaw cycling on stress–strain characteristics and volume change of a till subjected to repetitive loading. Canadian Geotechnical Journal, 8(3), pp.359-371.

Czurda, K.A. and Hohmann, M., 1997. Freezing effect on shear strength of clayey soils. Applied clay science, 12(1-2), pp.165-187.

Dagesse, D.F., 2006. Effect of the Freeze/thaw Process on the Structural Stability of Soil Aggregates. Doctoral thesis, University of Guelph, Guelph, Canada.

Dagesse, D.F., 2010. Freezing-induced bulk soil volume changes. Canadian journal of soil science, 90(3), pp.389-401.

Dagesse, D.F., 2016. Analysis of freezing induced soil shrinkage with implications regarding structural change. In Proceedings of the 69th Canadian Geotechnical Conference, Vancouver, Canada.

Dall'Amico, M., 2010. Coupled water and heat transfer in permafrost modeling (Doctoral dissertation, University of Trento).

Dash, J.G., Fu, H. and Wettlaufer, J.S., 1995. The premelting of ice and its environmental consequences. Reports on Progress in Physics, 58(1), p.115.

De Guzman, E.M.B., Stafford, D., Alfaro, M.C., Doré, G. and Arenson, L.U., 2018. Large-scale direct shear testing of compacted frozen soil under freezing and thawing conditions. Cold Regions Science and Technology, 151, pp.138-147.

Dillon, H.B. and Andersland, O.B., 1966. Predicting unfrozen water contents in frozen soils. Canadian geotechnical journal, 3(2): 53-60.

Edwards, A.C. and Cresser, M.S., 1992. Freezing and its effect on chemical and biological properties of soil. In Advances in soil science (pp. 59-79). Springer, New York, NY.

Eigenbrod, K.D., 1996. Effects of cyclic freezing and thawing on volume changes and permeabilities of soft fine-gained soils. Canadian Geotechnical Journal, 33(4), pp.529-537.

Feldman, G.M. 1988. Reference book for the forecast of the soils temperature behaviour. Ac. Sci.

Flerchinger, G.N., Seyfried, M.S. and Hardegree, S.P. 2006. Using soil freezing characteristics to model multi-season soil water dynamics. Vadose Zone Journal, 5(4): 1143-1153.

Fredlund, D.G. 1996. The scope of unsaturated soil mechanics: An overview. In Proceedings of the first international conference on unsaturated soils. Unsat'95, Paris, France, 3: 1155-1177.

Fredlund, D.G., Bergan, A.T. and Sauer, E.K. 1975. Deformation characterization of subgrade soils for highways and runways in northern environments. Canadian Geotechnical Journal, 12(2): 213-223.

Fredlund, D.G. and Rahardjo, H. 1993. Soil mechanics for unsaturated soils. John Wiley & Sons, Inc., Hoboken, New Jersey, USA.

Fredlund, D.G., Rahardjo, H., and Fredlund, M.D. 2012. Unsaturated Soil Mechanics in Engineering Practice. John Wiley & Sons, Inc., Hoboken, New Jersey, USA.

Gallipoli, D., Wheeler, S.J. and Karstunen, M., 2003. Modelling the variation of degree of saturation in a deformable unsaturated soil. Géotechnique, 53(1), pp.105-112.

Gens, A., 2010. Soil-environment interactions in geotechnical engineering. Géotechnique, 60(1), p.3.

Ghazavi, M. and Roustaei, M., 2013. Freeze–thaw performance of clayey soil reinforced with geotextile layer. Cold Regions Science and Technology, 89, pp.22-29.

Graham, J. and Au, V.C.S., 1985. Effects of freeze–thaw and softening on a natural clay at low stresses. Canadian Geotechnical Journal, 22(1), pp.69-78.

Grant, S.A. 1994. Some physical factors affecting contaminant hydrology in cold environments. Transportation Research Record: Journal of the Transportation Research Board, 1434: 61-69.

Grant, S.A. and Sletten, R.S., 2002. Calculating capillary pressures in frozen and ice-free soils below the melting temperature. Environmental geology, 42(2-3), pp.130-136.

Grant, S.A., Boltnott, G.E. and Tice, A.R., 1999. Effect of Dissolved NaC1 on Freezing Curves of Kaolinite, Montmorillonite, and Sand Pastes (No. CRREL-SR-99-2). Cold Regions Research and Engineering Laboratory, Hanover, N.H.

Hamilton, A.B., 1966. Freezing shrinkage in compacted clays. Canadian Geotechnical Journal, 3(1), pp.1-17.

Hansson, K., Šimůnek, J., Mizoguchi, M., Lundin, L.C. and Van Genuchten, M.T., 2004. Water flow and heat transport in frozen soil. Vadose Zone Journal, 3(2), pp.693-704.

He, H. and Dyck, M., 2013. Application of multiphase dielectric mixing models for understanding the effective dielectric permittivity of frozen soils. Vadose Zone Journal, 12(1): 1-22.

He, H., Dyck, M.F., Si, B.C., Zhang, T., Lv, J. and Wang, J., 2015. Soil freezing–thawing characteristics and snowmelt infiltration in Cryalfs of Alberta, Canada. Geoderma Regional, 5: 198-208.

Hohmann-Porebska, M., 2002. Microfabric effects in frozen clays in relation to geotechnical parameters. Applied clay science, 21(1-2), pp.77-87.

Homshaw, L.G., 1980. Freezing and melting temperature hysteresis of water in porous materials: Application to the study of pore form. Journal of Soil Science, 31(3), pp.399-414.

Hunsicker, S.E. 1987. The Effect of Freeze-Thaw Cycles on the Permeability and Macro Structure of Fort Edwards Clay. Master of Engineering Thesis, Thayer School of Engineering, Dartmouth College, Hanover, NH.

Ishikawa, T. and Tokoro, T., 2013. Influence of freeze-thaw action on hydro-mechanical behavior of unsaturated crushable volcanic soils. In Multiphysical Testing of Soils and Shales (pp. 143-148). Springer, Berlin, Heidelberg.

Ishikawa, T., Tokoro, T., Ito, K. and Miura, S., 2010. Testing methods for hydro-mechanical characteristics of unsaturated soils subjected to one-dimensional freeze-thaw action. Soils and Foundations, 50(3), pp.431-440.

Ishizaki, T., Fukuda, M., Xu, X.Z., and Chuvilin, E.M., 1994. Temperature dependence of unfrozen water film thickness in frozen soils. In Ground Freezing 94, Fremond (ed.), Balkema, Rotterdam.

Janoo, V. and Cortez, E., 2002. Pavement Evaluation in Cold Regions. Cold Regions Engineering, 360-371.

Jessberger, H.L., 1981. A state-of-the-art report. Ground freezing: Mechanical properties, processes and design. Engineering Geology, 18, 5-30.

Johnson, T.C., Cole, D.M. and Chamberlain, E.J., 1979. Effect of freeze—thaw cycles on resilient properties of fine-grained soils. Engineering Geology, 13(1-4), pp.247-276.

Jong, D.T., Bosscher, P. and Benson, C. 1998. Field assessment of changes in pavement moduli caused by freezing and thawing. Transportation Research Record: Journal of the Transportation Research Board, (1615), 41-48.

Konrad, J.M., 1989. Physical processes during freeze-thaw cycles in clayey silts. Cold Regions Science and Technology, 16(3), pp.291-303.

Konrad, J.M. 1994. Sixteenth Canadian Geotechnical Colloquium: Frost heave in soils: concepts and engineering. Canadian Geotechnical Journal, 31(2): 223-245.

Konrad, J.M. 2001. Cold region engineering. In: Rowe, R.K. (Ed.), Geotechnical and Geoenvironmental Engineering Handbook. Kluwer Academic Publishers, Boston, Mass, 591–613.

Konrad, J.M. and Lemieux, N., 2005. Influence of fines on frost heave characteristics of a well-graded base-course material. Canadian geotechnical journal, 42(2), pp.515-527.

Koopmans, R.W.R. and Miller, R.D. 1966. Soil freezing and soil water characteristic curves. Soil Science Society of America Journal, 30(6), 680-685.

Kozlowski, T., 2003. A comprehensive method of determining the soil unfrozen water curves: 1. Application of the term of convolution. Cold Regions Science and Technology, 36(1): 71-79.

Kozlowski, T., 2016. A simple method of obtaining the soil freezing point depression, the unfrozen water content and the pore size distribution curves from the DSC peak maximum temperature. Cold Regions Science and Technology, 122, pp.18-25.

Kumar, P. and Singh, S.P., 2008. Fiber-reinforced fly ash subbases in rural roads. Journal of transportation engineering, 134(4), pp.171-180.

Kurylyk, B.L. and Watanabe, K. 2013. The mathematical representation of freezing and thawing processes in variably-saturated, non-deformable soils. Advances in Water Resources, 60: 160-177.

Lai, Y., Xu, X., Dong, Y. and Li, S., 2013. Present situation and prospect of mechanical research on frozen soils in China. Cold Regions Science and Technology, 87, pp.6-18.

Lebeau, M. and Konrad, J.M., 2012. An extension of the capillary and thin film flow model for predicting the hydraulic conductivity of air‐free frozen porous media. Water Resources Research, 48(7).

Lee, W., Bohra, N.C., Altschaeffl, A.G. and White, T.D., 1995. Resilient modulus of cohesive soils and the effect of freeze–thaw. Canadian Geotechnical Journal, 32(4), pp.559-568.

Leong, E.C. and Rahardjo, H., 1997. Review of soil-water characteristic curve equations. Journal

of Geotechnical and Geoenvironmental Engineering, 123(12), pp.1106-1117.
Li, G., Ma, W., Zhao, S., Mao, Y. and Mu, Y., 2012. Effect of freeze-thaw cycles on mechanical behavior of compacted fine-grained soil. In Cold Regions Engineering 2012: Sustainable Infrastructure Development in a Changing Cold Environment (pp. 72-81).
Li, H., Yang, Z.J. and Wang, J., 2018. Unfrozen water content of permafrost during thawing by the capacitance technique. Cold Regions Science and Technology, 152: 15-22.
Li, L., Shao, W., Li, Y. and Cetin, B., 2015. Effects of climatic factors on mechanical properties of cement and fiber reinforced clays. Geotechnical and Geological Engineering, 33(3), pp.537-548.
Lin, B., Zhang, F. and Feng, D., 2017. Long-term resilient behaviour of thawed saturated silty clay under repeated cyclic loading: experimental evidence and evolution model. Road Materials and Pavement Design, pp.1-15.
Liu, J., Chang, D. and Yu, Q., 2016. Influence of freeze-thaw cycles on mechanical properties of a silty sand. Engineering geology, 210, pp.23-32.
Liu, J., Hayakawa, N., Lu, M., Dong, S. and Yuan, J., 2003. Winter streamflow, ground temperature and active‐layer thickness in northeast China. Permafrost and Periglacial Processes, 14(1), pp.11-18.
Liu, Z. and Yu, X., 2013. Physically based equation for phase composition curve of frozen soils. Transportation Research Record: Journal of the Transportation Research Board, (2349): 93-99.
Liu, Z. and Yu, X. 2014. Predicting the phase composition curve in frozen soils using index properties: A physico-empirical approach. Cold Regions Science and Technology, 108: 10-17.
Liu, Z., Yu, X.B., Yu, X. and Gonzalez, J., 2012b. Time domain reflectometry sensor-assisted freeze/thaw analysis in geomaterials. Cold Regions Science and Technology, 71, pp.84-89.
Liu, Z., Zhang, B., Yu, X.B. and Tao, J., 2012a. A new method for soil water characteristic curve measurement based on similarities between soil freezing and drying. Geotechnical Testing Journal, 35(1), pp.2-10.
Lu, N. and Khorshidi, M., 2015. Mechanisms for soil-water retention and hysteresis at high suction range. Journal of Geotechnical and Geoenvironmental Engineering, 141(8), p.04015032.
Lu, N. and Likos, W.J., 2004. Unsaturated soil mechanics. John Wiley & Sons, Inc., Hoboken, USA.
Lu, J., Pei, W., Zhang, X., Bi, J. and Zhao, T., 2019a. Evaluating of calculation models for the unfrozen water content of freezing soils. Journal of Hydrology. (in press)
Lu, Y., Liu, S., Alonso, E., Wang, L., Xu, L. and Li, Z., 2019b. Volume changes and mechanical degradation of a compacted expansive soil under freeze-thaw cycles. Cold Regions Science and Technology, 157, pp.206-214.
Lu, Z., Xian, S., Yao, H., Fang, R. and She, J., 2019c. Influence of freeze-thaw cycles in the presence of a supplementary water supply on mechanical properties of compacted soil. Cold Regions Science and Technology, 157, pp.42-52.

Ma, T.T., Wei, C.F., Zhou, J.Z., and Tian, H.H., 2015. Freezing characteristic curves and water retention characteristics of soils. Chinese Journal of Geotechnical Engineering, 37(1), pp.172-177. (in Chinese)

Ma, W. and Wang, D.Y., 2012. Studies on frozen soil mechanics in China in past 50 years and their prospect. Chinese Journal of Geotechnical Engineering, 34(4), pp.625-640. (in Chinese)

Mahoney, J.P., J.A. Lary, J. Sharma, and N. Jackson. 1985. Investigation of Seasonal Load Restrictions in Washington State. In Transportation Research Record 1043. TRB, National Research Council, Washington, D.C., 58–67.

Mao, Y., Romero Morales, E.E. and Gens Solé, A., 2018. Ice formation in unsaturated frozen soils. In Unsaturated Soils: UNSAT 2018: The 7th International Conference on Unsaturated Soils (pp. 597-602). The Hong Kong University of Science and Technology (HKUST).

Miller, R.D., 1973. Soil freezing in relation to pore water pressure and temperature. In 2nd International Conference on Permafrost. National Acad. Sci. Washington, D.C., 344-352.

Miller, R.D., 1980. Freezing phenomena in soils. Applications of soil physics, Academic Press, Inc., New York, USA, pp. 254-299.

Mizoguchi, M. 1990. Water, heat and salt transport in freezing soil. Doctoral thesis, University of Tokyo, Tokyo, Japan. (in Japanese)

Mu, Q.Y., Ng, C.W.W., Zhou, C., Zhou, G.G.D. and Liao, H.J., 2018. A new model for capturing void ratio-dependent unfrozen water characteristics curves. Computers and Geotechnics, 101, pp.95-99.

Na, S., 2018. Multiscale thermo-hydro-mechanical-chemical coupling effects for fluid-infiltrating crystalline solids and geomaterials: theory, implementation, and validation. Doctoral dissertation, Columbia University, USA.

Nersesova, Z.A. and Tsytovich, N.A. 1963. Unfrozen water in frozen soils. In Permafrost: Proceedings of 1st International Conference, 11-15.

Othman, M.A., Benson, C.H., Chamberlain, E.J. and Zimmie, T.F., 1994. Laboratory testing to evaluate changes in hydraulic conductivity of compacted clays caused by freeze-thaw: state-of-the-art. In Hydraulic conductivity and waste contaminant transport in soil. ASTM International, 227-254.

Overduin, P.P., Kane, D.L. and van Loon, W.K., 2006. Measuring thermal conductivity in freezing and thawing soil using the soil temperature response to heating. Cold Regions Science and Technology, 45(1), pp.8-22.

Parkin, G., von Bertoldi, A.P. and McCoy, A.J., 2013. Effect of tillage on soil water content and temperature under freeze–thaw conditions. Vadose Zone Journal, 12(1): 1-9.

Patterson, D.E. and Smith, M.W., 1980. The use of time domain reflectometry for the measurement of unfrozen water content in frozen soils. Cold Regions Science and Technology, 3(2-3): 205-210.

Patterson, D.E. and Smith, M.W., 1981. The measurement of unfrozen water content by time domain reflectometry: Results from laboratory tests. Canadian Geotechnical Journal, 18(1), pp.131-144.

Patterson, D.E. and Smith, M.W., 1985. Unfrozen water content in saline soils: results using time-domain reflectometry. Canadian Geotechnical Journal, 22(1), pp.95-101.

Pham, H.Q., Fredlund, D.G., and Barbour, S.L. 2005. A study of hysteresis models for soil-water characteristic curves. Canadian Geotechnical Journal, 42(6): 1548-1568.

Qi, J., and Ma, W., 2006. Influence of freezing-thawing on strength of overconsolidated soils. Chinese Journal of Geotechnical Engineering, 28(12), pp.2082-2086. (in Chinese)

Qi, J., Ma, W. and Song, C. 2008. Influence of freeze–thaw on engineering properties of a silty soil. Cold regions science and technology, 53(3): 397-404.

Qi, J., Vermeer, P.A. and Cheng, G., 2006. A review of the influence of freeze‐thaw cycles on soil geotechnical properties. Permafrost and periglacial processes, 17(3), pp.245-252.

Qi, J.L., Xu, G. and Wu, W., 2016, April. State of the art of study on strength of frozen soils. In EGU General Assembly Conference Abstracts (Vol. 18).

Schafer, H., 2018. Freezing Characteristics of Mine Waste Tailings and their Relation to Unsaturated Soil Properties. Master thesis, University of Alberta, Edmonton, Canada.

Schofield, R.K., 1935. The pF of the water in soil. p. 37–48. Trans. Int. Congr. Soil Sci., 3rd, Oxford, UK. July–Aug. 1935. Vol. 2. The pF of the water in soil. p. 37–48.

Shastri, A., and Sanchez, M. 2012. Mechanical modeling of frozen soils incorporating the effect of cryogenic suction and temperature. In Unsaturated Soils: Research and Applications, Springer Berlin Heidelberg., 159-164.

Simonsen, E. and Isacsson, U., 2001. Soil behavior during freezing and thawing using variable and constant confining pressure triaxial tests. Canadian Geotechnical Journal, 38(4), pp.863-875.

Simonsen, E., Janoo, V.C. and Isacsson, U., 2002. Resilient properties of unbound road materials during seasonal frost conditions. Journal of Cold Regions Engineering, 16(1), pp.28-50.

Skaggs, R.B., 1992. Effects of freeze-thaw and overload conditions on the resilient modulus of frost-susceptible soils. Master thesis, University of Wyoming, Wyoming, USA.

Smith, M.W. and Tice, A.R., 1988. Measurement of the unfrozen water content of soils. Comparison of NMR (nuclear magnetic resonance) and TDR (time domain reflectometry) methods (No. CRREL-88-18). Cold Regions Research and Engineering Lab, Hanover, NH.

Spaans, E.J., 1994. The soil freezing characteristic: Its measurement and similarity to the soil moisture characteristic. Phd thesis, University of Minnesota, Minneapolis, Minnesota, USA.

Spaans, E.J. and Baker, J.M. 1996. The soil freezing characteristic: its measurement and similarity to the soil moisture characteristic. Soil Science Society of America Journal, 60: 13–19.

SU, S.L., Singh, D.N. and Baghini, M.S., 2014. A critical review of soil moisture measurement. Measurement, 54: 92-105.

Tan, L., Wei, C., Tian, H., Zhou, J., and Wei, H., 2015. Experimental study of unfrozen water content of frozen soils by low-field nuclear magnetic resonance. Rock and soil mechanics, 36(6): 1566-1572. (in Chinese)

Tian, H., Wei, C., Wei, H. and Zhou, J., 2014. Freezing and thawing characteristics of frozen soils: Bound water content and hysteresis phenomenon. Cold Regions Science and

Technology, 103: 74-81.
Tian, S., Tang, L., Ling, X., Li, S., Kong, X. and Zhou, G., 2019. Experimental and analytical investigation of the dynamic behavior of granular base course materials used for China's high-speed railways subjected to freeze-thaw cycles. Cold Regions Science and Technology, 157, pp.139-148.
Topp, G.C., Davis, J.L. and Annan, A.P., 1980. Electromagnetic determination of soil water content: Measurements in coaxial transmission lines. Water resources research, 16(3), pp.574-582.
Tucker, A., 1985. The effects of cyclic freeze-thaw on the properties of high water content clays. Master thesis, McGill University, Montreal, Canada.
Vanapalli, S.K., Fredlund, D.G. and Pufahl, D.E. 1999. The influence of soil structure and stress history on the soil-water characteristics of a compacted till. Géotechnique, 49(2): 143-159.
Vanapalli, S.K., Fredlund, D.G., Pufahl, D.E. and Clifton, A.W., 1996. Model for the prediction of shear strength with respect to soil suction. Canadian Geotechnical Journal, 33(3), pp.379-392.
Viklander, P., 1998. Permeability and volume changes in till due to cyclic freeze/thaw. Canadian Geotechnical Journal, 35(3), pp.471-477.
Viklander, P. and Eigenbrod, D., 2000. Stone movements and permeability changes in till caused by freezing and thawing. Cold Regions Science and Technology, 31(2), pp.151-162.
Wang, C., Lai, Y. and Zhang, M., 2017. Estimating soil freezing characteristic curve based on pore-size distribution. Applied Thermal Engineering, 124: 1049-1060.
Wang, D.Y., Ma, W., Niu, Y.H., et al. 2007. Effects of cyclic freezing and thawing on mechanical properties of Qinghai–Tibet clay. Cold regions science and technology, 48(1): 34-43.
Watanabe, K. and Osada, Y., 2016. Comparison of hydraulic conductivity in frozen saturated and unfrozen unsaturated soils. Vadose Zone Journal, 15(5).
Weimer, H.F., 1972. The strength, resilience, and frost durability characteristics of a lime-stabilized till. M.Sc. Thesis, University of Saskatchewan, Saskatoon, Canada.
Williams, P.J., 1967. The nature of freezing soil and its field behaviour. Norwegian Geotechnical Institute, Publication, 72.
Williams, P.J., and Smith, M.W. 1989. The frozen earth: fundamentals of geocryology. Cambridge University Press, Cambridge.
Wu, M., Tan, X., Huang, J., Wu, J. and Jansson, P.E., 2015. Solute and water effects on soil freezing characteristics based on laboratory experiments. Cold Regions Science and Technology, 115, pp.22-29.
Xie, S.B., Jian-jun, Q., Yuan-ming, L., Zhi-wei, Z. and Xiang-tian, X., 2015. Effects of freeze-thaw cycles on soil mechanical and physical properties in the Qinghai-Tibet Plateau. Journal of Mountain Science, 12(4), pp.999-1009.
Xu, G., Qi, J. and Wu, W., 2019. Temperature Effect on the Compressive Strength of Frozen Soils: A Review. In Recent Advances in Geotechnical Research (pp. 227-236). Springer, Cham.
Xu, J., Ren, J., Wang, Z., Wang, S. and Yuan, J., 2018. Strength behaviors and meso-structural

characters of loess after freeze-thaw. Cold Regions Science and Technology, 148, pp.104-120.

Xu, X.Z., Oliphant, J.L. and Tice, A.R., 1985. Soil-water potential and unfrozen water content and temperature. Journal of Glaciology and Geocryology, 7(1), pp. 1-14. (in Chinese)

Yin, P. and Vanapalli, S.K., 2018. Model for predicting tensile strength of unsaturated cohesionless soils. Canadian Geotechnical Journal, 55(9), pp.1313-1333.

Yoshikawa, K. and Overduin, P.P., 2005. Comparing unfrozen water content measurements of frozen soil using recently developed commercial sensors. Cold Regions Science and Technology, 42(3): 250-256.

Yu, L., Zeng, Y., Wen, J. and Su, Z., 2018. Liquid‐Vapor‐Air Flow in the frozen soil. Journal of Geophysical Research: Atmospheres, 123(14), pp.7393-7415.

Zhang, S., Teng, J., He, Z., Liu, Y., Liang, S., Yao, Y. and Sheng, D., 2016. Canopy effect caused by vapour transfer in covered freezing soils. Géotechnique, 66(11), pp.927-940.

Zhang, Y., Ishikawa, T., Tokoro, T. and Nishimura, T., 2014. Influences of degree of saturation and strain rate on strength characteristics of unsaturated granular subbase course material. Transportation Geotechnics, 1(2), pp.74-89.

Zhou, Y., Zhou, J., Shi, X.Y. and Zhou, G.Q., 2019. Practical models describing hysteresis behavior of unfrozen water in frozen soil based on similarity analysis. Cold Regions Science and Technology, 157, pp.215-223.

Zhou, Z., Ma, W., Zhang, S., Mu, Y. and Li, G., 2018. Effect of freeze-thaw cycles in mechanical behaviors of frozen loess. Cold Regions Science and Technology, 146, pp.9-18.

Chapter 3 Soil freezing process and different expressions for the soil-freezing characteristic curve

The contents presented in this chapter are from the manuscript of the publication:

Ren, J., Vanapalli, S.K. and Han, Z., 2017. Soil freezing process and different expressions for the soil-freezing characteristic curve. Science in Cold and Arid Regions, 9(3): 221-228.

DOI: 10.3724/SP.J.1226.2017.00221

3.1 Abstract

The soil-freezing characteristic curve (SFCC), which represents the relationship between unfrozen water content and subzero temperature (or cryogenic suction at ice-water interface) in a frozen soil, can be used for understanding the transport of heat, water, and solute in frozen soils. In this paper, the soil freezing process and the similarity between the SFCC of saturated frozen soil and soil-water characteristic curve (SWCC) of unfrozen unsaturated soil are reviewed. Based on the similar characteristics between SWCC and SFCC, a conceptual SFCC is drawn for illustrating the main features of soil freezing and thawing processes. Various SFCC expressions from the literature are summarized. Four widely used expressions (i.e., the power relationship, exponential relationship, van Genuchten (1980) equation, and Fredlund and Xing (1994) equation) are evaluated using published experimental data on four different soils (i.e., sandy loam, silt, clay, and saline silt). Results show that the exponential relationship and van Genuchten (1980) equation are more suitable for sandy soils. The simple power relationship can be used to reasonably best-fit the SFCC for soils with different particle sizes; however, it has limitations when fitting the saline silt data. The Fredlund and Xing (1994) equation is suitable for fitting the SFCCs for all soils studied in this paper.

3.2 Introduction

The effects of harsh climate on geotechnical infrastructure in cold regions such as Canada,

northern United States, and northeast Asia should be considered by designers and contractors (Bronfenbrener and Bronfenbrener, 2012). For example, in the Province of Quebec, Canada, with freezing indices ranging from 800 to over 2000 degree-days, frost penetrates to a depth typically greater than 1.5 m. The frost action mainly develops in frost-susceptible soils, which leads to the formation of ice lens, surface heave, and eventual distress to the infrastructure (Konrad, 2005). In frozen soils, ice and unfrozen water coexist. Variation in the unfrozen water and ice contents significantly influences the physical and mechanical properties of frozen soils.

The relationship between the unfrozen water content and subzero temperature or cryogenic suction at ice-water interface is defined as the soil-freezing characteristic curve (SFCC). Since the SFCC links the degree of phase transition to the subzero temperature, the frozen soil properties, such as the segregation potential for frost heave, resilient modulus, and shear strength, can be interpreted using SFCC as a tool (Liu and Yu, 2014). For example, Azmatch et al. (2012b) predicted the hydraulic conductivity function of partially frozen Devon silt using the SFCC, saturated hydraulic conductivity, and empirical relationships for estimating hydraulic conductivity developed by Fredlund et al. (1994). Berg et al. (1996) conducted resilient modulus tests on several pavement materials from the Minnesota Road Research Project (Mn/ROAD) to characterize their behavior under seasonal frost conditions. The resilient modulus of pavement materials under frozen condition was expressed as a function of unfrozen water content, which is related to subzero temperature by SFCC. Similarly, the strength of frozen soils can be predicted based on their unfrozen water contents as per the study by Hivon and Sego (1995).

The SFCC has been recognized as a fundamental relationship in cold region engineering (Anderson and Morgenstern, 1973). Therefore, it is of critical importance to rigorously describe SFCC with reliable expressions. During the past decades, different equations and relationships have been proposed for representing SFCC (Kurylyk and Watanabe, 2013). They are either empirical relationships developed between the unfrozen water content and subzero temperature, or equations that exploit the similarity between SFCC and soil-water characteristic curve (SWCC), which correlates the water content to soil suction at air-water interface in unfrozen

unsaturated soils. The soil freezing process and the similarity between SFCC and SWCC are reviewed in this paper. A conceptual SFCC is highlighted to illustrate the main characteristics of soil freezing and thawing. In addition, various SFCC expressions proposed in the literature are succinctly summarized. Amongst them, two empirical relationships and two equations were selected and evaluated by fitting the experimental data on four different soils ranging from coarse-grained to fine-grained soils. This study provides useful information of SFCC expressions for their use in engineering practice in cold regions.

3.3 Soil freezing process

Figure 3.1 shows the soil freezing process in an open-system. When the air temperature is lower than the soil temperature, heat is extracted from the soil to the environment, which results in a temperature profile as presented in **Figure 3.1**(a). The freezing front (0 °C isotherm) progresses as a function of the imbalance associated with heat supplied to the heat removed as the pore water freezes in situ (Konrad and Morgenstern, 1980). As the freezing front advances, the upper portion of the soil becomes frozen while the lower portion remains unfrozen. A partly frozen layer, namely the frozen fringe, exists between the frozen and unfrozen soil layers (**Figure 3.1**(b)). Thermodynamic processes occurring in the frozen fringe contribute to the generation of negative pore water pressure (Williams, 1966; Konrad and Morgenstern, 1980), as presented in **Figure 3.1**(c). As a result, hydraulic gradient develops and water migrates from the unfrozen soil to frozen soil.

Ice lenses will form if sufficient amount of water is accumulated behind the freezing front, resulting in soil mass heave (**Figure 3.1**(b)). The thickness and spacing of the ice lenses depend on the relative magnitudes of the rate of freezing and water availability (Penner, 1961). Near the surface, the temperature gradient is large, thus the rate of freezing is also high. However, the pore water does not have enough time to form thick ice lenses. Instead, thin ice lenses form with a relatively close spacing for this situation. As the freezing front penetrates to deeper soil layers, the rate of freezing is relatively low due to lower temperature gradient. In this case, there is

enough time for water to migrate towards the freezing front from the lower unfrozen zone and to freeze. Therefore, thick ice lenses form. The non-uniform distribution of ice lenses in the soil mass contributes to the development of cracks, which occur more frequently near the surface and decrease in frequency with increasing depth (Benson and Othman, 1993). These cracks pose a significant influence on the performance of different infrastructure constructed in frozen soils.

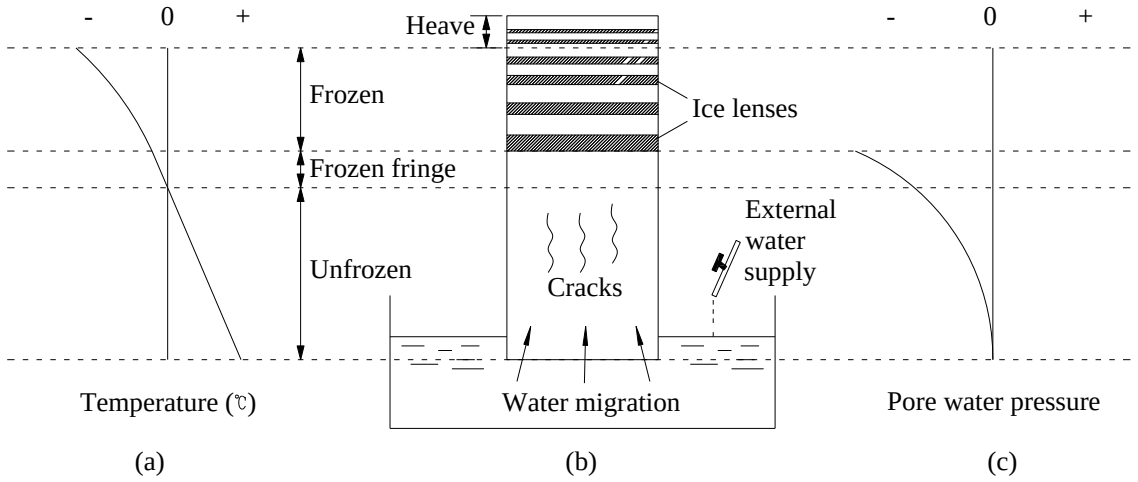

Figure 3.1 Soil freezing in an open-system: (a) temperature profile; (b) soil profile, water migration and ice lenses formation; and (c) negative pore water pressure profile (modified from Benson and Othman, 1993)

3.4 SFCC and its similarity to SWCC

In a frozen soil, unfrozen water and pore ice coexist. The principal factor determining the quantity of unfrozen water is temperature (Nersesova and Tsytovich, 1963). Pressure is a less important but a valid influencing factor. An increase in pressure increases the unfrozen water content at a given temperature. Besides, solute concentration, particle size distribution, chemical and mineralogical nature of the soil matrix also influence the unfrozen water content (Nersesova and Tsytovich, 1963; Anderson and Tice, 1973).

The relationship between unfrozen water content and subzero temperature (or cryogenic suction) in a frozen soil is characterized by SFCC (Koopmans and Miller, 1966; Spaans and

Baker, 1996; Azmatch et al., 2012b). The Clapeyron equation can be used to convert subzero temperature to cryogenic suction or vice versa with assumptions that (i) the pore ice pressure in a saturated frozen soil is equal to the atmospheric pressure, and (ii) the solute effect is negligible (Konrad and Morgenstern, 1980; Black and Tice, 1989). The Clapeyron equation is as follows (Azmatch et al., 2012b; Kurylyk and Watanabe, 2013),

$$\psi_{cryo} = -L\rho_w \ln\frac{T+273.15}{T_0+273.15} \tag{3.1}$$

where ψ_{cryo} is cryogenic suction (kPa); L is latent heat of fusion of water (L = 334 kJ/kg); T is subzero temperature in °C; T_0 is normal freezing temperature of water (T_0 = 0 °C); and ρ_w is water density (ρ_w = 1000 kg/m^3). A decrease in soil temperature by 1 °C typically increases the cryogenic suction by about 1250 kPa (Zhou et al., 2014).

Eq. (3.1) can be further simplified to Eq. (3.2) since ln((T+273.15)/(T_0+273.15)) is approximately equal to T/(273.15) when T is close to 0 °C (Kurylyk and Watanabe, 2013),

$$\psi_{cryo} = -L\rho_w \frac{T}{273.15} \tag{3.2}$$

Koopmans and Miller (1966) measured both the SFCC and SWCC for three different soils and showed that SFCC is similar to SWCC. This is due to the similarity in the physical processes experienced during drying and wetting in unfrozen unsaturated soils and freezing and thawing in saturated frozen soils. When soils are subjected to drying, water is gradually removed and replaced by air, leaving the remaining water at an increasingly lower potential. The physical process that occurs in freezing soils is similar, except that liquid water changes phase and becomes ice. The same forces that prevent soil water from draining also prevent it from freezing (Spaans and Baker, 1996). In other words, the temperature gradient in frozen soils can be considered to act in a manner similar to the potential gradient in unsaturated soils (Zhou et al., 2014).

Based on their similarity, a conceptual SFCC can be drawn, as presented in **Figure 3.2**. Ice will form in the largest pores first when soil temperature decreases (cryogenic suction gradually increases). The corresponding subzero temperature or cryogenic suction at this stage is referred to as the ice-entry value (IEV) (Azmatch et al., 2012a). The unfrozen water content in the soil

gradually decreases along the freezing curve. Most of the pore water turns into ice at a certain subzero temperature. However, beyond this temperature extremely low temperature (i.e. high cryogenic suction) would be required for achieving further reduction in the unfrozen water. This critical unfrozen water content is referred to as the residual unfrozen water content. Similar to SWCC, SFCC could be divided into three zones, i.e. boundary effect zone (where no pore ice forms), transition zone (where sharp drop in the unfrozen water content is experienced), and residual zone of unfrozen state (where variation in the unfrozen water content is insignificant in spite of significant changes in subzero temperature or cryogenic suction). These characteristics are similar to the descriptions provided for SWCC by Vanapalli et al. (1999). In addition, the SFCC also shows hysteretic behavior (Koopmans and Miller, 1966) which is similar to SWCC. This can be attributed to several possible mechanisms such as the phenomenon of metastable nucleation, the effect of electrolyte, and pore blocking (Tian et al., 2014).

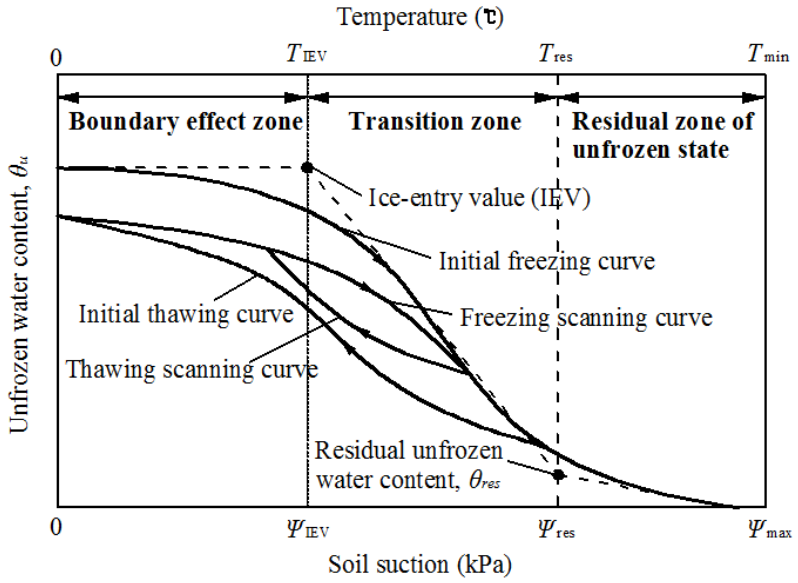

Figure 3.2 Typical soil-freezing characteristic curve

3.5 Different expressions for the SFCC

Several SFCC expressions are available in the literature. These expressions can be divided into two groups. The first group was based on empirical relationships between the unfrozen

water content and subzero temperature. The second group was developed by exploiting the similarity between SFCC and SWCC, with the aid of the Clapeyron equation correlating the subzero temperature to cryogenic suction at the ice-water interface.

3.5.1 Empirical relationships

Anderson and Tice (1972) found that the unfrozen water contents of most frozen soils can be conveniently expressed as a function of temperature by a simple power curve,

$$\theta_u = \frac{\rho_d}{\rho_w}\alpha(-T)^{\beta} \tag{3.3}$$

where θ_u is volumetric unfrozen water content, ρ_d is soil dry density (g/cm^3), α and β are model parameters.

Mckenzie et al. (2007) suggested an exponential function for the relationship between degree of saturation in frozen soil and temperature. Eq. (3.4) can be used for estimating the volumetric unfrozen water content,

$$\theta_u = \theta_{res} + (\theta_{sat} - \theta_{res})\exp[-(\frac{T - T_0}{\gamma})^2] \tag{3.4}$$

where θ_{sat} is volumetric unfrozen water content at saturated condition (θ_{sat} is equal to soil porosity), θ_{res} is residual volumetric unfrozen water content, and γ is model parameter.

Kozlowski (2007) developed a non-linear piecewise function for SFCC. It is expressed as,

$$\begin{cases} \theta_u = \theta_{sat} & \text{for } T > T_0 \\ \theta_u = \theta_{res} + (\theta_{sat} - \theta_{res})\exp[\delta(\frac{T_0 - T}{T - T_{res}})^{\varepsilon}] & \text{for } T_{res} < T \le T_0 \\ \theta_u = \theta_{res} & \text{for } T \le T_{res} \end{cases} \tag{3.5}$$

where T_{res} is the temperature corresponding to θ_{res} (°C), δ and ε are model parameters.

In addition to the power, exponential, and non-linear piecewise relationships, simple linear piecewise relationships can be used to achieve reasonable approximations for the SFCC (McKenzie et al., 2007; Kurylyk and Watanabe, 2013).

3.5.2 Relationship based on the similarity between SFCC and SWCC

The SFCC is derived from SWCC by relating cryogenic suction with subzero temperature, through the Clapeyron equation (Dall'Amico, 2010). Different SWCC equations, such as those proposed by Brooks and Corey (1964), van Genuchten (1980), and Fredlund and Xing (1994), have been used as SFCC equations by simply replacing the suction at the air-water interface in unsaturated unfrozen soil with the cryogenic suction at the ice-water interface in saturated frozen soil (e.g. Shoop and Bigl, 1997; Dall'Amico, 2010; Sheshukov and Nieber, 2011; Azmatch et al. 2012b).

By combining the simplified Clapeyron equation (Eq. (3.2)) with the Brooks and Corey (1964) equation, Sheshukov and Nieber (2011) obtained a relationship for unfrozen water content and subzero temperature,

$$\theta_u = \theta_{res} + (\theta_{sat} - \theta_{res})(\frac{-1}{\psi_{IEV}} \frac{L\rho_w T}{273.15})^{-1/b} \tag{3.6}$$

where ψ_{IEV} is ice-entry value (kPa), and b is the Brooks and Corey (1964) SWCC model parameter.

Zhang et al. (2016) incorporated the Clapeyron equation (Eq. (3.1)) into the van Genuchten (1980) SWCC equation and proposed the following SFCC relationship,

$$\theta_u = \theta_{res} + (\theta_{sat} - \theta_{res})[1 + (a_{vg} L\rho_w \ln \frac{T + 273.15}{T_0 + 273.15})^{n_{vg}}]^{-m_{vg}} \tag{3.7}$$

where a_{vg}, n_{vg}, and m_{vg} are the van Genuchten (1980) SWCC model parameters.

Azmatch et al. (2012b) showed that the Fredlund and Xing (1994) equation can be used to reasonably approximate SFCC by replacing the suction at the air-water interface with the cryogenic suction at the ice-water interface. By employing Eq. (3.1), the SFCC can be expressed as:

$$\theta_u = \frac{\theta_{sat}}{\{\ln[2.718 + (\frac{L\rho_w}{a_f} \ln(\frac{T + 273.15}{T_0 + 273.15}))^{n_f}]\}^{m_f}} \tag{3.8}$$

where a_f, n_f, and m_f are the Fredlund and Xing (1994) SWCC model parameters.

3.6 Comparison of different SFCC expressions and discussion

Four different SFCC expressions (two from each group), namely, the power relationship (Eq. (3.3)), exponential relationship (Eq. (3.4)), van Genuchten (1980) equation (Eq. (3.7)), and Fredlund and Xing (1994) equation (Eq. (3.8)), were selected to best-fit the measured SFCC data of four different types of soils from the literature (Smith and Tice, 1988). The four soils were saturated with distilled water and the volumetric unfrozen water contents were measured using time domain reflectometry (TDR), which is widely used for measuring unfrozen water content in frozen soils. The basic properties of the four soils are summarized in **Table 3.1**. **Figure 3.3** shows the measured SFCCs for these four soils. The residual unfrozen water content was determined by extending the linear transition zone to intersect a linear extension of the residual zone of unfrozen state, following the procedures summarized by Vanapalli et al. (1999) (see **Figure 3.2**).

Table 3.1 Basic properties of the four studied soils

Soil	Dry density (g/cm^3)	Saturated unfrozen water content, θ_{sat}	Residual unfrozen water content, θ_{res}	Specific surface area (m^2/g)
Castor sandy loam	1.475	0.385	0.020	/
Lanzhou silt (saline)	1.655	0.364	0.100	34
Niagara silt	1.645	0.365	0.091	37
Regina clay	0.961	0.572	0.190	291

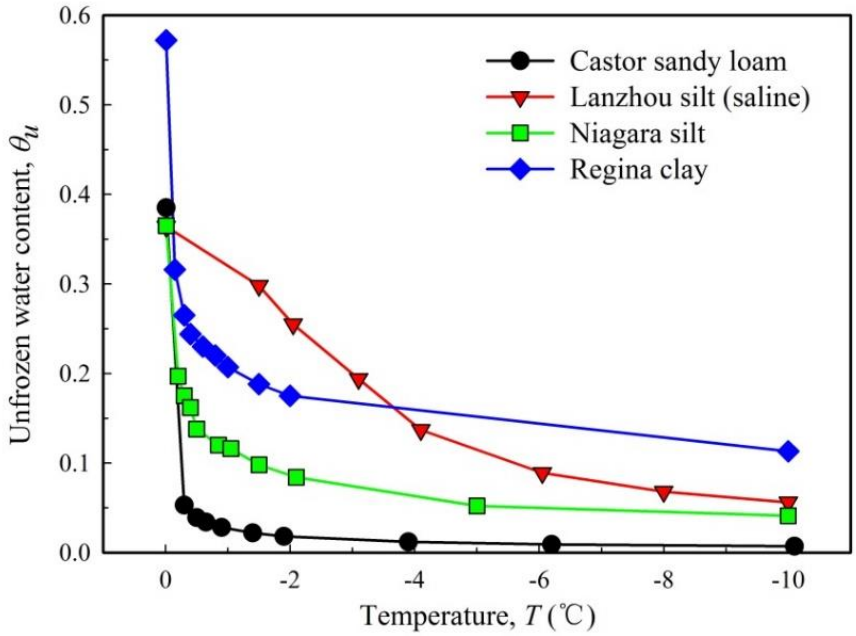

Figure 3.3 SFCCs of the four studied soils

It can be seen from **Figure 3.3** that the SFCCs of different non-saline soils show similar trends in their variation. The unfrozen water content significantly decreases as temperature drops from 0 to -2 °C, after which it gradually becomes constant. The Regina clay has much higher unfrozen water content than the Niagara silt and the Castor sandy loam at lower temperatures. The reason is that the Regina clay has much larger amount of fine platy particles that can adsorb more water on their surfaces, resulting in higher unfrozen water content even when the temperature drops below -10 °C. When the pore water of a soil contains salinity, its SFCC is different from that of a non-saline soil. As an example, the unfrozen water content of the saline Lanzhou silt does not show dramatic reduction when the temperature drops to -2 °C, and the slope of the freezing curve is much smaller than that of the Niagara silt, although both of these soils are silty soils and have approximately the same specific surface area (see **Table 3.1**).

The four selected SFCC expressions were used to best-fit the measured SFCCs of the four soils, and the fitting results are summarized in **Table 3.2** and **Figure 3.4**.

Table 3.2 Fitting results of the four selected SFCC expressions

	Power relationship			Exponential relationship		van Genuchten (1980) eq.				Fredlund and Xing (1994) eq.			
	α	β	R^2	γ	R^2	a_{vg}	n_{vg}	m_{vg}	R^2	a_f	n_f	m_f	R^2
Castor sandy loam	0.018	-0.583	1.00	0.194	0.99	0.013	3.369	0.449	0.99	80.6	2.541	1.423	1.00
Lanzhou silt (saline)	0.116	-0.152	0.53	2.909	0.96	0.0002	2.374	2.845	0.96	2933.5	2.130	1.648	0.99
Niagara silt	0.070	-0.256	0.96	0.268	0.86	0.002	1.044	2.095	0.93	119.0	1.071	1.231	0.99
Regina clay	0.212	-0.224	0.99	0.150	0.88	0.012	1.769	0.666	0.93	50.9	1.600	0.650	0.99

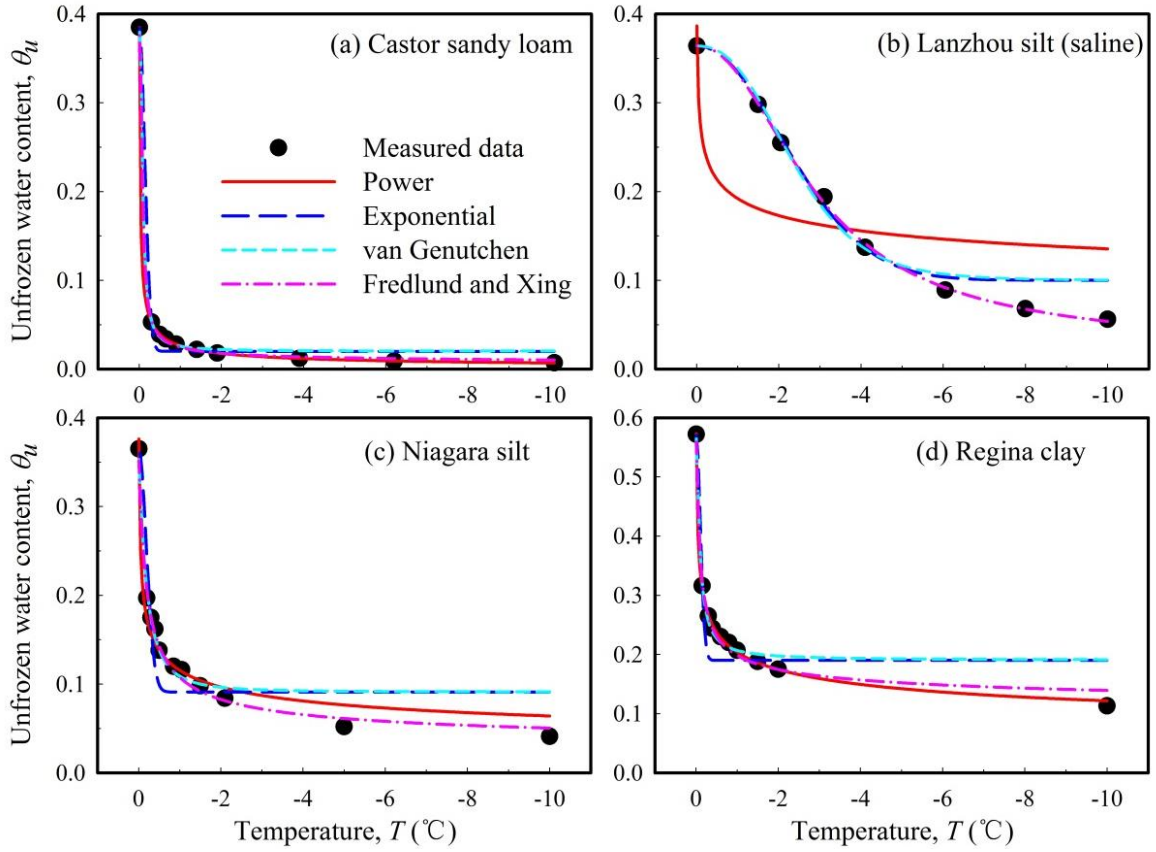

Figure 3.4 Comparison between the measured and best-fitted SFCCs for (a) Castor sandy loam, (b) Lanzhou silt, (c) Niagara silt, and (d) Regina clay

Figure 3.4 shows the comparison between the measured and best-fitted SFCCs for the four soils. All the four relationships / equations can reasonably fit the measured SFCCs of soils without salinity. The measured data of the Castor sandy loam is well fitted by the four expressions. However, the exponential relationship and van Genuchten (1980) equation are less accurate than the power relationship and the Fredlund and Xing (1994) equation for the Niagara silt and Regina clay. The reason is that for the exponential relationship and van Genuchten (1980) equation, the minimum value of unfrozen water content is limited by the residual unfrozen water content (θ_{res}). In other words, the minimum value of the predicted unfrozen water content is equal to θ_{res} by employing these two expressions. As can be seen from **Figure 3.3** and **Figure 3.4**, the unfrozen water content of the Castor sandy loam levels off after -2 °C, but the unfrozen water contents of the Niagara silt and Regina clay still decrease with a relatively lower rate, due to their relatively small particle sizes. This implies that the θ_{res} can be well defined for the sandy loam compared to the silt and clay.

The exponential relationship and the Fredlund and Xing (1994) equation are able to provide good fit for the saline Lanzhou silt. On the contrary, the power relationship is not as accurate as it is for the other three soils. For giving reasonable fitting for SFCC of saline silt, the parameter a_{vg} of the van Genuchten (1980) equation was fixed to 0.0002. Of all the various expressions used in the present study, the Fredlund and Xing (1994) equation is able to provide excellent approximation for all the four soils, including the saline soil.

In summary, the exponential relationship seems to be a good choice for sands and sandy soils whose unfrozen water content drops dramatically with temperature slightly below 0 °C and levels off afterwards. The power relationship provides good fits for sandy loam, silt, and clay; however, for the saline silt studied, only a fair fit was achieved. The power and exponential relationships are empirical but simple, and they are smooth and can be easily differentiated for determining the apparent heat capacity (McKenzie et al., 2007). On the contrary, the van Genuchten (1980) and Fredlund and Xing (1994) equations are relatively complex and require the use of the Clapeyron equation, which is valid when thermodynamic equilibrium condition

has been achieved. Moreover, the assumptions on which the Clapeyron equation is based need further investigations for employing them for SFCC equations. The exponential relationship and the van Genuchten (1980) equation are more suitable for sandy soils in comparison with silt or clay. The Fredlund and Xing (1994) equation well fitted the SFCCs for all the four soils, showing higher flexibility for use on soils with different particle sizes.

3.7 Conclusions

The variation in unfrozen water and ice contents with the change in subzero temperature significantly influences the physical and mechanical properties of frozen soils. The SFCC is required to understand the flow of heat, water, and solute in frozen soils (Spaans and Baker, 1996). A succinct review of the soil freezing process and the similarity between SFCC and SWCC is provided in this paper. A conceptual SFCC is drawn to illustrate key features of soil freezing and thawing. Four different SFCC expressions (i.e. two empirical relationships, and the other two equations based on the similarity between SFCC and SWCC) were selected for providing comparisons between the measured and fitted unfrozen water contents for four different soils. The results suggest that the exponential relationship and van Genuchten (1980) equation are more suitable for sandy soils. The power relationship could reasonably fit the SFCC for soils with different particle sizes, but not for saline silt. The Fredlund and Xing (1994) equation provides good fits for all the four soils investigated in the present study, showing its flexibility for different types of soils. However, more efforts should be put into investigating the theoretical background for employing the Clapeyron equation and the similarity between SFCC and SWCC for predicting the unfrozen water content in frozen soils.

3.8 References

Anderson, D.M., Morgenstern, N.R. 1973. Physics, chemistry, and mechanics of frozen ground: a review. In Permafrost: The North American Contribution to the Second International Conference, National Academy of Sciences, Washington, DC, 257-288.

Anderson, D.M., Tice, A.R., 1972. Predicting unfrozen water contents in frozen soils from

surface area measurements. Highway Research Record, 393: 12-18.
Anderson, D.M., Tice, A.R., 1973. The unfrozen interfacial phase in frozen soil water systems. In: Hadas A., et al. (ed.). Springer Berlin Heidelberg, pp. 107-124.
Azmatch, T.F., Sego, D.C., Arenson, L.U., et al., 2012a. New ice lens initiation condition for frost heave in fine-grained soils. Cold Regions Science and Technology, 82: 8-13.
Azmatch, T.F., Sego, D.C., Arenson, L.U., et al., 2012b. Using soil freezing characteristic curve to estimate the hydraulic conductivity function of partially frozen soils. Cold Regions Science and Technology, 83: 103-109.
Benson, C.H., Othman, M.A., 1993. Hydraulic conductivity of compacted clay frozen and thawed in situ. Journal of Geotechnical Engineering, 119(2): 276-294.
Berg, R.L., S.R. Bigl, J. Stark, et al., 1996. Resilient modulus testing of materials from Mn/ROAD, Phase 1. USA Cold Regions Research and Engineering Laboratory, Special Report 96- 19, Mn/DOT Report 96-21.
Black, P.B., Tice, A.R., 1989. Comparison of soil freezing curve and soil water curve data for Windsor sandy loam. Water Resources Research, 25(10): 2205-2210.
Bronfenbrener, L., Bronfenbrener, R., 2012. A temperature behavior of frozen soils: Field experiments and numerical solution. Cold Regions Science and Technology, 79: 84-91.
Brooks, R.H., Corey, A.T., 1964. Hydraulic properties of porous media. Transactions of the ASAE, 7(1): 1-27.
Dall'Amico, M., 2010. Coupled water and heat transfer in permafrost modeling. PhD Thesis, University of Trento, pp. 43.
Fredlund, D.G., Xing, A., 1994. Equations for the soil-water characteristic curve. Canadian Geotechnical Journal, 31(4): 521-532.
Fredlund, D.G., Xing, A., Huang, S., 1994. Predicting the permeability function for unsaturated soils using the soil-water characteristic curve. Canadian Geotechnical Journal, 31(4): 533-546.
Hivon, E.G. and Sego, D.C., 1995. Strength of frozen saline soils. Canadian Geotechnical Journal, 32(2): 336-354.
Konrad, J.M., 2005. Estimation of the segregation potential of fine-grained soils using the frost heave response of two reference soils. Canadian Geotechnical Journal, 42(1): 38-50.
Konrad, J.M., Morgenstern, N.R., 1980. A mechanistic theory of ice lens formation in fine-grained soils. Canadian Geotechnical Journal, 17(4): 473-486.
Koopmans, R.W.R., Miller, R.D., 1966. Soil freezing and soil water characteristic curves. Soil Science Society of America Journal, 30(6), 680-685.
Kozlowski, T. 2007. A semi-empirical model for phase composition of water in clay–water systems. Cold Regions Science and Technology, 49(3): 226-236.
Kurylyk, B.L. Watanabe, K., 2013. The mathematical representation of freezing and thawing processes in variably-saturated, non-deformable soils. Advances in Water Resources, 60: 160-177.
Liu, Z., Yu, X., 2014. Predicting the phase composition curve in frozen soils using index properties: A physic - empirical approach. Cold Regions Science and Technology, 108:

10-17.
McKenzie, J.M., Voss, C.I., Siegel, D.I., 2007. Groundwater flow with energy transport and water–ice phase change: numerical simulations, benchmarks, and application to freezing in peat bogs. Advances in Water Resources, 30(4): 966-983.
Nersesova, Z.A., Tsytovich, N.A. 1963. Unfrozen water in frozen soils. In Permafrost: Proceedings of 1st International Conference, 11-15.
Penner, E., 1961. The importance of freezing rate in frost action in soils. In Proceedings of the American Society for Testing and Materials, 60: 1151-1165.
Sheshukov, A.Y., Nieber, J.L., 2011. One-dimensional freezing of nonheaving unsaturated soils: Model formulation and similarity solution. Water Resources Research, 47(11): W11519.
Shoop, S.A., Bigl, S.R., 1997. Moisture migration during freeze and thaw of unsaturated soils: modeling and large scale experiments. Cold Regions Science and Technology, 25(1): 33-45.
Smith, M.W., Tice, A.R., 1988. Measurement of the unfrozen water content of soils - comparison of nmr (nuclear magnetic resonance) and tdr (time domain reflectometry) methods. No. CRREL-88-18. Cold Regions Research and Engineering Lab, Hanover, NH.
Spaans, E.J. and Baker, J.M. 1996. The soil freezing characteristic: its measurement and similarity to the soil moisture characteristic. Soil Science Society of America Journal, 60: 13–19.
Tian, H., Wei, C., Wei, H., et al., 2014. Freezing and thawing characteristics of frozen soils: Bound water content and hysteresis phenomenon. Cold Regions Science and Technology, 103: 74-81.
Vanapalli, S.K., Fredlund, D.G., Pufahl, D.E., 1999. The influence of soil structure and stress history on the soil-water characteristics of a compacted till. Géotechnique, 49(2): 143-159.
van Genuchten, M.T., 1980. A closed-form equation for predicting the hydraulic conductivity of unsaturated soils. Soil Science Society of America Journal, 44(5): 892-898.
Williams, P.J., 1966. Pore pressures at a penetrating frost line and their prediction. Géotechnique, 16(3): 187-208.
Zhang, S., Teng, J., He, Z., et al., 2016. Importance of vapor flow in unsaturated freezing soil: a numerical study. Cold Regions Science and Technology, 126: 1-9.
Zhou, X., Zhou, J., Kinzelbach, W., et al., 2014. Simultaneous measurement of unfrozen water content and ice content in frozen soil using gamma ray attenuation and TDR. Water Resources Research, 50(12): 9630-9655.

Chapter 4 Comparison of soil-freezing and soil-water characteristic curves of two Canadian soils

The contents presented in this chapter are from the manuscript of the publication:

Ren, J. and Vanapalli, S.K., 2019. Comparison of soil-freezing and soil-water characteristic curves of two Canadian soils. Vadose Zone Journal, 18:180185.

DOI: 10.2136/vzj2018.10.0185

4.1 Abstract

The drying / wetting and freezing / thawing cycles significantly influence the soil pore water in the vadose zone in permafrost and seasonally frozen regions. Soil-freezing characteristic curve (SFCC) describes the relationship between unfrozen water content and subzero temperature in a soil at frozen condition. Several studies suggest that the SFCC of a frozen saturated soil is similar to soil-water characteristic curve (SWCC), which describes the relationship between water content and suction for a soil under unfrozen unsaturated condition. In the present study, the similarity between SFCC and SWCC, and possible reasons for the hysteresis of SFCC are succinctly reviewed. The SFCC and SWCC of two Canadian soils were measured and critically interpreted to understand the fundamental behavior of SFCC in comparison with the SWCC. The observed hysteresis of SFCC for the two soils was mainly associated with the supercooling of pore water. The measured SFCC and SWCC of the two soils show quantitative dissimilarity rather than similarity. This may be attributed to the experimental limitations and possible fundamental differences between drying / wetting and freezing / thawing processes. In addition, several concerns regarding the similarity between SFCC and SWCC were discussed. The present study highlights that rigorous investigations are required for better understanding the SFCC to facilitate its use for cold regions engineering practice applications.

4.2 Introduction

The soil pore water in the vadose zone in permafrost and seasonally frozen regions is significantly influenced by both drying / wetting and freezing / thawing cycles. Unfrozen water and ice coexist in a frozen soil. The amount of unfrozen water and ice is predominantly dependent on subzero temperature. The relationship between unfrozen water content and subzero temperature is commonly referred to as the soil-freezing characteristic curve (SFCC) (e.g., Koopmans and Miller, 1966; Spaans and Baker, 1996; Azmatch et al., 2012). The subzero temperature can be converted to cryogenic suction (which is defined as the pressure difference between pore ice and pore water) by using the Clapeyron equation, based on certain assumptions and thermodynamic equilibrium condition between ice and water phases.

The amount of unfrozen water change contributes to the variation of the physical and mechanical properties of frozen soils. For this reason, SFCC can be used as a tool in the interpretation of frozen soil behavior. Several studies highlight that the SFCC of frozen saturated soil is similar to soil-water characteristic curve (SWCC), which describes the relationship between water content and suction, of unfrozen unsaturated soil (e.g., Koopmans and Miller, 1966; Spaans and Baker, 1996). The wide use of SWCC in the prediction of unsaturated soil properties is encouraging researchers and practitioners in recent years to extend similar philosophy in engineering practice for frozen soils using the SFCC.

For example, Azmatch et al. (2012) measured the SFCC of Devon silt specimens that were consolidated using different pressures. The SFCC of these specimens were expressed as a relationship between unfrozen water content versus cryogenic suction and fitted using the well-known Fredlund and Xing (1994) equation. The hydraulic conductivities of the frozen Devon silt specimens were estimated using the fitted SFCC along with a saturated hydraulic conductivity value extending the same philosophy used for unfrozen unsaturated soils.

Ren and Vanapalli (2018) proposed a semi-empirical model for estimating the resilient modulus of frozen soils at saturated condition using SFCC as a tool. The unfrozen water content versus subzero temperature relationship was converted to the relationship between degree of

unfrozen water saturation and cryogenic suction. The later relationship was then fitted using the Fredlund and Xing (1994) equation. Experimental data of seven different saturated soils were used to validate the model and a good agreement was achieved between the measured and estimated frozen resilient modulus values.

The reliable determination of SFCC is the primary step to employ SFCC in the prediction of frozen soil properties. Two different approaches are commonly used for determining the SFCC. The first approach focuses on the direct measurement of SFCC. Several methods such as the dilatometry, calorimetry, frequency domain reflectometry (FDR), time domain reflectometry (TDR), and nuclear magnetic resonance (NMR), have been used in laboratory and in situ during the past few decades (e.g., Anderson and Morgenstern, 1973; Yoshikawa and Overduin, 2005). A significant amount of data is published in the literature following these methods. The second approach focuses on the estimation of SFCC from soil physical properties, or using the similarity between SFCC and SWCC and / or physical and theoretical mechanisms (e.g., Anderson and Tice, 1972; Liu and Yu, 2013; Wang et al., 2017; Amiri et al., 2018).

There are limited studies in the literature for better understanding the fundamental behavior of SFCC to facilitate the development of reliable models for the design of civil infrastructure such as pavements, foundations, and pipelines. For this reason, it is important to understand the strengths and limitations of the presently used experimental and empirical methods for the determination or estimation of SFCC. To address these objectives, the SFCC and SWCC of two soils from Toronto, Canada (i.e. Toronto silty clay and Toronto lean clay) were investigated. Several different testing conditions were imposed to determine the SFCC. Some of the testing scenarios were directed to study the freezing and thawing branches of SFCC to understand the hysteretic characteristics of the two soils. In addition, comparisons were provided between the SFCC and SWCC for both the soils. The results of the study provide valuable information for better understanding the SFCC in general and the two tested soils from Toronto, Canada in particular.

4.3 Background

4.3.1 Similarity between SFCC and SWCC

The physical process that a soil undergoes during drying and wetting cycles under unfrozen condition has similar characteristics to that when the soil is subjected to freezing and thawing cycles. When an initially saturated soil is subjected to drying, water is gradually removed and replaced by air, leaving the remainder water at an increasingly lower matric potential. In a similar fashion, liquid water in a saturated soil changes phase and gradually becomes ice when it is subjected to freezing. Two different mechanisms contribute to matric potential; namely, the adsorptive force and capillary force. The adsorptive force acts on the mineral-water interface. Water is adsorbed by soil particles as thin films. Therefore, it is considered immaterial whether ice or air is present on the other side of the water film; for this reason, reductions of soil matric potential in frozen and unfrozen conditions due to adsorptive forces can be considered identical (Spaans and Baker, 1996). The capillary force at the interface of different phases, such as air-water, ice-water, and air-ice interfaces, is proportional to the surface energy of the interface. The surface energy of air-water interface is higher than that of ice-water interface (Spaans, 1994). For this reason, reductions of soil matric potential associated with capillary force are different in a soil that is at frozen and unfrozen conditions.

Koopmans and Miller (1966) were the pioneers who measured both SFCC and SWCC for three different types of soils (i.e. SS, SLS, and SSLS). The SS soil is free of colloidal materials and represents soils such as sand, silt, or coarse clay fractions that have direct solid-to-solid (SS) contacts between particles. In SS type soils, each particle is wedged with the other adjacent particles and the pore geometry is fixed. A change in water content causes a displacement of the air-water interface within the pore system; however, there will be no change in the bulk volume of the soil. The other extreme scenario relates to the soil particles are always separated by liquid water, designated as the SLS (i.e. solid-liquid-solid) soil. A change in water content is accompanied by corresponding changes in particle spacing and in the bulk volume. Macroscopic cracks may open or close due to changes in water content; however, the air phase does not

penetrate the spaces between particles. The schematic representation of the SS and SLS soils is available in Miller (1980). In reality, the behavior of a majority of natural soils lies in between the SS and SLS; for this reason, they are designated as SSLS soil.

It is assumed that adsorptive force dominates the water retention behavior of the SLS soil. The SFCC and SWCC are expected to be identical and do not require any adjustment if soil water is at a similar state in the frozen and unfrozen SLS soil. However, because of the difference between the surface energy of air-water and ice-water interfaces in a SS soil, an adjustment factor is required to relate its SWCC to SFCC (Koopmans and Miller, 1966; Miller, 1980). **Figure 4.1** shows the measured SFCC and SWCC of these three different types of soils. As can be seen, by using an adjustment factor of 2.2 for the SS and SSLS soils and with no adjustment for the SLS soil, good agreement was achieved between the SFCC and SWCC. However, it is of interest to note that a value of 2.2 would lead to erroneous result for the SSLS soil from a theoretical point of view. Investigators were also inspired to find an adjustment factor that is dependent on temperature since most soils behave as SSLS soil, which is not predominantly influenced by either capillary or adsorptive force (Kurylyk and Watanabe, 2013). Soil pore water freezes gradually and the governing force (capillary or adsorptive) may switch with a decrease in temperature. At higher subzero temperature, pore water is mainly present as the result of capillary force since the curvature of ice-water interface is significant in this situation. However, when there is a further decrease in temperature, most pore water becomes ice and thin adsorbed film of water is predominantly available. At this stage, adsorptive force dominates and no capillary force is considered (Lebeau and Konrad, 2012; Kurylyk and Watanabe, 2013).

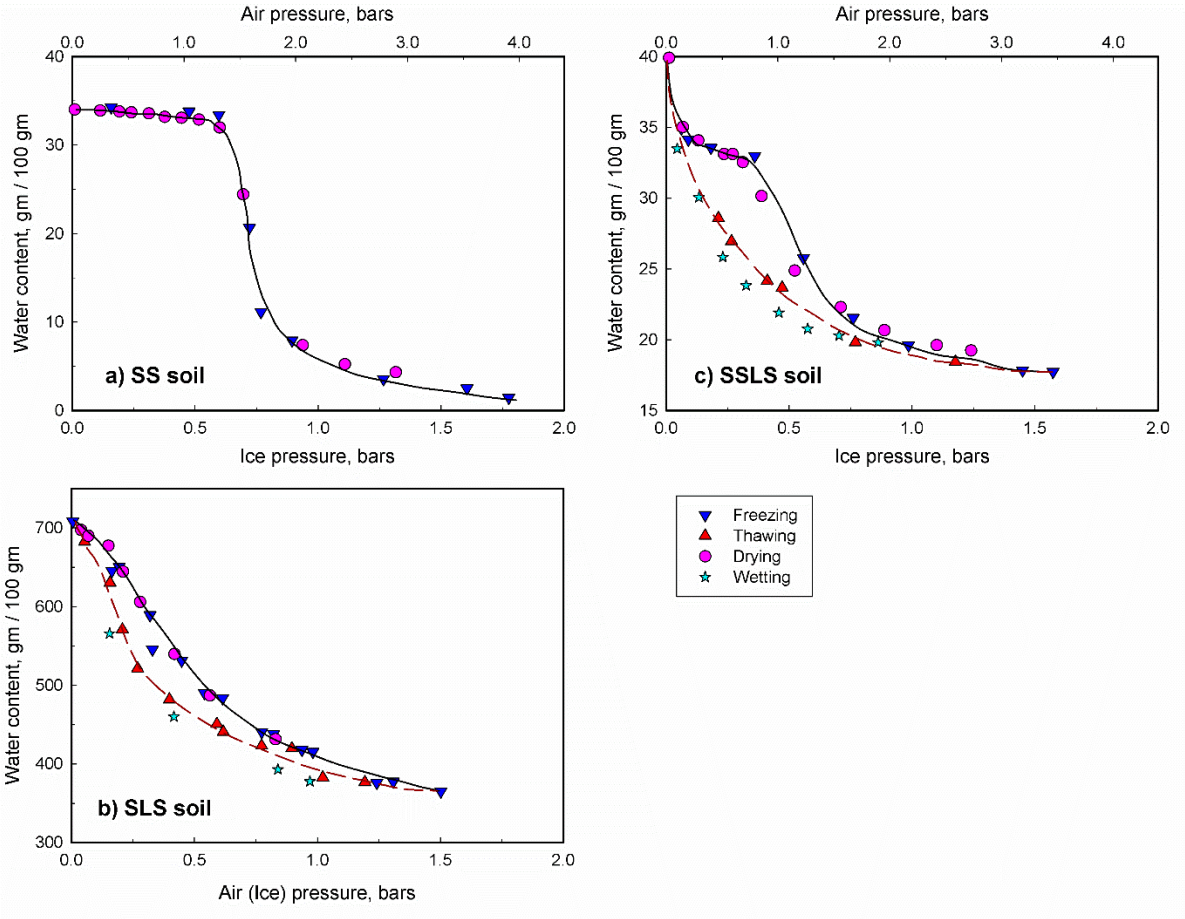

Figure 4.1 (a) SS soil: SFCC for second freezing and SWCC for drying, (b) SFCC and SWCC for SLS soil, and (c) SSLS soil: SFCC for third freeze-thaw cycle and SWCC for dry-wet cycle (modified after Koopmans and Miller, 1966)

4.3.2 Hysteresis of SFCC

SFCC exhibits hysteretic behavior similar to the SWCC. This can be attributed to several possible mechanisms: (1) Supercooling of pore water (Bittelli et al., 2003; He and Dyck, 2013; Tian et al., 2014; He et al., 2015). Soil pore water does not necessarily freeze when its freezing temperature is reached. Instead, pore water remains in a liquid phase and is supercooled to a lower temperature, until freezing is induced by ice nucleation. (2) The effect of electrolytes (Bittelli et al., 2003; He and Dyck, 2013; Tian et al., 2014; He et al., 2015). Since electrolytes will be excluded from ice when soil is subjected to freezing, the solute concentration in the

remainder of pore water becomes larger, which contributes to freezing point depression of pore water and yields hysteresis. (3) Pore geometry (Anderson et al., 2009). Hysteresis may be attributed to differences in ice-water interface curvatures during crystallization and melting, especially in soil that contains a notable component of pores that are cylindrical. (4) Pore blocking (Bittelli et al., 2003; Anderson et al., 2009). Bottle neck effect (originating from large pores with narrow necks), which is considered as a primary cause of the hysteresis commonly observed for air-water phase transition in soil with a wide distribution of interconnected pores of different radii, may similarly lead to the hysteresis for ice-water phase transition in the soil. (5) The effect of contact angle (Liu and Yu, 2013; Zhou et al., 2019). The advancing contact angle during soil freezing is different from the receding contact angle during soil thawing. (6) The change in pore structure. The thixotropic property and aging effects that influence pore size distribution, may contribute to hysteresis (Liu and Yu, 2013).

In addition, soil particles typically move from their original positions as soil pores are enlarged due to ice expansion during the freezing process. Therefore, there would be more large pores than prior to soil freezing. When soil is subjected to thawing, pore ice melting initiates in small pores first and then progresses successively to larger pores (Tan et al., 2015). Due to this reason, for the same unfrozen water content, temperature on the thawing branch is higher than that on the freezing branch. In other words, the thawing branch is below the freezing branch (i.e. hysteresis). Nevertheless, the reasons for hysteresis in porous media such as soils are still not well understood. This may be associated with the complexity of pore structure, which may likely comprise of various heterogeneous (at the pore scale) pore geometries, a wide range of pore diameters and varying degrees of interconnectivity (Anderson et al., 2009).

4.4 Specimens preparation and experimental setup

The Toronto silty clay (TSC) and Toronto lean clay (TLC) were collected from 0 to 3m below the natural ground surface in Toronto, Canada. The two soils were air dried for two weeks and then ground and passed through a 2 mm sieve. The standard Proctor compaction test (ASTM

D698-12) was conducted on the two soils, whose optimum moisture contents were determined as 13.5% and 12.3%, respectively. The basic physical properties of TSC and TLC are summarized in **Table 4.1**. **Figure 4.2** presents their gradation curves.

Table 4.1 Basic physical properties of TSC and TLC

	w_L (%)	w_p (%)	I_p (%)	w_{opt} (%)	ρ_{dmax} (kg/m^3)	G_s	%sand	%silt	%clay	USCS
TSC	19.6	13.6	6	13.5	1915	2.68	3	81	16	CL-ML
TLC	25	13	12	12.3	1962	2.69	31	50	19	CL

Note: w_L = liquid limit; w_p = plastic limit; I_p = plasticity index; w_{opt} = optimum moisture content; ρ_{dmax} = maximum dry density; G_s = specific gravity; USCS = Unified Soil Classification System (ASTM D2487-11).

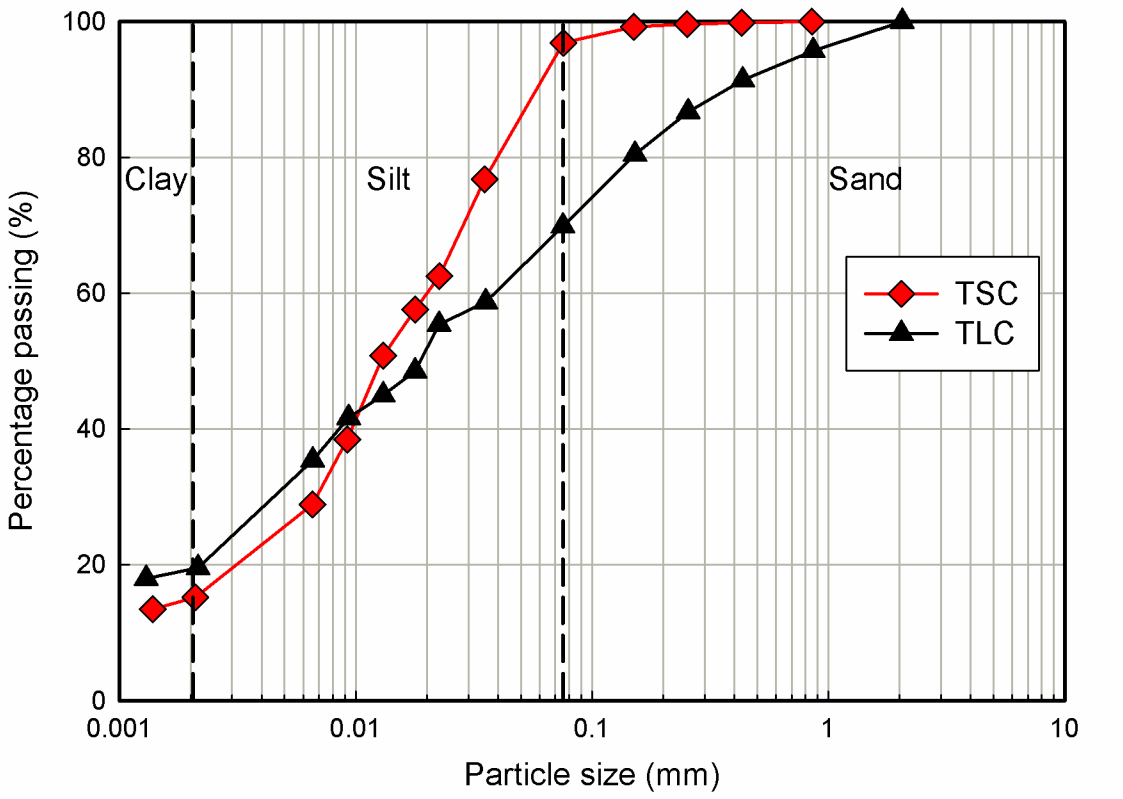

Figure 4.2 Particle size distribution of TSC and TLC

4.4.1 SFCC measurement

Compacted specimens were saturated and used for measuring the SFCC. A pre-calculated

amount of dry soil and tap water were mixed and statically compacted at the optimum moisture content to achieve the maximum dry density by volume control method. The soil specimen was compacted in five equal layers. Each layer was 20 mm high and the final soil specimen was 100 mm in height with a diameter of 50 mm. After compaction, the specimen was securely wrapped with filter paper. A cling wrap with small holes was used to cover the filter paper wrapped specimen. The specimen was then put into plastic tube (which was drilled with small holes and was used to constrain the lateral expansion of the soil specimen) and was submerged in a plastic tank with tap water for saturation. On top of the specimen, a mass of 2 kg was placed to limit its vertical expansion, as shown in **Figure 4.3**. The specimen absorbed water gradually along its height and achieved a constant mass after a period of one week. At this time, the soil specimens were close to fully saturated condition (i.e., 100%). In spite of careful experimental procedures that were followed to prevent specimen expansion during the saturation process, the soil specimen expanded slightly (for TLC: the changes in height and diameter were approximately 0.8% and 1.0%, respectively; for TSC, the changes were insignificant).

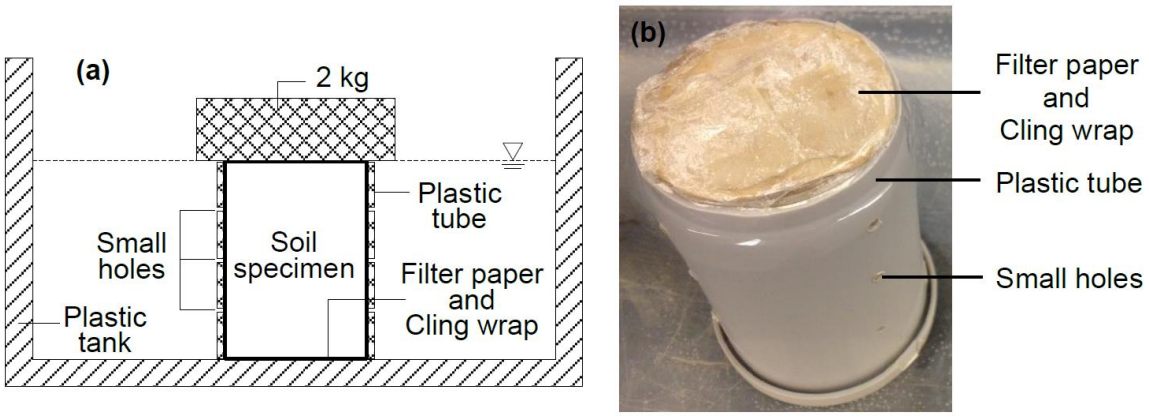

Figure 4.3 (a) Schematic diagram and (b) Photo of the setup for saturating soil specimen

The EC-5 moisture sensor, RT-1 temperature sensor, and EM50 data logger (all manufactured by the METER Group, Inc., Pullman, USA) were used for measuring SFCC of the two soils. The EC-5 can determine volumetric water content by measuring dielectric constant of

the soil using FDR technique. The 70 MHz frequency minimizes salinity and textural effects, making this a reliable sensor for use (with an accuracy better than 0.03 m^3/m^3 in typical soils). The RT-1 is an easy-to-use instrument for reliably measuring soil temperature and has a temperature resolution of 0.1°C. The dimensions of the two sensors are shown in **Figure 4.4**(a). The two sensors were calibrated prior to their use, as summarized in the following section.

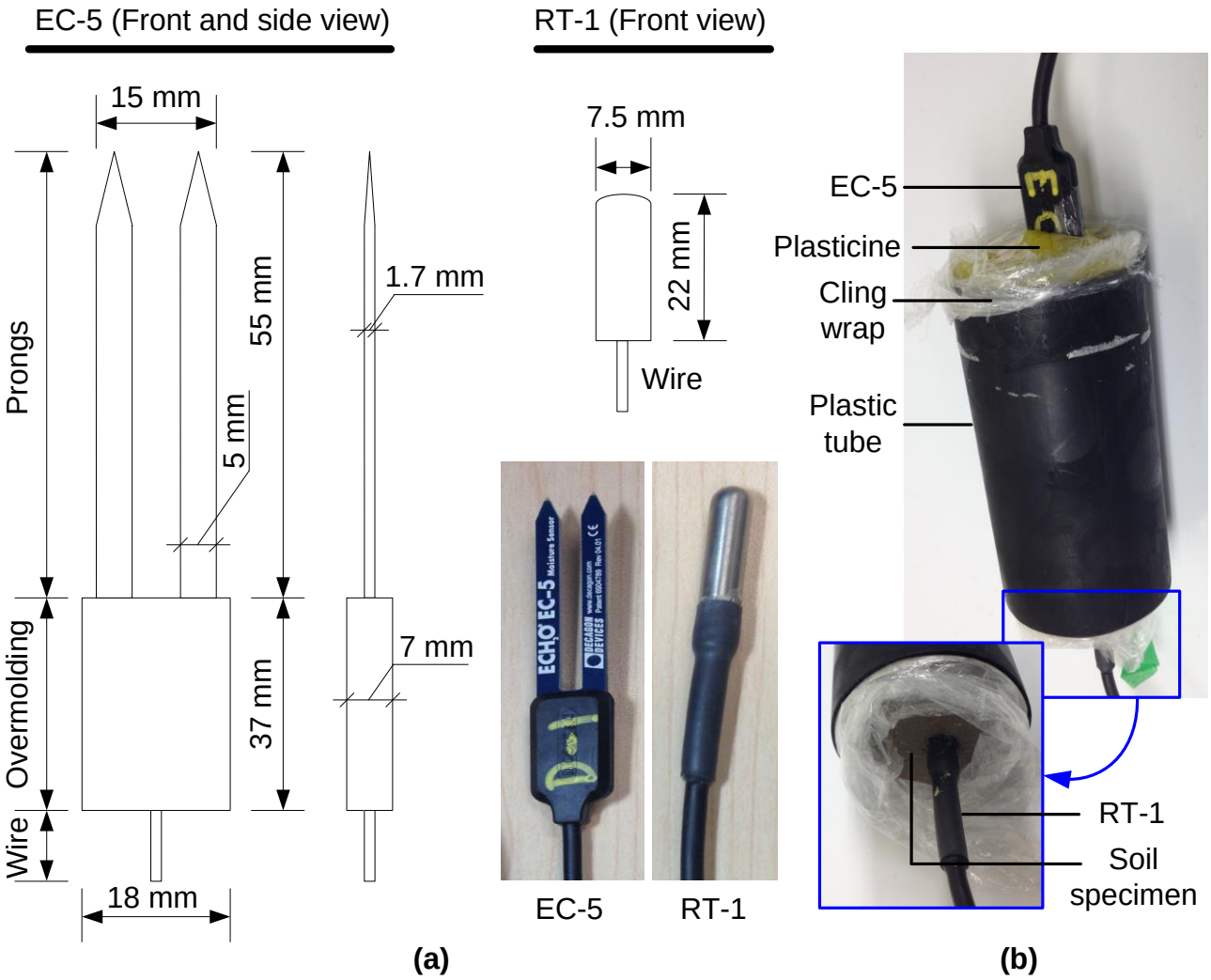

Figure 4.4 Schematic diagram and photo of (a) EC-5 and RT-1, and (b) experimental setup

The RT-1 was inserted into one end of the specimen, and the EC-5 into the other end (with its two prongs completely in the specimen). A small amount of plasticine was pasted around the

overmolding of the EC-5 (see **Figure 4.4**(b)). This was aimed to prevent the direct contact, if any, between the EC-5 prongs and air, which may influence the EC-5 reading. The two sensors were then connected to the EM50 data logger. The time intervals for data collection were typically 5 min and 15 min. The soil specimen was tightly sealed by cling wrap to prevent moisture loss during the testing period. Three-dimensional freezing of the specimen (under zero external stress) was fulfilled by putting it in a freezer, in which the ambient temperature was controlled. In the present study, 14 specimens were tested; of which seven were TSC (labeled as TSC-1 to TSC-7) and the remainder seven were TLC (labeled as TLC-1 to TLC-7). All these specimens were saturated except for TSC-7, which was kept at its initial optimum moisture content. **Table 4.2** summarizes the imposed testing conditions for these specimens. For achieving uniform temperature condition, the soil specimens were kept 12h under each controlled temperature. After 12h, the controlled temperature was changed to next value, following the sequence shown in **Table 4.2**.

Table 4.2 Types of freezing test and controlled temperatures for the TSC and TLC specimens

No.	Controlled temperatures (°C)	Freezing test used
TSC-1	RT, -20.0, -15.0, -10.0, -7.0, -5.0, -3.5, -2.5, -2.0, -1.5, -1.0, -0.5, 0.0, RT	Direct freezing, step thawing
TSC-2	RT, -20.0, -16.0, -12.0, -9.0, -7.0, -5.0, -4.0, -3.0, -2.0, -1.0, 0.0, RT	
TSC-3		
TSC-4	RT, -0.1, -0.5, -1.0, -1.5, -2.0, -2.5, -3.0, -4.0, -6.0, -10.0, -15.0, -20.0, -15.0, -10.0, -6.0, -4.0, -3.0, -1.0, 0.0, RT	Step freezing, step thawing
TSC-5		
TSC-6	RT, -0.5, -0.8, -1.0, -1.5, -2.0, -2.5, -3.0, -3.5, -4.0, -5.0, -7.0, -10.0, -15.0, -20.0	Step freezing
TSC-7		
TLC-1	Same as for TSC-1	Direct freezing, step thawing
TLC-2	Same as for TSC-2 and TSC-3	
TLC-3		

TLC-4	RT, -0.5, -0.8, -1.0, -1.5, -2.0, -2.5, -3.0, -3.5, -4.0, -5.0, -7.0, -10.0, -15.0, -20.0, -15.0, -10.0, -7.0, -5.0, -3.5, -2.5, -2.0, -1.5, -1.0, -0.5, 0.0, RT	Step freezing, step thawing
TLC-5		
TLC-6	RT, -0.5, -1.0, -1.5, -2.0, -2.5, -3.0, -3.5, -4.0, -4.5, -5.0, -7.0, -10.0, -15.0, -20.0, -15.0, -10.0, -7.0, -5.0, -4.5, -4.0, -3.5, -3.0, -2.5, -2.0, -1.5, -1.0, -0.5, RT	Step freezing, step thawing
TLC-7		

Note: RT: Room temperature, around 23 °C.

Two freezing methods (i.e. direct freezing and step freezing) were used to freeze the specimens, and the specimens were then gradually thawed under different temperatures for determining SFCC. For example, specimens TSC-1 to TSC-3 (initially at room temperature, which was around 23 °C) were directly exposed to -20 °C. The controlled temperature was then gradually increased until it reached back to room temperature. The thawing branch of SFCC was measured using this technique. For specimens TSC-4 and TSC-5, the controlled temperature was gradually decreased from room temperature to -20 °C and was then increased back to room temperature. In other words, both the freezing and thawing branches of SFCC were obtained. Specimens TSC-6 and TSC-7 were only subjected to step decreasing temperatures, facilitating the measurement of the freezing branch of SFCC.

4.4.2 Sensors calibration

For calibrating the EC-5 moisture sensor, four TLC cylindrical specimens were compacted at its optimum moisture content (i.e. 12.3%), with dimensions of 100 mm in length and 50 mm in diameter. After compaction, one specimen was dried and the other three were wetted by covering them with dry and wet filter paper, respectively. The final gravimetric water contents of the four specimens were determined by oven dry method as 14.68%, 13.87%, 13.01%, and 11.96%. The corresponding volumetric water contents were calculated as 0.280 m^3/m^3, 0.266 m^3/m^3, 0.252 m^3/m^3, and 0.234 m^3/m^3, respectively, based on the measured dry soil mass and volume of the specimens (i.e., volumetric water content = gravimetric water content * dry soil mass / volume). The volumetric water contents of the four TLC specimens at room temperature, 15 °C, 10 °C, 6 °C, and 2 °C were measured by the EC-5. During this process, the water contents of the four

specimens were kept unchanged by tightly sealing them with cling wrap and storing them in plastic container. From the results summarized in **Figure 4.5**(a), it can be observed that under constant water content condition, the measured volumetric water content by EC-5 decreases against the controlled temperature. This suggests that above 0 °C, temperature change influences the EC-5 reading. The relationship between the calculated volumetric water content and the measured value for the soil specimen under each controlled temperature can be derived from these results. In the present study, a linear relationship (i.e. calculated volumetric water content = A * measured volumetric water content + B) was used to best-fit the data points. The constants A, B and coefficient of determination (R^2) for the five controlled temperatures are summarized in **Table 4.3**. For SFCC measurement in the present study, when the temperature of soil specimen was above 0 °C, the volumetric water content measured by EC-5 (i.e. total water content) was calibrated by using these relationships. For example, if the soil specimen achieved equilibrium under room temperature (or 2 °C), the linear relationship obtained for room temperature (or 2 °C) was used to calibrate the EC-5 measured volumetric water content.

Table 4.3 EC-5 calibration constants *A* and *B*

Temperature	*A*	*B*	R^2
Room temperature	0.5200	0.1134	0.99
15 °C	0.5158	0.1331	1.00
10 °C	0.5983	0.1217	0.99
6 °C	0.6347	0.1182	0.95
2 °C	0.6372	0.1223	0.94

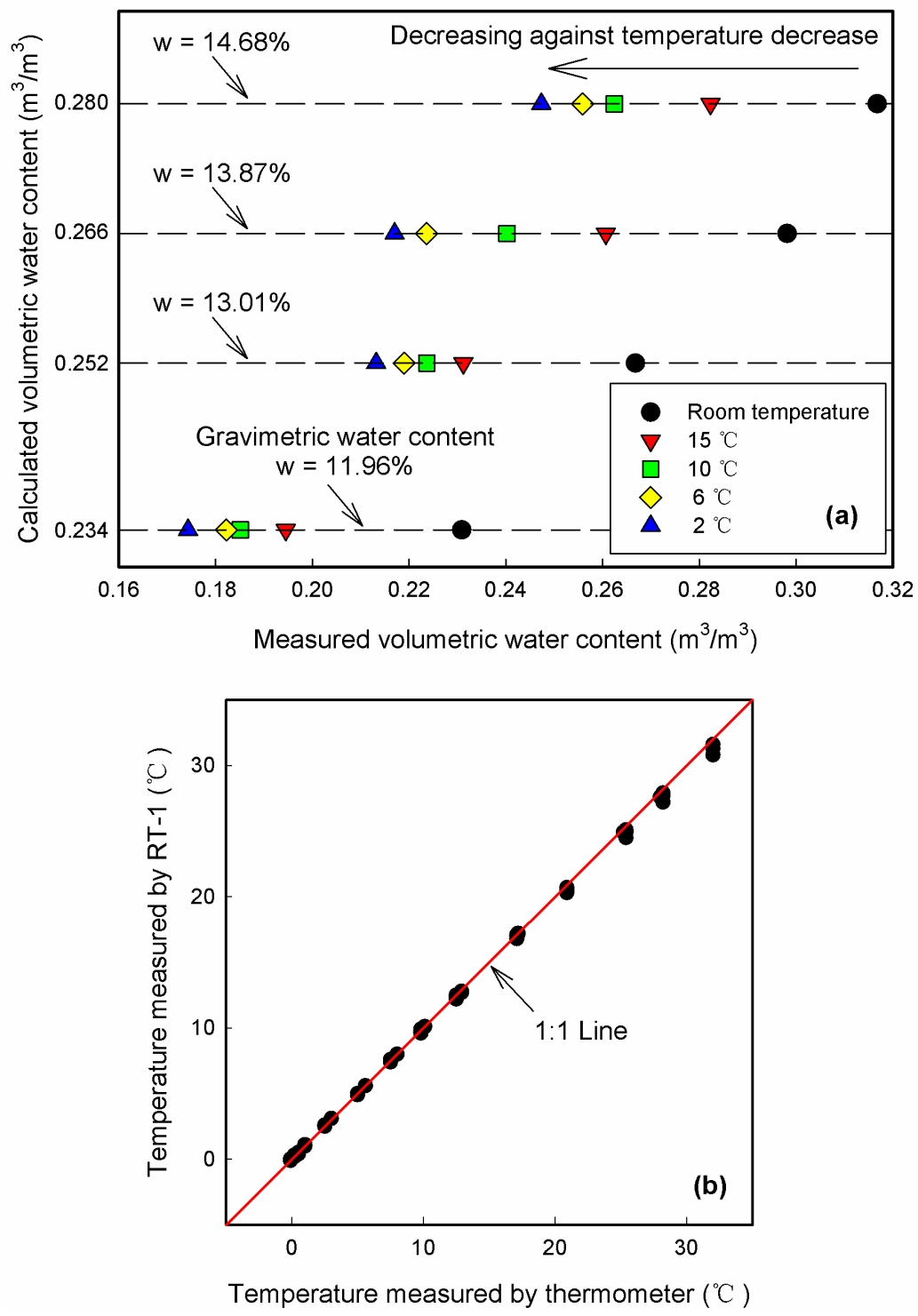

Figure 4.5 (a) The calculated and measured volumetric water contents of four TLC specimens under different temperatures, and (b) temperatures measured by thermometers and RT-1

On the other hand, when the soil specimen was under subzero temperatures (i.e. frozen condition), no direct calibration was carried out due to the lack of reliable equipment for quantifying unfrozen water and ice contents in the soil specimen. However, Smith and Tice (1988) conducted unfrozen water content test on various types of soils by using TDR and NMR. A general relationship was found between the measured apparent dielectric constant (K_a) by TDR and the measured unfrozen water content by NMR for these soils. This relationship (Eq. (4.1)) was used in the present study for obtaining the volumetric unfrozen water content (θ_u) under subzero temperatures based on K_a of the soil specimen, which can be determined from EC-5 raw output according to the manufacturer.

$$\theta_u = -1.458\times10^{-1} + 3.868\times10^{-2}K_a - 8.502\times10^{-4}K_a^{\,2} + 9.920\times10^{-6}K_a^{\,3} \qquad (4.1)$$

The calibration of the RT-1 temperature sensor was done by comparing the measured values with two thermometers. A couple of different temperature values were selected and the results are shown in **Figure 4.5**(b). It can be seen that the measured temperature values by RT-1 are close to the values measured by the two thermometers (data points are closely located along the 1:1 line), suggesting that RT-1 provided good accuracy.

4.4.3 SWCC measurement

Three different methods, namely, pressure plate method (ASTM D6836-16), vapor equilibrium method (Fredlund et al., 2012), and WP4-T measurement (ASTM D6836-16), were used for determining the SWCC of the two soils, as shown in **Figure 4.6**. For the first two methods, saturated compacted specimens were used. Similar procedure that was used for preparing SFCC specimens (i.e. compaction and saturation) was followed for preparing the required specimens. The dimension of the specimen used for the pressure plate method was 63 mm in diameter and 20 mm in height. A small piece of the saturated specimen was cut and used for the vapor equilibrium method. For the WP4-T measurement, certain amounts of dry soil and tap water were mixed to prepare wet soil aggregates with different initial water contents. The wet

soil aggregates (with sizes typically lower than 2 mm) were stored in plastic bags for two days to achieve uniform moisture distribution, which were used for measurement.

Figure 4.6 Three methods used for SWCC measurement: (a) Pressure plate method, (b) Vapor equilibrium method and cut saturated specimen, and (c) WP4-T measurement and wet soil aggregates

The ceramic disk with an air-entry value of 500 kPa was used in the pressure plate extractor (Soil-moisture Equipment Corp., California, USA). The air pressures ranging from 10

kPa to 300 kPa were applied while the pore water pressure was kept at the atmospheric pressure for gathering SWCC data. Each applied air pressure was maintained at least for seven days for achieving equilibrium condition. For the vapor equilibrium method, three different solutions were used, i.e. $CuSO_4 \cdot 5H_2O$, K_2SO_4 and NaCl, which approximately correspond to the total suction values of 1.9 MPa, 4.4 MPa and 38 MPa, respectively. The saturated specimen was kept in desiccator for three months, ensuring the soil pore water equilibrated with the solution vapor. The WP4-T device (METER Group, Inc., Pullman, USA) was calibrated by using the standard KCl solution provided by the manufacturer. The suction measurement for the wet soil aggregates with different water contents was carried out at the temperature set in the WP4-T chamber, which was 25 °C. The gravimetric water content was determined from these three methods using oven dry method. The osmotic suction of the soil specimens (i.e. 6 kPa, calculated by using the van't Hoff equation (Fredlund et al., 2012)) was assumed negligible, due to the low solute concentrations in the tap water (Jiang et al., 2017).

4.5 Experimental results

4.5.1 Temperature – time curves of the two soils

Figure 4.7(a) shows the temperature - time curves of TSC-1, TSC-2 and TSC-3, under direct freezing and step thawing condition. There is distinct supercooling phenomenon as can be seen from the inset of **Figure 4.7**(a). However, the phase change part is not well defined because only certain amount of pore water can transform into ice at the freezing temperature of soil specimen. The corresponding latent heat released therefore could not fully counteract the cooling effect exerted by the controlled temperature, which is low (i.e. -20 °C). The temperature - time curves of TLC-1, TLC-2 and TLC-3 under direct freezing and step thawing condition are similar to those of the TSC specimens. For direct freezing and step thawing condition, the volumetric unfrozen water content of soil specimen under each thawing temperature was measured. As a result, the thawing branch of SFCC was obtained.

Figure 4.7(b) shows the temperature - time curves of specimens TSC-4 to TSC-7 under

step freezing / step thawing condition. For TSC-4 and TSC-5, their temperature - time curves appear to be the same (due to the same controlled temperatures), except for the different supercooling temperatures and the time when ice starts nucleation. Similarly, TSC-6 and TSC-7 have approximately the same temperature - time curve; in spite of the latter was at the optimum moisture rather than saturated condition. However, it should be noted that TSC-7 has lower supercooling and freezing temperatures than TSC-6. In addition, the temperature increment of TSC-7 is lower than that of TSC-6. This is reasonable since initially more water existed in the soil pores of saturated specimen and therefore larger amount of latent heat was generated and contributed to the temperature rise within the soil specimen. Similar conclusions can be drawn for the four saturated TLC specimens (i.e. TLC-4 to TLC-7) under step freezing and thawing condition (shown in **Figure 4.8**). Under step freezing and thawing condition, both the freezing and thawing branches of SFCC were measured.

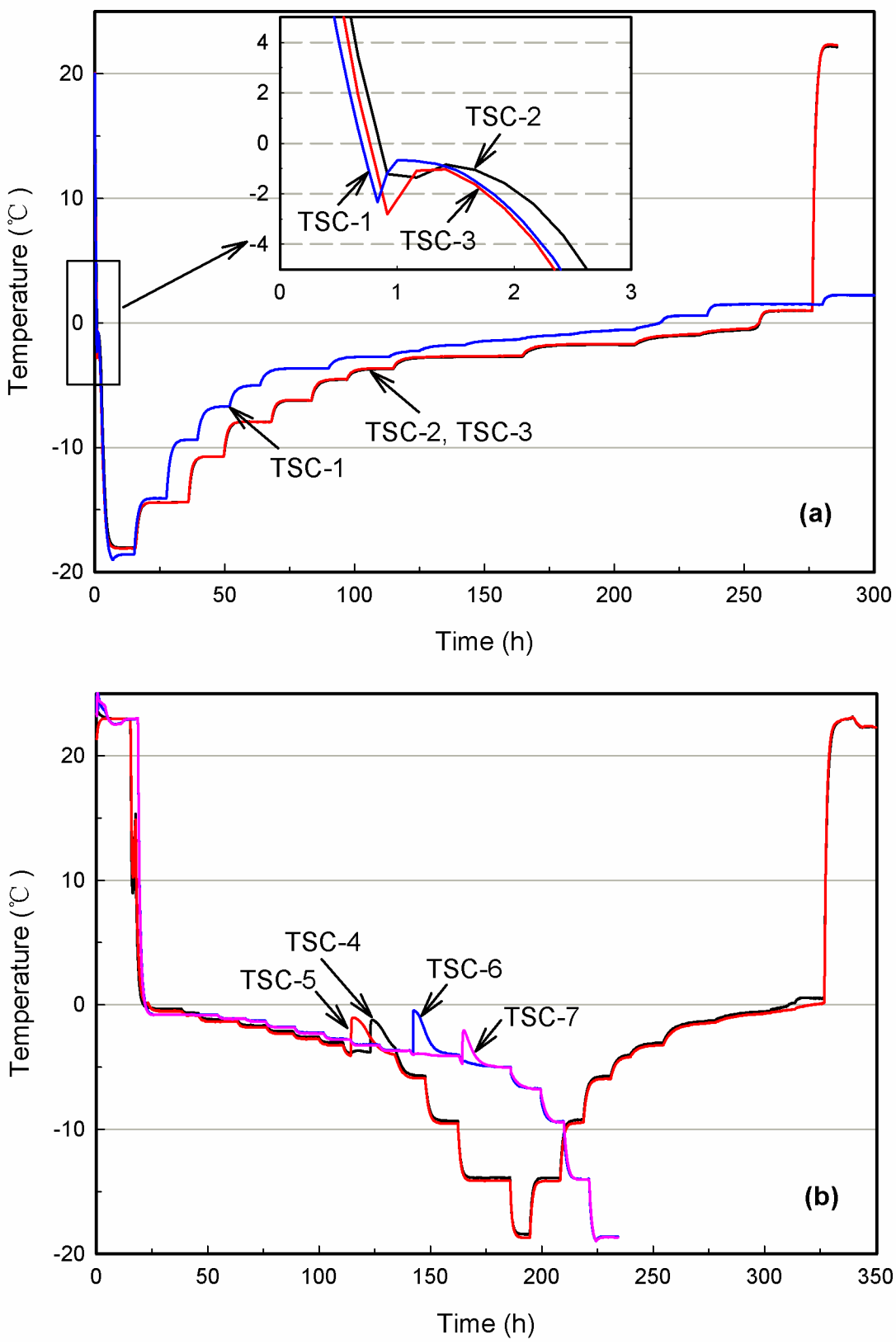

Figure 4.7 Temperature – time curves of (a) TSC-1 to TSC-3, and (b) TSC-4 to TSC-7

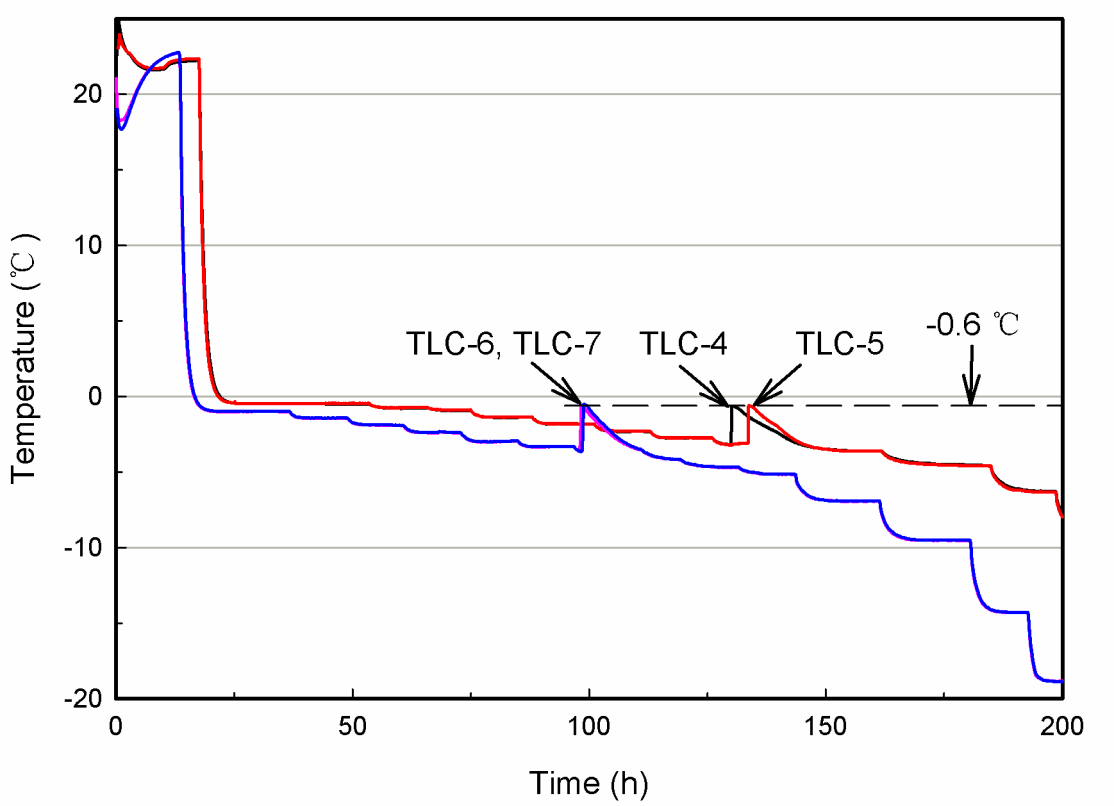

Figure 4.8 Temperature – time curves of TLC-4 to TLC-7

In the present study, the freezing temperature of soil specimen was determined based on its temperature - time curve (i.e. the highest temperature after supercooling). Under the direct freezing condition, the soil specimen (initially at room temperature) was directly exposed to -20 °C. Therefore, the temperature change in the soil specimen was dramatic during the initial period of freezing. Since the time interval for data collection was 15 min for some tests, it was likely that the RT-1 did not capture the actual freezing temperature (the highest point after supercooling), but measured the temperature values that were close to the freezing temperature. On the other hand, the controlled temperature in the step freezing condition was gradually decreased (i.e. temperature change rate was low). There was relatively well-defined phase change period (the soil specimen maintained at the same temperature for approximately 1 hour). This indicates that the freezing temperature under step freezing condition can be reliably determined.

The supercooling and freezing temperatures of the specimens under step freezing condition are summarized in **Table 4.4**. The supercooling temperatures of the two soils are scattered due to the random nature of supercooling. The saturated TSC specimens show fluctuation with respect to freezing temperature. This may be attributed to specimen structure change during the saturation process and crack formation when inserting sensors into the specimen, which contribute to differences between specimens. On the other hand, the freezing temperatures of TLC specimens are more consistent with a value around -0.6 °C (see **Figure 4.8**). This suggests that better integrity was achieved with TLC during the testing process and hence its experimental results experienced relatively limited fluctuation.

Table 4.4 Supercooling and freezing temperatures of the specimens tested under step freezing condition

	TSC-4	TSC-5	TSC-6	TSC-7
Supercooling temperature (°C)	-3.8	-4.1	-3.9	-4.8
Freezing temperature (°C)	-1.2	-1.0	-0.5	-2.0
	TLC-4	TLC-5	TLC-6	TLC-7
Supercooling temperature (°C)	-3.2	-3.1	-3.6	-3.6
Freezing temperature (°C)	-0.6	-0.6	-0.6	-0.5

Note: TSC-7 was at the optimum moisture content.

4.5.2 Results of SFCC measurement

The measured SFCC of TSC and TLC are summarized in **Figure 4.9** and **Figure 4.10**. The corresponding open data point is the initial volumetric water content of each specimen calculated based on its gravimetric water content and maximum dry density before testing. **Figure 4.9**(a) and **Figure 4.10**(a) show the thawing branch of SFCC of the two soils respectively. It can be seen that the unfrozen water content changes rapidly in the temperature range from 0 to -5 °C, after which the unfrozen water content gradually levels off. The rapid change in unfrozen water content is attributed to the phase change of capillary and adsorbed water in relatively large pores. With a further decrease in temperature, most of the pore water is frozen, and the strongly

adsorbed water and those confined in small pores (which have low matric potential) gradually transform into ice. It is also noted that the measured thawing branches of TSC are not consistent, which may be partly attributed to the structure change of TSC specimen, and its poor ability of maintaining water during experimental process. On the other hand, the measured thawing branches of TLC are relatively consistent, especially for the low temperature range. This is reasonable since the TLC specimen was typically intact and did not crack during the testing period.

The freezing and thawing branches of SFCC of the two soils are shown in **Figure 4.9**(c) and **Figure 4.10**(b), respectively. It can be seen that unfrozen water content is relatively stable (i.e. around the measured initial water content since no ice was formed) until the supercooling temperature is achieved. As ice crystals start to nucleate and continue to grow in soil pores, the quantity of unfrozen water drops dramatically. Finally, when most capillary and adsorbed water turned into ice, unfrozen water content decreases with a gentle slope and gradually levels off. On the contrary, the thawing branch of SFCC is smooth and does not show abrupt change in unfrozen water content or superheating phenomenon (Tan et al., 2015). Therefore, significant hysteresis is observed between the freezing and thawing branches. For the two soils under the present experimental conditions, hysteresis occurs mainly in the temperature range from 0 to -5 °C. After -5 °C, hysteresis is insignificant.

Figure 4.9(b) shows the freezing branch of SFCC of TSC. This is similar to the freezing branch shown in **Figure 4.9**(c). It is interesting to note that the freezing branch of SFCC is supposed to behave as the line shown with dashes in **Figure 4.9**(b). It means that soil specimen temperature would change to its freezing temperature (i.e. ice-entry value (IEV), at which ice first begins to form in the largest soil pores) from the supercooling temperature due to the release of latent heat. The freezing temperature is theoretically maintained for a short period while unfrozen water content plunges. Afterwards, unfrozen water content gradually decreases with the decrease in soil temperature. However, in reality as ice crystals form in large soil pores, the amount of latent heat released is small and not able to maintain soil temperature at the freezing

temperature (for a period that is long enough to ensure equilibrium condition that facilitates reliable measurement) since the ambient temperature inside the freezer at this time is relatively low (i.e. around the supercooling temperature). Instead, the soil temperature keeps decreasing until an equilibrium condition is achieved under the current controlled temperature (e.g., see **Figure 4.8**). As a result, the unfrozen water content during this period could not be reasonably measured, as equilibrium condition is not fully established. In other words, the theoretical freezing branch shown in **Figure 4.9**(b) is not measurable in the present study.

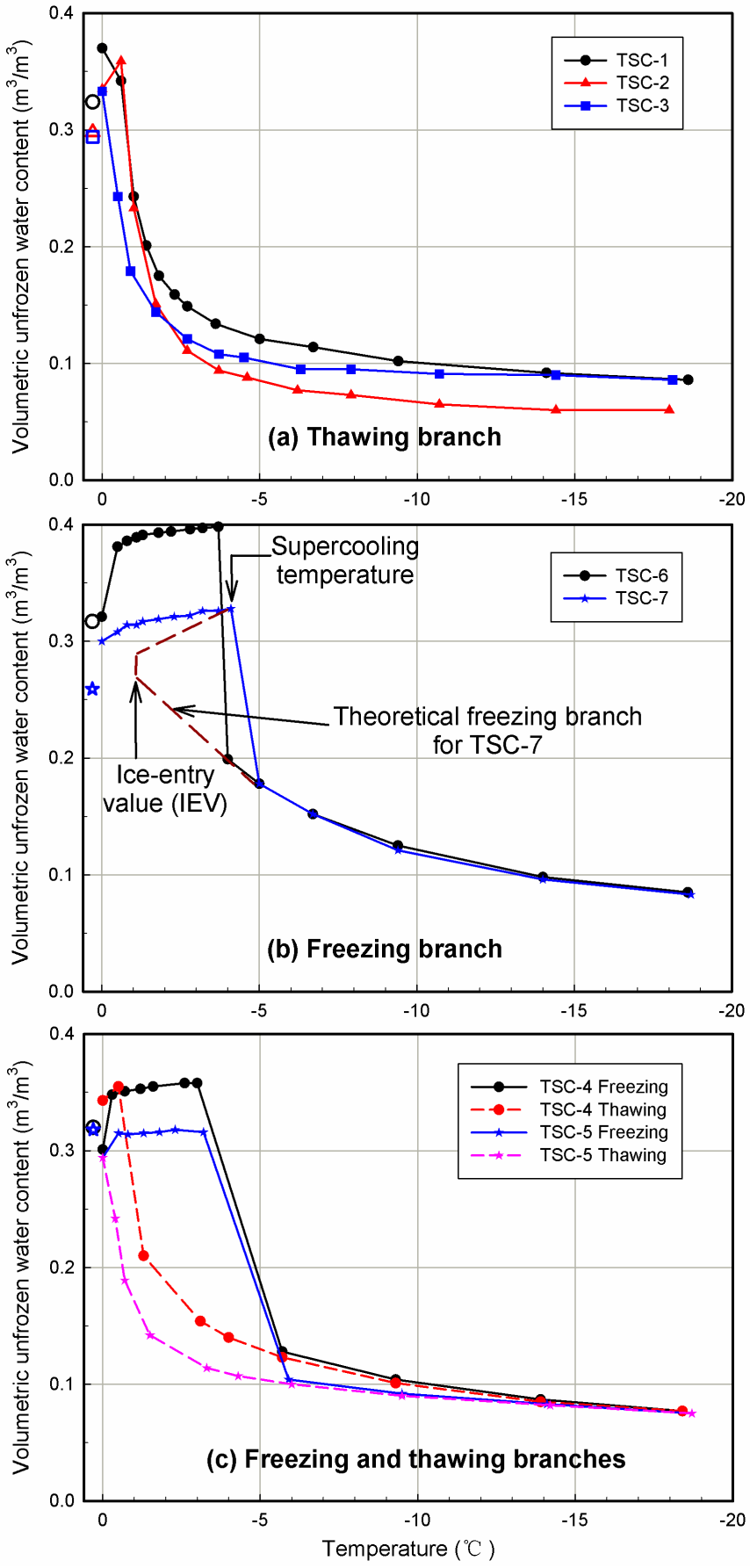

Figure 4.9 (a) Thawing branch, (b) Freezing branch, and (c) Freezing and thawing branches of TSC (Open data points: see text)

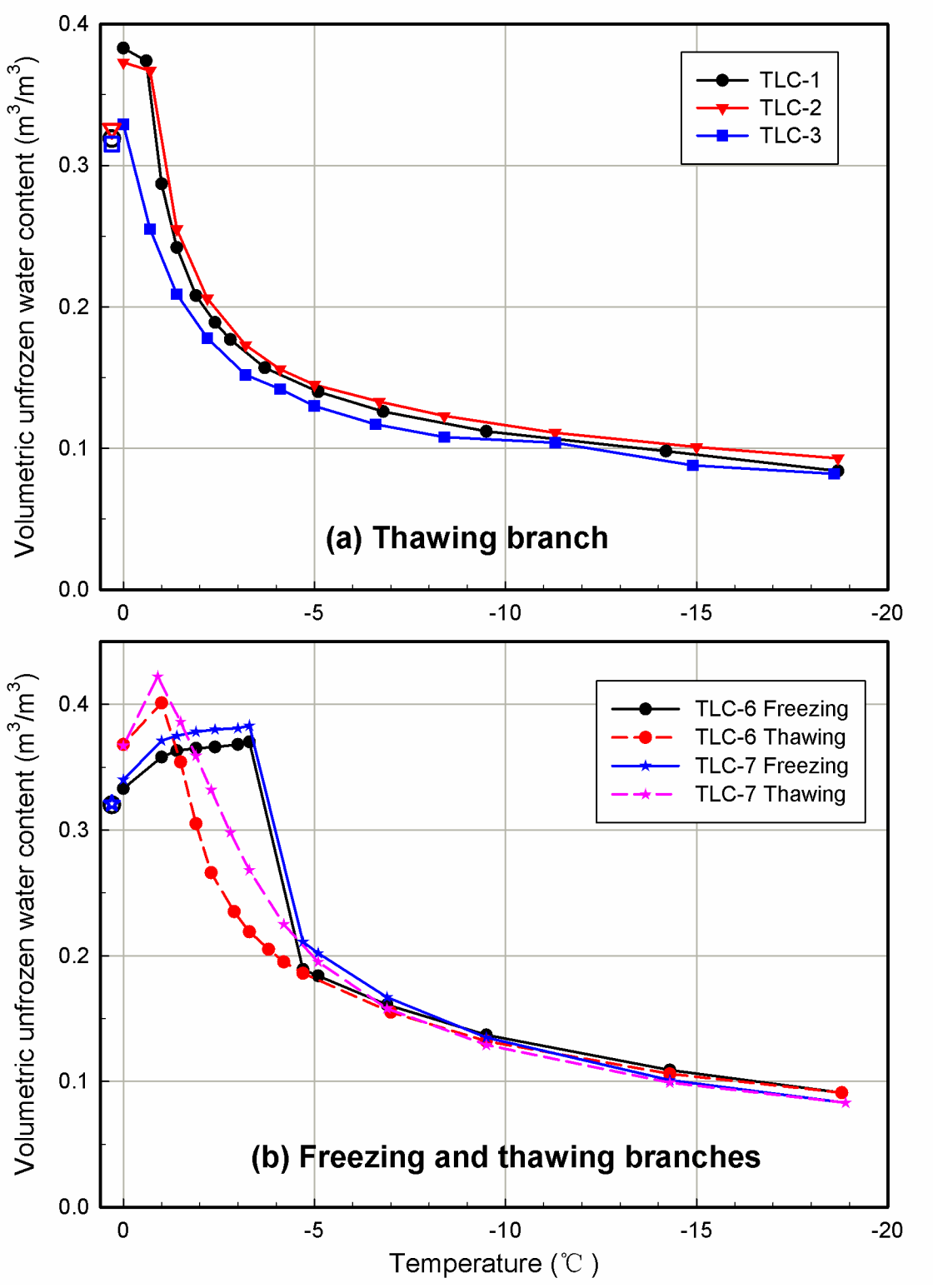

Figure 4.10 (a) Thawing branch, and (b) Freezing and thawing branches of TLC (Open data points: see text)

4.5.3 Results of SWCC measurement and its comparison to SFCC

The SWCC of the two soils are shown in **Figure 4.11**. It can be seen that the data points measured by the three methods are consistent and form a smooth curve (especially for TLC) in spite of some scatter in the data. This suggests that the measured SWCC is reliable. Comparison between SWCC and the three thawing branches of SFCC of the two soils (i.e. TSC-1 to TSC-3, and TLC-1 to TLC-3) are shown in **Figure 4.12**. The gravimetric water content obtained in SWCC measurement is converted to volumetric water content by multiplying by the maximum dry density of each soil shown in **Table 4.1** (assuming that the volume of specimens was unchanged during SWCC measurement). The measured subzero temperature is converted to cryogenic suction by multiplying by 1225 kPa/°C, as suggested by Ren and Vanapalli (2018). It can be observed from **Figure 4.12** that the measured SWCC does not agree well with the SFCC. The suction value obtained from SWCC is lower than that obtained from SFCC at the same unfrozen water content. The disagreement cannot be compensated by multiplying the cryogenic suction by an adjustment factor of 2.2, because it introduces more discrepancy to the two retention curves. In other words, there is only qualitative but no quantitative similarity between SWCC and SFCC for the two soils under the investigated experimental conditions. The discrepancy can be partly attributed to the slightly different initial water contents of the specimens used for SWCC and SFCC measurements, and to possible errors associated with the sensors.

The measured SWCC and SFCC were fitted using the Fredlund and Xing (1994) equation. The fitted curves are shown in **Figure 4.12** and the fitting parameters (i.e. a_f, n_f, m_f, and ψ_r) are summarized in **Table 4.5**. It can be seen that the Fredlund and Xing (1994) equation provides good fitting for both the SWCC and SFCC of the two soils. However, the fitting parameters for the two retention curves of the same soil are different, especially with respect to the slope of the retention curves (controlled by parameter n_f) and the residual suction value (ψ_r).

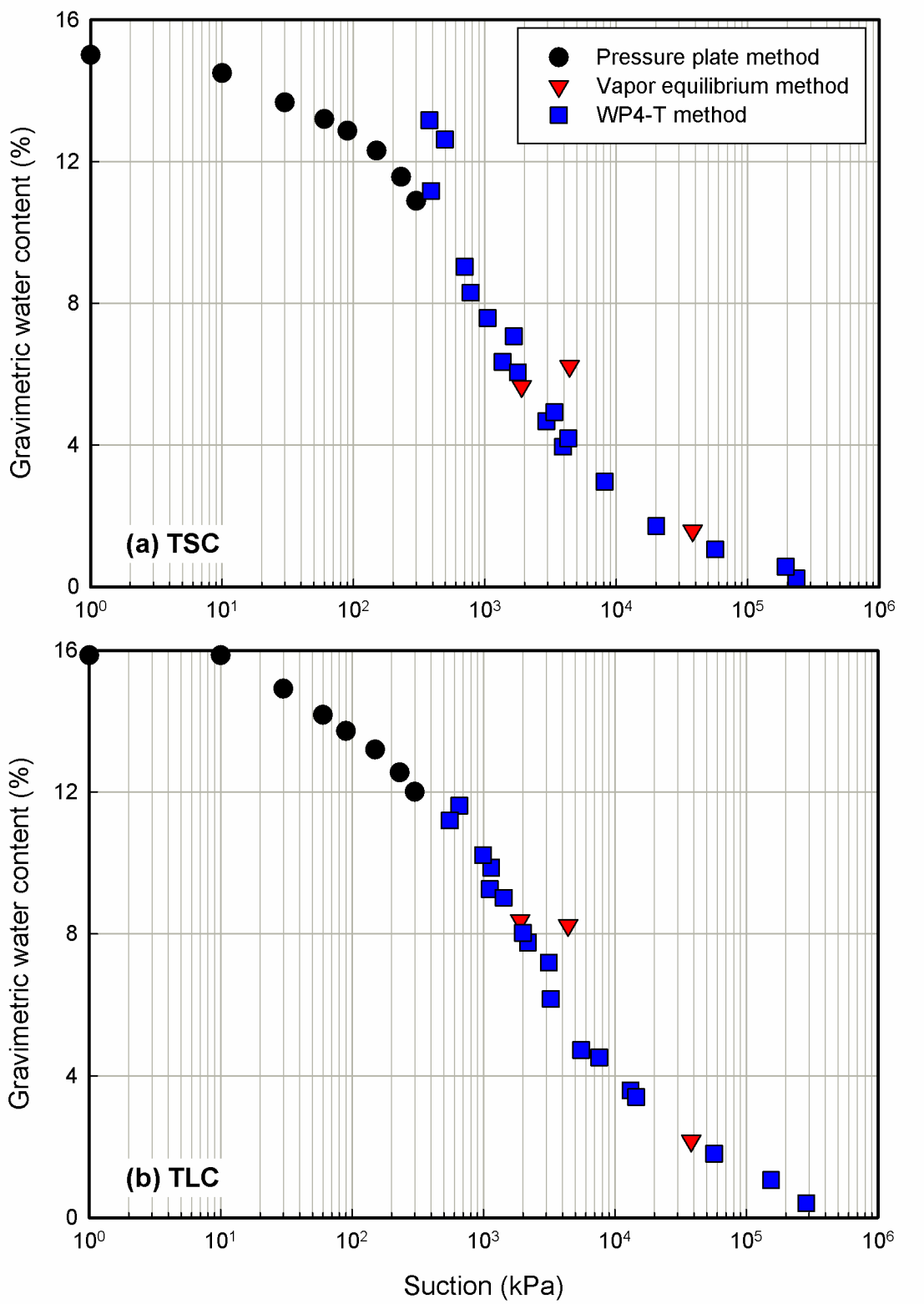

Figure 4.11 Measured SWCC of (a) TSC and (b) TLC

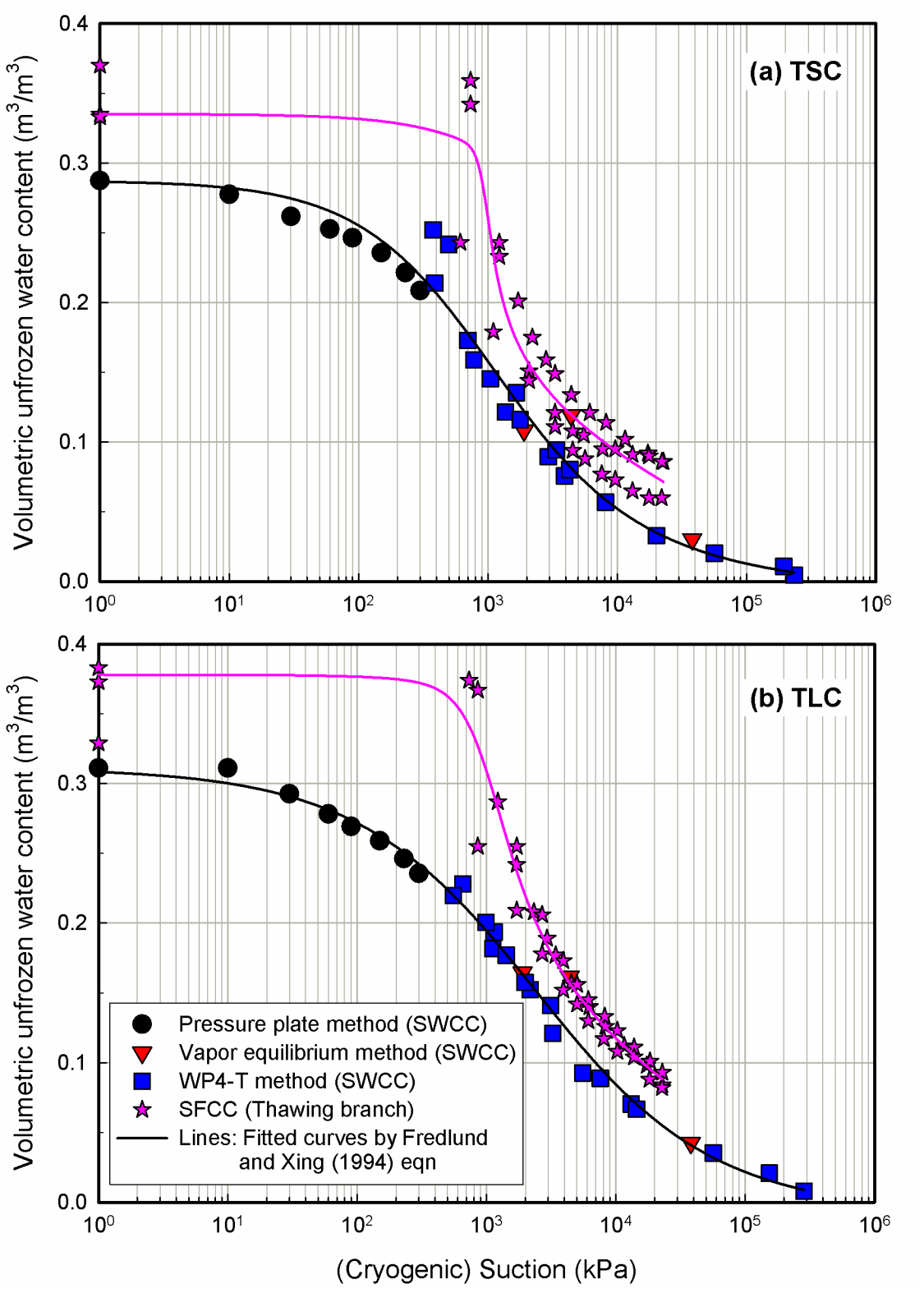

Figure 4.12 Comparison between the thawing branch of SFCC and SWCC of (a) TSC and (b) TLC

Table 4.5 Fitting parameters for SWCC and SFCC using Fredlund and Xing (1994) equation

	a_f	n_f	m_f	ψ_r	R^2
TSC-SWCC	665	0.81	1.41	904	0.96
TSC-SFCC	895	11.91	0.27	1447	0.92
TLC-SWCC	1217	0.59	1.67	2718	0.99
TLC-SFCC	876	3.34	0.45	5189	0.95

4.6 Discussion

4.6.1 Measurement of SFCC

The reliable measurement of SFCC depends on the accurate determination of temperature and unfrozen water content. The difficulties in accurately measuring temperature are not only associated with the resolution and precision requirement for the temperature sensor (the resolution of RT-1 is 0.1 °C, which is considered sufficient for an accurate temperature measurement), but also with the time required to achieve uniform temperature within the bulk soil specimen. If this is not achieved, the measured temperature may only be the temperature of soil surrounding the temperature sensor. Moreover, during the freezing process, once ice has started nucleation, soil temperature changes relatively fast under the low controlled temperature (see **Figure 4.7** and **Figure 4.8**). Therefore, during this period, the reliable measurement of unfrozen water content is difficult since equilibrium condition is not fully established.

A number of concerns have to be addressed carefully with respect to the measurement of unfrozen water content. Firstly, temperatures above 0 °C were observed to have influence on EC-5 reading. Hence, the total water content needs to be calibrated taking into account the influence of temperature at which it is measured. In addition, the EC-5 was calibrated by using four TLC specimens at different water contents. The resulting calibration curves were used for both the TLC and TSC specimens. However, specific calibration for TSC is suggested for reliable determination of its SFCC. Secondly, the measurement of dielectric constant in frozen soils is influenced not only by water content, but also by other parameters, which include ice

content, soil structure and bulk density that influence the sensor's performance (Yoshikawa and Overduin, 2005). The water content at which soil specimen is compacted, imparting a particular soil structure, would have significant influence on the measured SFCC. Thirdly, unfrozen water content in high subzero temperature range (e.g., from 0 to -5 °C) shows significant change with respect to temperature. For this reason, more precautions are required in this temperature range such that the measured SFCC is reliable. Fourthly, the accuracy of EC-5 sensor is about 0.03 m^3/m^3, which may result in considerable difference between the measured and actual unfrozen water content, especially when the soil temperature is low. In addition, the use of plasticine for covering the overmolding of EC-5 should be avoided in future studies since the plasticine has high water content, which can likely contribute to additional experimental error. Finally, pore water supercooling during the freezing process causes significant hysteresis of SFCC. The hysteresis measured in the present study is also mainly attributed to this reason. It is difficult to obtain representative freezing branch of SFCC since the degree of supercooling may be influenced by many factors such as freezing rate, presence and concentration of solutes, and electromagnetic fields exerted by EC-5. Due to this reason, comparisons were not provided between SWCC and the freezing branch of SFCC in the present study.

4.6.2 Concerns regarding the similarity between SFCC and SWCC

Several researches have shown similarities between SFCC and SWCC for several soils (Koopmans and Miller, 1966; Spaans and Baker, 1996; Watanabe and Wake, 2008; Liu et al., 2012; Schafer and Beier, 2017). Good agreement was also observed between the measured soil water potential or subzero temperature with the one obtained from the Clapeyron equation (Watanabe et al., 2012; Caicedo, 2016). However, several investigators have also obtained results showing dissimilarity between SFCC and SWCC.

For example, Ma et al. (2015) measured both the SWCC and SFCC of a silt and a clay. The soil specimens were statically compacted at specified water contents and to targeted dry densities. The unfrozen water content was obtained by using NMR. In order to avoid the effect of

supercooling, only the thawing branch of SFCC was measured. The soil water potential of the frozen soil is derived from a generalized Clapeyron equation. The results show that at the same unfrozen water content, the soil water potential of an unsaturated soil is significantly lower than that of its frozen counterpart, which means that there is no similarity between SFCC and SWCC. In the study by Azmatch et al. (2012), the SWCC and SFCC of the Devon silt specimens with and without salinity were measured. The specimens prepared from slurry were consolidated under different pressures. The unfrozen water content was measured by using TDR. The results display significant discrepancy between SWCC and SFCC of the specimen with salinity. This suggests that the tap water used in the present study may have contributed to the observed discrepancy between SFCC and SWCC of the two investigated soils due to the influence of various ions (i.e., water salinity).

In the present study, the slightly different initial water contents of the specimens used for SWCC and SFCC measurements, and the accuracy of EC-5 may be the major reasons for the dissimilarity between the measured SFCC and SWCC. In other words, the limitations associated with testing sensors prohibit a reliable characterization of the quantitative similarity between the two retention curves. However, besides the experimental limitations, some more concerns with respect to the similarity between SFCC and SWCC are summarized below.

Firstly, it is important to understand the temperature range within which the similarity between SFCC and SWCC could be achieved. The classic work by Koopmans and Miller (1966) experimentally showed the similarity within a narrow temperature range (i.e. from 0 to -0.2 °C). It should also be noted that their results were based on certain assumptions (Miller, 1980), in addition to following careful specimen preparation and experimental procedures. Williams (1976) stated that the free energy of soil unfrozen water, calculated from the Clapeyron equation, is essentially equivalent to the negative pore water pressure before temperature lower than -1.5 °C. This suggests that using the Clapeyron equation to convert subzero temperature to cryogenic suction and adopting the latter for the comparison of SFCC and SWCC is applicable, in the temperature range between 0 °C to about -1.5 °C. Brown and Payne (1990) also concluded that

in the absence of solutes, the Schofield (1935) equation (which is a simplified form of the Clapeyron equation) relating cryogenic suction to subzero temperature can be used at least down to -0.73 °C and almost certainly to several degrees lower without serious error. It has also been shown that in fine glass capillary tube at temperatures near 0 °C, ice-water interface has a hemispherical appearance with zero contact angle at the walls (Skapski et al., 1957). This is the same as air-water interface in a capillary tube (Miller, 1980). Ma et al. (2015) pointed out that the Clapeyron equation is valid for phase equilibrium state where pressure and temperature remain constant with respect to time. Sufficiently slow freezing or thawing rate is required to ensure equilibrium condition. Freezing or thawing at a relatively fast rate will lead to significant discrepancy between SFCC and SWCC (Liu et al., 2012). In addition, fast freezing may cause ice crystals to form in smaller pores first (Colbeck, 1982), rather than typically assumed that ice fills larger pores first in frozen soils (Williams, 1999).

Secondly, it is difficult to precisely control temperature around 0 °C from typical experimental studies. For this reason, there are difficulties associated with the reliable SFCC measurements at high subzero temperatures (i.e. small suction range). In addition, the determination of SWCC becomes increasingly inaccurate as soil dries (i.e. large suction range). Therefore, the quantitative comparison between SFCC and SWCC in these two ranges is questionable. For example, coarse-grained soils generally have an air-entry value of a few kilopascals. According to the Clapeyron equation (e.g., using a value of 1225 kPa/°C for conversion), a suction value of 8 kPa corresponds to a temperature value around -0.007 °C, which is difficult to be accurately measured or controlled. This causes difficulty in comparing the air-entry value and ice-entry value of a soil.

Thirdly, Black and Tice (1989) showed that the SFCC and SWCC data of Windsor sandy loam could be best fitted by one single equation. They achieved better results when the soil specimens used for SFCC and SWCC measurement had approximately the same densities. However, worse results were obtained when there was a difference between the densities. It was also suggested that the SFCC of frozen saturated soils and SWCC of unfrozen unsaturated soils

are comparable only for the same soil at the same bulk density and with similar histories. In other words, theoretically, only freezing and drying curves or thawing and wetting curves can be compared. In addition, the soil must meet similar structure requirements as proposed by Miller and Miller (1956). Konrad (1990) concluded that the unfrozen water content of a given soil is strongly dependent upon the soil structure. This is similar to the influence of soil structure on the SWCC (Vanapalli et al., 1999). Therefore, the difference between the structures of the SWCC and SFCC specimens in the present study (due to slight variation in compaction water content and uncontrollable structure changes during the saturation process) is possibly another important factor that contributed to the dissimilarity.

Finally, some fundamental differences may also contribute to the dissimilarity between the SFCC and SWCC. Williams (1968) showed that there are at least three distinct processes by which air may replace water in soil pores: (i) a process explained by normal capillary equation for air-water interface, (ii) a process involving diffusion of external air to entrapped air bubbles, which are then slowly enlarged and tend to penetrate smaller pores, and (iii) a process of slow advance of air-water interface into the soil. Additionally, the nucleation of air bubbles was not experimentally observed in his study (Williams, 1968). However, spontaneous ice nucleation and the associated replacement of water by ice may occur at anywhere inside soil pores, if the freezing condition is favorable (e.g., at sufficiently low temperature for a long freezing time). The ice may then percolate further and extrude into adjacent pores. No “ice diffusion” process corresponding to the second process of the replacement of water by air (i.e. air diffusion) is expected. Rempel (2012) pointed out that the strengths and nature of the dominant wetting interactions that cause liquid films to coat soil particles in the unsaturated zone are different from those that cause premelted films to separate soil particles from pore ice (i.e. the former involve intermolecular forces between particles, liquid and vapor, whereas the latter involve intermolecular forces between particles, liquid and ice). The existence of solutes further complicates the problem.

From a theoretical point of view, there is similarity between the SWCC of unfrozen

unsaturated soil and the SFCC of the same soil at frozen saturated condition. However, researchers also showed the similarity between SWCC and SFCC of variably saturated soils. For example, Zhou et al. (2014) determined the SWCC on initially saturated specimen, while the unfrozen water contents (i.e. SFCC) were measured at different depths of initially unsaturated soil column subjected to unidirectional freezing with water migration and varying total water content. Except for some dissimilarities when the soil temperature was approximately around 0 °C (e.g., higher than -0.2 °C), the results showed that there was a good agreement between the SWCC and SFCC of variably saturated soils. These investigators suggested that the dissimilarity was partly because unfrozen water content is dependent on both temperature and total water content in the high subzero temperature range. An adjustment factor with the value of 1.0 was obtained for the unsaturated soil used in their study. However, extensive experimental investigations are required for better understanding the similarities and differences between the SWCC and SFCC of variably saturated soils.

4.7 Summary

The SFCC and SWCC are physically similar since both of these two water retention curves describe the relationship between the amount of pore water and its energy state in a soil. Some of the possible reasons for the hysteresis of SFCC proposed in the literature (e.g., the effects of pore blocking and contact angle, and the change in pore structure) are based on their similarity. In the present study, the SFCC and SWCC of two Canadian soils (i.e. Toronto silty clay (TSC) and Toronto lean clay (TLC)) were experimentally determined and analyzed. Many factors have a significant influence on the reliable measurement of SFCC, which include the sensors resolution and their stability, specific sensor calibration for each soil under investigation, thermodynamic equilibrium condition, and continuous soil structure changes that arise during freezing / thawing processes. The observed hysteresis of SFCC for the two Canadian soils is mainly attributed to the supercooling of pore water.

The measured SFCC and SWCC of the two soils show significant differences, indicating

their quantitative dissimilarity. Many reasons may contribute to the dissimilarity. For example, specimens structure variations during the compaction and saturation processes, and during freezing / thawing processes, and cracks formation when sensors were inserted into the specimens. The performance and calibration of sensors would also significantly influence the comparison between SFCC and SWCC. In other words, the limitations associated with testing sensors prohibit a reliable characterization of the quantitative similarity between the two retention curves.

In addition, some fundamental differences may exist between drying / wetting and freezing / thawing processes. For example, the way that ice replaces water may be different from that air replaces water in a soil (Williams, 1967). The dominant wetting interactions that cause liquid films to coat soil particles in the unsaturated zone are different from those that cause premelted films to separate soil particles from pore ice. The existence of salinity further complicates the problem. The present study highlights that rigorous investigations are required for better understanding the fundamental behavior of SFCC of fine-grained soils.

4.8 References

Amiri, E.A., Craig, J.R. and Kurylyk, B.L., 2018. A theoretical extension of the soil freezing curve paradigm. Advances in Water Resources, 111: 319-328.

Anderson, D.M. and Morgenstern, N.R., 1973. Physics, chemistry and mechanics of frozen ground: A review. In Permafrost: The North American Contribution to the Second International Conference, National Academy of Sciences, Washington, DC (pp. 257-288).

Anderson D.M., and Tice A.R., 1972. Predicting unfrozen water contents in frozen soils from surface area measurements. Highway Research Record, 393: 12–18.

Anderson, R., Tohidi, B. and Webber, J.B.W., 2009. Gas hydrate growth and dissociation in narrow pore networks: capillary inhibition and hysteresis phenomena. Geological Society, London, Special Publications, 319(1): 145-159.

ASTM. 2011. Designation: D2487-11. Standard practice for classification of soils for engineering purposes (Unified Soil Classification System). American Society for Testing and Materials, West Conshohocken, PA.

ASTM. 2012. Designation: D698-12: Standard Test Methods for Laboratory Compaction Characteristics of Soil Using Standard Effort (12400 ft-lbf/ft3 (600 kN-m/m3)). American Society for Testing and Materials. West Conshohocken, PA.

ASTM, 2016. Designation: D6836-16. Standard test methods for determination of the soil water

characteristic curve for desorption using hanging column, pressure extractor, chilled mirror hygrometer, or centrifuge. American Society for Testing and Materials. West Conshohocken, PA.

Azmatch, T.F., Sego, D.C., Arenson, L.U. and Biggar, K.W., 2012. Using soil freezing characteristic curve to estimate the hydraulic conductivity function of partially frozen soils. Cold Regions Science and Technology, 83: 103-109.

Bittelli, M., Flury, M. and Campbell, G.S., 2003. A thermodielectric analyzer to measure the freezing and moisture characteristic of porous media. Water Resources Research, 39(2): 1-10.

Black, P.B. and Tice, A.R., 1989. Comparison of soil freezing curve and soil water curve data for Windsor sandy loam. Water Resources Research, 25(10): 2205-2210.

Brown, S.C. and Payne, D., 1990. Frost action in clay soils. II. Ice and water location and suction of unfrozen water in clays below 0° C. Journal of Soil Science, 41(4), pp.547-561.

Caicedo, B., 2016. Physical modelling of freezing and thawing of unsaturated soils. Géotechnique, 67(2): 106-126.

Colbeck, S.C., 1982. Configuration of ice in frozen media. Soil science, 133(2), pp.116-123.

Fredlund, D.G., Rahardjo, H. and Fredlund, M.D., 2012. Unsaturated soil mechanics in engineering practice. John Wiley & Sons.

Fredlund, D.G. and Xing, A., 1994. Equations for the soil-water characteristic curve. Canadian geotechnical journal, 31(4): 521-532.

He, H. and Dyck, M., 2013. Application of multiphase dielectric mixing models for understanding the effective dielectric permittivity of frozen soils. Vadose Zone Journal, 12(1): 1-22.

He, H., Dyck, M.F., Si, B.C., Zhang, T., Lv, J. and Wang, J., 2015. Soil freezing–thawing characteristics and snowmelt infiltration in Cryalfs of Alberta, Canada. Geoderma Regional, 5: 198-208.

Jiang, H., Fall, M. and Cui, L., 2017. Freezing behaviour of cemented paste backfill material in column experiments. Construction and Building Materials, 147: 837-846.

Konrad, J.M., 1990. Unfrozen water as a function of void ratio in a clayey silt. Cold regions science and technology, 18(1): 49-55.

Koopmans, R.W.R. and Miller, R.D., 1966. Soil freezing and soil water characteristic curves. Soil Science Society of America Journal, 30(6): 680-685.

Kurylyk, B.L. and Watanabe, K., 2013. The mathematical representation of freezing and thawing processes in variably-saturated, non-deformable soils. Advances in Water Resources, 60: 160-177.

Lebeau, M. and Konrad, J.M., 2012. An extension of the capillary and thin film flow model for predicting the hydraulic conductivity of air‐free frozen porous media. Water Resources Research, 48(7).

Liu, Z. and Yu, X., 2013. Physically based equation for phase composition curve of frozen soils. Transportation Research Record: Journal of the Transportation Research Board, (2349): 93-99.

Liu, Z., Zhang, B., (Bill) Yu, X., and Tao, J., 2012. A new method for soil water characteristic curve measurement based on similarities between soil freezing and drying. Geotechnical Testing Journal, 35(1): 2-10.

Ma, T., Wei, C., Xia, X., Zhou, J. and Chen, P., 2015. Soil freezing and soil water retention characteristics: connection and solute effects. Journal of Performance of Constructed Facilities, D4015001.

Ma, W., Zhang, L. and Yang, C., 2015. Discussion of the applicability of the generalized Clausius–Clapeyron equation and the frozen fringe process. Earth-Science Reviews, 142: 47-59.

Miller, E.E. and Miller, R.D., 1956. Physical theory for capillary flow phenomena. Journal of Applied Physics, 27(4): 324-332.

Miller, R.D., 1980. Freezing phenomena in soils. Applications of soil physics, Academic Press, Inc., New York, USA, pp. 254-299.

Rempel, A.W., 2012. Hydromechanical processes in freezing soils. Vadose Zone Journal, 11(4): 1-10.

Ren, J. and Vanapalli, S.K., 2018. Prediction of the resilient modulus of frozen unbound road materials using the soil-freezing characteristic curve. Canadian Geotechnical Journal, 55: 1200-1207.

Schafer, H.L. and Beier, N.A., 2017. Development of soil freezing characteristic curves for fluid fine tailings using TDR. In Proceedings of the 70th Canadian Geotechnical Conference, Ottawa, Canada, 1-8.

Schofield, R.K., 1935. The pF of water in soil. In Trans. of the Third International Congress on Soil Science, 2, Plenary Session Papers, 30 July-7 August, 1935 Oxford, UK (pp. 37-48).

Skapski, A., Billups, R. and Rooney, A., 1957. Capillary cone method for determination of surface tension of solids. The Journal of chemical physics, 26(5): 1350-1351.

Smith, M.W. and Tice, A.R., 1988. Measurement of the unfrozen water content of soils. Comparison of NMR (nuclear magnetic resonance) and TDR (time domain reflectometry) methods (No. CRREL-88-18). Cold Regions Research and Engineering Lab, Hanover, NH.

Spaans, E.J., 1994. The soil freezing characteristic: Its measurement and similarity to the soil moisture characteristic. Phd thesis, University of Minnesota, Minneapolis, Minnesota, USA.

Spaans, E.J. and Baker, J.M., 1996. The soil freezing characteristic: its measurement and similarity to the soil moisture characteristic. Soil Science Society of America Journal, 60: 13–19.

Tan, L., Wei, C., Tian, H., Zhou, J., and Wei, H., 2015. Experimental study of unfrozen water content of frozen soils by low-field nuclear magnetic resonance. Rock and soil mechanics, 36(6): 1566-1572. (in Chinese)

Tian, H., Wei, C., Wei, H. and Zhou, J., 2014. Freezing and thawing characteristics of frozen soils: Bound water content and hysteresis phenomenon. Cold Regions Science and Technology, 103: 74-81.

Vanapalli, S.K., Fredlund, D.G. and Pufahl, D.E., 1999. The influence of soil structure and stress history on the soil-water characteristics of a compacted till. Geotechnique, 49(2): 143-159.

Wang, C., Lai, Y. and Zhang, M., 2017. Estimating soil freezing characteristic curve based on pore-size distribution. Applied Thermal Engineering, 124: 1049-1060.

Watanabe, K., Takeuchi, M., Osada, Y. and Ibata, K., 2012. Micro-chilled-mirror hygrometer for measuring water potential in relatively dry and partially frozen soils. Soil Science Society of America Journal, 76(6): 1938-1945.

Watanabe, K. and Wake, T., 2008, June. Hydraulic conductivity in frozen unsaturated soil. In Proceedings of the 9th International Conference on Permafrost (Vol. 29, pp. 1927-1932). Fairbanks, Alaska: Univ. of Alaska Fairbanks.

Williams, P.J., 1967. The nature of freezing soil and its field behavior. In Properties and behavior of freezing soils. Norwegian Geotechnical Institute publication, NR. 72, Oslo, Norway.

Williams, P.J., 1968. Replacement of water by air in soil pores. Norwegian Geotechnical Institute, 75-90.

Williams, P.J., 1976. Volume change in frozen soils. Laurits Bjerrum memorial volume. Norwegian Geotechnical Institute, Oslo, 233-246.

Williams, P.J., 1999. The freezing of soils: Ice in a porous medium and its environmental significance. In Ice physics and the natural environment. Springer Berlin Heidelberg, 219-239.

Yoshikawa, K. and Overduin, P.P., 2005. Comparing unfrozen water content measurements of frozen soil using recently developed commercial sensors. Cold Regions Science and Technology, 42(3): 250-256.

Zhou, X., Zhou, J., Kinzelbach, W. and Stauffer, F., 2014. Simultaneous measurement of unfrozen water content and ice content in frozen soil using gamma ray attenuation and TDR. Water Resources Research, 50(12): 9630-9655.

Zhou, Y., Zhou, J., Shi, X.Y. and Zhou, G.Q., 2019. Practical models describing hysteresis behavior of unfrozen water in frozen soil based on similarity analysis. Cold Regions Science and Technology, 157, pp.215-223.

Chapter 5 Prediction of the resilient modulus of frozen unbound road materials using the soil-freezing characteristic curve

The contents presented in this chapter are from the manuscript of the publication:

Ren, J. and Vanapalli, S.K., 2017. Prediction of the resilient modulus of frozen unbound road materials using the soil-freezing characteristic curve. Canadian Geotechnical Journal, 55: 1200-1207.

DOI: 10.1139/cgj-2017-0153.

5.1 Abstract

The resilient modulus is a key parameter required in the mechanistic design of pavements. Experimental determination of the resilient modulus requires elaborate equipment for testing and requires trained personnel; for this reason, it is expensive. There are several models for predicting the resilient modulus for unbound road materials that take account of the influence of wetting and drying conditions. However, well-established models are not available for the prediction of the resilient modulus of these materials in a frozen state. In this paper, a semi-empirical model, which uses soil-freezing characteristic curve (SFCC) as a tool, is proposed for predicting the variation of the resilient modulus with subzero temperature and the associated cryogenic suction for frozen soils. Experimental data on seven different unbound materials were used to validate the proposed model. It is shown that the model can reasonably predict the resilient modulus of the investigated soils that are in a state of frozen condition. More investigations on different types of soils would be useful to better understand the strengths and limitations of the proposed model.

5.2 Introduction

The resilient modulus, which is defined as the ratio of the cyclic deviator stress to the recoverable strain, is the key material property required for the rational design of pavements as

per the *Guide for Mechanistic-Empirical Design of New and Rehabilitated Pavement Structures* (also known as MEPDG) (ARA, Inc., 2004). In permafrost and seasonally frozen regions, temperature has a significant influence on the resilient modulus of pavement materials. As the soil temperature drops below 0 °C, ice crystals start to nucleate in the soil's pore spaces. The growing ice crystals interfere with each other and adjacent soil particles, resulting in the movement and rearrangement of the soil particles that contribute to changes in the original soil fabric (Chamberlain and Blouin, 1977; Andersland and Anderson, 1978). The freezing process contributes to an increase in the resilient modulus, which has been measured by several investigators on different frozen pavement materials (e.g., Berg et al., 1996; Simonsen et al., 2002; Li et al., 2011).

Experimental determination of the temperature influence on the resilient modulus of unbound road materials is challenging due to the complex and time-consuming testing procedures associated with the control and equilibrium of temperature. It is desirable to develop simple prediction models for estimating resilient modulus of the frozen unbound soils to facilitate the design of pavement structures in cold regions. In the MEPDG, empirical values are recommended as the resilient modulus for frozen unbound soils based on different physical properties (i.e. 2.5×10^6 psi (approximately, 17000 MPa) for non-plastic soils, and 1×10^6 psi (approximately, 7000 MPa) for plastic soils). However, a single value for frozen resilient modulus may not be reasonable because the resilient modulus of frozen soils varies with subzero temperatures (e.g., Berg et al., 1996; Simonsen et al., 2002). For example, the frozen resilient modulus of the New Hampshire marine clay is around 200 MPa at -2 °C. However, it reaches a value higher than 1500 MPa at -5 °C, and is approximately 3000 MPa at -10 °C (Simonsen et al., 2002).

This paper exploits the similarity between the drying-wetting processes in an unsaturated unfrozen soil and the freezing-thawing processes in a saturated frozen soil. This can be achieved by using the similarity between the soil-water characteristic curve (SWCC, representing the relationship between water content and suction in unsaturated unfrozen soil) and the soil-freezing

characteristic curve (SFCC, representing the relationship between unfrozen water content and cryogenic suction at ice-water interface in saturated frozen soil). Both the SFCC and SWCC describe the soil water retention characteristics (Spaans and Baker, 1996). Since the SWCC has been widely used as a tool in the implementation of the mechanics of unsaturated soils in engineering practice, it has been postulated that the SFCC can also be used for predicting the frozen soils behavior. A semi-empirical model is proposed to predict the resilient modulus of saturated soils that are in a state of frozen condition by extending this philosophy. The proposed model has been validated using experimental data on different types of soils. The proposed model is simple and provides reasonable predictions for the resilient modulus of the investigated frozen soils. It is promising for use in the rational design of pavement structures in cold regions; in addition, it can be used in better understanding the artificial frozen soil techniques, which usually require the strength and stiffness properties of the frozen soils (Sayles et al., 1987).

5.3 Soil-freezing characteristic curve (SFCC)

In a frozen soil, unfrozen water and pore ice coexist. The unfrozen water exists as thin films adsorbed on the surfaces of soil particles in equilibrium with the pore ice at temperatures below 0 °C (Harlan, 1973). The relationship between unfrozen water content and subzero temperature (T) or cryogenic suction (ψ_{cryo}) in a frozen soil is defined as SFCC (Koopmans and Miller, 1966; Spaans and Baker, 1996; Azmatch et al., 2012a). Since the constitutive relationships for hydraulic, thermal, and mechanical properties of frozen soils are functions of the quantity of unfrozen water, the SFCC is essential to modeling the transport mechanism of water, heat, and solutes in frozen soils (Black and Miller, 1985; Spaans and Baker, 1996; Zhang et al., 2016). The cryogenic suction, which is associated with the potential that develops between the ice and water in the frozen soils, is conceptually similar to the suction developed between the air and water in unfrozen unsaturated soils (Gens, 2010; Caicedo, 2017). The cryogenic suction contributes to increase the shear strength, apparent preconsolidation pressure, and stiffness of the frozen soils (Shastri and Sanchez, 2012). The Clapeyron equation (Eq. (5.1)) can be used to

convert the subzero temperature to cryogenic suction or vice versa based on the assumptions that the pressure of pore ice in a frozen soil is equal to atmospheric pressure and the solute effect is negligible (Azmatch et al., 2012a; Kurylyk and Watanabe, 2013).

$$\psi_{cryo} = -L\rho_w \ln \frac{T + 273.15}{T_0 + 273.15} \tag{5.1}$$

where ψ_{cryo} is the cryogenic suction in kPa; T is the subzero temperature in °C; L is the latent heat of fusion of water (L = 334 kJ/kg); T_0 is the normal freezing temperature of water (T_0 = 0 °C); ρ_w is the density of water (ρ_w = 1000 kg/m^3). The calculated cryogenic suction versus subzero temperature relationship by Eq. (5.1) is approximately linear with a slope of about 1225 kPa/°C, when the temperature is not too low. This is in close agreement with the relations provided by Konrad (1994), Williams and Smith (1989), and Grant (1994), which suggest a slope value of 1250, 1200, and 1221 kPa/°C, respectively.

5.4 Similarity between the SFCC and SWCC

Koopmans and Miller (1966) measured both the SFCC and SWCC for three different soils, namely: SS, SLS, and SSLS. The SS soil is free of colloidal materials. It represents soils such as sand, silt, or coarse clay fractions which have direct solid-to-solid (SS) contacts between particles. Each particle is wedged with the other adjacent particles and the pore geometry is fixed. A change in water content causes a displacement of the air-water interface within the pore system, but there will be no change in the bulk volume of the soil. The other extreme is soil in which the soil particles are separated by liquid water (i.e. solid-liquid-solid), designated as the SLS soil. A change in water content is accompanied by corresponding changes in particle spacing and in the bulk volume. Macroscopic cracks may open or close, but the air phase does not penetrate the spaces between the particles. In reality, the behavior of a majority of natural soils lies in between the SS and SLS; hence they are designated as SSLS soil.

Figure 5.1 shows the SFCC (i.e. freezing-thawing curve) and SWCC (i.e. drying-wetting curve) for both the SS and SSLS soils. As can be seen, the shape of the SFCC is similar to that of

the SWCC. This is due to the similarity in the physical processes that the soil experiences both during drying and wetting at unfrozen condition and freezing and thawing at frozen condition. When soils are subjected to drying, water is gradually removed and replaced by air, leaving the remainder water at an increasingly lower matric potential. The physical process that occurs in freezing soils is similar, except that liquid water changes phase and becomes ice. The same forces that prevent soil water from draining also prevent it from freezing (Spaans and Baker, 1996). In other words, the temperature gradient in frozen soil can be considered to act in a similar manner to the potential gradient in an unfrozen soil (Harlan, 1973; Zhou et al., 2014). Temperature is actually a thermal potential (Oonk and Calvet, 2007). For this reason, the SFCC can be used as a tool to estimate or predict the SWCC (Black and Tice, 1989; Spaans and Baker, 1996; Bittelli et al. 2003; Cheng et al., 2014). Although, SWCC is conventionally measured, it is rather difficult and time-consuming in comparison with measuring the SFCC. The SFCC can be measured using time domain reflectometry (TDR) technique, which is presently a well-established method to reliably measure the unfrozen water content in frozen soils (Azmatch et al., 2012a).

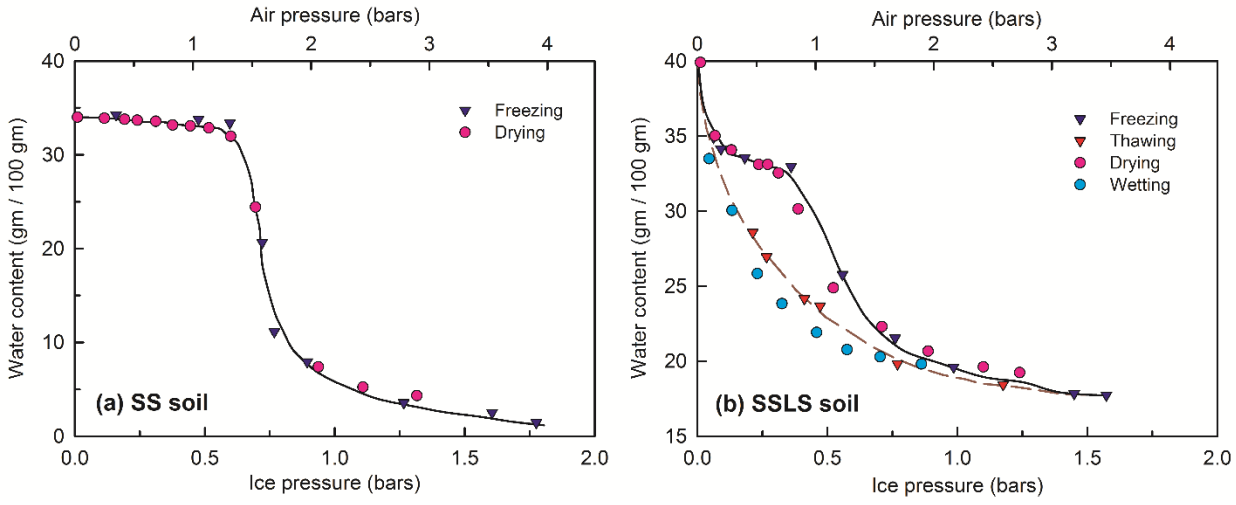

Figure 5.1 (a) SFCC for second freeze-thaw cycle and SWCC for drying path for SS soil; (b) SFCC for third freeze-thaw cycle and SWCC for dry-wet cycle for SSLS soil (data from Koopmans and Miller 1966)

As shown in **Figure 5.1**(b), the SFCC exhibits hysteretic behavior similar to SWCC. This can be attributed to several possible mechanisms such as supercooling of pore water, the effect of electrolyte, and pore blocking (Bittelli et al., 2003; Tian et al., 2014). The hysteretic branches of SWCC contain main drying / wetting curves, and an infinite number of scanning curves inside the hysteresis loop (Pham et al., 2005). A conceptual SFCC can be drawn to illustrate main features of soil freezing and thawing processes, as shown in **Figure 5.2**. As temperature drops, pore water starts to crystalize. The remainder of unfrozen water will be in a state of thinner adsorbed layers with decreasing radii of curvature upon temperature decrease. For coarse-grained soils, the decrease in unfrozen water content occurs in a narrow temperature range. Their freezing curves have steep slopes. Azmatch et al. (2012a) measured the SFCC curves for Devon silt sample and showed that its SFCC curves dropped dramatically within a small range of temperature from -0.04 °C to about -1 °C. On the other hand, the SFCC of fine-grained soils are relatively flat due to their fairly smaller size particles, which can retain large amount of water by adsorptive forces. In fine-grained soils, even at low temperatures (e.g., -20 °C), considerable amount of water in the pores remains unfrozen and is available for the soil grains in the form of thin layers of adsorbed water (Andersland and Ladanyi, 1994). The larger the surface area of the soil particles, the greater the amount of unfrozen water is adsorbed on the particles' surface (Christ and Kim, 2009). The freezing and thawing branches form bounds of the unfrozen water content versus cryogenic suction (or subzero temperature) relationship (i.e. SFCC). Similar to the SWCC, there are infinite number of freezing and thawing scanning curves that bridge between the initial freezing and thawing curves (Spaans and Baker, 1996), as shown in **Figure 5.2**.

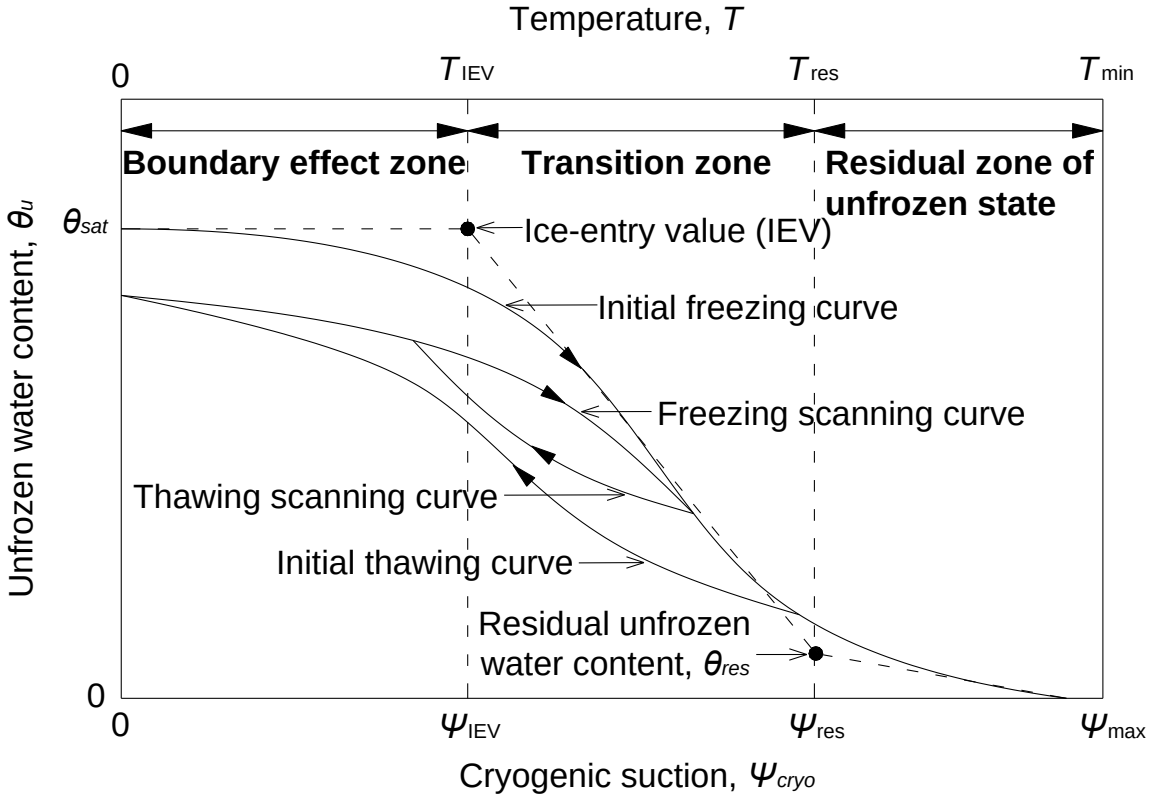

Figure 5.2 Conceptual sketch for a typical soil-freezing characteristic curve

Figure 5.3 shows the probable variation of unfrozen water and ice in a saturated freezing soil. The soil pores were originally filled by unfrozen water (i.e. no ice has formed as shown in **Figure 5.3**(a)). With decreasing temperature or increasing cryogenic suction, ice crystals start to form in the large soil pores, as shown in **Figure 5.3**(b). The corresponding cryogenic suction or subzero temperature at this stage is called the ice-entry cryogenic suction or ice-entry subzero temperature, which can be referred to as the ice-entry value (IEV) (Azmatch et al., 2012b). The unfrozen water content in the soil continues to decrease with a decrease in the soil temperature (i.e. the ice crystals increase in size and penetrate smaller pores as shown in **Figure 5.3**(c)). At certain subzero temperature, most pore water turns into ice and beyond which extremely low temperature (i.e. very high cryogenic suction) would be required to reduce the unfrozen water further. This critical unfrozen water content is referred to as the residual unfrozen water content, at which the unfrozen water is firmly held by and close to the soil particles (Harlan, 1973; Sheng

et al., 2014), as shown in **Figure 5.3**(d). Similar to the SWCC (Vanapalli et al., 1996; Vanapalli et al., 1999), the SFCC could be divided into three zones; namely, boundary effect zone (where no pore ice forms, indicating freezing point depression of soil water; see **Figure 5.3**(a)), transition zone (where ice crystals start to form and gradually increase in size, and sharp drop in the unfrozen water content is experienced; see **Figure 5.3**(b) and (c)), and residual zone of unfrozen state (where most pore water turned into ice and the variation in the unfrozen water content is insignificant under large change in temperature or cryogenic suction; see **Figure 5.3**(d)), as shown in **Figure 5.2**.

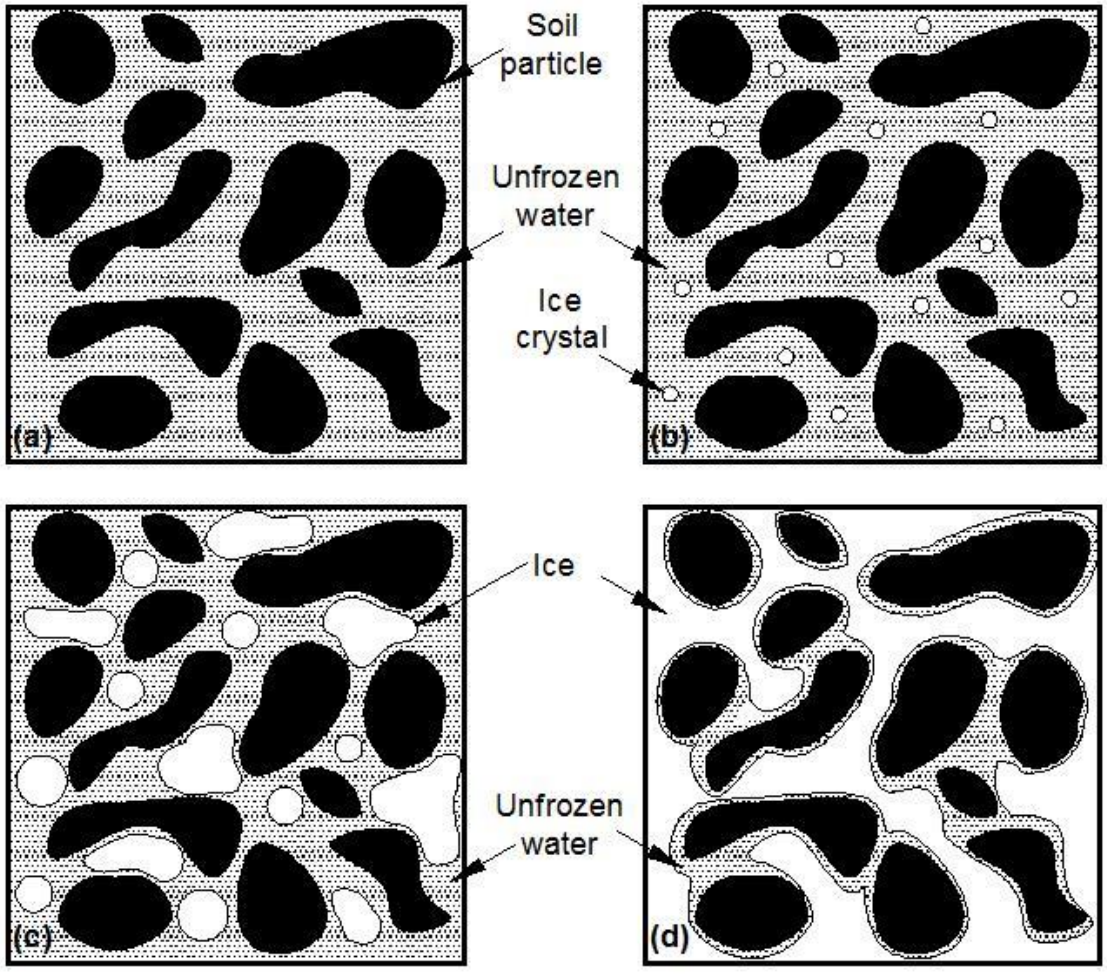

Figure 5.3 Probable variation of unfrozen water and ice in a saturated freezing soil: (a) no ice has formed; (b) formation of ice crystals; (c) increase of ice crystals; (d) residual state

5.5 The proposed semi-empirical model

Temperature has the most significant impact on the amount of unfrozen water in a frozen soil. It has been shown that unfrozen water content can be directly expressed as a function of temperature (Bigl and Berg, 1996b) and thus can be correlated to the cryogenic suction at ice-water interface using Eq. (5.1). Because of the similar shape of the SWCC and SFCC, equations developed for SWCC can also be used to best-fit SFCC. Azmatch et al. (2012a) successfully fitted the measured SFCC data for Devon silt samples consolidated to different pressures (i.e. 100 kPa and 400 kPa) using the Fredlund and Xing (1994) SWCC equation, which is shown below.

$$\theta = C(\psi)\frac{\theta_{sat}}{\{\ln[2.718+(\psi/a_f)^{n_f}]\}^{m_f}} \tag{5.2a}$$

$$C(\psi) = 1-\frac{\ln(1+\psi/\psi_r)}{\ln[1+(10^6/\psi_r)]} \tag{5.2b}$$

where θ is the volumetric water content; θ_{sat} is the saturated volumetric water content (equals to soil porosity); ψ is the suction in the unsaturated unfrozen soil (kPa); ψ_r is the suction corresponding to the residual water content (kPa); a_f, n_f, and m_f are fitting parameters. The $C(\psi)$ contributes to force the fitting curve to be zero at a ψ value of 10^6 kPa.

A semi-empirical model is proposed to predict the resilient modulus of saturated soils in a state of frozen condition (i.e. $M_{RSAT(\text{frozen})}$) by extending the concepts proposed by Han and Vanapalli (2014) using the SFCC as a tool. This model is based on extending observed similarities between the freezing-thawing and drying-wetting processes. It is assumed that the rate at which the cryogenic suction contributes towards frozen resilient modulus can be related to the degree of unfrozen water saturation, S_u, which is the ratio of the volume of unfrozen water to the total volume of the unfrozen water and ice. The value of S_u varies from unity before the ice-entry value has reached to a small value at large cryogenic suction. The semi-empirical model is expressed as:

$$M_{RSAT(\text{frozen})} = M_{RSAT(0℃)}(1+\chi\psi_{cryo}S_u^{\ \delta}) \tag{5.3}$$

where $M_{RSAT(0\ ^\circ C)}$ is the saturated resilient modulus at 0 °C (MPa); χ and δ are model parameters. The relationship between the S_u (i.e. $S_u = \theta / \theta_{sat}$ assuming constant volume of the specimen) and ψ_{cryo} (i.e. the SFCC) can be described by Eq. (5.2). Eq. (5.3) suggests that $M_{RSAT(\text{frozen})}$ changes remarkably with an increase in the ψ_{cryo} in a saturated frozen soil.

5.6 Model validation

Experimental data of seven different saturated soils from the literature were used in the validation of the proposed model. The basic properties of these soils are summarized in **Table 5.1**.

Table 5.1 Physical properties of the seven saturated soils

No.	Soil	Type	γ_d	w_{sat}	G_s	w_L	I_p	AASHTO[a]	USCS[b]	Data from
1	Subgrade 1206	Sandy lean clay	16.8	23.4	2.70	37.0	18.5	A-6	CL	Berg et al., 1996; Bigl and Berg, 1996a; Bigl and Berg, 1996b
2	Subgrade 1232	Sandy lean clay	17.1	19.3	2.71	26.4	10.9	A-6	CL	
3	Class 6 base	Well-graded gravel	21.0	9.4	2.74	/	/	/	GW	
4	Class 3 subbase	Well-graded sand	20.3	9.7	2.69	17.0*	1.2*	A-1-b	SW	
5	Taxiway A base	Crushed stone	19.4	7.5	/	/	/	/	/	Cole et al., 1987
6	Taxiway A subbase	Silty sand	20.9	7.5	2.73	/	/	A-1-b	SM	
7	Taxiway B subbase	Silty sandy gravel	20.0	5.5	2.68	/	/	/	GM	

[a] American Association of State Highway and Transportation Officials.
[b] Unified Soil Classification System (ASTM D2487-11).
* Fraction that passed No. 40 sieve.
/ Not available.
γ_d: dry unit weight (kN/m^3); w_{sat}: saturated gravimetric moisture content (%); G_s: specific gravity; w_L: liquid limit (%); I_p: plasticity index.

5.6.1 Soil 1 through 4 from Berg et al. (1996)

The subgrade 1206 (Soil 1) and subgrade 1232 (Soil 2) respectively represent the high- and low-heaving sandy lean clay subgrades. The class 6 base (Soil 3) has a relatively small amount of fines while the class 3 subbase (Soil 4) is a material with a high percentage of fines. These materials were saturated, frozen, and then tested at three temperatures below freezing and tested in a thawed, saturated state at room temperature. The volume changes of class 6 base and class 3 subbase during freezing process were generally small since they are coarse-grained soils. Subgrade 1206 and subgrade 1232 should have larger volume change during freezing, but since surcharge was placed on the top of the specimens, the volume change was considered acceptable. The resilient modulus tests were conducted using repeated-load triaxial test equipment. The confining pressure was held constant while the cyclic deviator stress varied. The pulse length is approximately 1-s with 2-s between pulses. Detailed test procedures are available in Berg et al. (1996).

Bigl and Berg (1996b) showed that the variation in unfrozen water contents of these four soils with subzero temperature can be expressed as,

$$w_u = \frac{c}{100}\left(\frac{-T}{T_{ref}}\right)^d \tag{5.4}$$

where w_u is the gravimetric unfrozen water content (in decimal); T_{ref} is the reference temperature (T_{ref} = 1 °C); c and d are constants. The values of c and d for the four soils are listed in **Table 5.2**.

Table 5.2 Constants *c* and *d* for the seven saturated soils

No.	Soil	*c*	*d*
1	Subgrade 1206	11.085	-0.274
2	Subgrade 1232	8.121	-0.303
3	Class 6 base	0.567	-1.115
4	Class 3 subbase	1.497	-0.709
5	Taxiway A base	3.000	-0.250
6	Taxiway A subbase	3.000	-0.250
7	Taxiway B subbase	3.000	-0.220

The degree of unfrozen water saturation at any subzero temperature can be calculated from Eq. (5.4) and the saturated gravimetric water content in **Table 5.1** (i.e. $S_u = w_u / w_{sat}$). The subzero temperature can be further converted to cryogenic suction at the ice-water interface by Eq. (5.1). **Figure 5.4** shows the variation in the degree of unfrozen water saturation in the four frozen saturated soils with the increasing cryogenic suction (i.e. SFCC). These data were fitted using Eq. (5.2a), based on the least square method. The fitted SFCCs are shown in **Figure 5.4**. and their fitting parameters are summarized in **Table 5.3**. The summarized results suggest that Eq. (5.2a) is suitable for fitting the degree of unfrozen water saturation. From **Figure 5.4**, it can be seen that the desorption rate is relatively low for subgrades 1206 and 1232. The unfrozen water contents of these two soils are greater than 20% in spite of relatively high cryogenic suction value of 10 MPa. On the contrary, the unfrozen water contents of class 6 base and class 3 subbase decrease significantly within a small range of cryogenic suction and reach values lower than 10% when the cryogenic suction is higher than 2 MPa. It is reasonable to see that the class 3 subbase has greater unfrozen water content than the class 6 base does since the former has higher percentage of fines.

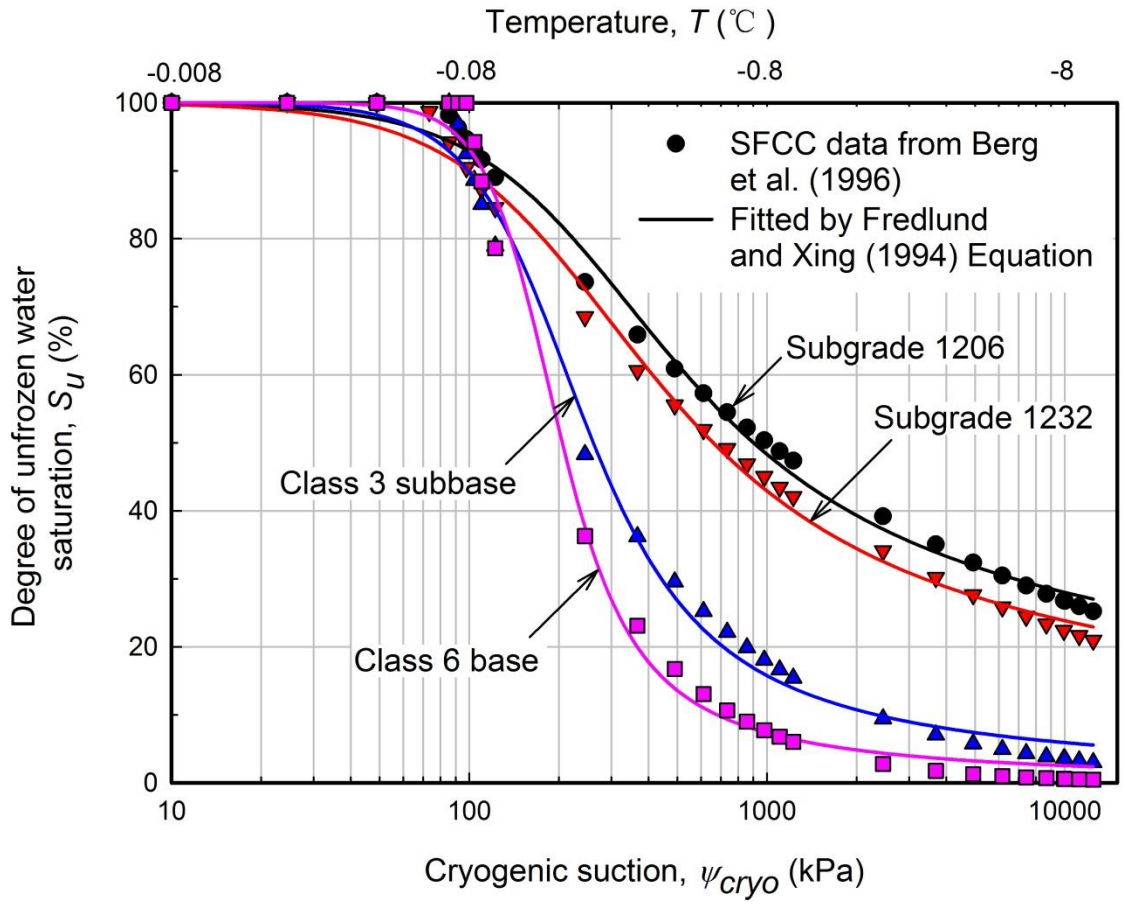

Figure 5.4 SFCCs of Subgrade 1206, Subgrade 1232, Class 6 base, and Class 3 subbase (SFCC data from Berg et al. (1996))

The resilient modulus for frozen soils that are in a state of saturation ($M_{RSAT(\text{frozen})}$) can be predicted using the fitted SFCC and Eq. (5.3). The prediction results for the four soils are shown in **Figure 5.5**, together with the measured values of frozen resilient modulus, several data points of which were obtained under each subzero temperature. The measured data were not exactly the same and showed fluctuations due to difficulties associated with conducting the resilient modulus test. The regression analysis in the present study obtained the best-fit curve for the originally measured data. The fitted model parameters, the coefficient of determination (R^2), and the saturated resilient modulus at 0 °C (i.e. $M_{RSAT(0\,^\circ\text{C})}$) are summarized in **Table 5.3**. The results suggest that the proposed semi-empirical model can reliably predict the variation in resilient modulus of these four soils at subzero temperatures.

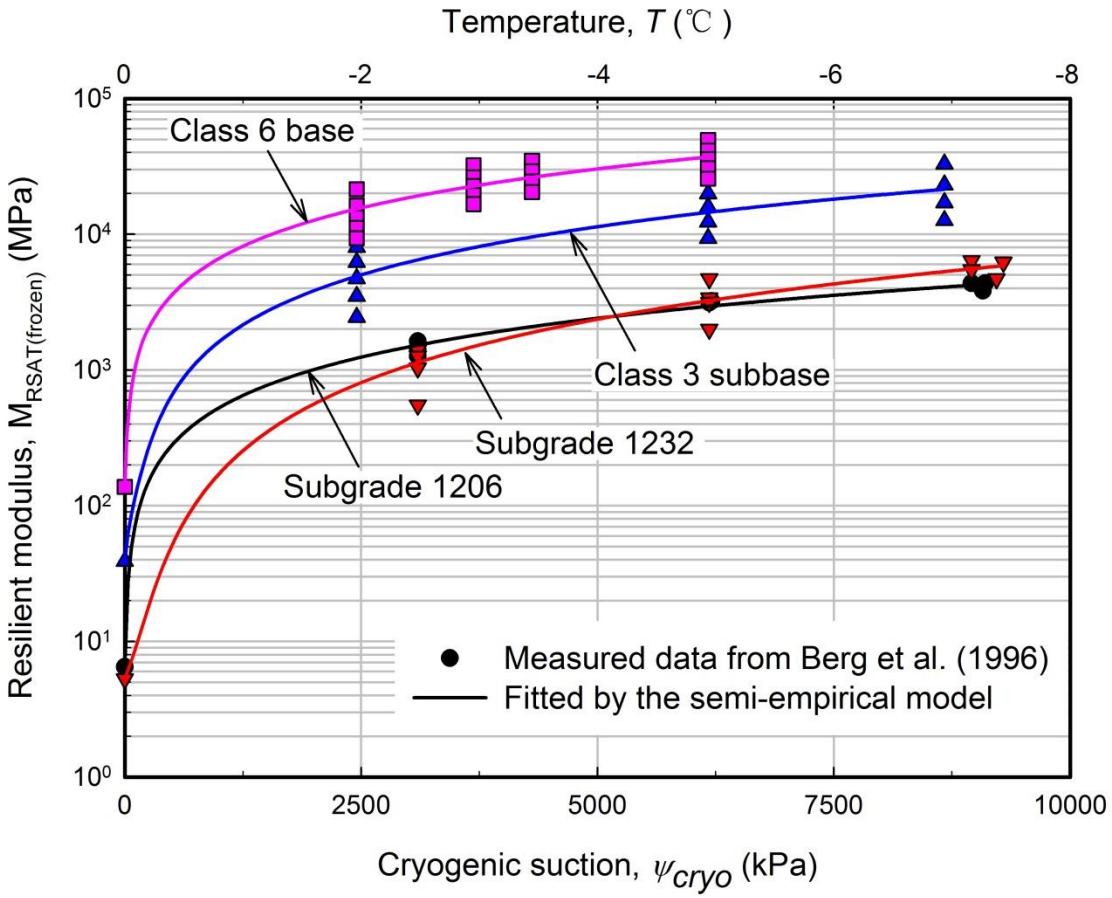

Figure 5.5 Comparison between the measured and predicted resilient modulus values for Subgrade 1206, Subgrade 1232, Class 6 base, and Class 3 subbase (measured data from Berg et al. (1996))

Table 5.3 Summary of the results by using the semi-empirical model

No.	Soil	Parameters of Fredlund and Xing (1994) Equation				Model parameters		$M_{RSAT(0\ °C)}$ (MPa)	R^2
		a_f	n_f	m_f	R^2	χ	δ		
1	Subgrade 1206	189.306 (9.000)	1.701 (0.105)	0.666 (0.030)	0.99	0.037 (0.055)	0.197 (0.436)	6.49	0.97
2	Subgrade 1232	165.278 (9.145)	1.629 (0.110)	0.754 (0.040)	0.99	190.144 (709.725)	-2.314 (1.161)	5.28	0.89
3	Class 6 base	159.552 (7.797)	3.996 (0.365)	1.310 (0.109)	0.99	0.039 (0.022)	0.092 (0.459)	137.71	0.71
4	Class 3 subbase	165.821 (9.612)	2.598 (0.215)	1.195 (0.090)	0.99	0.150 (0.276)	-0.473 (0.984)	38.97	0.69
5	Taxiway A base	78.826 (5.421)	1.151 (0.086)	0.807 (0.049)	0.99	346.050 (133.882)	-2.877 (0.117)	61.4	0.99
6	Taxiway A subbase	78.826 (5.421)	1.151 (0.086)	0.807 (0.049)	0.99	9.467×10^{-5} (6.306×10^{-5})	1.966 (0.204)	33.7	0.99
7	Taxiway B subbase	187.581 (8.491)	1.611 (0.095)	0.557 (0.024)	0.99	9×10^{-4} (1×10^{-4})	1.037 (0.032)	56.4	0.99

Note: Number in parenthesis is the Standard Error.

5.6.2 Soil 5 through 7 from Cole et al. (1987)

Taxiway A base and subbase are crushed stone base and gravelly sand subbase, respectively. Taxiway B subbase is silty sandy gravel. These three soils were compacted and then frozen at a rate of 25 mm/day under open-system condition. The samples did not heave appreciably. An electro-hydraulic, closed-loop testing machine operated with load control method was used for determining the resilient modulus. A total of 200 loading cycles were applied at each stress level to achieve a steady-state response. The applied load was a 28-ms haversine and repeated every 2-s, simulating the load pulse produced by the Falling Weight Deflectometer (Cole et al., 1987). The degree of unfrozen water saturation of these three soils were calculated using the parameters *c* and *d* (shown in **Table 5.2**) which were from the relationship between unfrozen water content and subzero temperature provided by Cole et al. (1987), and the saturated water contents that are summarized in **Table 5.1**. The SFCCs of these soils were drawn by calculating the cryogenic suctions corresponding to the subzero temperatures. The SFCCs shown in **Figure 5.6** were fitted by Eq. (5.2a). The Taxiway A base and subbase have the same SFCC since these two soils have the same parameters *c* and *d*, and saturated gravimetric water content.

The prediction results for the three soils are shown in **Figure 5.7**, together with the measured values of frozen resilient modulus. The fitted model parameters and R^2, and the saturated resilient modulus at 0 °C (i.e. $M_{RSAT(0\ ^\circ C)}$) are summarized in **Table 5.3**. The results suggest that the variation in frozen resilient modulus of these three soils can be reliably predicted by the semi-empirical model.

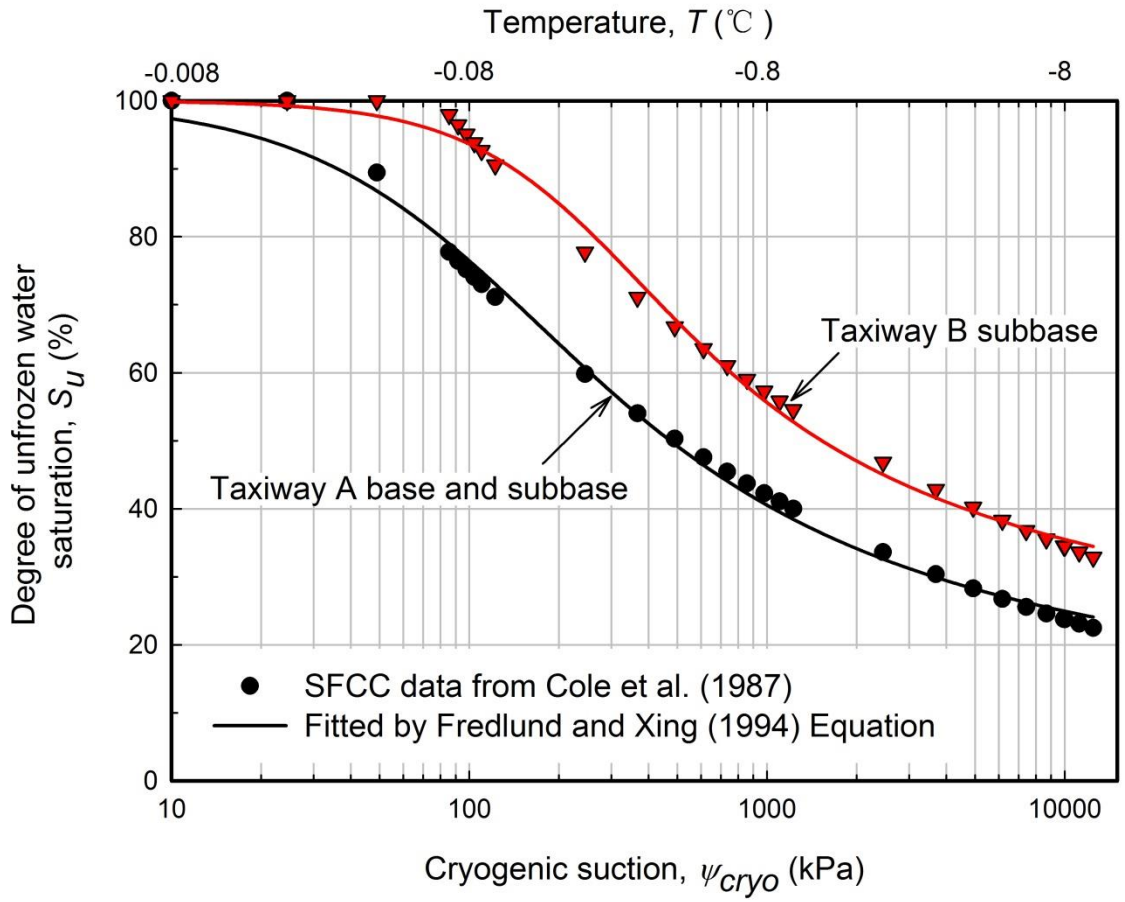

Figure 5.6 SFCCs of Taxiway A base, Taxiway A subbase, and Taxiway B subbase (SFCC data from Cole et al. (1987))

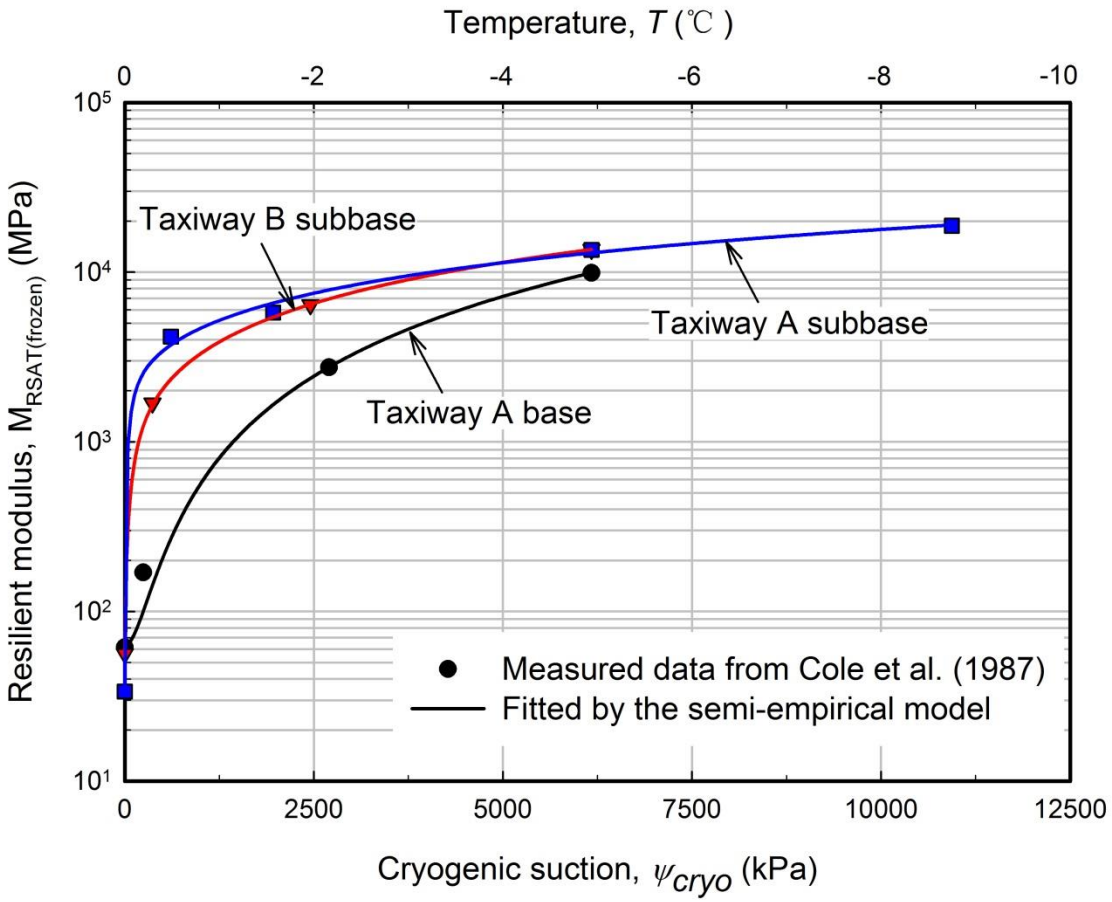

Figure 5.7 Comparison between the measured and predicted resilient modulus values for Taxiway A base, Taxiway A subbase, and Taxiway B subbase (measured data from Cole et al. (1987))

5.7 Discussion

The proposed semi-empirical model well predicts the resilient modulus for both fine- and coarse-grained saturated frozen soils. The model has a theoretical basis. The relationship between the unsaturated unfrozen soils and saturated frozen soils is used for developing the model. In unsaturated unfrozen soils, the suction at air-water interface contributes to soil's mechanical properties, such as the shear strength, modulus of elasticity, and resilient modulus. The meniscus water associated with capillary tension forces clings at the contact points of soil particles and holds the soil particles tightly (Karube and Kawai, 2001), resulting in high soil

strength and stiffness. In saturated frozen soils, the cryogenic suction at ice-water interface, which increases with decreasing subzero temperature, contributes to the frozen soil's mechanical properties, such as the strength and stiffness (Shastri and Sanchez, 2012; Kweon and Hwang, 2013). The proposed model is only valid for soils that are in a state of saturated condition and the suction in these soils is considered at the ice-water interface, rather than at the air-ice or air-water interface or combination of them. In addition, to employ the Clapeyron equation, thermodynamic equilibrium condition should be achieved at the ice-water interface (Ma et al., 2015; Caicedo, 2017). Theoretically, this can be achieved by slow and gradual freezing of the soil sample. However, for some scenarios, large rate of temperature changes may not ensure the thermodynamic equilibrium to employ the proposed model (Kurylyk and Watanabe, 2013).

No relationships could be proposed for the model parameters χ and δ because of the limited data. However, from Eq. (5.3), it is known that parameter χ should be greater than zero. On the other hand, parameter δ can be either positive or negative (see **Table 5.3**). One possible explanation is that the frozen soil is complex because it typically constitutes of four different phases, namely, soil particle, ice, unfrozen water, and air. The resilient modulus of frozen soil is significantly influenced by such as the subzero temperature, soil type, water content, and testing conditions. Due to this reason, there are large differences in model parameter δ for different soils at different conditions. It is also observed from **Table 5.3**, **Figure 5.5**, and **Figure 5.7** that: when the parameter χ is large, the parameter δ is relatively small. However, a small value of parameter χ is obtained when there is a significant growth in the frozen resilient modulus within a narrow temperature range just below 0 °C. More evidence is required to propose a well-defined or unique relationship between the model parameters and soil physical properties, such as the pore size characteristics, plasticity index, and unfrozen water content.

The proposed semi-empirical model only requires the $M_{RSAT(0\,°C)}$ and SFCC along with two fitting parameters (i.e. χ and δ) to predict the frozen resilient modulus. Similar to the SWCC, the SFCC can be predicted based on soil's basic property indices coupled with one-point measurement (Liu and Yu, 2014). Such a technique reduces the need for conducting cumbersome

experiments.

5.8 Summary

In this paper, the similarity between the soil-water characteristic curve (SWCC) in an unfrozen unsaturated soil and the soil-freezing characteristic curve (SFCC) in a frozen saturated soil is discussed. A conceptual SFCC is highlighted to illustrate key features of soil freezing and thawing processes. Using the SFCC as a tool, a semi-empirical model is proposed for predicting the resilient modulus of frozen saturated soils by exploiting the similarity between freezing / thawing and drying / wetting processes. Seven saturated soils were used to validate the proposed model. The results show that the model can predict the resilient modulus of frozen saturated soils with a reasonable degree of accuracy. However, no relationships could be obtained for the model parameters because of the limited data. The model proposed in the present study is simple and promising. However, more efforts are needed to further improve the model and validate it with additional experimental data on different types of soils. In addition, the influence of stress level should be investigated and incorporated into the model.

5.9 References

Andersland, O.B., and Anderson, D.M. 1978. Geotechnical engineering for cold regions. McGraw-Hill Book Co., Inc., New York.

Andersland, O.B., and Ladanyi, B. 1994. An introduction to frozen ground engineering. Springer Science & Business Media, Berlin.

ARA, Inc., ERES Consultants Division. 2004. Guide for mechanistic–empirical design of new and rehabilitated pavement structures. Final report, NCHRP Project 1-37A. Transportation Research Board of the National Academies, Washington, D.C.

Azmatch, T.F., Sego, D.C., Arenson, L.U., and Biggar, K.W. 2012a. Using soil freezing characteristic curve to estimate the hydraulic conductivity function of partially frozen soils. Cold Regions Science and Technology, 83: 103-109.

Azmatch, T.F., Sego, D.C., Arenson, L.U., and Biggar, K.W. 2012b. New ice lens initiation condition for frost heave in fine-grained soils. Cold Regions Science and Technology, 82: 8-13.

Berg, R.L., Bigl, S.R., Stark, J.A., and Durell, G.D. 1996. Resilient modulus testing of materials from Mn/ROAD, Phase 1. CRREL-96-19, U.S, Army Cold Regions Research and

Engineering Laboratory, Hanover, N.H.
Bigl, S.R. and Berg, R.L. 1996a. Material Testing and Initial Pavement Design Modeling-Minnesota Road Research Project. CRREL-96-14, U.S, Army Cold Regions Research and Engineering Laboratory, Hanover, N.H.
Bigl, S.R., and Berg, R.L. 1996b. Testing of Materials from the Minnesota Cold Regions Pavement Research Test Facility. CRREL-96-20, U.S, Army Cold Regions Research and Engineering Laboratory, Hanover, N.H.
Bittelli, M., Flury, M. and Campbell, G.S. 2003. A thermodielectric analyzer to measure the freezing and moisture characteristic of porous media. Water Resources Research, 39(2): 11-1:10.
Black, P.B., and Miller, R.D. 1985. A continuum approach to modeling of frost heaving. In Freezing and Thawing of Soil-Water Systems. In Technical Council on Cold Regions Engineering Monograph. Edited by D.M. Anderson and P.J. Williams. ASCE, pp. 36-45.
Black, P.B., and Tice, A.R. 1989. Comparison of soil freezing curve and soil water curve data for Windsor sandy loam. Water Resources Research, 25(10): 2205-2210.
Caicedo, B., 2017. Physical modelling of freezing and thawing of unsaturated soils. Geotechnique, 67(2): 106-126.
Cheng, Q., Sun, Y., Xue, X. and Guo, J., 2014. In situ determination of soil freezing characteristics for estimation of soil moisture characteristics using a dielectric tube sensor. Soil Science Society of America Journal, 78(1), pp.133-138.
Chamberlain, E.J., and Blouin, S.E. 1977. Freeze-thaw enhancement of the drainage and consolidation of fine-grained dredged material in confined disposal areas. CRREL-77-16, U.S, Army Cold Regions Research and Engineering Laboratory, Hanover, N.H.
Christ, M., and Kim, Y.C. 2009. Experimental study on the physical-mechanical properties of frozen silt. KSCE Journal of Civil Engineering, 13(5): 317-324.
Cole, D.M., Bentley, D.L., Durell, G.D. and Johnson, T.C. 1987. Resilient modulus of freeze-thaw affected granular soils for pavement design and evaluation. Part 3. Laboratory tests on soils from Albany County Airport. CRREL-87-2, U.S, Army Cold Regions Research and Engineering Laboratory, Hanover, N.H.
Fredlund, D.G., and Xing, A. 1994. Equations for the soil-water characteristic curve. Canadian Geotechnical Journal, 31(4): 521-532.
Gens, A. 2010. Soil–environment interactions in geotechnical engineering. Geotechnique, 60(1): 3-74.
Grant, S.A. 1994. Some physical factors affecting contaminant hydrology in cold environments. Transportation Research Record: Journal of the Transportation Research Board, 1434: 61-69.
Han, Z., and Vanapalli, S.K. 2014. Predicting the variation of resilient modulus with respect to suction using the soil-water characteristic curve as a tool. In Proc. ASCE Geo-Institute's 2014 Annual Congress, 1463-1472.
Harlan, R.L. 1973. Analysis of coupled heat‐fluid transport in partially frozen soil. Water Resources Research, 9(5): 1314-1323.

Karube, D. and Kawai, K. 2001. The role of pore water in the mechanical behavior of unsaturated soils. In Unsaturated Soil Concepts and Their Application in Geotechnical Practice, Springer Netherlands, 211-241.

Konrad, J.M. 1994. Sixteenth Canadian Geotechnical Colloquium: Frost heave in soils: concepts and engineering. Canadian Geotechnical Journal, 31(2): 223-245.

Koopmans, R.W.R., and Miller, R.D. 1966. Soil freezing and soil water characteristic curves. Soil Science Society of America Journal, 30(6): 680-685.

Kurylyk, B.L. and Watanabe, K. 2013. The mathematical representation of freezing and thawing processes in variably-saturated, non-deformable soils. Advances in Water Resources, 60: 160-177.

Kweon, G. and Hwang, T. 2013. Deformational characteristics of subgrade soils and subbase materials with freeze-thaw. KSCE Journal of Civil Engineering, 17(6): 1317-1322.

Li, L., Liu, J., Zhang, X., and Saboundjian, S. 2011. Resilient modulus characterization of Alaska granular base materials. Transportation Research Record: Journal of the Transportation Research Board, 2232: 44-54.

Liu, Z., and Yu, X. 2014. Predicting the phase composition curve in frozen soils using index properties: A physico-empirical approach. Cold Regions Science and Technology, 108: 10-17.

Ma, W., Zhang, L. and Yang, C. 2015. Discussion of the applicability of the generalized Clausius–Clapeyron equation and the frozen fringe process. Earth-Science Reviews, 142: 47-59.

Oonk, H.A. and Calvet, M.T., 2007. Equilibrium between phases of matter: phenomenology and thermodynamics. Springer Science & Business Media, Berlin.

Pham, H.Q., Fredlund, D.G., and Barbour, S.L. 2005. A study of hysteresis models for soil-water characteristic curves. Canadian Geotechnical Journal, 42(6): 1548-1568.

Sayles, F.H., Baker, T.H.W., Gallavres, F., Jessberger, H.L., Kinosita, S., Sadovskiy, A.V., Sego, D., and Vyalov, S.S. 1987. Classification and laboratory testing of artificially frozen ground. Journal of Cold Regions Engineering, 1(1): 22-48.

Shastri, A., and Sanchez, M. 2012. Mechanical modeling of frozen soils incorporating the effect of cryogenic suction and temperature. In Unsaturated Soils: Research and Applications. Edited by N. Khalili, A. Russell, and A. Khoshghalb. Springer Berlin Heidelberg, pp. 159-164.

Sheng, D.C., Zhang, S., Niu, F.J. and Cheng, G. 2014. A potential new frost heave mechanism in high-speed railway embankments. Géotechnique, 64(2): 144-154.

Simonsen, E., Janoo, V.C., and Isacsson, U. 2002. Resilient properties of unbound road materials during seasonal frost conditions. Journal of Cold Regions Engineering, 16(1): 28-50.

Spaans, E.J., and Baker, J.M. 1996. The soil freezing characteristic: its measurement and similarity to the soil moisture characteristic. Soil Science Society of America Journal, 60(1): 13–19.

Tian, H., Wei, C., Wei, H., and Zhou, J. 2014. Freezing and thawing characteristics of frozen soils: Bound water content and hysteresis phenomenon. Cold Regions Science and

Technology, 103: 74-81.
Vanapalli, S.K., Fredlund, D.G., Pufahl, D.E. and Clifton, A.W. 1996. Model for the prediction of shear strength with respect to soil suction. Canadian Geotechnical Journal, 33(3): 379–392.
Vanapalli, S.K., Fredlund, D.G., and Pufahl, D.E. 1999. The influence of soil structure and stress history on the soil-water characteristics of a compacted till. Géotechnique, 49(2): 143-159.
Williams, P.J., and Smith, M.W. 1989. The frozen earth: fundamentals of geocryology. Cambridge University Press, Cambridge.
Zhang, S., Teng, J., He, Z., Liu, Y., Liang, S., Yao, Y. and Sheng, D., 2016. Canopy effect caused by vapour transfer in covered freezing soils. Géotechnique, 66(11): 927-940.
Zhou, X., Zhou, J. Kinzelbach, W., and Stauffer, F. 2014. Simultaneous measurement of unfrozen water content and ice content in frozen soil using gamma ray attenuation and TDR. Water Resources Research, 50(12): 9630-9655.

Chapter 6 Empirical model for predicting the resilient modulus of frozen unbound road materials using a hyperbolic function

The contents presented in this chapter are from the manuscript of the publication:

Ren, J. and Vanapalli, S.K., 2018. Empirical model for predicting the resilient modulus of frozen unbound road materials using a hyperbolic function. Transportation Geotechnics, 1-9.

DOI: 10.1016/j.trgeo.2018.09.011.

6.1 Abstract

The resilient modulus (M_R) is a key parameter required in the mechanistic-empirical methods, which are widely used for the rational design of pavement structures. However, experimental determination of the M_R is expensive and time-consuming since it requires elaborate equipment for testing and trained personnel. Due to this reason, several researchers have proposed models for predicting the M_R of unbound road materials that take into account the influence of wetting and drying conditions. However, the presently available models in the literature have some limitations for the prediction of the M_R of these materials at a frozen state. In this paper, a model with two-constants is proposed for predicting the variation of the M_R with subzero temperature for unbound road materials exploiting the hyperbolic shape of the frozen resilient modulus - subzero temperature relationship. Experimental data on eighteen different unbound road materials including both fine- and coarse-grained soils, and under both saturated and unsaturated conditions, were used to validate the proposed model. It is shown that the proposed model can reasonably well-predict the M_R of the investigated soils that are in a state of frozen condition. More investigations on different types of soils would be useful for better understanding the strengths and limitations of the proposed model. In addition, the effect of stress should be incorporated for further improving the model.

6.2 Introduction

The resilient modulus (M_R), which is defined as the ratio of the cyclic deviator stress (σ_d) to the recoverable strain (ε_r), is the key material property required for the rational design of pavements as per the *Guide for Mechanistic-Empirical Design of New and Rehabilitated Pavement Structures* (also known as MEPDG) (ARA, Inc., 2004). The M_R can be determined from experimental results with the aid of elaborate testing equipment that require highly trained technical personnel. For this reason, gathering information about the M_R from experimental methods is both expensive and time-consuming. Several models have been proposed in the literature for predicting the M_R considering various influencing factors such as the external stresses, soil types and / or soil physical properties using limited and easy-to-obtain experimental data (e.g., Drumm et al., 1990; ARA, Inc., 2004; Rahim, 2005; Han and Vanapalli, 2016).

Pavements' unbound aggregates and subgrade soils, throughout their design period life cycle, typically stay in a state of unsaturated condition (Ba et al., 2013). Suction, which is the energy potential of pore water in the unsaturated condition, influences the mechanical properties such as the shear strength and the resilient modulus of these materials (e.g., Vanapalli et al., 1996; Cary and Zapata, 2011; Salour and Erlingsson, 2015; Han and Vanapalli, 2015). The pavement structure is directly exposed to the external environment; due to this reason, environmental factors such as the evaporation and infiltration pose remarkable influence on the moisture content and suction within the pavement materials, and therefore on their mechanical properties (Cary and Zapata, 2010). In recent years, many researchers have proposed models that incorporate the contribution of suction for estimating resilient modulus under different moisture conditions. Han and Vanapalli (2016) provide a comprehensive summary of these models.

In addition to the moisture content variations, temperature is another key factor that has a significant influence on the behavior of the unbound materials (e.g., Simonsen and Isacsson, 1999; Berg et al., 1996; Simonsen et al., 2002). Typical variation of stiffness of unbound materials subjected to freezing-thawing is shown in **Figure 6.1**. When the soil temperature drops below 0 °C, ice crystals start to nucleate in the soil's pores. As the pore water changes to ice, its

volume increases approximately by 9% due to the opening of the lattice of its hexagonal crystal structures. The growing ice crystals interfere with each other and adjacent soil particles, resulting in the movement and rearrangement of the soil particles that contribute to changes in the original soil structure (Chamberlain and Blouin, 1977; Andersland and Anderson, 1978). The freezing process contributes to the significant increase in the original value of stiffness or resilient modulus, as shown in **Figure 6.1**. Such a behavior may be associated with different factors, which include the original soil strength, pore ice strength, and the synergistic strengthening effects between the soil and ice matrix preventing the collapse of the soil skeleton (Andersland and Ladanyi, 2004). On the other hand, if the temperature of frozen soil increases to positive values, pore ice within the soil melts which contributes to an increase in soil water content. The original soil structure changes due to pore ice melting and contributes to the loss of soil particles' cementation and loosening of soil fabric. The excess pore water that generated after the melting of ice is not able to drain at a relatively fast rate. Due to this reason, there will be a significant reduction in the soil resilient modulus after thawing. This period is critical (see **Figure 6.1**) for a pavement structure since the stiffness and capacity of the pavement structure decreases to its minimum value. The situation will be even worse when ice lenses are formed during the freezing process. The resilient modulus of unbound material, however, will gradually increase to its unfrozen value after the excess pore water pressure is fully dissipated. This is called the recovery period for pavement structure, as shown in **Figure 6.1**. The thaw-weakening period consists of the critical and recovery periods, during which the resilient modulus of unbound materials is lower than its unfrozen value and the pavement structure has low capacity. Therefore, it is common that spring load restriction is used as a pavement preservation strategy in cold regions (Yu et al., 2009).

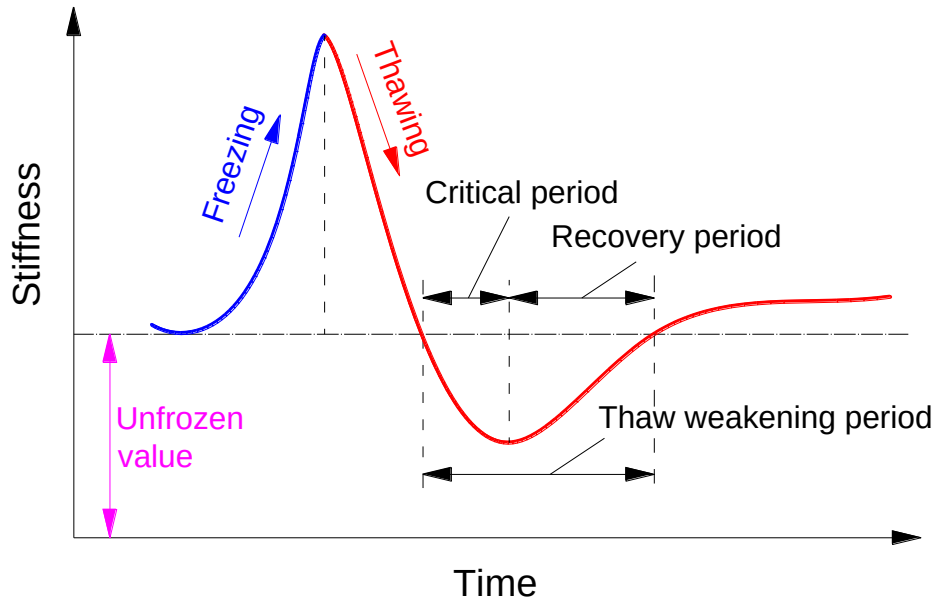

Figure 6.1 Variation in pavement stiffness under freezing-thawing (modified after Janoo and Cortez, 2002)

Experimental determination of the influence of temperature on the resilient modulus of unbound soils is challenging due to the complex and time-consuming testing procedures associated with the control and equilibrium of low negative values of temperature. It is desirable to develop reliable prediction models for estimating resilient modulus of unbound soils to facilitate the design of pavement structures in cold regions. Although the resilient modulus of the just thawed soil (i.e. during the critical period) or of the soil undergoing recovery is important for the rational design and preservation of pavement structure (e.g., determining the duration of the spring load restriction), the resilient modulus of the unbound soils at frozen state is equally important. In the MEPDG (ARA, Inc., 2004), constant values are assigned for the frozen resilient modulus of unbound soils based on different soil physical properties (i.e. 2.5×10^6 psi (approximately, 17000 MPa) for non-plastic soils, and 1×10^6 psi (approximately, 7000 MPa) for plastic soils). These assigned values are used to calculate the frozen adjustment factor, which is one of the key parameters for estimating the composite adjustment factor that is used to quantify the influence of environmental effect on the resilient modulus of unbound soils when designing

pavement structure. However, using a constant value for frozen resilient modulus may not be reasonable because the resilient modulus of frozen unbound soils varies with subzero temperatures (e.g., Berg et al., 1996; Simonsen et al., 2002). For example, the frozen resilient modulus of the New Hampshire marine clay is around 200 MPa at -2 °C; however, it reaches a value higher than 1500 MPa at -5 °C, and is approximately 3000 MPa at -10 °C (Simonsen et al., 2002).

The variation of frozen resilient modulus against subzero temperature is hyperbolic in nature. Due to this reason, a hyperbolic model is proposed in the present study for estimating the resilient modulus for both saturated and unsaturated frozen unbound soils, with the aid of two constants. The proposed model has been validated using experimental data on eighteen different soils, which include both fine- and coarse-grained soils under both saturated and unsaturated conditions. The proposed model is simple and provides reasonable predictions for the resilient modulus of the investigated eighteen frozen soils. For this reason, it is promising for use in the rational mechanistic-empirical design of pavement structures in cold regions.

6.3 Various Models for predicting the resilient modulus considering environmental effects

6.3.1 Models that consider the variation of moisture

Han and Vanapalli (2016) suggested that the relationships of M_R to moisture content or suction (ψ) in unsaturated unfrozen soils can be categorized into three groups; which include: (i) Empirical relationships (derived from regression analysis using extensive experimental data); (ii) Constitutive models (that incorporate ψ into applied shearing or confining stresses); and (iii) Extending stress state variables approach by considering the independent contribution of ψ to M_R.

For example, the MEPDG (ARA, Inc., 2004) recommends using Eq. (6.1) to estimate the M_R considering the influence of seasonal moisture content fluctuations, by referring to the M_R at the optimum moisture content (i.e. M_{ROPT}),

$$\log(\frac{M_R}{M_{ROPT}}) = a + \frac{b-a}{1+\exp[\ln(-b/a) + k_m(S - S_{OPT})]} \quad (6.1)$$

where S is the degree of saturation in the unsaturated unfrozen soil; S_{OPT} is the degree of saturation at the optimum moisture content; a is the minimum of $\log(M_R/M_{ROPT})$; b is the maximum of $\log(M_R/M_{ROPT})$; k_m is the regression parameter. The suggested values for a, b, and k_m are: -0.3123, 0.3, and 6.8157 for coarse-grained soils, and -0.5934, 0.4, and 6.1324 for fine-grained soils.

Han and Vanapalli (2014) proposed a semi-empirical model (Eq. (6.2)) to predict the variation in the M_R with respect to the ψ using the soil-water characteristic curve (SWCC), which represents the relationship between water content or S and ψ in an unsaturated unfrozen soil. Eq. (6.2) is similar to the models proposed by Vanapalli et al. (1996) and Oh et al. (2009) for predicting the unsaturated shear strength and the modulus of elasticity, respectively,

$$M_R = M_{RSAT} + \alpha\psi S^{\beta} \quad (6.2)$$

where M_{RSAT} is the M_R at the saturated condition (MPa); α and β are model parameters.

By incorporating ψ as a stress state variable, Cary and Zapata (2011) proposed the following equation, which was derived for a granular soil and a clayey sand from Arizona, USA over the soil suction range of 0 to 250 kPa,

$$M_R = k_1 P_a (\frac{\theta_{net} - 3\Delta u_{w-sat}}{P_a})^{k_2} (\frac{\tau_{oct}}{P_a} + 1)^{k_3} (\frac{\psi_0 - \Delta\psi}{P_a} + 1)^{k_4} \quad (6.3)$$

where P_a is the atmospheric pressure; θ_{net} is the net bulk stress; $\Delta u_{w\text{-}sat}$ is the build-up of pore water pressure under saturated conditions; τ_{oct} is the octahedral shear stress; ψ_0 is the initial suction; $\Delta\psi$ is the relative change of suction with respect to ψ_0 due to build-up of pore water pressure under unsaturated conditions; k_1, k_2, k_3, and k_4 are fitting parameters.

6.3.2 Models that consider the variation of temperature

The unfrozen water content has a significant influence on the physical and mechanical properties of frozen soils. Johnson et al. (1986) used the unfrozen water content as the key

variable and proposed an empirical equation for predicting the M_R of frozen soils ($M_{R(\text{frozen})}$), which is given below,

$$M_{R(\text{frozen})} = C_1(w_u / w)^{C_2} \tag{6.4}$$

where w_u is the gravimetric unfrozen water content; w is the total gravimetric water content (i.e. the sum of unfrozen water content and ice content); C_1 and C_2 are constants.

Similarly, Berg et al. (1996) used statistical regression techniques to interpret resilient modulus data of frozen and unfrozen soils. The nonlinear form of the equation used to model the resilient modulus is shown as Eq. (6.5),

$$M_{R(\text{frozen})} = K_1 P^{K_2} \tag{6.5}$$

where P is the governing parameter; K_1 and K_2 are constants. For frozen soils, three different governing parameters, all related to the unfrozen water contents: (i) gravimetric unfrozen water content normalized to the total gravimetric water content, w_u/w; (ii) gravimetric unfrozen water content normalized to a unit gravimetric unfrozen water content (w_0, equals to 1.0), w_u/w_0; and (iii) volumetric unfrozen water content (θ_u) normalized to a unit volumetric unfrozen water content (θ_0, equals to 1.0), θ_u/θ_0, can be used.

Simonsen et al. (2002) recommended several models for estimating the $M_{R(\text{frozen})}$ of different frozen soils from New Hampshire, USA as shown below:

For glacial till and silty fine sand,

$$M_{R(\text{frozen})} = k_1\left(\frac{|T|}{T_{\text{ref}}}\right)^{k_2}\left(\frac{\sigma_d}{\sigma_{\text{ref}}}\right)^{k_3} \tag{6.6a}$$

For coarse gravelly sand,

$$M_{R(\text{frozen})} = \exp\left(k_1 + k_2\left(\frac{T_{\text{ref}}}{T}\right)\right) \tag{6.6b}$$

For fine sand,

$$M_{R(\text{frozen})} = k_1\left(\frac{|T|}{T_{\text{ref}}}\right)^{k_2}\left(\frac{J_1}{\sigma_{\text{ref}}}\right)^{k_3}\left(\frac{\sigma_d}{\sigma_{\text{ref}}}\right)^{k_4} \tag{6.6c}$$

For marine clay,

$$M_{R(\text{frozen})} = k_1\left(\frac{|T|}{T_{\text{ref}}}\right)^{k_2}\left(\frac{\sigma_3}{\sigma_{\text{ref}}}\right)^{k_3} \tag{6.6d}$$

where T is the subzero temperature (°C); T_{ref} is the reference temperature (T_{ref} = 1 °C); σ_d is the deviator stress (MPa); J_1 is the bulk stress (MPa); σ_3 is the confining stress (MPa); σ_{ref} is the reference stress (σ_{ref} = 1 MPa); k_1, k_2, k_3, and k_4 are fitting parameters derived from regression analysis using experimental results and are different for different types of soils.

Ren and Vanapalli (2017) proposed a semi-empirical model for predicting $M_{R(\text{frozen})}$ for saturated unbound road materials (i.e. Eq. (6.7)). The model exploits the similarity between the drying-wetting processes in an unsaturated unfrozen soil and the freezing-thawing processes in a saturated frozen soil, and uses cryogenic suction (ψ_{cryo}) and degree of unfrozen water saturation (S_u) for prediction. The semi-empirical model has similar shape as Eq. (6.2).

$$M_{RSAT(\text{frozen})} = M_{RSAT(0℃)}\left(1+\chi\psi_{cryo}S_u^{\ \delta}\right) \tag{6.7}$$

where $M_{RSAT(0\,°C)}$ is the saturated resilient modulus at 0 °C (MPa); χ and δ are model parameters.

Models proposed by Johnson et al. (1986) and Berg et al. (1996) are empirical relationships between the resilient modulus of frozen soils and unfrozen water content. However, the models proposed for different types of soils by Simonsen et al. (2002) considered the influence of stress (e.g., deviator stress, confining stress, and bulk stress) on the resilient modulus of frozen soils. These models require different fitting parameters for the prediction of resilient modulus of different types of soils. Therefore, these models are valid only for soils and the conditions for which they have been developed. The model proposed by Ren and Vanapalli (2017) works well for different types of saturated soils and has a theoretical basis. However, the model is only applicable to saturated soils. For this reason, there is a need for a model for predicting the in-situ resilient modulus of unbound soils, where the field water content is typically less than their saturated water content.

6.4 The proposed hyperbolic model

Unfrozen water and pore ice coexist in frozen soils. The quantity, composition, and properties of the unfrozen water and pore ice are not constant, but change with variations of external factors, with which they are in dynamic equilibrium (Tsytovich, 1975). The principal factor is the subzero temperature (Nersesova and Tsytovich, 1963; Anderson, 1967). Pore ice can firmly bond or cement soil particles together, resulting in the significant increase in soil strength and stiffness, and decrease in hydraulic conductivity (e.g., Chamberlain and Gow, 1979; Hivon and Sego, 1995; Berg et al., 1996; Andersland and Ladanyi, 2004). Due to this reason, freezing is sometimes used to stabilize soils during the construction of foundations, tunnels, and retaining walls where weak soils are encountered (Chamberlain and Gow, 1979).

Experimental studies by several investigators on resilient modulus of frozen soils suggest that the variation in resilient modulus of frozen soils is closely related to a decrease in subzero temperature, and the variation curve resembles the shape of hyperbola (e.g., Berg et al., 1996; Simonsen et al., 2002). On the other hand, various stress combinations do not have significant impact on the frozen resilient modulus (Berg et al., 1996), especially considering the significant value of resilient modulus at subzero temperatures. In addition, according to the *Standard Method of Test for Determining the Resilient Modulus of Soils and Aggregate Materials* (AASHTO T307-99, 2007), the applied stress levels for determining the resilient modulus of unbound road materials are relatively low. In other words, it can be assumed that the effect of general stress combinations encountered by unbound road materials on their frozen resilient modulus is negligible. Extending this assumption, a simple two-constant hyperbolic model is proposed in the present study to predict the Log($M_{R(\text{frozen})}$) – subzero temperature relationship for unbound road materials. The model can be expressed as below:

$$\text{Log}(M_{R(\text{frozen})}) = \text{Log}(M_{R(0℃)})(1+\frac{(-T)}{A+B(-T)}) \tag{6.8}$$

where $M_{R(0\,°C)}$ is the resilient modulus at 0 °C (MPa); T is the subzero temperature (°C); A and B are model parameters. For simplicity, the units of the resilient modulus and subzero temperature are ignored when using the proposed model.

6.5 Model validation

Experimental data of eighteen different soils from the literature were used in the validation of the proposed model. Soils 1 through 7 were saturated soils while Soils 8 through 18 were unsaturated soils. The basic properties of these soils are summarized in **Table 6.1**. **Figure 6.2** shows the grain size distribution of these soils.

6.5.1 Soils 1 through 7

The subgrade 1206 (Soil 1) and subgrade 1232 (Soil 2) are, respectively, the high- and low-heaving sandy lean clay subgrade. The class 6 base (Soil 3) has a relatively small amount of fines while the class 3 subbase (Soil 4) is a material with a high percentage of fines. These materials were compacted and saturated. Once saturated, the specimens were frozen from the top down with a surcharge of 3.4 kPa and at a rate of about 25 mm/day under an open-system condition. They were then tested at three different temperatures below freezing. In addition, they were also tested in a thawed, saturated state at room temperature. Taxiway A base (Soil 5) and subbase (Soil 6) are crushed stone base and gravelly sand subbase, respectively. Taxiway B subbase (Soil 7) is silty sandy gravel. These three soils were compacted and then frozen at a rate of 25 mm/day under an open-system condition. The samples did not heave appreciably. More details of the testing techniques for these seven soils such as the triaxial equipment used, the applied load pulse waveforms, stress levels and testing procedures are available in Berg et al. (1996) and Cole et al. (1987).

The test results of the variation in resilient modulus in frozen state with a decrease in subzero temperature resembles the shape of hyperbola. Eq. (6.8), which is a two-constant hyperbolic function, is employed to best-fit the frozen resilient modulus for the seven saturated soils. The fitted results are shown in **Figure 6.3** and **Figure 6.4**, and summarized in **Table 6.2**. Good agreement between the measured and best-fitted data has been achieved using the proposed hyperbolic model for the seven saturated frozen soils (as indicated by the high value of the coefficient of determination (R^2) in **Table 6.2**).

Table 6.1 Physical properties of soils used in the study

No.	Soil	Type	γ_d	w_{sat}	G_s	w_L	I_p	C_u	C_c	AASHTO[a]	USCS[b]	Data from
1	Subgrade 1206	Sandy lean clay	16.8	23.4	2.70	37.0	18.5	/	/	A-6	CL	Berg et al., 1996; Bigl and Berg, 1996a; Bigl and Berg, 1996b
2	Subgrade 1232	Sandy lean clay	17.1	19.3	2.71	26.4	10.9	/	/	A-6	CL	
3	Class 6 base	Well-graded gravel	21.0	9.4	2.74	/	/	21.3#	2.1#	/	GW	
4	Class 3 subbase	Well-graded sand	20.3	9.7	2.69	17.0*	1.2*	16.2#	2.2#	A-1-b	SW	
5	Taxiway A base	Crushed stone	19.4	7.5	/	/	/	494.7#	1.3#	/	/	Cole et al., 1987
6	Taxiway A subbase	Silty sand	20.9	7.5	2.73	/	/	72.8#	1.8#	A-1-b	SM	
7	Taxiway B subbase	Silty sandy gravel	20.0	5.5	2.68	/	/	275.9#	4.7#	/	GM	
No.	**Soil**	**Type**		γ_{dmax}	w_{opt}	C_u	C_c	**AASHTO[a]**			**USCS[b]**	**Data from**
8	NH1	Silty glacial till		20.5	9.0	/	/	A-4			SM	Janoo et al., 1999; Simonsen et al., 2002
9	NH2	Silty fine sand		17.2	14.5	/	/	A-2-4			SM	
10	NH3	Coarse gravelly sand		17.3	9.5	7.5#	0.7#	A-1-a			SP	
11	NH4	Medium fine sand		16.4	13.6	10.0#	1.2#	A-1-b			SP	
12	NH5	Marine clay		16.1	23.5	/	/	A-7-5			ML	
No.	**Soil**	G_s	γ_d	w		w_L	I_p	C_u		C_c		**Data from**
13	Dense graded stone	2.81	17.9	21.8		23	3	32.8		7.1		Cole et al., 1986
14	Ikalanian sand	2.70	14.8	22.7		/	/	4.5		0.96		
15	Hart brothers sand	2.76	15.5	18.6		/	/	8.0		0.92		
16	Sibley till	2.74	18.3	12.5		19	4	235.0		4.1		
17	Graves sand	2.70	12.9	31.0		/	/	39.1		1.6		
18	Hyannis sand	2.67	14.4	29.1		/	/	4.7		1.2		

[a] American Association of State Highway and Transportation Officials.
[b] Unified Soil Classification System (ASTM D2487-11).
* Fraction that passed No. 40 sieve.
# Calculated from grain size distribution curve.
/ Not available.
γ_d: dry unit weight (kN/m^3); γ_{dmax}: maximum dry unit weight (kN/m^3); w: moisture content (%); w_{opt}: optimum moisture content (%); w_{sat}: saturated moisture content (%); G_s: specific gravity; w_L: liquid limit (%); I_p: plasticity index; C_u: coefficient of uniformity; C_c: coefficient of curvature.

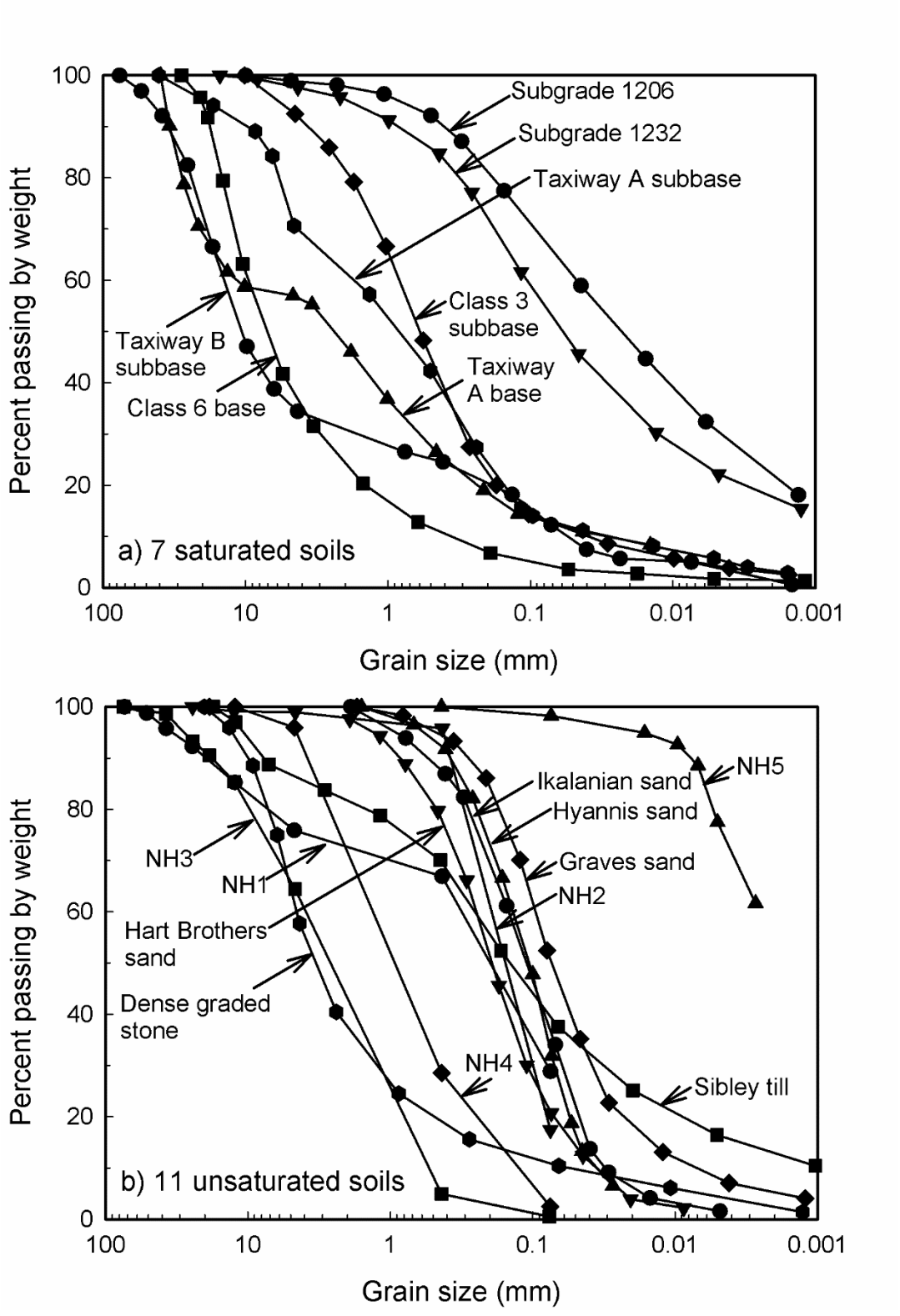

Figure 6.2 Grain size distribution of the eighteen soils

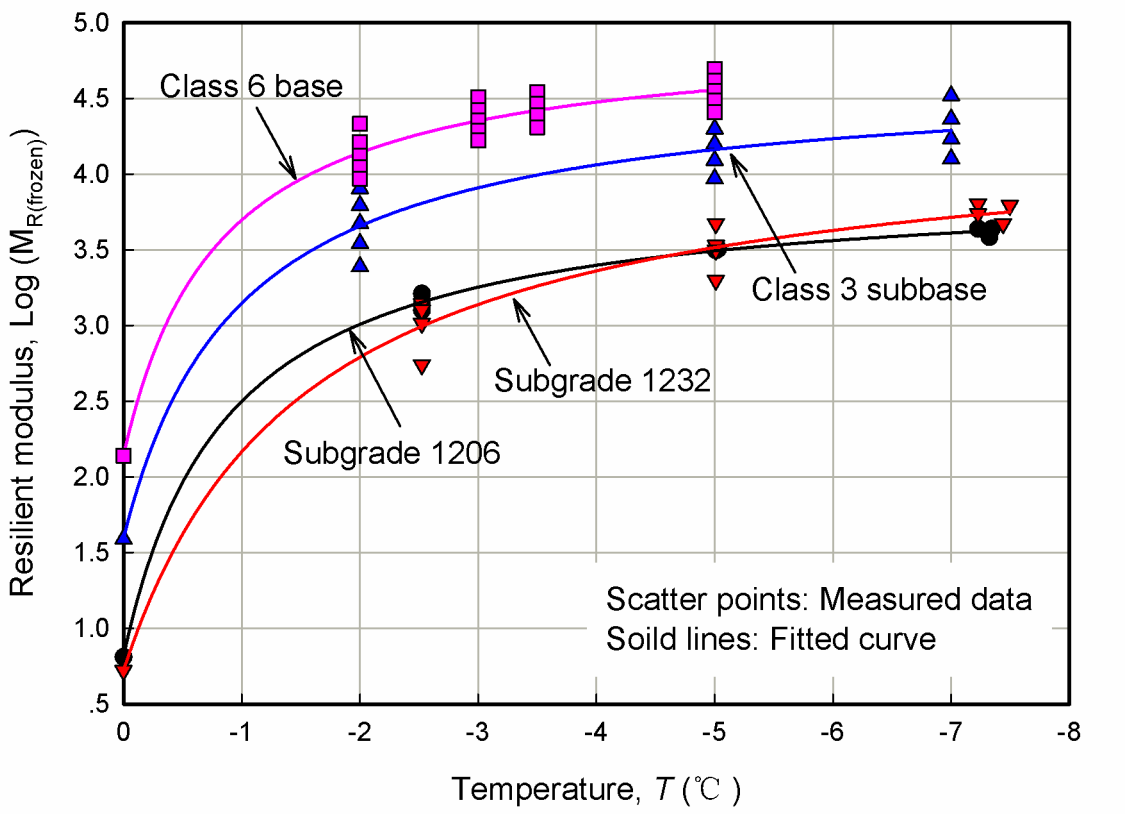

Figure 6.3 Comparison between the measured and predicted resilient modulus values for Subgrade 1206, Subgrade 1232, Class 6 base, and Class 3 subbase (measured data from Berg et al. (1996))

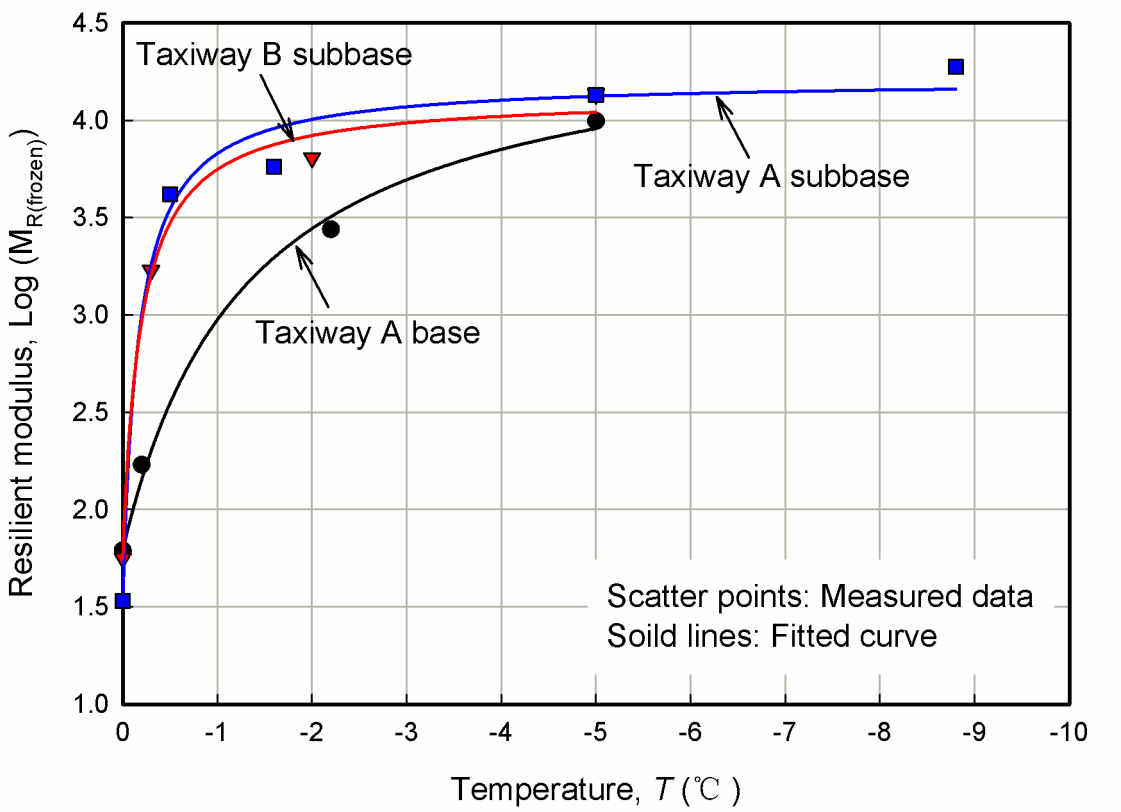

Figure 6.4 Comparison between the measured and predicted resilient modulus values for Taxiway A base, Taxiway A subbase, and Taxiway B subbase (measured data from Cole et al. (1987))

Table 6.2 Summary of the results by using the hyperbolic model

No.	Soil	M_R data points	Model parameters		Log($M_{R(0\,°C)}$)	R^2
			A	*B*		
1	Subgrade 1206	9	0.222 (0.014)	0.257 (0.003)	0.81	0.99
2	Subgrade 1232	13	0.301 (0.040)	0.198 (0.009)	0.72	0.97
3	Class 6 base	20	0.612 (0.102)	0.763 (0.033)	2.14	0.96
4	Class 3 subbase	14	0.504 (0.090)	0.517 (0.024)	1.59	0.95
5	Taxiway A base	4	0.856 (0.155)	0.655 (0.049)	1.79	0.99
6	Taxiway A subbase	5	0.094 (0.030)	0.571 (0.023)	1.53	0.98
7	Taxiway B subbase	4	0.141 (0.030)	0.736 (0.031)	1.75	0.99
8	NH1	5	0.274 (0.074)	0.661 (0.037)	1.72	0.97
9	NH2	5	0.461 (0.038)	0.758 (0.015)	1.79	0.99
10	NH3	4	0.502 (0.021)	2.405 (0.006)	2.48	1.00
11	NH4	5	0.080 (0.004)	0.554 (0.003)	1.55	0.99
12	NH5	5	2.144 (0.536)	0.434 (0.083)	1.40	0.97
13	Dense graded stone	4	0.081 (0.021)	0.704 (0.046)	1.87	0.98
14	Ikalanian sand	5	0.308 (0.097)	0.602 (0.039)	1.65	0.97
15	Hart Brothers sand	8	0.357 (0.041)	0.497 (0.013)	1.38	0.99
16	Sibley till	4	0.225 (0.014)	0.489 (0.005)	1.47	0.99
17	Graves sand	6	0.351 (0.019)	0.435 (0.007)	1.36	0.99
18	Hyannis sand	5	0.121 (0.031)	0.472 (0.018)	1.53	0.98

Note: Number in parenthesis is the Standard Error.

6.5.2 Soils 8 through 18

The NH soils (Soils 8 through 12) were from different investigation sites from New Hampshire, USA. The five soils were compacted at their optimum moisture contents in five equal layers by means of a kneading compactor. They were then subjected to omnidirectional closed-system freezing and generally tested at five temperatures below freezing. The soils were mounted in a triaxial cell that was accommodated inside a mechanically cooled climate chamber, which was placed between the columns of a closed-loop servo-hydraulic load frame. The soil samples were tested using a 0.1-s haversine pulse and a 0.9-s rest period. Detailed testing

procedures can be found in Simonsen et al. (2002). Soils 13 through 18 were collected from the experimental pavement sections at a site in Winchendon, Massachusetts, USA. These coarse soils were also molded in five equal layers with sufficient compaction effort to achieve the estimated in-situ density. The specimens were frozen unidirectionally at about 25 mm/day in insulated cabinets using open-system freezing (Cole et al., 1986). The same triaxial machine and applied load as in Cole et al. (1987) were used. Detailed procedures that were followed for performing these tests are available in Cole et al. (1986).

The best-fit results using the hyperbolic model are shown in **Figure 6.5** and **Figure 6.6**, and **Table 6.2**. Good agreement between the measured and best-fitted data has been achieved for the eleven unsaturated frozen soils. The hyperbolic model provides good comparisons with the measured results of the soil samples that were tested at their saturated water contents (see results of Soils 1 through 7 in **Figure 6.3** and **Figure 6.4**). Thus, it can be concluded that the proposed hyperbolic model can be used for the prediction of resilient modulus of both saturated and unsaturated frozen soils with a reasonably high degree of accuracy (see R^2 values in **Table 6.2**).

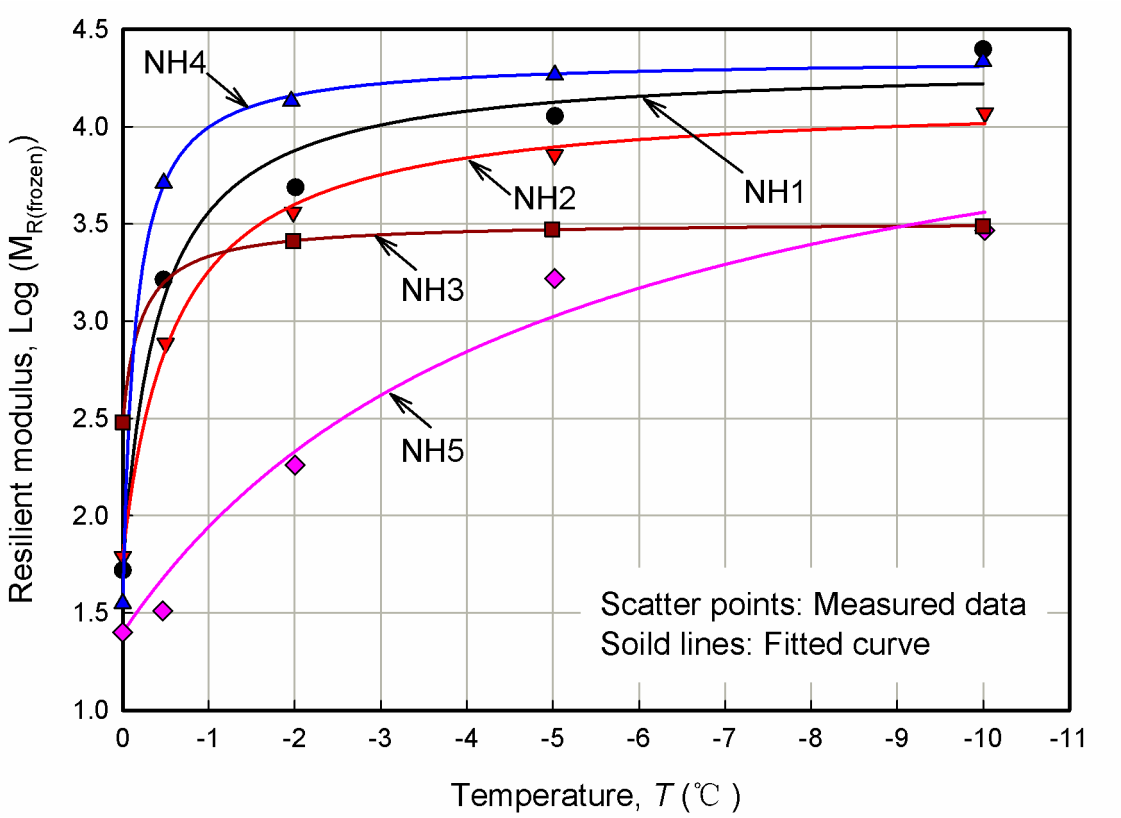

Figure 6.5 Comparison between the measured and predicted resilient modulus values for NH1, NH2, NH3, NH4, and NH5 (measured data from Simonsen et al. (2002))

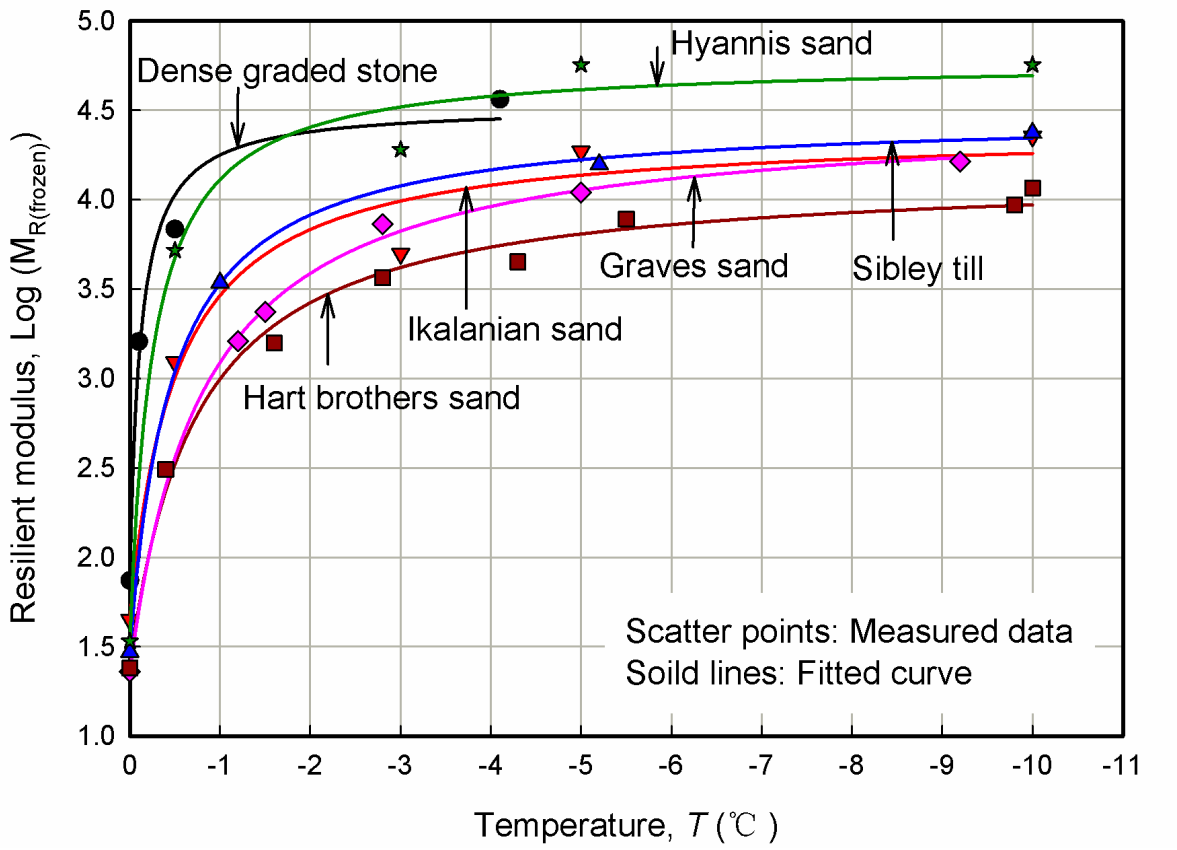

Figure 6.6 Comparison between the measured and predicted resilient modulus values for Dense graded stone, Ikalanian sand, Hart brothers sand, Sibley till, Graves sand, and Hyannis sand (measured data from Cole et al. (1986))

From **Figure 6.3** to **Figure 6.6**, it can be observed that the frozen resilient moduli of the eighteen soils increase significantly within the temperature range from 0 to -2 °C. This is particularly true for the coarse-grained soils. The pore water crystalizes and transforms into ice in the relatively large pores of coarse-grained soils quickly in small temperature range. This is consistent with the variation in the resilient modulus of coarse-grained frozen soils, which also increases rapidly within 0 to -1 °C and then becomes relatively constant. On the other hand, small pores and adsorptive forces of clay particles that dominate in fine-grained soils require a relatively large temperature range for the pore water to transform into ice. This observation can be derived from the result that an increase in the frozen resilient modulus with decreasing

temperatures even for values lower than -10 °C. Therefore, the significant influence of subzero temperature on the resilient modulus can be manifested by the amount of unfrozen water, or more precisely, the ice content in the soils. As observed by Janoo et al. (1999), the frozen resilient modulus of the NH soils except for the marine clay (NH5) at -20 °C was similar to that obtained at -10 °C. This suggests that most water is in a state of frozen condition as temperature is lowered to -10 °C in these soils.

6.6 Discussion

6.6.1 Model parameters *A* and *B*

The proposed hyperbolic model (i.e. Eq. (6.8)) can be written as Eq. (6.9),

$$\frac{\mathrm{Log}(M_{R(\mathrm{frozen})})}{\mathrm{Log}(M_{R(0℃)})} = 1 + \frac{(-T)}{A + B(-T)} \tag{6.9}$$

Eq. (6.9) can be rearranged as below:

$$\frac{\mathrm{Log}(M_{R(0℃)})}{\mathrm{Log}(M_{R(\mathrm{frozen})}) - \mathrm{Log}(M_{R(0℃)})} = \frac{A + B(-T)}{(-T)} \tag{6.10}$$

Eq. (6.10) can be written in a form as Eq. (6.11) assuming $-T = (0 - T) = \Delta T$,

$$\frac{1}{\mathrm{Log}(M_{R(\mathrm{frozen})}) - \mathrm{Log}(M_{R(0℃)})} = \frac{1}{\Delta T}\frac{A}{\mathrm{Log}(M_{R(0℃)})} + \frac{B}{\mathrm{Log}(M_{R(0℃)})} \tag{6.11}$$

The relationship between the parameter A, ΔT, and the change in the resilient modulus (i.e. $\mathrm{Log}(M_{R(\mathrm{frozen})}) - \mathrm{Log}(M_{R(0\,℃)})$) is illustrated in **Figure 6.7**. If ΔT is kept constant, from Eq. (6.11), it can be seen that parameter A is influenced by the change in the resilient modulus (Note that B is constant). A larger change in the resilient modulus corresponds to a relatively smaller value of parameter A. **Figure 6.8** shows the influence of parameter A on the prediction curve while keeping the value of parameter B constant for different soils (see the B values shown in **Table 6.2**). As can be seen, for the selected six soils investigated in the present study, lower value of parameter A results in more rapid change in the prediction curve within the temperature range of 0 to -2 °C. The rapid change in the resilient modulus is due to the decrease in unfrozen water

content in the soils, or to the formation of pore ice, which firmly bonds soil particles together and increases the soil stiffness significantly. This suggests that parameter A may be related to the unfrozen water content, which is influenced by the soil structure and physical properties at certain subzero temperatures. Attempts to suggest a relationship between the parameter A and soil physical properties (e.g., dry unit weight, initial water content, plasticity index, and coefficient of uniformity) were not successful. This may be attributed to the eighteen soils from various investigations have significantly different physical properties (see **Table 6.1**). In addition, the soil specimens were prepared under various conditions and tested following different techniques. The structure of these soils (both coarse- and fine-grained) is likely different. Due to this reason, the pore ice structure and distribution that develop at subzero temperatures in these soils can be also complex. All these reasons, may have contributed to difficulties in developing a well-defined or unique relationship.

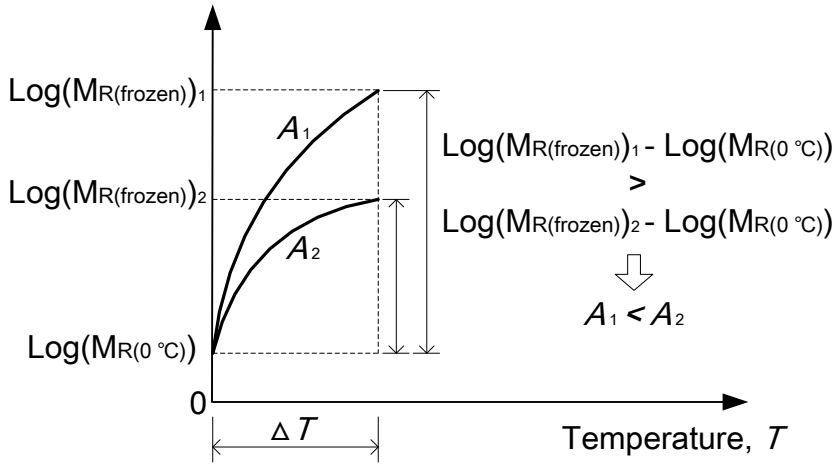

Figure 6.7 Illustration of the relationship between (Log($M_{R(\text{frozen})}$) - Log($M_{R(0\ ^\circ\text{C})}$)) and model parameter A when ΔT is kept constant

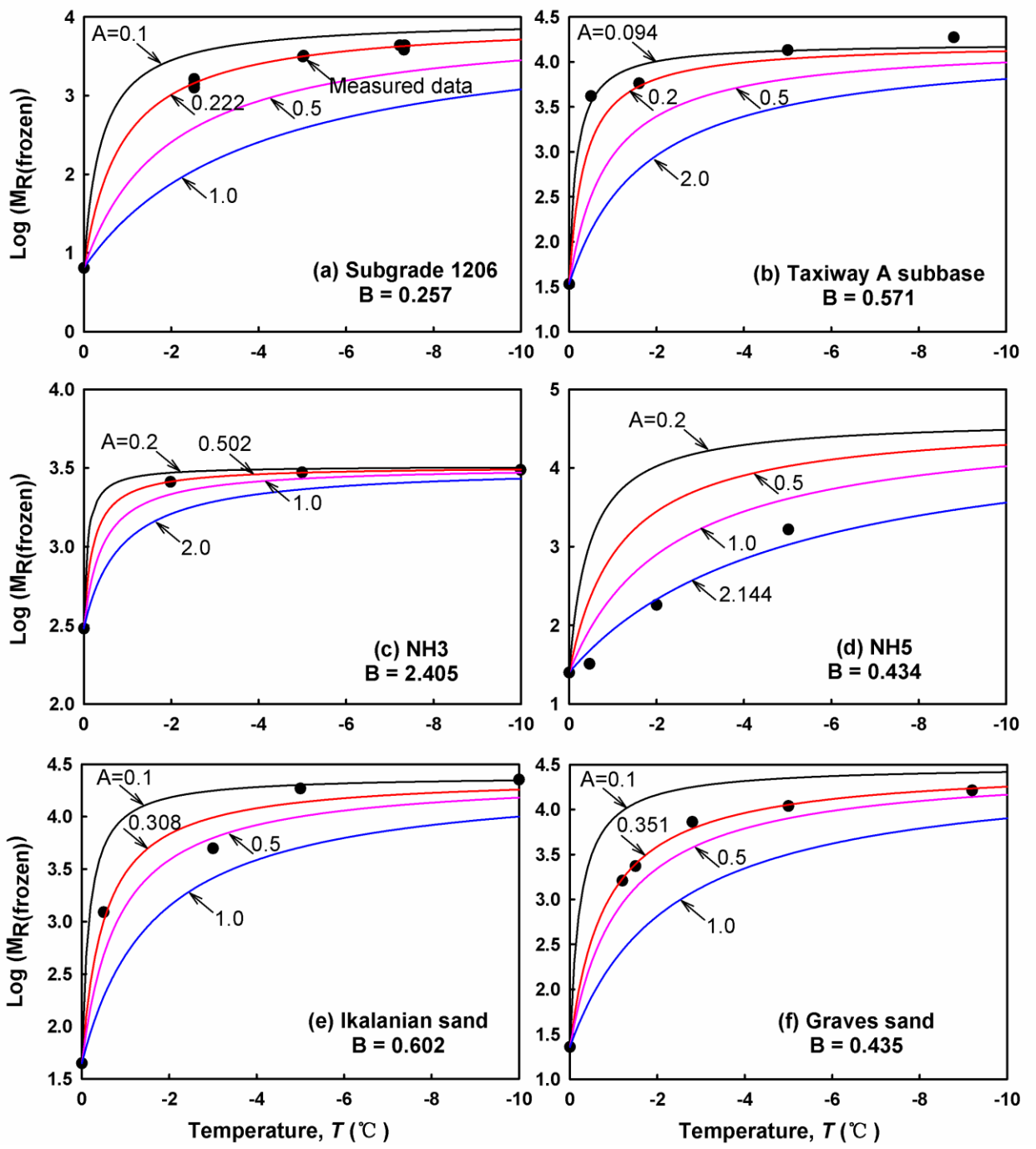

Figure 6.8 Influence of parameter *A* on the prediction results for (a) Subgrade 1206, (b) Taxiway A subbase, (c) NH3, (d) NH5, (e) Ikalanian sand, and (f) Graves sand

On the other hand, parameter *B* is not influenced by the change in the resilient modulus. The parameter *B*, however, was found to be strongly dependent on the resilient modulus at 0 °C (i.e. Log($M_{R(0\,°C)}$)). **Figure 6.9** shows that the variation in parameter *B* with the Log($M_{R(0\,°C)}$) for fourteen soils investigated in this paper can be well-fitted with an exponential equation (i.e. Eq. (6.12) with the Adj. R^2 of 0.88). The parameter *B* increases gradually before the value of Log($M_{R(0\,°C)}$) reaching 2.0; however, it increases rapidly with a further increase in Log($M_{R(0\,°C)}$).

$$B = 0.0392 \times \exp[1.6241 \times \mathrm{Log}(M_{R(0℃)})] \tag{6.12}$$

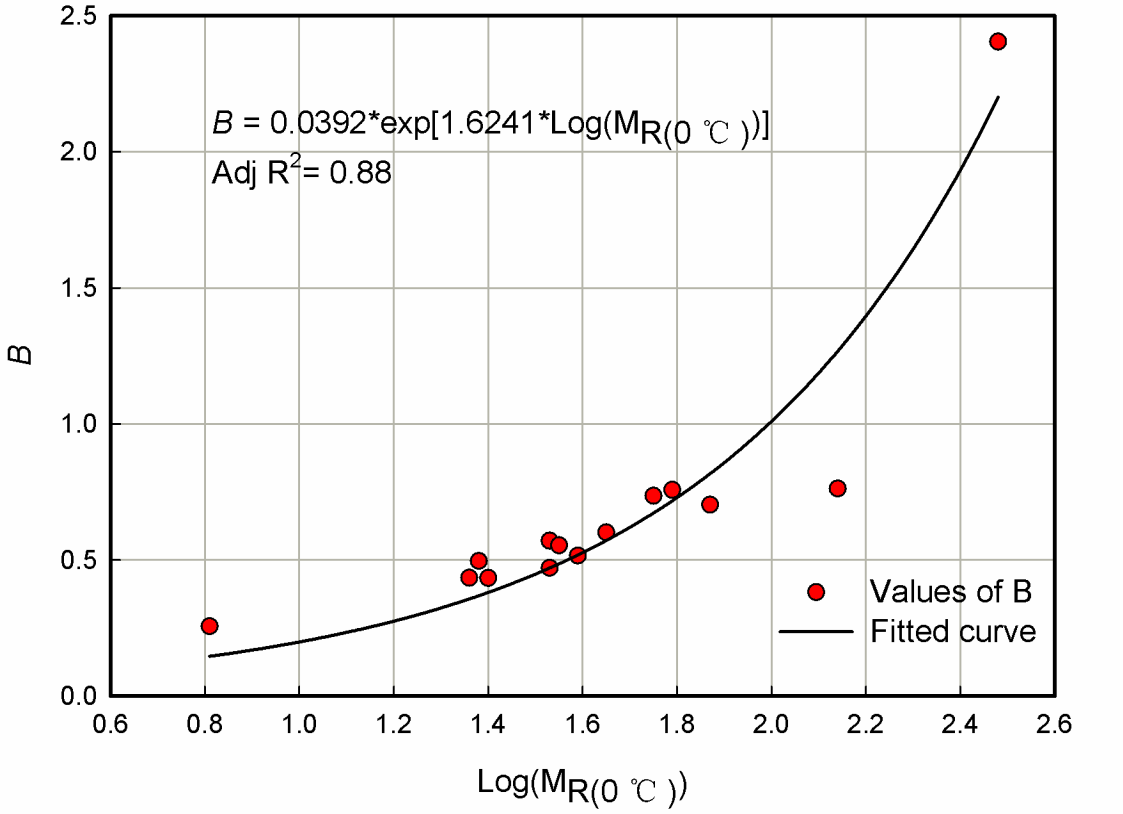

Figure 6.9 The relationship between parameter *B* and Log($M_{R(0\,°C)}$)

The resilient modulus data of the other four soils (i.e. Subgrade 1232, Taxiway A base, NH1, and Sibley till) were used to validate the relationship between parameter *B* and Log($M_{R(0\,°C)}$). The parameter *B* can be calculated for these four soils as 0.126, 0.718, 0.640, and 0.427, respectively, with the aid of Eq. (6.12). Using the calculated values of parameter *B*, the

measured experimental data were fitted for the four soils and summarized in **Figure 6.10**. The results highlight a good fit for the four soils, suggesting that the parameter *B* can be reliably estimated using Eq. (6.12).

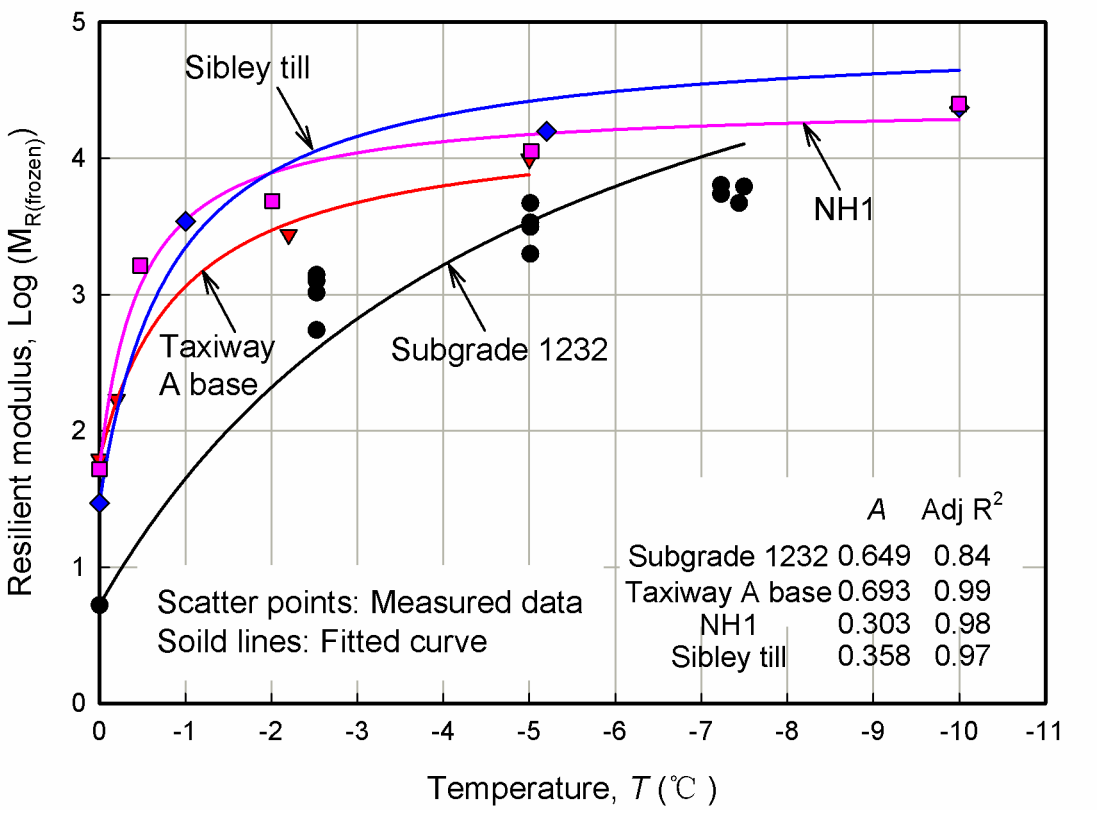

Figure 6.10 Comparison between the measured and predicted resilient modulus values using calculated *B* values for Subgrade 1232, Taxiway A base, NH1, and Sibley till

6.6.2 Strengths and limitations of the proposed model

The proposed hyperbolic model in the present study well predicts the resilient modulus for both fine- and coarse-grained frozen soils, and for both saturated and unsaturated conditions. In order to determine the parameters (i.e. *A* and *B*) in the model, at least two measured data points information is required. However, if more measured data is available, it would enhance the reliability of these fitting parameters. The investigations of the present study highlight that parameter *B* has strong relationship with the initial resilient modulus (i.e. Log($M_{R(0\ ^\circ C)}$)) (see

Figure 6.9). This relationship is useful for quick and reliable estimation of the parameter *B*. The parameter *A* could be related to unfrozen water content in the soil. In other words, in spite of the hyperbolic model being an empirical method, both the parameters *A* and *B* are related to frozen soil properties. The use of parameters *A* and *B* can reduce the empirical nature in predicting frozen resilient modulus for different types of soils. As suggested by Simonsen et al. (2002), the differences between soil types and conditions may be reflected through model parameters with physical meanings. In their study, different empirical regression equations were suggested for different types of soils (see Eq. (6.6)). Due to this reason, such equations are valid only for the soils and to the conditions close to which they were developed (Simonsen et al., 2002).

Another advantage of the proposed hyperbolic model is that it does not require the soil to be in a state of fully saturated condition (the model was validated on different soils with various initial water contents from 5.5% to 31% (see **Table 6.1**)). Therefore, it has wider application since most unbound road soils are generally compacted at their optimum moisture contents at which they are in a state of unsaturated condition. In addition, resilient modulus of soils at a specific stress and moisture content level is generally considered constant for the temperatures above 0 °C (e.g., Janoo et al., 1999; Li et al., 2010). Hence, the resilient modulus at ambient temperature (e.g., 20 °C) can be used to represent $M_{R(0\,^{\circ}C)}$. This eliminates the need to measure resilient modulus precisely at 0 °C, which is cumbersome and difficult.

The eighteen soils used for validation were tested under different conditions (e.g., different loading forms and stress levels). For example, the loading form on Soils 1-4 and 13-18 had the pulse length approximately one second with two seconds interval between successive pulses. For Soils 5-7, a 28 milliseconds haversine was repeated every two seconds. However, for Soils 8-12 a 0.1 second haversine pulse and a 0.9 second rest period was used, which is consistent with AASHTO T307-99 (2007). This suggests that the proposed model is suitable for modeling a variety of different testing conditions. In other words, the standard AASHTO T307-99 (2007) could be followed in order to use the proposed model.

The proposed model only considers subzero temperature as the single independent variable

and assumes that the effect of general stress combinations encountered by unbound road materials on their frozen resilient modulus is negligible, which makes the model simple and easy to use. The assumption used does not contribute to significant errors as supported by the good fitting results obtained for the eighteen soils, whose frozen resilient moduli were determined using confining and deviator stress values that were generally lower than 150 kPa and 1 MPa respectively, by different researchers. On the other hand, it should also be noted that relatively large stress levels have influence on the frozen resilient modulus of unbound soils. For example, pore ice may melt under large stress levels, which makes the soil specimen unstable and introduces difficulties to resilient modulus measurement. Furthermore, the energy dissipation under cyclic loading condition is significant under large deviator stress level, making the soil specimen even more unstable.

6.7 Summary

In this paper, a hyperbolic model with two fitting parameters (i.e. A and B) was proposed for predicting the resilient modulus of unbound road materials at frozen state, based on the shape of the experimental data determined for frozen resilient modulus versus subzero temperature. The model was validated using the data of eighteen soils comprising of both fine- and coarse-grained soils that were tested under both saturated and unsaturated conditions. The parameter A has significant influence on the prediction results and can be related to the unfrozen water content in the frozen soils. A lower value of parameter A results in more rapid change in the prediction results within the temperature range of 0 to -2 °C. The parameter B was found to have a strong relationship with the initial resilient modulus (i.e. $\mathrm{Log}(M_{R(0\ ^\circ\mathrm{C})})$) which was used for prediction. The model is simple and promising for use in pavement engineering practice. However, more efforts are needed to further improve the proposed model and validate it with additional experimental data on different types of soils. In addition, the influence of stress level should be investigated and incorporated into the model. It would be a good practice to follow the standard AASHTO T307-99 (2007) for future studies and use the proposed model.

6.8 References

AASHTO Designation: T307-99. 2007. Standard Method of Test for Determining the Resilient Modulus of Soils and Aggregate Materials, American Association of State Highway and Transportation Officials, Washington, D.C.

Andersland, O.B., and Anderson, D.M. 1978. Geotechnical engineering for cold regions. McGraw-Hill Book Co., Inc., New York.

Andersland, O.B. and Ladanyi, B. 2004. Frozen ground engineering. John Wiley & Sons, New Jersey.

Anderson, D.M. 1967. Ice nucleation and the substrate-ice interface. Nature, 216: 563-566.

ARA, Inc., ERES Consultants Division. 2004. Guide for mechanistic–empirical design of new and rehabilitated pavement structures. Final report, NCHRP Project 1-37A. Transportation Research Board of the National Academies, Washington, D.C.

Ba, M., Nokkaew, K., Fall, M., and Tinjum, J.M. 2013. Effect of matric suction on resilient modulus of compacted aggregate base courses. Geotechnical and Geological Engineering, 31(5): 1497-1510.

Berg, R.L., Bigl, S.R., Stark, J.A., and Durell, G.D. 1996. Resilient modulus testing of materials from Mn/ROAD, Phase 1. CRREL-96-19, U.S, Army Cold Regions Research and Engineering Laboratory, Hanover, N.H.

Bigl, S.R. and Berg, R.L. 1996a. Material Testing and Initial Pavement Design Modeling-Minnesota Road Research Project. CRREL-96-14, U.S, Army Cold Regions Research and Engineering Laboratory, Hanover, N.H.

Bigl, S.R., and Berg, R.L. 1996b. Testing of Materials from the Minnesota Cold Regions Pavement Research Test Facility. CRREL-96-20, U.S, Army Cold Regions Research and Engineering Laboratory, Hanover, N.H.

Cary, C.E., and Zapata, C.E. 2010. Enhanced model for resilient response of soils resulting from seasonal changes as implemented in mechanistic-empirical pavement design guide. Transportation Research Record: Journal of the Transportation Research Board, 2170: 36-44.

Cary, C.E., and Zapata, C.E. 2011. Resilient modulus for unsaturated unbound materials. Road Materials and Pavement Design, 12(3): 615-638.

Chamberlain, E.J., and Blouin, S.E. 1977. Freeze-thaw enhancement of the drainage and consolidation of fine-grained dredged material in confined disposal areas. CRREL-77-16, U.S, Army Cold Regions Research and Engineering Laboratory, Hanover, N.H.

Chamberlain, E.J. and Gow, A.J., 1979. Effect of freezing and thawing on the permeability and structure of soils. Engineering geology, 13(1-4): 73-92.

Cole, D.M., Bentley, D.L., Durell, G.D. and Johnson, T.C. 1986. Resilient modulus of freeze-thaw affected granular soils for pavement design and evaluation. Part 1. Laboratory tests on soils from Winchendon, Massachusetts, test Sections. CRREL-86-4, U.S, Army Cold Regions Research and Engineering Laboratory, Hanover, N.H.

Cole, D.M., Bentley, D.L., Durell, G.D. and Johnson, T.C. 1987. Resilient modulus of freeze-thaw affected granular soils for pavement design and evaluation. Part 3. Laboratory

tests on soils from Albany County Airport. CRREL-87-2, U.S, Army Cold Regions Research and Engineering Laboratory, Hanover, N.H.

Drumm, E.C., Boateng-Poku, Y., and Johnson Pierce, T. 1990. Estimation of subgrade resilient modulus from standard tests. Journal of Geotechnical Engineering, 116(5): 774-789.

Han, Z., and Vanapalli, S.K. 2014. Predicting the variation of resilient modulus with respect to suction using the soil-water characteristic curve as a tool. In Proc. ASCE Geo-Institute's 2014 Annual Congress, 1463-1472.

Han, Z. and Vanapalli, S.K., 2015. Model for predicting resilient modulus of unsaturated subgrade soil using soil-water characteristic curve. Canadian Geotechnical Journal, 52(10): 1605-1619.

Han, Z., and Vanapalli, S.K. 2016. State-of-the-art: prediction of resilient modulus of unsaturated subgrade soils. International Journal of Geomechanics, 16(4): 1-15.

Hivon, E.G. and Sego, D.C., 1995. Strength of frozen saline soils. Canadian Geotechnical Journal, 32(2): 336-354.

Janoo, V.C., Bayer Jr., J.J., Durell, G.D., and Smith Jr., C.E. 1999. Resilient Modulus for New Hampshire Subgrade Soils for Use in Mechanistic AASHTO Design. CRREL-SR-99-14. U.S, Army Cold Regions Research and Engineering Laboratory, Hanover, N.H.

Janoo, V.C., and Cortez, E., 2002. Pavement Evaluation in Cold Regions. Cold Regions Engineering, 360-371.

Johnson, T.C., Berg, R.L., Chamberlain, E.L., and Cole, D.M. 1986. Frost action predictive techniques for roads and airfields. A comprehensive survey of research findings. CRREL-86–18. U.S, Army Cold Regions Research and Engineering Laboratory, Hanover, N.H.

Li, L., Liu, J., Zhang, X., and Saboundjian, S. 2010. Laboratory investigation of seasonal variations in resilient modulus of Alaskan base course material. ASCE Geotechnical Special Publication, 203: 270-278.

Nersesova, Z.A., and Tsytovich, N.A. 1963. Unfrozen water in frozen soils. In Proceedings of 1st Permafrost International Conference, Lafayette, Indiana, 11-15 November 1963. National Research Council, Washington D.C., pp. 230-234.

Oh, W.T., Vanapalli, S.K., and Puppala, A.J. 2009. Semi-empirical model for the prediction of modulus of elasticity for unsaturated soils. Canadian Geotechnical Journal, 46(8): 903–914.

Rahim, A.M. 2005. Subgrade soil index properties to estimate resilient modulus for pavement design. International Journal of Pavement Engineering, 6(3): 163-169.

Ren, J.P., and Vanapalli, S.K. 2017. Prediction of the resilient modulus of frozen unbound road materials by using soil-freezing characteristic curve. Canadian Geotechnical Journal, 55: 1200-1207.

Salour, F., and Erlingsson, S. 2015. Resilient modulus modelling of unsaturated subgrade soils: laboratory investigation of silty sand subgrade. Road Materials and Pavement Design, 16(3): 553-568.

Simonsen, E., and Isacsson, U. 1999. Thaw weakening of pavement structures in cold regions.

Cold Regions Science and Technology, 29(2): 135-151.
Simonsen, E., Janoo, V.C., and Isacsson, U. 2002. Resilient properties of unbound road materials during seasonal frost conditions. Journal of Cold Regions Engineering, 16(1): 28-50.
Tsytovich, N.A., 1975. Mechanics of frozen ground. Scripta Book Co., Washington, D.C.
Vanapalli, S.K., Fredlund, D.G., Pufahl, D.E. and Clifton, A.W. 1996. Model for the prediction of shear strength with respect to soil suction. Canadian Geotechnical Journal, 33(3): 379–392.
Yu, X., Yu, X., Zhang, B. and Li, N., 2009. An innovative sensor for assisting spring load restrictions: results of field demonstration study. In Cold Regions Engineering 2009: Cold Regions Impacts on Research, Design, and Construction, 417-428.

Chapter 7 Experimental study on the resilient moduli of five Canadian soils subjected to freezing

The contents presented in this chapter are from the manuscript:

Ren, J.P., and Vanapalli, S.K. 2019. Experimental study on the resilient moduli of five Canadian soils subjected to freezing. Under peer review with a Journal.

7.1 Abstract

The resilient modulus (M_R) of soils in the permafrost and seasonally frozen regions is sensitive to variations in soil temperature and moisture content. In the present study, the M_R of five frozen Canadian soils that were subjected to wetting conditions was experimentally determined using an advanced triaxial testing equipment. In addition, the influences of stress level and loading frequency were investigated. A freezing system was established for maintaining desired temperatures to investigate frozen M_R of the five soils. The results suggest that (i) the effect of subzero temperature (0 to -15 °C) is significant on the M_R of the five soils tested. The relationship between the frozen M_R and subzero temperature can be best-fit with a hyperbolic model; (ii) the frozen M_R versus subzero temperature relationship of the saturated specimen typically has a steeper slope than specimen with the optimum water content, for the temperature range of 0 to -5 °C for four of the five soils; (iii) the effect of stress levels on the measured M_R is dependent on soil type, water content, and temperature; and (iv) the loading frequency does not show a significant influence on the measured frozen M_R. More investigations on different soils are recommended to better understand the resilient behavior of frozen soils.

7.2 Introduction

The soil resilient modulus (M_R) is defined as the ratio of cyclic deviator stress to recoverable (resilient) strain. The M_R is a key material property used for the rational design of pavement structures based on the mechanistic-empirical methods (e.g., MEPDG (ARA, Inc.,

2004)). The pavements are exposed to external environment throughout their service life. Due to this reason, environmental factors such as evaporation and infiltration have a significant influence on the water content within the pavement materials (which are porous media), and therefore on their physical and mechanical properties (e.g., hydraulic conductivity, shear strength, and stiffness / modulus). In addition to water content, temperature is another key factor that influences the properties of pavement materials, and therefore on the pavement performance. The effects of the harsh climate on pavement structures cannot be neglected in the permafrost and seasonally frozen regions such as the north America, north Europe, Russia, and the Qinghai-Tibet plateau of China.

In cold regions, when the air temperature is lower than the soil temperature, heat is extracted from the soil to the environment that results in a temperature profile. The freezing front (0 °C isotherm) progresses as a function of the imbalance associated with heat supplied to heat removed as the pore water freezes (Konrad and Morgenstern, 1980). As the freezing front advances, the portion of the soil close to natural ground surface becomes frozen while the lower portion is still in a state of unfrozen condition (Ren et al., 2017). The depth that the freezing front penetrates the pavement structure depends on many factors, which include the air temperature, thermal properties and water contents of the base, subbase and subgrade soils. For example, the frost penetration depth in southern Ontario, Canada is around 1 to 2 m; however, it can exceed 3 m in northern Ontario (MTO, 2013). In cold climate regions such as the Siberia in Russia, freezing indices of 4000 to 6000 degree-days are found with frost penetration to depths greater than 2.5 m (Feldman, 1988). In some seasonally frozen areas in northeast China, the frost penetration ranges between 1.6 to 1.9 m (Liu et al., 2003). The soils located in these cold regions are typically subjected to freezing and thawing, depending on the time of a year and associated environmental factors.

The phase change of pore water (from liquid to solid or vice versa) has significant influence on the resilient behavior of the base, subbase, subgrade and foundation soils. When pore water freezes, ice bonds adjacent soil particles together (Andersland and Ladanyi, 2004),

resulting in a dramatic increase in soil modulus (Jong et al., 1998). For example, Bigl and Berg (1996) showed that the resilient moduli of subbase and subgrade soils could increase two orders of magnitude when the soil freezes. Bosscher and Nelson (1987) reported a 20-fold increase in the modulus of frozen Ottawa sand. Similar increases in moduli for frozen granular base soils were observed by Cole et al. (1987). Therefore, artificial freezing technique has been used temporarily to stabilize soils during the construction of retaining walls, foundations, tunnels, and other projects where weak soils are encountered (Chamberlain and Gow, 1979). A large cryogenic suction (i.e. the pressure difference between pore ice and pore water due to curved ice-water interface) is generated in the frozen soils when pore water freezes (Sheng et al., 2013). Such a phenomenon contributes to water migration from the lower portion of subgrade or foundation soils to upper frozen subgrade soils.

Several models have been proposed in the literature for the prediction of M_R of pavement materials. These prediction models were based on regression analysis or relationships between the M_R and soil properties considering the influence of environmental factors (e.g., Cary and Zapata, 2011; Han and Vanapalli, 2016; Caicedo, 2018; Ren and Vanapalli, 2018). However, experimental methods are still the most reliable way to determine the M_R of pavement materials, despite its drawbacks of being expensive because they require elaborate equipment and time-consuming test procedures.

In the present study, the M_R of five Canadian soils (one from Saskatchewan and the remainder four from southern Ontario) considering the influence of moisture and temperature was determined, with the aid of an advanced cyclic loading triaxial testing system. The effect of subzero temperature on the M_R, i.e. the frozen M_R of the five soils at both the optimum and saturated water contents, was investigated. Modifications were introduced to the triaxial testing system by establishing a freezing system with cooling unit and thermal insulation for accurately maintaining the soil specimens under the desired testing temperatures. In addition, the effects of stress level and frequency of the cyclic loading on the frozen M_R were investigated.

The above experimental program for determining the variation of the frozen M_R of the five

soils is valuable to understand the resilient (cyclic) behavior of typical Canadian frozen soils. The study is also useful for characterization of the pavement materials and the rational implementation of MEPDG in the design of pavement structures in Canada and other permafrost and seasonally frozen regions. Furthermore, the soil resilient behavior under cyclic loading can promote better understanding of the mechanical response of soils subjected to other types of long-term low-level dynamic loadings, such as those induced by trains, earthquakes, ocean waves, wind, and construction work (e.g., pile driving, tunneling or blasting) (Ishikawa et al., 2011; Ling et al., 2013).

7.3 Materials and specimen preparation

Five Canadian soils, i.e., Toronto silty clay (TSC), Toronto lean clay (TLC), Kincardine lean clay (KLC), Ottawa Leda clay (OLC), and Indian Head till (IHT), were investigated in the present study. The first four soils were collected from 0 to 3 m below the natural ground surface in the southern region of Ontario province, which has the most widely used pavement grid network in Canada due to national trade with the United States (Ho and Gough, 2006). The fifth soil, Indian Head till was collected from Indian Head, Saskatchewan. This soil is a representative candidate of glacial tills that are extensively available in Saskatchewan, Alberta, and Manitoba provinces of Canada. The investigated soils were air dried for two weeks and then pulverized and passed through a 2 mm sieve. The basic physical properties of the five soils are summarized in **Table 7.1**. Their chemical and mineralogical compositions are shown in **Table 7.2**. **Figure 7.1** presents their gradation curves.

Table 7.1 Physical properties of the five soils

	Toronto silty clay (TSC)	Toronto lean clay (TLC)	Kincardine lean clay (KLC)	Ottawa Leda clay (OLC)	Indian Head till (IHT)
w_L (%)	20	25	31	48	36
w_P (%)	14	13	21	22	17
PI (%)	6	12	10	26	19

w_{opt} (%)	13.5	12.3	20.3	23.0	13.9
γ_{dmax} (kN/m^3)	19.15	19.62	16.31	16.16	18.39
G_s	2.68	2.69	2.71	2.75	2.72
%sand	3	31	15	20	28
%silt	81	50	60	48	42
%clay	16	19	25	32	30
AASHTO	A-4	A-6	A-4	A-6	A-6
USCS	CL-ML	CL	CL	CL	CL
ψ_{opt} (kPa)	40	260	90	200	190

Note: w_L = liquid limit; w_P = plastic limit; PI = plasticity index; w_{opt} and γ_{dmax} = optimum water content and maximum dry unit weight (determined by the Standard Proctor compaction test, ASTM D698-12); G_s = specific gravity; AASHTO = American Association of State Highway and Transportation Officials soil classification system (AASHTO M145-91); USCS = Unified Soil Classification System (ASTM D2487-11); ψ_{opt} = approximate suction of the soil specimen at the w_{opt} (based on the measured soil-water characteristic curve (SWCC) of the five soils by using the pressure plate method, vapor equilibrium method, and WP4-T measurement as described in Section 4.4.3).

Table 7.2 The chemical and mineralogical compositions of the five soils (data from Han et al. (2018))

		TSC	TLC	KLC	OLC	IHT
Chemical composition (% by mass)	Na_2O	2.35	0.28	1.67	2.85	1.29
	MgO	5.34	0.47	2.65	4.19	3.73
	Al_2O_3	9.97	1.77	10.44	14.77	9.89
	SiO_2	50.20	89.38	59.69	54.74	59.43
	P_2O_5	0.21	0	0.09	0.19	0.09
	K_2O	2.27	0.33	2.50	3.16	1.83
	CaO	12.27	0.33	5.11	5.99	6.88
	TiO_2	0.43	0.09	0.53	0.79	0.43
	MnO	0.09	0.01	0.09	0.11	0.08
	Fe_2O_3	3.45	0.85	3.67	7.05	3.69
	H_2O	13.20	0.74	13.37	5.83	11.11
Mineralogical composition (by dominance)		Quartz	Quartz	Quartz	Quartz	Quartz
		Dolomite	Calcite	Muscovite	Labradorite	Dolomite
		Calcite	Albite	Anorthite	Ferro-Pargasite	Calcite
		Albite	Dolomite		Titanite	Albite
		Microline	Blodite		Montmorillonite	Muscovite

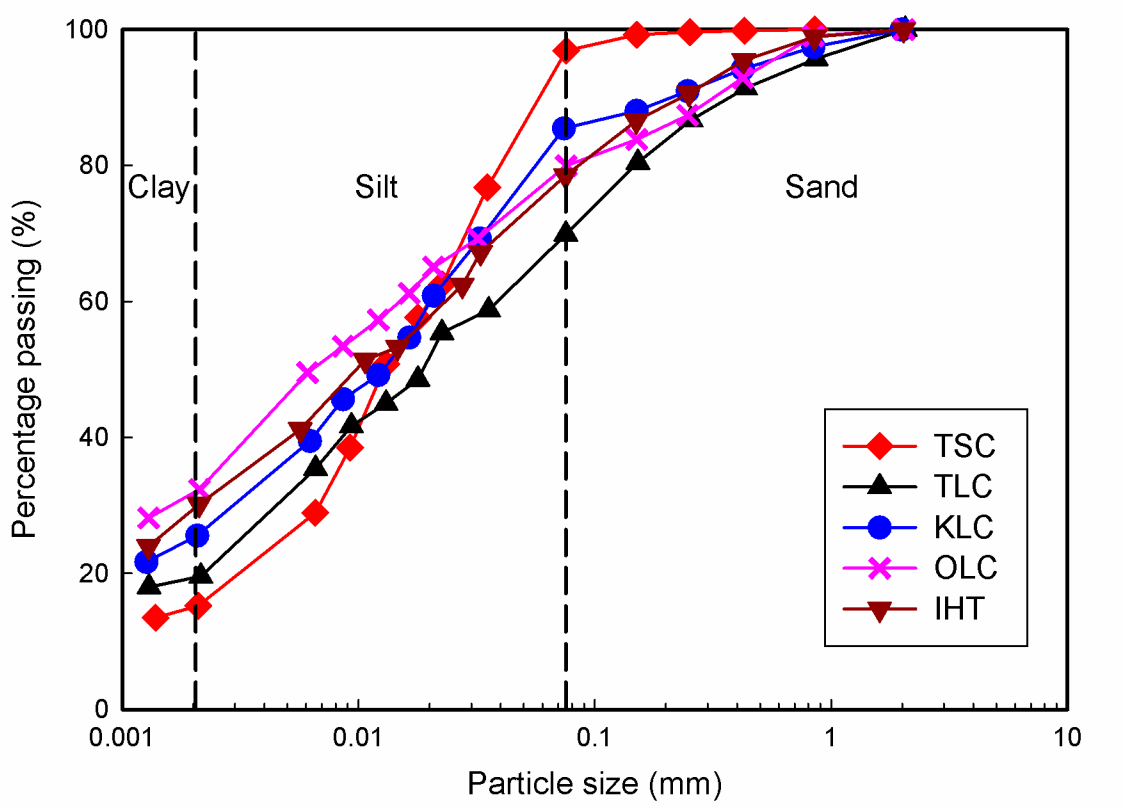

Figure 7.1 The gradation curves of the five soils

A pre-calculated amount of dry soil and water were mixed and statically compacted at the optimum water content for achieving the maximum dry density. The test specimens were compacted in five equal layers. Each layer was 20 mm high and the final soil specimen was 100 mm in height and 50 mm in diameter, as shown in **Figure 7.2**(a). In order to simulate the wetting process that in-situ subgrade soils typically undergo, one compacted specimen of each soil was wetted to the saturated water content condition. During the wetting process, the top, bottom, and side surfaces of the soil specimens were covered with wet filter paper and sealed using cling wrap. The soil specimens were then stored in plastic containers (see **Figure 7.2**(b)). The specimens were allowed to absorb water gradually from the wet filter paper (with no external stress applied) until the saturated water content was achieved. The TSC specimen did not attain saturated condition; possibly due to its high fraction of silt and low clay content (see **Table 7.1**). **Table 7.3** summarizes the final water contents of the tested soil specimens together with their

void ratios assuming constant volume condition during the wetting process. In addition, the degrees of saturation, which were calculated from the volume-mass relationships of the five soils, are summarized. In the present study, the frozen M_R of soil specimens at both the optimum and higher or saturated water contents were tested.

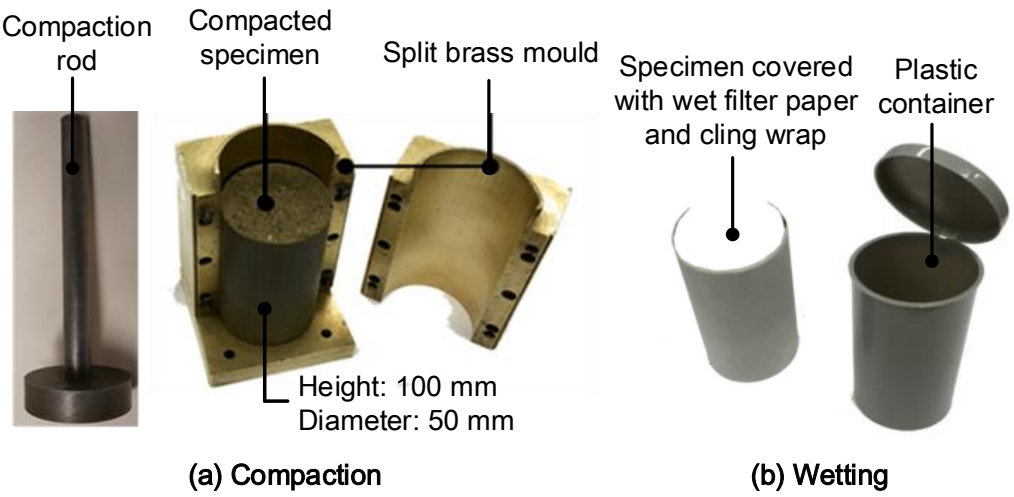

Figure 7.2 Soil specimen preparation: (a) compaction, and (b) wetting

7.4 Experimental setup and details

The M_R of the five soils was experimentally determined using the Entry Level Dynamic (ELDyn) triaxial testing system, manufactured by the GDS Instruments, UK. The main components of the testing system include GDS controllers, pneumatic actuator, loading frame, and triaxial chamber, as shown in **Figure 7.3**(a). The pneumatic actuator facilitates the application of cyclic load (through either stress- or strain-control), and a pneumatic regulator with air as fluid is used to apply the confining stress (σ_c) on the soil specimen. The schematic representation and more details of this equipment are available in Han (2016).

The prepared soil specimen was placed on the base pedestal and sealed with a rubber membrane and O-rings (shown in **Figure 7.3**(b)). Two temperature sensors (with wire diameter around 0.5 mm) were inserted into the specimen for monitoring soil temperature at two different locations during the test (see **Figure 7.3**(b) and **Figure 7.4**). In order to freeze the specimen (for

the measurement of frozen M_R), a copper coil was made and placed around the specimen (see **Figure 7.3**(c)). There was some space between the wrapped copper coil and specimen. This space was intentionally allowed to facilitate the easy installation of the copper coil. As a result, air gap existed between the copper coil and specimen. It was found from trial tests that the specimen could not achieve the desired freezing temperatures due to the low thermal conductivity of air (i.e. 0.026 W/(m•K) at 25 °C). For this reason, the gap between the copper coil and specimen was filled with lead pellets (see **Figure 7.3**(e)), which have high thermal conductivity of 35.5 W/(m•K) at 0 °C. The lead pellets provided good thermal conduction for transferring cold energy from the copper coil to the specimen. Antifreeze liquid (i.e. the mixture of ethylene glycol and water) was circulated through the copper coil by using an isotemp bath circulator. Two plastic tubes were used to connect the copper coil and bath circulator (see **Figure 7.3**(c)). The base of the triaxial testing system was modified for passing through the inlet and outlet connection tubes, and temperature sensor wires. Fiberglass was used as thermal insulation material to minimize the thermal exchange between the soil specimen and its surrounding environment (see **Figure 7.3**(d)).

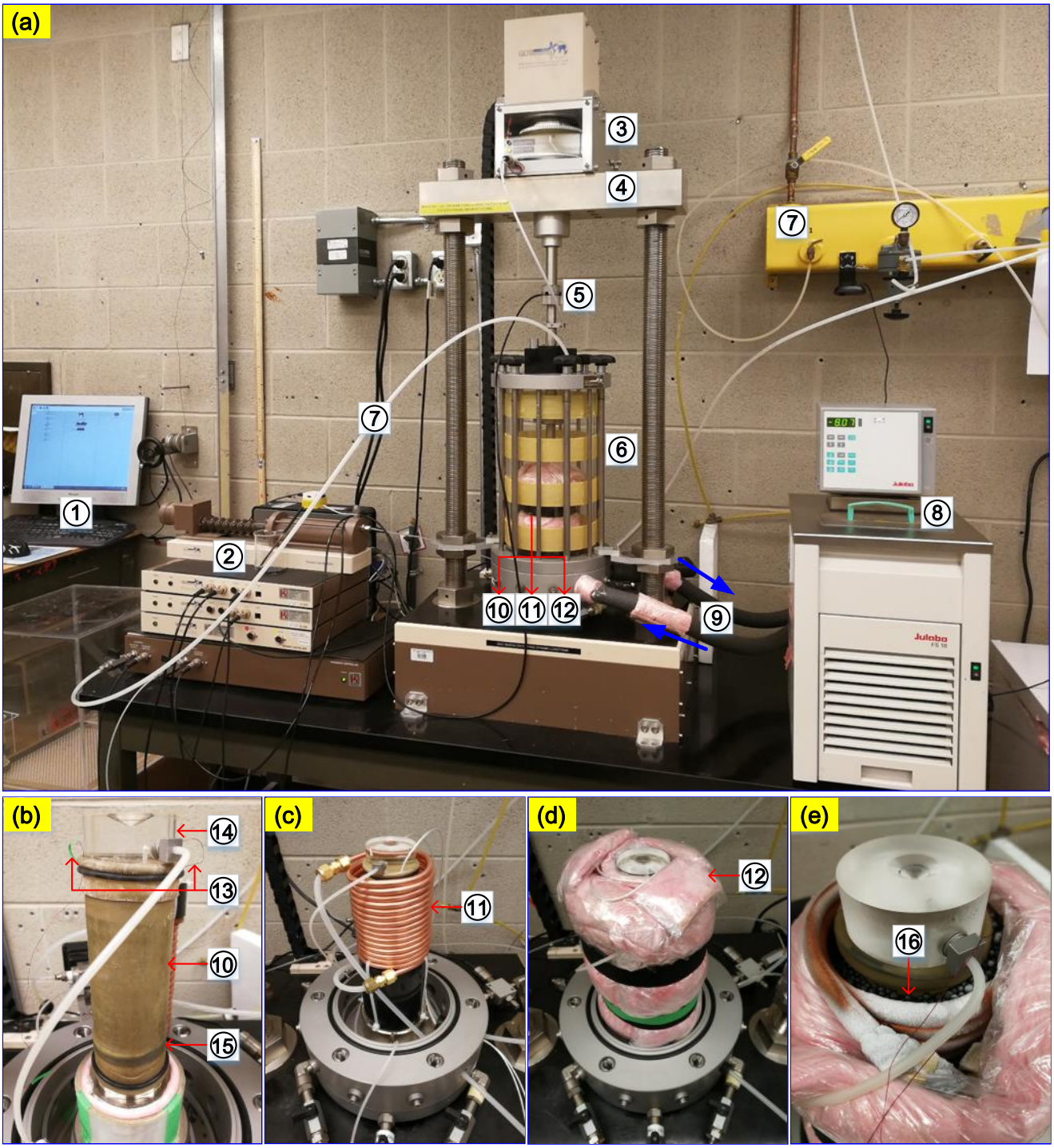

① GDS control panel ② GDS controllers ③ Pneumatic actuator ④ Loading frame ⑤ Loading rod ⑥ Triaxial chamber ⑦ Cell pressure supply ⑧ Isotemp bath circulator ⑨ Antifreeze liquid circulation ⑩ Soil specimen (inside rubber membrane) ⑪ Copper coil ⑫ Thermal insulation ⑬ Temperature sensors ⑭ Acrylic top cap ⑮ Solid PVC disk (1 cm thick) ⑯ Lead pellets

Figure 7.3 The experimental setup for frozen M_R test: (a) ELDyn triaxial testing system, (b) soil specimen, (c) copper coil, (d) thermal insulation, and (e) frozen specimen

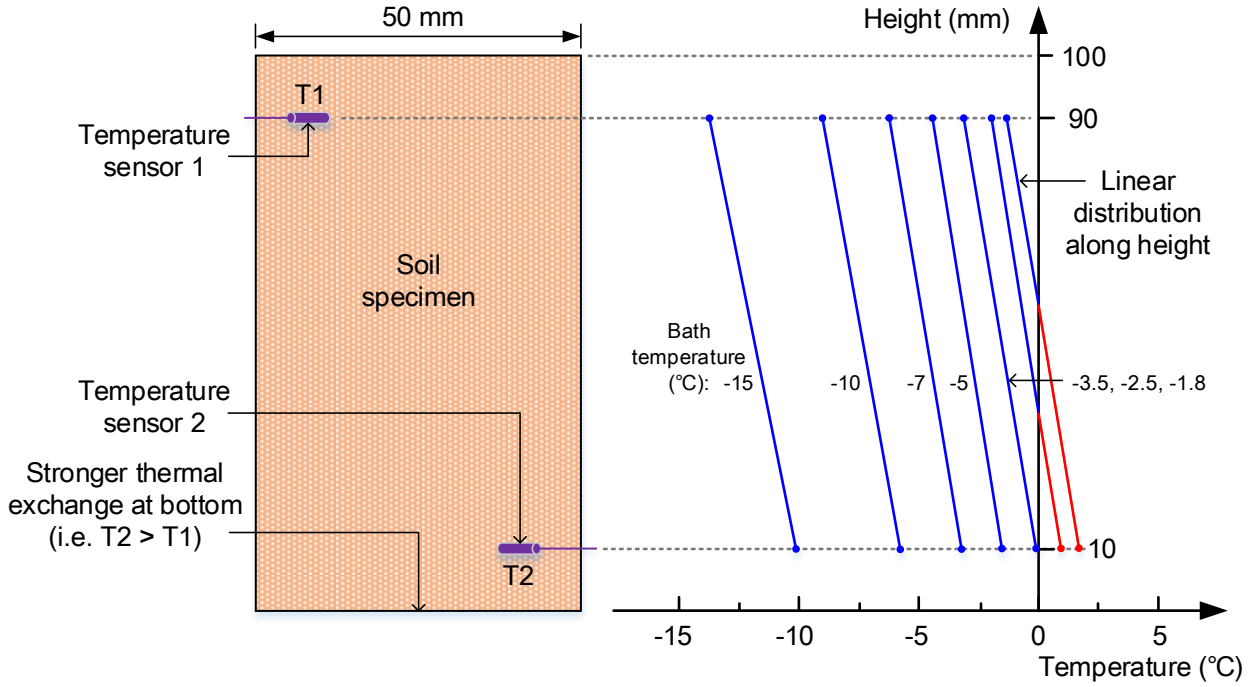

Figure 7.4 The schematic representation of temperature distribution in the specimen

The bath temperature in the circulator can be accurately controlled. However, a temperature gradient existed within the soil specimen. This can be attributed to the difference in the losses associated with cold energy from the top and bottom parts of the specimen (i.e. different thermal boundary conditions). The top surface of the specimen was covered by an acrylic top cap and exposed to chamber environment, while the bottom surface was placed on a solid PVC disk which was sitting on the metal pedestal (i.e. good thermal conductor) (see **Figure 7.3**(b)). Therefore, thermal exchange at the bottom part of the specimen was relatively stronger with respect to the surrounding environment, resulting in higher subzero temperature compared to the upper part.

The temperature distribution in the specimen can be considered linear. This conclusion was derived based on a verification test in which three additional temperature sensors were inserted into the specimen (located between T1 and T2) and the temperature distribution was measured. In other words, five temperature sensors were used. All the temperature sensors were calibrated by referring to two thermistors prior to their use. The temperature distributions along the specimen's height under different controlled bath temperatures are summarized in **Figure 7.5**. It

can be seen that the temperature distribution is approximately linear, based on the high coefficients of determination (R^2) of the linear regression. For this reason, only two temperature sensors (i.e. T1 and T2) were used for monitoring the specimen's temperature during the M_R test to alleviate possible specimen damage associated with sensor insertion and for simplifying experimental procedures. In addition, it is noticed that the temperature gradients (T_G), or the slopes of the fitted lines under different bath temperatures have good consistency, with a value around 0.35 °C/cm. The temperature gradient within the test specimens better simulates the behavior of in-situ soils, in which a temperature gradient exists during freezing period. The schematic representation of the temperature distribution in the specimen under different bath temperatures are shown in **Figure 7.4**.

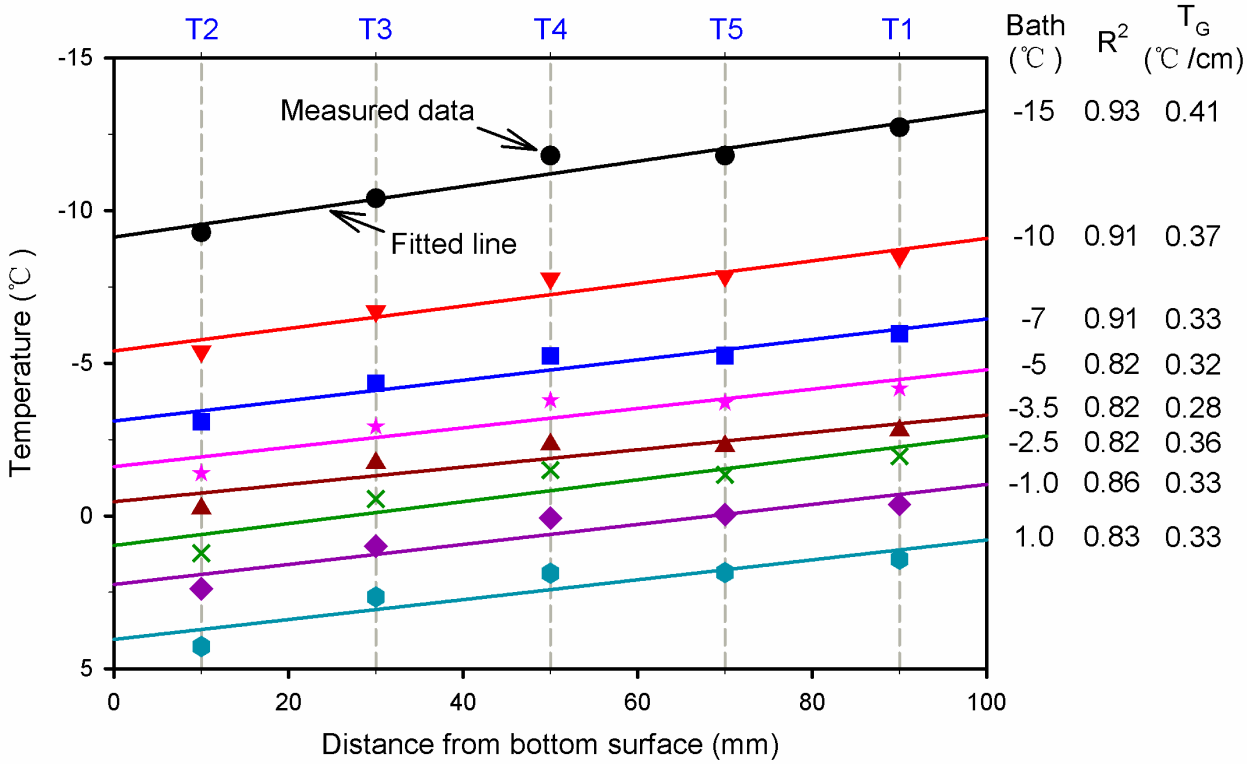

Figure 7.5 Measured temperature distributions in the specimen under different bath temperatures (T_G: Temperature gradient)

The bath temperature was set to -15 °C once the experimental setup was ready. Different higher subzero temperatures were controlled (following the sequence summarized in **Table 7.3**)

under which the M_R tests were carried out. The specimen was maintained for 24 hours under each controlled temperature, ensuring thermodynamic equilibrium condition. The same specimen was used for the M_R measurements along the thawing process; based on the assumption that M_R test is non-destructive and the axial displacement of the specimen under cyclic loading is insignificant at relatively low temperatures (i.e. the specimen is in frozen condition having a high stiffness). However, when the controlled bath temperature was relatively high (e.g., -2.5 °C), the soil specimen had certain amount of plastic deformation during the M_R test. Nevertheless, this deformation was ignored in the present study. In other words, the M_R test was continued on the same specimen until the final testing temperature (e.g., -1.0 °C) was achieved.

The *Standard Method of Test for Determining the Resilient Modulus of Soils and Aggregate Materials* (AASHTO T307-99, 2007) was followed to measure the M_R of the five soils under frozen condition. The standard haversine load pulse in AASHTO T307-99 was modified to a sinusoidal form of cyclic load, which can be applied by the ELDyn system. **Figure 7.6** shows the applied sinusoidal load versus load duration, which is 1 sec for one loading cycle (i.e. the loading frequency is 1 Hz). In order to understand the effect of loading frequency on M_R, four different frequencies (i.e. 0.2, 0.5, 4, and 5 Hz) were selected and M_R tests were conducted on an OLC specimen under different temperatures. There is a contact load (which is 10% of the maximum applied load during a loading cycle) acting on the specimen during the entire period of testing. The maximum applied load is equal to $A^*\sigma_d$, where A is the initial cross-sectional area of the specimen, and σ_d is the maximum deviator stress during a loading cycle. The cyclic load is 90% of the maximum applied load of a loading cycle. The M_R is equal to the cyclic stress (i.e. $0.9\sigma_d$) divided by the recovered axial strain. The M_R values of the specimens that were subjected to different combinations of σ_c (i.e. 41.4, 27.6, and 13.8 kPa) and σ_d (i.e. 55.2, 68.9, 137.8, 206.7, and 275.6 kPa) were determined in the present study. The pre-conditioning loading (i.e. 500 to 1000 cycles) was applied on the test specimens for minimizing the effects of initially imperfect contact between the top cap, specimen, and pedestal. For each stress level, 100 loading cycles were applied. The M_R was determined by averaging the values of the last five loading cycles.

Table 7.3 Physical properties and testing conditions of the soil specimens

Soil	Maximum dry unit weight (kN/m^3)	Void ratio	Gravimetric water content (%)	Degree of saturation (%)	Controlled bath temperature[3] (°C)
TSC	19.15	0.400	13.5[1]	90.5	-15, -10, -7, -5, -3.5, -2.5, -1.8
			13.8	92.1	-15, -10, -7, -5, -3.5, -2.5, -1.0
TLC	19.62	0.371	12.3[1]	89.0	-15, -10, -7, -5, -3.5, -2.5, -1.8
			13.8[2]	100.0	-15, -10, -7, -5, -3.5, -2.5, -1.8
KLC	16.31	0.662	20.3[1]	83.2	-15, -10, -7, -5, -3.5
			24.4[2]	100.0	-15, -10, -7, -5, -3.5, -2.5
OLC	16.16	0.702	23.0[1]	90.0	-15, -10, -7, -5, -3.5, -2.5, -1.8, -1.0
			25.5[2]	100.0	-15, -10, -5, -3.5, -2.5, -1.8, -1.0
IHT	18.39	0.479	13.9[1]	79.0	-15, -10, -7, -5, -3.5, -2.5, -1.0
			17.6[2]	100.0	-15, -10, -7, -5, -3.5, -2.5, -1.0

Note: [1]Optimum water content (w_{opt}); [2]Saturated water content (w_{sat}); [3]Each temperature was maintained for 24 hours.

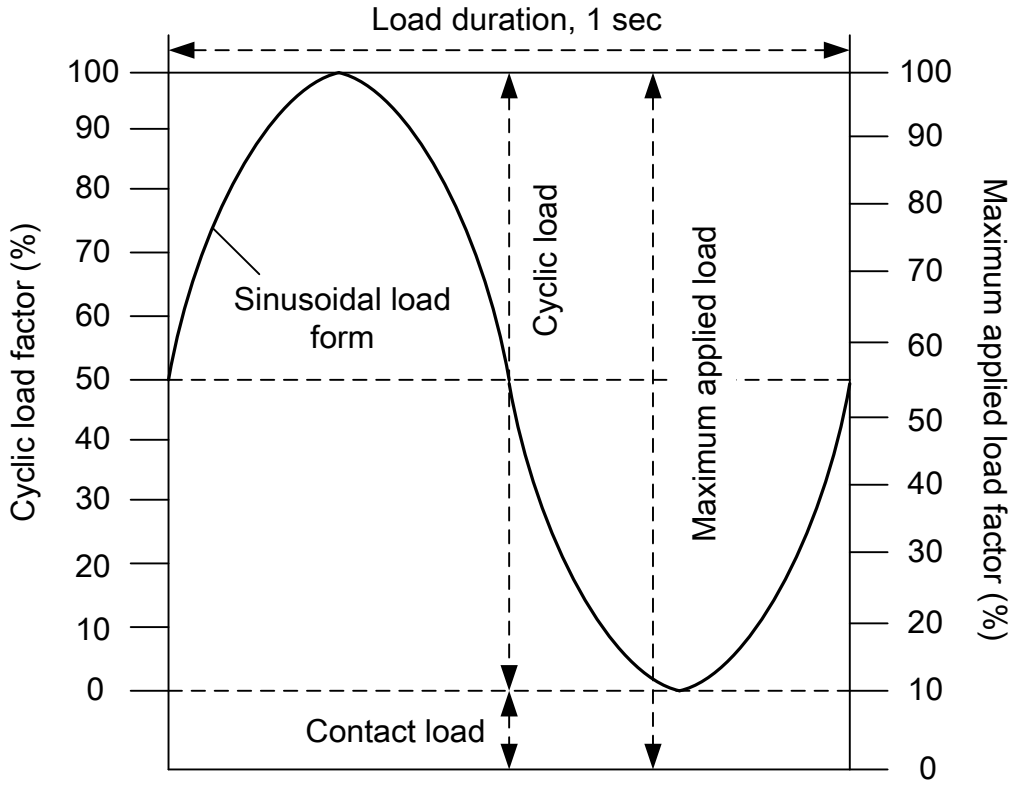

Figure 7.6 The sinusoidal load form used for M_R test

7.5 Experimental results and analysis

7.5.1 Effect of subzero temperature

Figure 7.7 shows the variation of M_R of TSC specimens associated with a decrease in the subzero temperature, under different stress levels. The controlled bath temperature is plotted as the abscissa. It can be seen that the relationships between frozen M_R and subzero temperature are similar for different stress levels. When the subzero temperature is not low, the M_R increases significantly with a decrease in the temperature. The resilient modulus curve is relatively flat after a certain value of subzero temperature (e.g., -5 °C), suggesting gentle increment or constant value against temperature. It can also be seen that the relationships resemble the shape of a hyperbola. However, these relationships are different in terms of M_R values and the rate of increase in M_R when the subzero temperature is not low (e.g., from 0 to -5 °C). The relationship curves of the specimen with the water content of 13.8% exhibit similar trend as for the case of the optimum water condition.

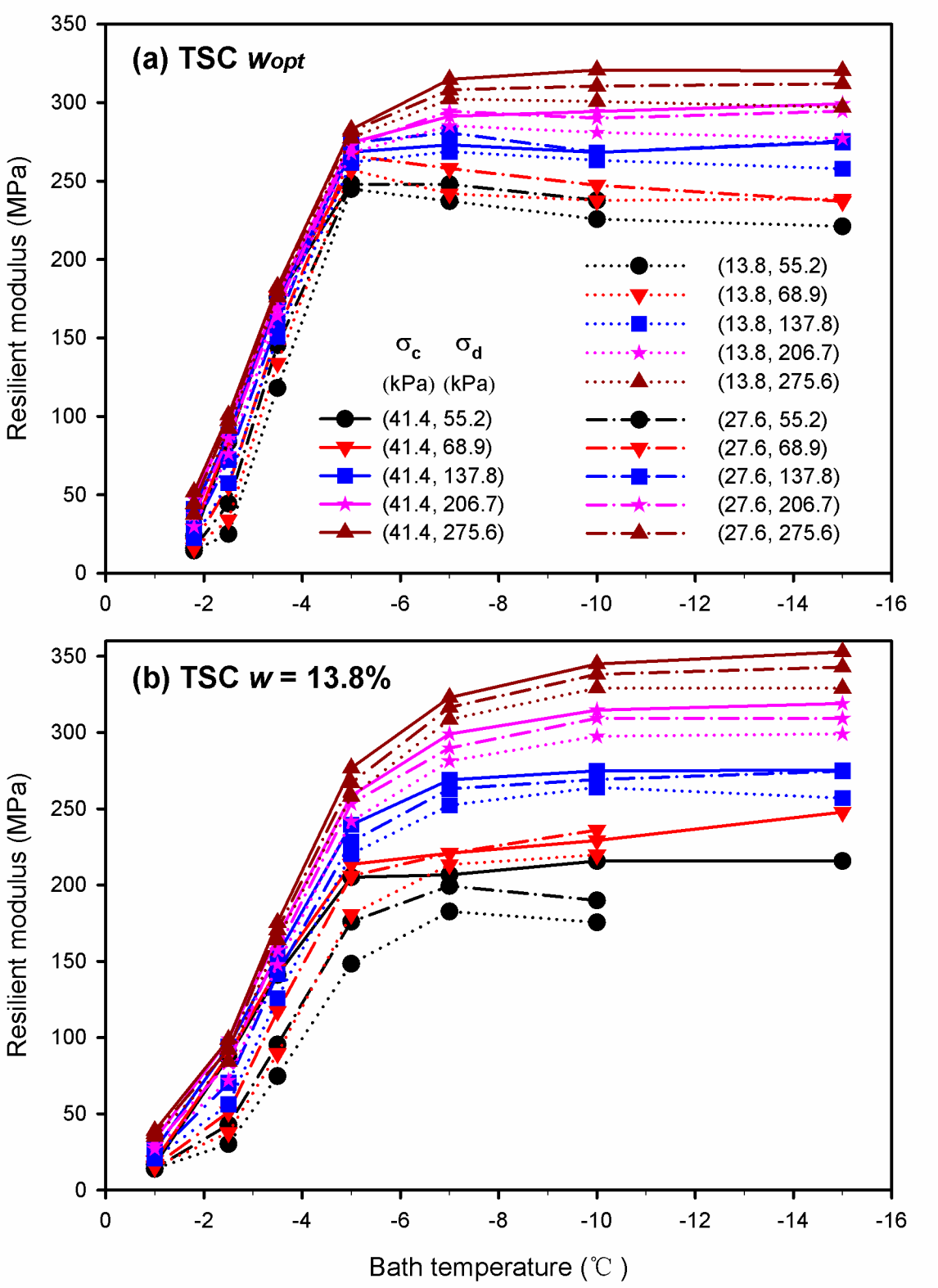

Figure 7.7 The effect of subzero temperature on the M_R of TSC at (a) w_{opt}, and (b) w = 13.8%

The frozen M_R versus subzero temperature relationships are similar for different stress levels. For this reason, the M_R of the five investigated soils under the stress levels of (σ_c = 41.4 kPa and σ_d = 275.6 kPa) and (σ_c = 13.8 kPa and σ_d = 137.8 kPa) are selected and compared as an example, as shown in **Figure 7.8**. The abscissa is the controlled bath temperature. The comparison between the five soils can be clearly seen from this figure.

The measured M_R values are typically lower under small stress level (i.e. **Figure 7.8**(b) and (d)) compared to those under large stress level (i.e. **Figure 7.8**(a) and (c)) for the five soils. The trends of the results for both the two water contents, i.e. optimum and saturated water contents are similar. The highest M_R values achieved for the five soils may fluctuate because many factors can have influences on the determination of frozen soil behavior, such as the specimen structure variations and lack of rigorous temperature control.

It can be observed from **Figure 7.8**(a) and (b) that at the optimum water content, TSC typically exhibits steeper slope than the other four soils in the high subzero temperature range (i.e. from 0 to -5 °C). The frozen M_R does not show significant increase but levels off after a certain value of temperature is achieved. This is, however, not applicable to KLC, which shows relatively large rate of increase when its temperature is lower than -10 °C (see **Figure 7.8**(a)). At the saturated condition (note that the TSC specimen had a water content of 13.8%), the variations in frozen M_R with a decrease in temperature for the five soils are similar under the two stress levels, except for IHT at the stress level of (σ_c = 13.8 kPa and σ_d = 137.8 kPa). In other words, the slopes of the frozen M_R – subzero temperature relationships appear to be close to each other. However, the variation characteristics are rather complex and not well-defined for the five soils. It is difficult to conclude that a certain soil has distinct M_R results in comparison with those of other soils. More discussions for such a behavior are summarized in later sections.

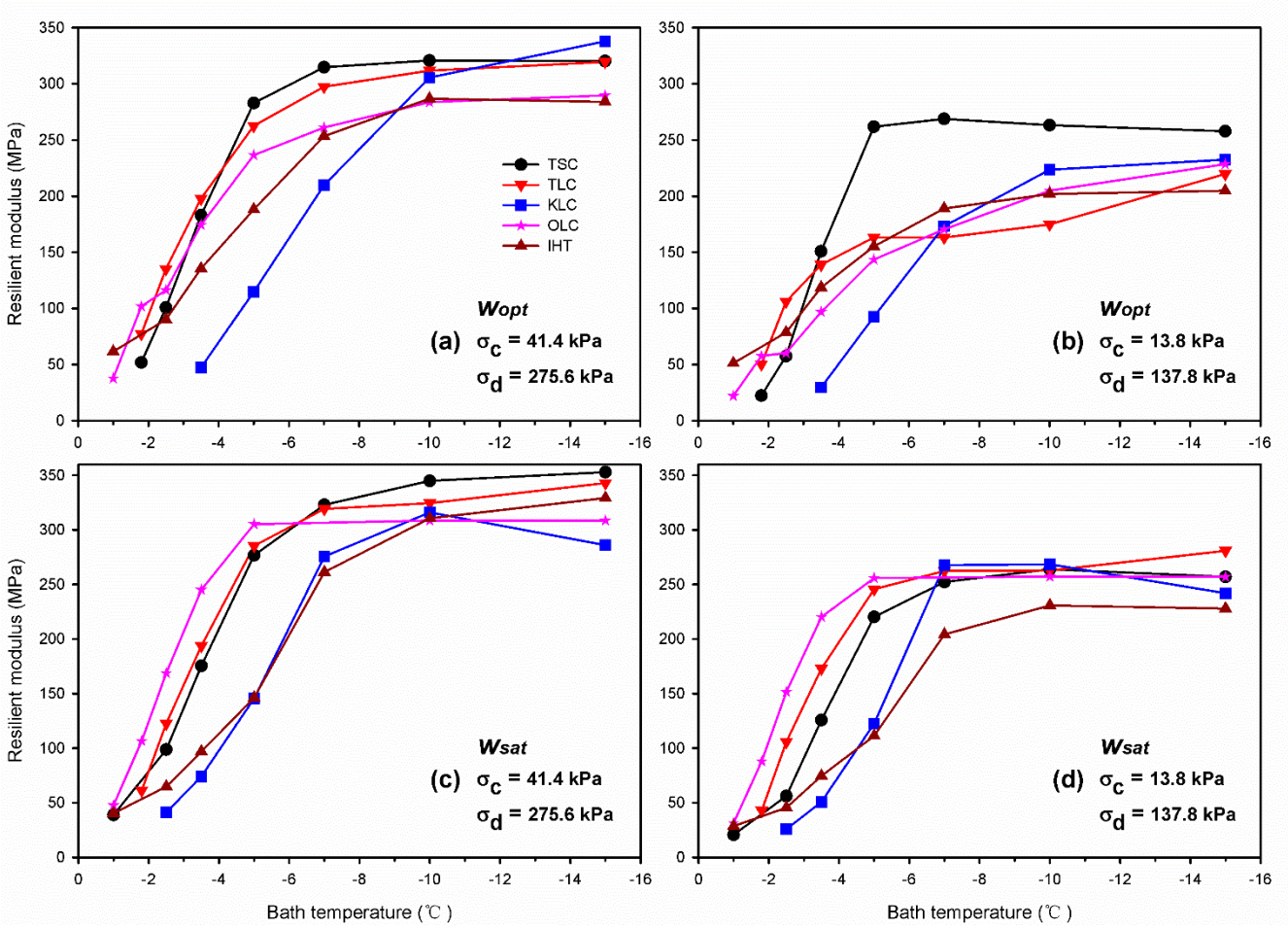

Figure 7.8 The M_R values of the five soils under two different stress levels (Note: TSC was at w = 13.8%)

7.5.2 Effect of water content

In order to observe the effect of water content, the measured frozen M_R values of the five soils at the optimum and saturated water contents are compared. The stress level of σ_c = 41.4 kPa and σ_d = 275.6 kPa was chosen as an example, as shown in **Figure 7.9**. The corresponding temperature values near the data points were measured by the two temperature sensors (i.e. T1 and T2) respectively.

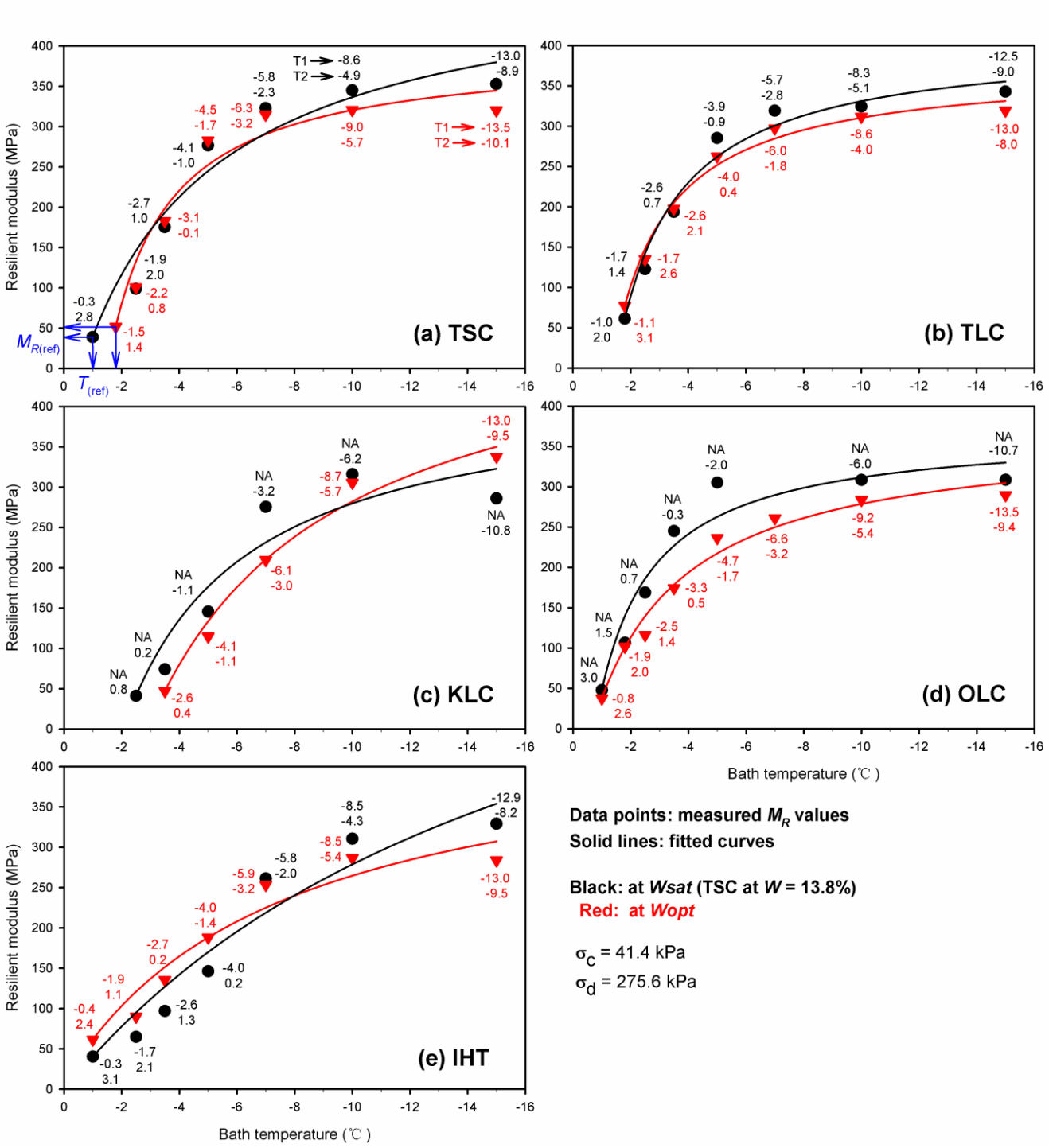

Figure 7.9 The effect of water content on the M_R of (a) TSC, (b) TLC, (c) KLC, (d) OLC, and (e) IHT under stress level of (σ_c = 41.4 kPa, σ_d = 275.6 kPa)

Ren and Vanapalli (2018) proposed an empirical hyperbolic model for best-fitting the relationship between the logarithmic scale of M_R of frozen soils and subzero temperature. This

model is expressed as,

$$\mathrm{Log}(M_{R(\mathrm{frozen})}) = \mathrm{Log}(M_{R(0\,^{\circ}\mathrm{C})})[1 + \frac{(-T)}{A + B(-T)}] \tag{7.1}$$

where, $\mathrm{Log}(M_{R(\mathrm{frozen})})$ is the logarithmic M_R of the frozen soil; $\mathrm{Log}(M_{R(0\,^{\circ}\mathrm{C})})$ is the logarithmic M_R of the frozen soil at 0 °C, which is a reference point; T is the subzero temperature (°C); A and B are model parameters. For simplicity purposes, the units of the M_R and subzero temperature are ignored when using this model.

It can be seen from **Figure 7.9** that the measured M_R values of the five soils versus subzero temperature relationship bears the same hyperbolic nature. In addition, this characteristic is applicable to both the optimum and saturated water conditions. Therefore, the above hyperbolic model (Eq. (7.1)) can be used to best-fit the M_R data points measured in the present study (i.e. $M_{R(\mathrm{frozen})}$). However, it should be noted that the reference temperature is no longer at 0 °C as in Eq. (7.1), but the highest subzero temperature at which the M_R test was conducted (e.g., see **Figure 7.9**(a)). In addition, since the measured frozen M_R values in the present study are relatively low, both the normal and logarithmic scales can be used. The normal scale of M_R is used and the modified hyperbolic model is shown below,

$$M_{R(\mathrm{frozen})} = M_{R(\mathrm{ref})}[1 + \frac{(-T + T_{(\mathrm{ref})})}{A + B(-T + T_{(\mathrm{ref})})}] \tag{7.2}$$

where, $M_{R(\mathrm{ref})}$ is the reference frozen M_R measured at the reference temperature $T_{(\mathrm{ref})}$ (°C) (see **Figure 7.9**(a)).

The measured frozen M_R versus subzero temperature relationships shown in **Figure 7.9** are best-fitted by using Eq. (7.2). The corresponding fitting curves are shown with solid lines. The fitting parameters (i.e. A and B) and their standard errors, and the coefficient of determination (R^2) are summarized in **Table 7.4**. From **Figure 7.9** and **Table 7.4**, it can be seen that the modified hyperbolic model provides good fitting for the experimental data points. In the high subzero temperature range (i.e. 0 to -5 °C), the slope of the frozen M_R versus subzero temperature relationship of the specimen at saturated condition is typically steeper than that of the specimen with the optimum water content. This is true for TLC, KLC, OLC, and IHT, but not for TSC. For the former four soils, the fitted parameter A value for specimen at saturated condition is less than that at the optimum water content, indicating a faster increase in the frozen M_R with the decrease of subzero temperature. This is consistent with the conclusion drawn by Ren and Vanapalli (2018). The observed phenomenon can be explained that for the specimen at

saturated condition, its pore spaces with different sizes are completely filled by water. When the saturated specimen is subjected to freezing, the phase change of pore water from liquid to solid occurs at a relatively fast rate. On the other hand, for specimen at the optimum water content, initially there is much less water available in its pore spaces (i.e. low degrees of saturation, see **Table 7.3**). This small amount of water is likely to be adsorbed on soil particles' surface and confined in small pore spaces. As a result, the pore water has lower freezing points and slower phase change rate. In other words, the specimen at the optimum water content has flatter shape in terms of the frozen M_R versus temperature relationship, compared to the saturated specimen.

Table 7.4 Fitting results by the modified hyperbolic model (σ_c = 41.4 kPa, σ_d = 275.6 kPa)

Soil	$T_{(ref)}$ (°C)	$M_{R(ref)}$ (MPa)	A	B	R^2
TSC w_{opt}	-1.8	51.8	0.344 (0.085)	0.151 (0.016)	0.95
TSC w = 13.8%	-1.0	38.9	0.419 (0.102)	0.084 (0.014)	0.93
TLC w_{opt}	-1.8	77.3	0.587 (0.072)	0.260 (0.014)	0.99
TLC w_{sat}	-1.8	61.3	0.409 (0.070)	0.177 (0.013)	0.97
KLC w_{opt}	-3.5	47.3	0.674 (0.127)	0.098 (0.017)	0.98
KLC w_{sat}	-2.5	41.2	0.493 (0.207)	0.107 (0.030)	0.88
OLC w_{opt}	-1.0	37.6	0.383 (0.051)	0.113 (0.008)	0.98
OLC w_{sat}	-1.0	47.8	0.296 (0.076)	0.148 (0.016)	0.93
IHT w_{opt}	-1.0	61.6	1.322 (0.325)	0.156 (0.039)	0.93
IHT w_{sat}	-1.0	40.4	1.024 (0.269)	0.056 (0.027)	0.92

Note: Number in the parenthesis is Standard error.

According to Ren and Vanapalli (2019), the unfrozen water contents of TSC and TLC show significant reduction in the temperature range of 0 to -5 °C. After -5 °C, a considerable amount of pore water has changed phase to ice, and the unfrozen water content is relatively small and only decreases slightly. The variation in the unfrozen water content versus subzero temperature (i.e. soil-freezing characteristic curve, SFCC) is similar to that of the relationship between frozen M_R and subzero temperature. Ren and Vanapalli (2017) proposed a semi-empirical model for estimating the frozen M_R of saturated soils by employing the SFCC as a tool. This model provided good estimation for seven soils collected from the literature. An attempt to apply this model for the five soils in the present study, however, was not successful due to the temperature gradient in the soil specimen. In other words, because the temperature values are different at various locations along the specimen's height, the unfrozen water contents at these locations are different. Therefore, each location will have its own SFCC, but there will be no unique SFCC for

the bulk specimen. This theoretically limits the application of the semi-empirical model for the five investigated soils.

The effect of water content on the frozen M_R is also observed for the stress level of σ_c = 13.8 kPa and σ_d = 137.8 kPa. The temperature values of the specimens measured by the two sensors are the same as in **Figure 7.9**. Similar procedures were followed to best-fit the data points. The fitting results are shown in **Figure 7.10**, and the fitting parameters together with their standard errors and R^2 are summarized in **Table 7.5**. Similar conclusions can be drawn for this stress level.

Table 7.5 Fitting results by the modified hyperbolic model (σ_c = 13.8 kPa, σ_d = 137.8 kPa)

Soil	$T_{(ref)}$ (°C)	$M_{R(ref)}$ (MPa)	A	B	R^2
TSC w_{opt}	-1.8	22.3	0.142 (0.054)	0.073 (0.011)	0.89
TSC w = 13.8%	-1.0	20.7	0.274 (0.093)	0.058 (0.013)	0.88
TLC w_{opt}	-1.8	50.2	0.495 (0.129)	0.300 (0.028)	0.94
TLC w_{sat}	-1.8	43.0	0.271 (0.047)	0.154 (0.010)	0.97
KLC w_{opt}	-3.5	29.6	0.403 (0.091)	0.103 (0.014)	0.97
KLC w_{sat}	-2.5	25.9	0.308 (0.166)	0.077 (0.025)	0.82
OLC w_{opt}	-1.0	22.1	0.517 (0.050)	0.067 (0.006)	0.99
OLC w_{sat}	-1.0	31.5	0.190 (0.051)	0.116 (0.012)	0.93
IHT w_{opt}	-1.0	51.1	1.221 (0.267)	0.219 (0.036)	0.94
IHT w_{sat}	-1.0	28.7	0.871 (0.282)	0.066 (0.031)	0.88

Note: Number in the parenthesis is Standard error.

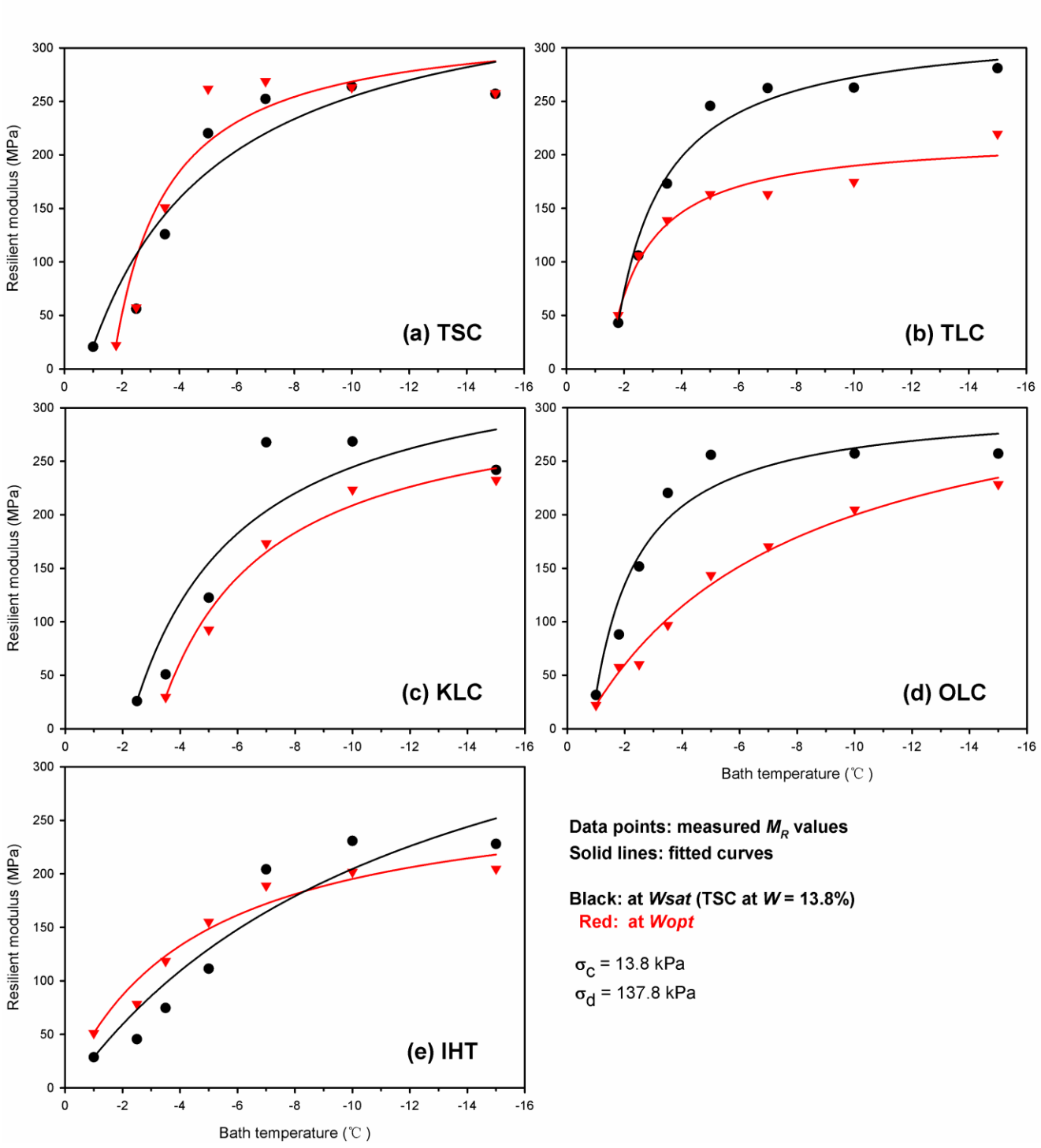

Figure 7.10 The effect of water content on the M_R of (a) TSC, (b) TLC, (c) KLC, (d) OLC, and (e) IHT under stress level of (σ_c = 13.8 kPa, σ_d = 137.8 kPa)

7.5.3 Effect of stress level

As can be seen from **Figure 7.7**, the frozen M_R versus subzero temperature relationships are different in terms of M_R values under various stress levels. The effect of stress levels on the measured M_R of the five soils are presented in **Figure 7.11**. Three different bath temperatures are selected and the results for both the optimum and saturated water contents are shown. The selected three bath temperatures are the representatives of three different stages of the specimen: (i) when the bath temperature is at -15 °C, the specimen has relatively low temperature (e.g., see **Figure 7.11**(a)) and is in a frozen condition. In this case, most of the pore water has been transformed into ice and only a small amount of unfrozen water is left in soil pores; (ii) when the bath temperature increases to a higher negative value (e.g., -3.5 °C), the specimen is still in a state of frozen condition but has relatively high temperature (see **Figure 7.11**(a)). At this stage, the specimen has much higher unfrozen water content; and (iii) when the bath temperature is controlled to a value close to 0 °C (e.g., -1.8 °C in **Figure 7.11**(a)), the upper part of the specimen is still frozen while the lower part thawed. In this condition, the specimen behaves similar to a thawed soil under cyclic loading since the lower thawed part undergoes large deformation, which contributes to the overall deformation of the specimen.

As can be seen from **Figure 7.11**, the specimen has much higher M_R values at -15 °C than those at the other two temperatures. The M_R values of specimen tested at the highest temperature are the lowest. These M_R values are around 50 MPa for all the five soils, and at both their optimum and saturated water contents. It can also be concluded from **Figure 7.11** that the effect of stress level on the measured M_R values depends on the types of soils and their water contents, and testing temperature.

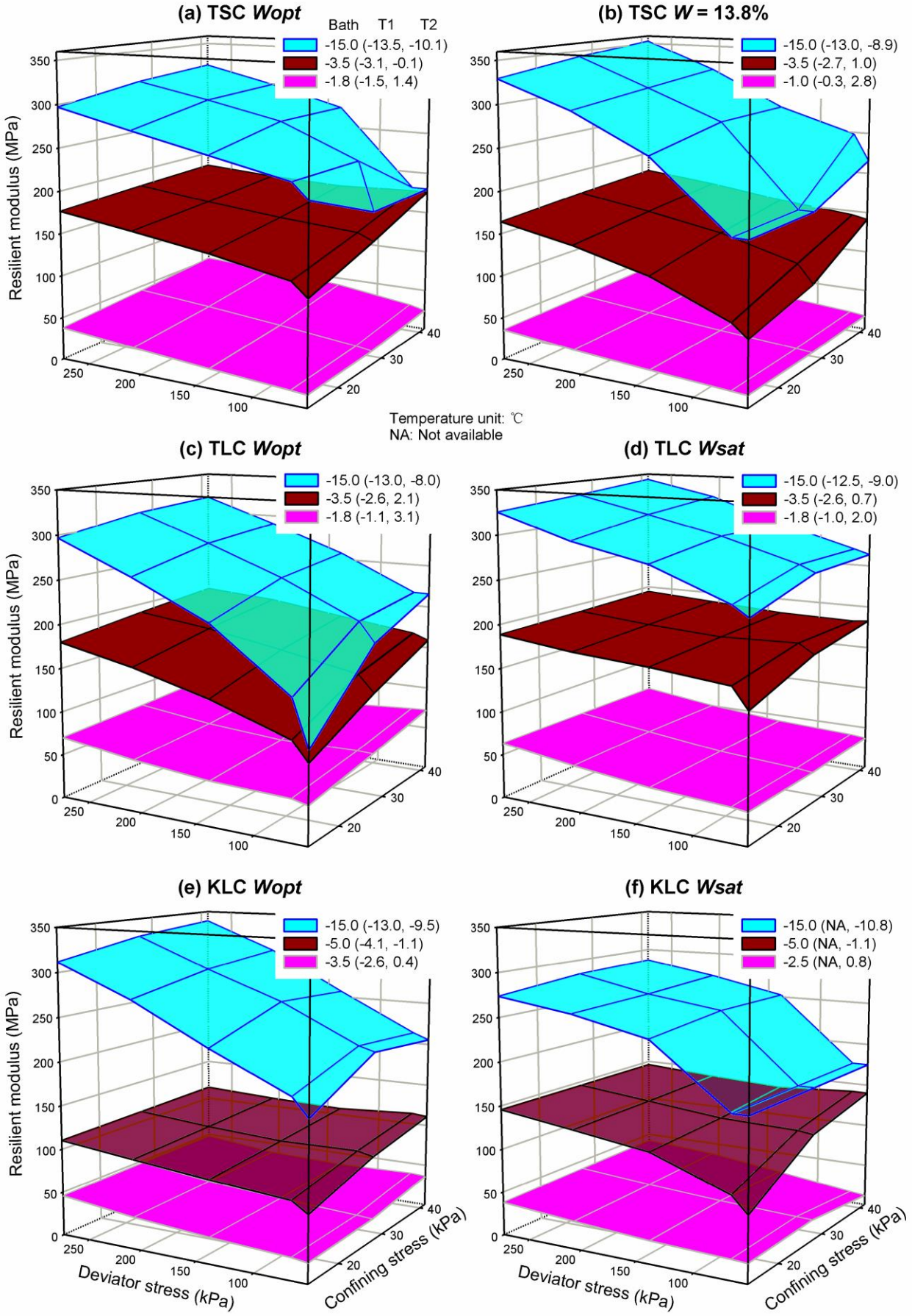

Figure 7.11 The effect of stress levels on the M_R of (a) TSC, (b) TLC, (c) KLC, (d) OLC, and (e) IHT at various temperatures and water contents

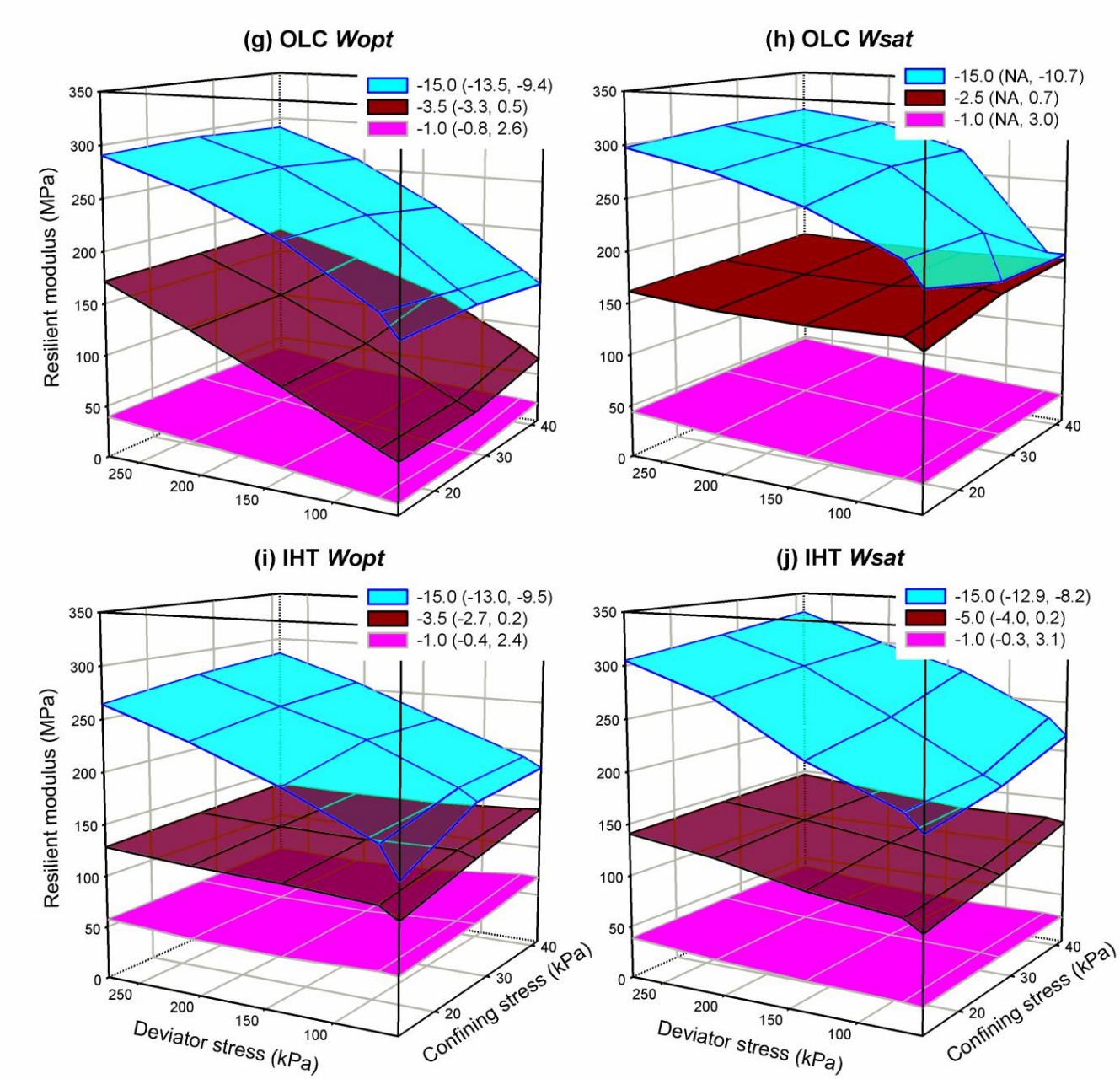

Figure 7.11 The effect of stress levels on the M_R of (a) TSC, (b) TLC, (c) KLC, (d) OLC, and (e) IHT at various temperatures and water contents (Cont'd)

The M_R values of frozen TSC specimens at relatively low temperatures (i.e. at -15 °C and -3.5 °C) increase with an increase in the deviator stress. The increment is larger for TSC specimen at the water content of 13.8% (**Figure 7.11**(b)) than that at the optimum water content (**Figure 7.11**(a)). At a certain value of deviator stress, the M_R does not show significant variation

due to the change in confining stress under these two temperatures. When the specimen has high temperature, i.e. its lower portion is thawed, the measured M_R values are low and stress levels do not significantly influence M_R. Similar conclusions hold for KLC (see **Figure 7.11**(e) and (f)).

The measured frozen M_R at -15 °C for TLC specimens (**Figure 7.11**(c) and (d)) increases with an increase in the deviator stress, for both the optimum and saturated water conditions. However, the increment for the latter case is relatively smaller. When the temperature is at -3.5 °C, for TLC specimen at the optimum water content (**Figure 7.11**(c)), both the increase in deviator and confining stresses contribute to an increase in the M_R. On the other hand, no significant influence is observed for the saturated specimen at the same temperature (**Figure 7.11**(d)). Similar to TSC at -1.8 °C, different stress combinations have insignificant influence on the measured M_R. In other words, the plotted surfaces are approximately horizontal. It is also noted that at -1.8 °C, the measured M_R values are higher for specimen at the optimum water content than those at the saturated condition. The measured results for IHT is approximately similar to those observed for TLC.

For OLC, the frozen M_R increases with an increase in the deviator stress when the controlled temperature is at -15 °C. This is true for both the optimum and saturated water conditions. When the temperature is adjusted to an intermediate value, the deviator stress has significant influence on the M_R of OLC specimen with the optimum water content (**Figure 7.11**(g)). However, only limited effect is observed for the specimen at the saturated condition (**Figure 7.11**(h)). The stress levels show limited influence on the measured M_R values when the specimen has high temperature.

In summary, the influence of deviator stress on frozen M_R is clearly observed when the soil specimen has low temperatures (e.g., -15 °C). The effect of confining stress, however, is not as significant as the deviator stress. This may be attributed to that the three confining stresses selected in this study are close (i.e., the confining stresses values are low in comparison with deviator stresses). When the soil specimen has high temperatures (e.g., -1.8 °C), neither the deviator stress nor confining stress contributes to a significant increase in the M_R. The reason is

that at high temperatures, the lower part of the specimen is thawed and hence the measured M_R values are low.

7.5.4 Effect of loading frequency

The effect of loading frequency on the measured frozen M_R are shown in **Figure 7.12**. The test was conducted on an OLC specimen at its optimum water content, and under three different bath temperatures (i.e. -15, -10, and -7 °C). Four different frequencies (i.e. 0.2, 0.5, 4, and 5 Hz) were selected. The comparisons between the case of 4 Hz and 0.5 Hz, 4 Hz and 5 Hz, and 4 Hz and 0.2 Hz are plotted in **Figure 7.12**(a), (b), and (c), respectively. It can be seen from **Figure 7.12**(a) and (c) that the measured M_R values under various stress levels at the loading frequency of 4 Hz are typically larger than those measured at lower loading frequencies (i.e. 0.2 and 0.5 Hz). However, the maximum difference in M_R of these two cases (i.e. 4 and 0.5 Hz, and 4 and 0.2 Hz) is around 20 MPa, which is considered not significant given the large difference between the two frequencies (e.g., 4 and 0.2 Hz). The exception occurs at σ_c = 41.4 kPa and σ_d = 55.2 kPa in **Figure 7.12**(a), which shows a difference value about 50 MPa. This difference, however, may likely be associated to experimental errors (e.g., initial imperfect contact between the top cap, specimen, and pedestal) rather than due to frequency effect. In addition, it can be seen from **Figure 7.12**(b) that, there is no significant difference between the results under 4 Hz and 5 Hz at the bath temperature of -10 °C. In other words, the measured M_R values for these two frequencies are approximately the same.

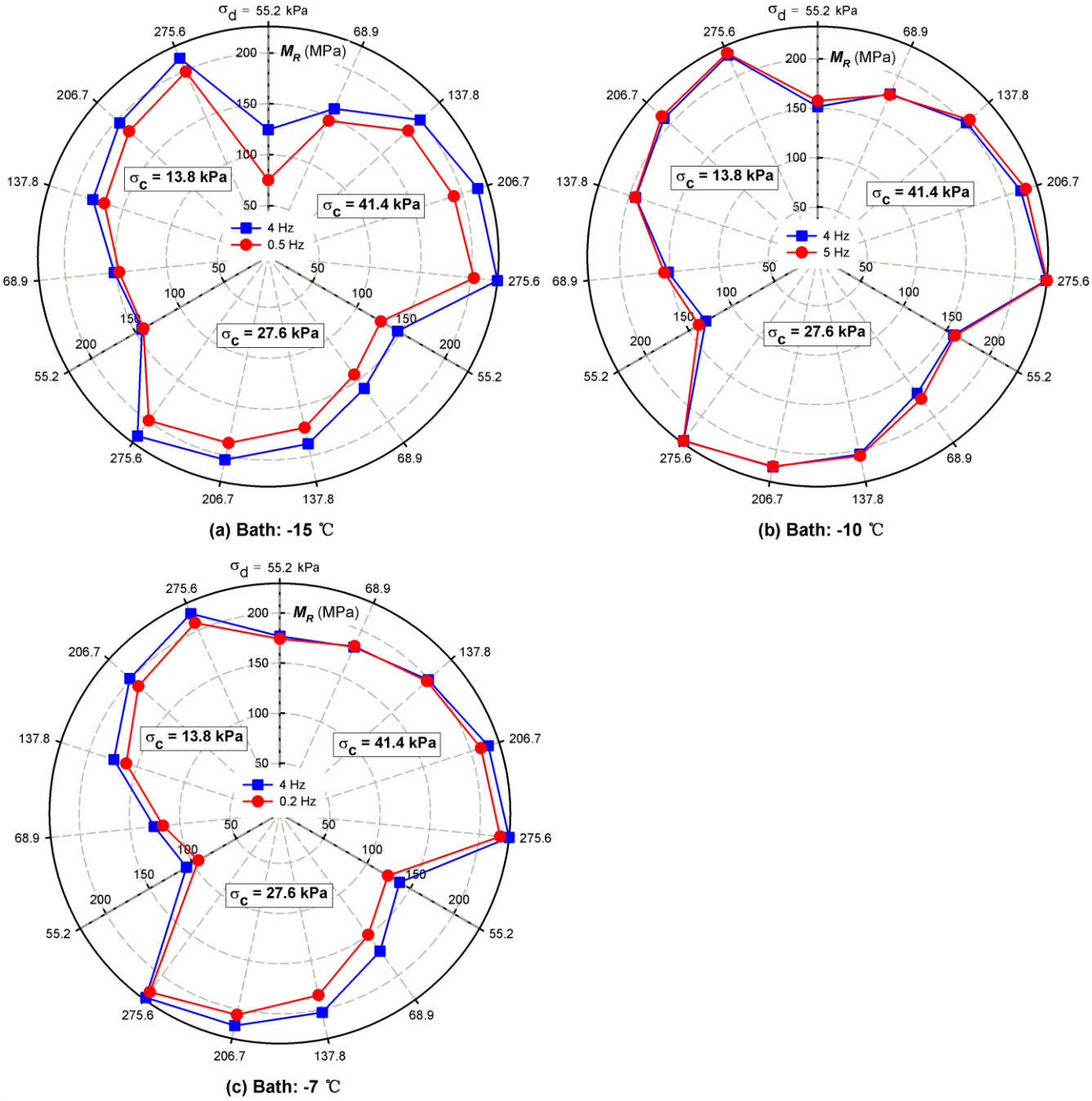

Figure 7.12 The effect of loading frequency on frozen M_R of OLC specimen at w_{opt} under bath temperature of: (a) -15 °C, (b) -10 °C, and (c) -7 °C

7.6 Discussion

The behavior of frozen soil is complex because it typically consists of four phases, i.e. solid particles, air, unfrozen water, and ice. The frozen soil behavior is dependent on the quantity of unfrozen water and ice, which is sensitive to temperature and pressure variations. The mechanical properties such as frozen resilient modulus under dynamic cyclic loading exhibit large fluctuations (e.g., Berg et al. (1996)) due to difficulties associated with experimental investigations on frozen soils (e.g., accurate temperature control and measurement, thermodynamic equilibrium condition). When a soil is subjected to freezing, pore water changes phase and becomes ice. The frozen soil typically has much higher strength and stiffness than those of unfrozen and thawed soils. The possible reasons for the significant increment include: (i) pore ice strength; (ii) soil strength, consisting of interparticle friction, particle interference, and dilatancy effects; (iii) increase in the effective stress due to the adhesive ice bonds, or the cryogenic suction; and (iv) synergistic strengthening effects between the soil and ice matrix preventing the collapse of soil skeleton (Andersland and Ladanyi, 2004).

In the present study, the five fine-grained soils were compacted at their optimum water contents to achieve their maximum dry density values. When they are subjected to closed-system radial freezing, water in large inter-aggregate pores near to the surface of the specimen freezes first and its volume increases by about 9%. At the same time, large cryogenic suction forms between the ice crystals and water phase that is adsorbed on soil particles' surfaces in these pores. These ice crystals grow at the expense of water in adjacent pores (e.g., in smaller intra-aggregate pores and pores inside the specimen) which is drawn towards the ice through water films under the cryogenic suction gradient. Therefore, the distribution of unfrozen water and ice is not likely to be uniform inside the specimen. The variation in the specimens' structure before freezing, influencing the final distribution of unfrozen water and ice after freezing, may yield fluctuation in the measured behavior of frozen soils. However, the influence of possible non-uniform distribution of unfrozen water and ice on the frozen M_R needs more investigations.

The effect of subzero temperature on the M_R of frozen soils is significant, compared to

other factors. When the temperature decreases from 0 to -5 °C, large amount of pore water changes phase to ice at a relatively fast rate. The large quantity of ice forms ice matrix and bonds soil particles together. As a result, the M_R of the investigated five soils show dramatic increase. The phase change of pore water in this temperature range can be seen from the SFCC of TSC and TLC specimens measured by Ren and Vanapalli (2019). As most pore water has transformed to ice, the remainder unfrozen water requires lower temperature to freeze (e.g., Sheng et al., 2014), and the reduction in its quantity is at a much slower rate compared to the initial freezing period. Therefore, the amount of ice formed during this stage is limited and hence there is no significant increase in the frozen M_R.

When the specimen is subjected to wetting, water migrates from the wet filter paper to the specimen due to suction gradient. The suction of the specimen that is initially at the optimum water content is relatively high (see **Table 7.1**). On the contrary, the wet filter paper has a relatively high amount of water and therefore low or zero suction. With the gradual migration of water towards the specimen, the original thin water films adsorbed on the soil particles' surfaces become thicker, and the radii of curvature of the air-water menisci become larger, resulting in lower suction and more deformable soil structure. As a result, the pore spaces of the specimen enlarge as effective stress reduces (due to the decrease in suction), and micro flow channels may form during water migration. Water phase in these large pores / channels has relatively high free energy. Therefore, the phase change of these pore water occurs easier and faster compared to those in smaller pore spaces. On the other hand, the amount of water that exists in the pore spaces of specimen at the optimum water content is less. Its pore water is confined in small pores and adsorbed on soil particles' surfaces, and therefore has low free energy. As a result, the pore water freezes under low temperatures at a slower rate. This can explain the observation that for the five investigated soils except for TSC, the frozen M_R versus subzero temperature relationship of the specimen at saturated water condition typically has steeper slope than that at the optimum water content, in the temperature range of 0 to -5 °C.

The effect of stress levels on the measured frozen M_R is dependent on soil type, water

content, and temperature. For the same soil tested under a specific water content, the influence of stress level is straightforward. When the specimen has low temperature (e.g., the controlled bath temperature is at -15 °C), the deviator stress has large influence on the frozen M_R of the five soils. This is true for specimens at both the optimum and saturated water contents. However, when the specimen has higher temperatures (e.g., the controlled bath temperature is higher than -5 °C), the effect of deviator stress is less significant. Compared to the deviator stress, the confining stress typically does not have notable influence on frozen M_R of the five soils.

In the present study, loading frequency showed limited influence on the frozen M_R. Such a behavior may be attributed to the differences between the selected frequencies, which is not large enough. An attempt to conduct M_R tests with higher frequencies (e.g., 6, 8, and 10 Hz) was not successful due to limitations of the equipment used in the present study. Zhu et al. (2011), is one of the investigators, who measured the dynamic shear modulus of a frozen clay under different frequencies (i.e. 2 to 10 Hz). The dynamic shear modulus does not show significant differences under the investigated frequencies in spite of a maximum value that is achieved at the frequency of 6 Hz. The study by Stevens (1973) showed that the investigated range of frequency (1 to 1000 kHz) does not have a significant influence on the measured dynamic shear modulus of a sand and a silt. On the other hand, it is generally recognized that the frequency of cyclic loading has a large influence on the dynamic behavior of soils. Higher loading frequency typically results in higher value of dynamic modulus of frozen soils (Li et al., 1979), frozen saline soils (Jessberger and Jordan, 1982), and soils subjected to freeze-thaw cycles (Lin et al., 2017). This is because the resilient strain under cyclic loading decreases when the loading frequency increases. Alternatively, lower loading frequency contributes to larger permanent strain (Guo et al., 2016; Lei et al., 2017).

The measured frozen M_R values of the five investigated soils are low compared to the results of other studies reported in the literature. For example, when the bath temperature is controlled at -15 °C, the highest M_R value measured in the present study is around 350 MPa (e.g., see **Figure 7.11**). However, the M_R results of two frozen subgrade soils at temperature around

-7 °C, measured by Berg et al. (1996), are significantly high and is about 10 times the M_R value measured in the present study. According to Simonsen et al. (2002), the frozen M_R of New Hampshire marine clay is around 200 MPa at −2 °C. However, it reaches a value higher than 1500 MPa at −5 °C, and is approximately 3000 MPa at −10 °C. The possible reasons for the significant differences include different soil types and water contents, different specimen preparation and freezing methods (which have a significant influence on the soil structure), different loading forms, frequencies and stress levels, as well as the hysteresis of unfrozen water or ice content during freezing and thawing processes. It should be noted that the M_R test was carried out following thawing path in the present study. By extending such an approach, the problem associated with supercooling in the initial freezing period is avoided. More investigations are however required to understand the effects of these factors on the M_R of different frozen soils.

7.7 Summary

The resilient modulus (M_R) characterizes the resilient (elastic) behavior of soils subjected to dynamic cyclic loading. The M_R is a key material property required for the rational design of pavement structures. In permafrost and seasonally frozen regions, temperature and moisture variations have significant influence on the M_R of subgrade and foundation soils. In the present study, the M_R of five Canadian soils considering wetting and freezing were experimentally determined with the aid of an advanced cyclic loading triaxial testing system. A freezing system with the cooling unit, thermal insulation, and modification to the triaxial testing system was established for accurately maintaining the desired testing temperatures within soil specimens. In addition, the effects of stress level and frequency of the cyclic loading on the frozen M_R were investigated.

The main conclusions drawn from the present study include: (i) The effect of subzero temperature on the M_R of the five investigated soils is significant. The relationship curve between the frozen M_R and subzero temperature resembles hyperbola. (ii) For four of the five soils, the

frozen M_R versus subzero temperature relationship of the saturated specimen typically has steeper slope than that at the optimum water content, for the temperature range of 0 to -5 °C. (iii) The effect of stress levels on the measured M_R is dependent on the type of soils, water contents of the specimens, and temperature. And (iv) Loading frequency does not show a significant influence on the measured frozen M_R in the present study.

The determination of frozen soil behavior such as M_R is prone to fluctuation due to the difficulties in experimental investigations on frozen soils. For example, the accurate temperature control throughout the specimen is difficult; and the non-uniform distribution of unfrozen water and ice may contribute to the variation in frozen soil behavior. The large difference in the measured M_R between the present study and other studies may be associated to different soil types and water contents, different specimen preparation and freezing methods, and different loading forms, frequencies, and stress levels. More investigations are required for better understanding the effects of these factors on the M_R of different frozen soils.

7.8 References

AASHTO, 2007. Designation: T307-99: Standard method of test for determining the resilient modulus of soils and aggregate materials, American Association of State Highway and Transportation Officials, Washington, D.C.

AASHTO, 2012. Designation M145-91: Classification of soil and soil-aggregate mixtures for highway construction purpose. American Association of State Highway and Transportation Officials, Washington, D.C.

Andersland, O.B., and Ladanyi, B., 2004. Frozen ground engineering. 2nd edition. John Wiley & Sons, Inc., Hoboken, NJ.

ARA, Inc., ERES Consultants Division. 2004. Guide for Mechanistic - Empirical Design of New and Rehabilitated Pavement Structures. Final report, NCHRP Project 1-37A. Transportation Research Board, Washington, D.C.

ASTM, 2011. Designation: D2487-11: Standard practice for classification of soils for engineering purposes (Unified Soil Classification System). American Society for Testing and Materials, West Conshohocken, PA.

ASTM. 2012. Designation: D698-12: Standard Test Methods for Laboratory Compaction Characteristics of Soil Using Standard Effort (12400 ft-lbf/ft^3 (600 kN-m/m^3)). American Society for Testing and Materials. West Conshohocken, PA.

Berg, R.L., Bigl, S.R., Stark, J.A., and Durell, G.D. 1996. Resilient modulus testing of materials

from Mn/ROAD, Phase 1. CRREL-96-19, U.S, Army Cold Regions Research and Engineering Laboratory, Hanover, N.H.

Bigl, S.R., and Berg, R.L. 1996. Material Testing and Initial Pavement Design Modeling: Minnesota Road Research Project. CRREL Report 96-14, USACE Cold Regions Research and Engineering Laboratory, Hanover, N.H.

Bosscher, P. J., and D. L. Nelson. 1987. Resonant Column Testing of Frozen Ottawa Sand. Geotechnical Testing Journal, 10(3), 123–134.

Caicedo, B., 2018. Geotechnics of Roads: Fundamentals. CRC Press, Boca Raton, Florida, USA.

Cary, C.E. and Zapata, C.E., 2011. Resilient modulus for unsaturated unbound materials. Road Materials and Pavement Design, 12(3), pp.615-638.

Chamberlain, E.J. and Gow, A.J. 1979. Effect of freezing and thawing on the permeability and structure of soils. Engineering Geology, 13(1): 73-92.

Cole, D.M., Bentley, D.L., Durell, G.D. and Johnson, T.C., 1987. Resilient Modulus of Freeze-Thaw Affected Granular Soils for Pavement Design and Evaluation. Part 3. Laboratory Tests on Soils from Albany County Airport (No. CRREL-87-2). Cold Regions Research and Engineering Laboratory, Hanover, N.H.

Feldman, G.M. 1988. Reference book for the forecast of the soils temperature behaviour. Ac. Sci.

Guo, L., Chen, J., Wang, J., Cai, Y. and Deng, P., 2016. Influences of stress magnitude and loading frequency on cyclic behavior of K0-consolidated marine clay involving principal stress rotation. Soil Dynamics and Earthquake Engineering, 84, pp.94-107.

Han, Z., 2016. Modelling Stiffness and Shear Strength of Compacted Subgrade Soils. Doctoral thesis, University of Ottawa, Ottawa, Canada.

Han, Z. and Vanapalli, S.K., 2016. State-of-the-Art: Prediction of resilient modulus of unsaturated subgrade soils. International Journal of Geomechanics, 16(4), p.04015104.

Han, Z., Vanapalli, S.K., Ren, J.P. and Zou, W.L., 2018. Characterizing cyclic and static moduli and strength of compacted pavement subgrade soils considering moisture variation. Soils and foundations, 58(5), pp.1187-1199.

Ho, E. and Gough, W.A., 2006. Freeze thaw cycles in Toronto, Canada in a changing climate. Theoretical and Applied Climatology, 83(1-4), pp.203-210.

Ishikawa, T., Sekine, E. and Miura, S., 2011. Cyclic deformation of granular material subjected to moving-wheel loads. Canadian Geotechnical Journal, 48(5), pp.691-703.

Jessberger, H.L. and Jordan, P., 1982. Frozen saline sand subjected to dynamic loads. In CRREL Proc. of the 3 d Intern. Symp. on Ground Freezing p 19-26 (SEE N 83-15691 06-42).

Jong, D.T., Bosscher, P. and Benson, C. 1998. Field assessment of changes in pavement moduli caused by freezing and thawing. Transportation Research Record: Journal of the Transportation Research Board, (1615), 41-48.

Konrad, J.M. and Morgenstern, N.R., 1980. A mechanistic theory of ice lens formation in fine-grained soils. Canadian Geotechnical Journal, 17(4), pp.473-486.

Lei, H., Liu, M., Zhang, W. and Li, B., 2017. Dynamic properties of reclaimed soft soil under the combined frequency cyclic loading. Road Materials and Pavement Design, 18(sup3), pp.54-64.

Li, J.C., Baladi, G.Y. and Andersland, O.B., 1979. Cyclic triaxial tests on frozen sand. Engineering Geology, 13(1-4), pp.233-246.

Lin, B., Zhang, F. and Feng, D., 2017. Long-term resilient behaviour of thawed saturated silty clay under repeated cyclic loading: experimental evidence and evolution model. Road Materials and Pavement Design, 20(3), pp.608-622.

Ling, X., Li, Q., Wang, L., Zhang, F., An, L. and Xu, P., 2013. Stiffness and damping radio evolution of frozen clays under long-term low-level repeated cyclic loading: experimental evidence and evolution model. Cold Regions Science and Technology, 86, pp.45-54.

Liu, J., Hayakawa, N., Lu, M., Dong, S. and Yuan, J., 2003. Winter streamflow, ground temperature and active‐layer thickness in northeast China. Permafrost and Periglacial Processes, 14(1), pp.11-18.

MTO, (Ministry of Transportation of Ontario). 2013. Pavement design and rehabilitation manual (Second Edition). Queen's Printer for Ontario, Canada.

Ren, J. and Vanapalli, S.K., 2017. Prediction of the resilient modulus of frozen unbound road materials using the soil-freezing characteristic curve. Canadian Geotechnical Journal, 55: 1200-1207.

Ren, J. and Vanapalli, S.K., 2018. Empirical model for predicting the resilient modulus of frozen unbound road materials using a hyperbolic function. Transportation Geotechnics, 17: 66-74.

Ren, J. and Vanapalli, S.K., 2019. Comparison of soil-freezing and soil-water characteristic curves of two Canadian soils. Vadose Zone Journal, (online).

Ren, J., Vanapalli, S.K. and Han, Z., 2017. Soil freezing process and different expressions for the soil-freezing characteristic curve. Sci Cold Arid Reg, 9(3), pp.221-228.

Sheng, D., Zhang, S., Niu, F. and Cheng, G., 2014. A potential new frost heave mechanism in high-speed railway embankments. Géotechnique, 64(2), pp.144-154.

Sheng, D., Zhang, S., Yu, Z. and Zhang, J., 2013. Assessing frost susceptibility of soils using PCHeave. Cold Regions Science and Technology, 95, pp.27-38.

Simonsen, E., Janoo, V.C., and Isacsson, U. 2002. Resilient properties of unbound road materials during seasonal frost conditions. Journal of Cold Regions Engineering, 16(1): 28–50.

Stevens, H.W., 1973. Viscoelastic properties of frozen soil under vibratory loads. In North American Contribution to the Second International Conference on Permafrost. Yakutsk, Siverua, USSR (pp. 400-409).

Zhu, Z.Y., Ling, X.Z., Wang, Z.Y., Lu, Q.R., Chen, S.J., Zou, Z.Y. and Guo, Z.H., 2011. Experimental investigation of the dynamic behavior of frozen clay from the Beiluhe subgrade along the QTR. Cold Regions Science and Technology, 69(1), pp.91-97.

Chapter 8 The resilient moduli of five Canadian soils under wetting and freeze-thaw conditions and their estimation by using an Artificial Neural Network (ANN) model

The contents presented in this chapter are from the manuscript:

Ren, J.P., Vanapalli, S.K., Han, Z., Omenogor, K.O., and Bai, Y. 2018. The resilient moduli of five Canadian soils under wetting and freeze-thaw conditions and their estimation by using an Artificial Neural Network model. Under peer review with a Journal.

8.1 Abstract

The resilient modulus (M_R) is a key parameter used in the mechanistic-empirical methods for the rational design of pavement structures. In permafrost and seasonally frozen regions, the M_R of subgrade soils is significantly influenced by the variations in moisture content and temperature. The M_R typically reduces due to the weathering action associated with wetting and freeze-thaw (F-T) cycles, which contributes to the reorientation of soil particles, loss in suction and cohesion, and formation of cracks in the subgrade soils. In the present study, the M_R values of five Canadian soils that are widely used as pavement subgrades were determined under wetting and F-T conditions. The key findings from the extensive experimental investigations suggest: (i) the M_R values of the soils at their respective optimum water contents significantly reduce up to the critical F-T cycle, which is typically the first or second F-T cycles; (ii) there is little change in the M_R values from the critical to the tenth F-T cycle; (iii) the percentage of reduction in the measured M_R at the optimum water content after the critical F-T cycle is strongly related to the soils plasticity index; (iv) the measured M_R values are typically low for the specimens subjected to wetting, and the effect of F-T cycles on these specimens is insignificant; and (v) the effect of stress levels on the M_R values is dependent on the initial water contents of the specimens and soil types. In addition, an artificial neural network (ANN) model was proposed and validated for estimating the M_R of the tested soils taking account of various

influencing factors. Both the experimental data and the developed ANN model provide valuable information for the rational design of pavements in Canada.

8.2 Introduction

The resilient modulus (M_R) is a key material property required for the rational design of pavement structures based on the mechanistic-empirical methods (e.g., MEPDG (ARA, Inc., 2004)). The pavement structures are directly exposed to the external environment; due to this reason, environmental factors such as the evaporation and infiltration have a significant influence on the water contents within the pavement materials, and therefore on their mechanical properties such as the M_R (Cary and Zapata, 2010). In addition to water content, temperature is another key factor that influences the properties of pavement materials and therefore the pavement performance. The effects of the harsh climate on pavement structures cannot be neglected in permafrost and seasonally frozen regions such as Canada, Russia, and the Qinghai-Tibet plateau of China.

The depth that the freezing front penetrates the pavement structure depends on many factors, which include the air temperature, thermal properties and water contents of base, subbase and subgrade soils. For example, the frost penetration depth in southern Ontario, Canada is around 1 to 2 m; however, it can exceed 3 m in northern Ontario (MTO, 2013). The pavement structures located in these areas are typically subjected to F-T cycles during a year. Several cycles of F-T can be expected in regions where the temperature varies significantly. Alternatively, fewer F-T cycles are expected if the temperature remains below freezing for a significant portion of winter (Othman et al., 1994). The number of F-T cycles also depends on the depth of the soils. The subgrade soils near the ground surface are subjected to more F-T cycles compared to those at a greater depth where temperature fluctuation is typically small.

The physical and mechanical properties of soils are significantly influenced by F-T cycles. The soils typically experience volume change, development of cracks, loss in shear strength and stiffness, and alteration in hydraulic conductivity due to F-T cycles (e.g., Graham and Au, 1985;

Eigenbrod, 1996; Ishikawa et al., 2010; Xu et al., 2018). Qi et al. (2008) highlighted the dual influence of F-T cycles on soil density, i.e. loose soils densify and dense soils loosen. The F-T cycles also influence the yielding and hardening characteristics of soils, which are essential for modeling soil behavior using constitutive models (Yao et al., 2009). For example, an increase in the vertical hydraulic conductivity of different fine-grained soils subjected to F-T cycles were observed by Chamberlain and Gow (1979). One of the main reasons for the increase in the hydraulic conductivity was attributed to the formation of polygonal shrinkage cracks. Wang et al. (2007) investigated the mechanical behavior of the Qinghai-Tibet clay subjected to a maximum of 21 closed-system F-T cycles. This study highlighted a strong relationship between the failure shear strength determined from triaxial compression tests and the number of F-T cycles. Li et al. (2018) investigated the independent effect of moisture variation (i.e. wetting-drying (W-D) cycles) and temperature variation (i.e. F-T cycles) on the mechanical properties (e.g., unconfined compressive strength, elastic modulus, compressibility and collapsibility) of densely compacted loess specimens. They concluded that the weathering associated W-D contributes to a more significant deterioration effect on the geotechnical properties of loess soils than the F-T weathering.

The M_R of pavement materials can be reliably determined from experimental results with the aid of elaborate testing equipment. However, they are time consuming, need trained professionals and hence it is expensive. For this reason, several models have been proposed in the literature for the prediction of the M_R of pavement materials. These predictive models were mostly established through regression analysis, based on relationships between the M_R and soil properties and stresses considering the influence of environmental factors (e.g., Cary and Zapata, 2011; Han and Vanapalli, 2016; Caicedo, 2018; Ren and Vanapalli, 2018). In recent years, the artificial neural network (ANN) models have been successfully used for the estimation of moduli of engineering materials (e.g., Tutumluer and Seyhan, 1998; Park et al., 2009; Zaman et al. 2010; Duan et al., 2013). For example, Park et al. (2009) developed ANN models for estimating M_R of subbase and subgrade soils based on basic soil properties and stress levels the soils are subjected

to. The ANN model correlates input variables to output variables through neurons, which are inter-connected to form a mathematical representation of the relationship that may be embedded in any set of data (Park et al., 2009; Saha et al., 2018). Various factors that influence the M_R of pavement materials can be considered by using ANN without fully understanding the nature of the relationship between the M_R and influencing variables. For this reason, ANN models can serve as a simple yet reliable predictive tool for the design of pavement structure alleviating cumbersome experimental determination of the M_R.

The purpose of the present study is to develop a reliable database of M_R values for five fine-grained soils that are widely used in pavement subgrade construction in Canada. The influence of both water content variation (i.e. wetting process) and F-T cycles on the M_R of the five soils was investigated from an extensive experimental program. In addition, the effect of different stress levels was investigated in the present study. An ANN model was developed and validated for estimating the M_R of the five soils taking account of the variation in water content, number of F-T cycles and various stress levels. Both the experimental results and the developed ANN model provide valuable information and facilitate the rational design of pavement structures in regions with frozen soils in Canada.

8.3 Materials and specimen preparation

Five Canadian soils, i.e., Toronto silty clay (TSC), Toronto lean clay (TLC), Kincardine lean clay (KLC), Ottawa Leda clay (OLC), and Indian Head till (IHT), were used in the present study. The first four soils were collected from 0 to 3 m below the natural ground surface in the southern region of Ontario province, which has the most widely used pavement grid network in Canada. The fifth soil, Indian Head till was collected from Indian Head, Saskatchewan. This soil is a representative candidate of glacial tills that are extensively available in Saskatchewan, Alberta and Manitoba provinces of Canada. The investigated soils were air dried for two weeks and then grinded and passed through a 2 mm sieve. The basic physical properties of the five soils are summarized in **Table 8.1**. **Figure 8.1** presents the gradation curves of the five soils. The

chemical and mineralogical compositions of the five soils are summarized in Chapter 7 (see **Table 7.2**) and also available in Han et al. (2018).

Table 8.1 Basic properties of the five soils

	Toronto silty clay (TSC)	Toronto lean clay (TLC)	Kincardine lean clay (KLC)	Ottawa Leda clay (OLC)	Indian Head till (IHT)
w_L (%)	20	25	31	48	36
w_P (%)	14	13	21	22	17
PI (%)	6	12	10	26	19
w_{opt} (%)	13.5	12.3	20.3	23.0	13.9
γ_{dmax} (kN/m^3)	19.15	19.62	16.31	16.16	18.39
G_s	2.68	2.69	2.71	2.75	2.72
%sand	3	31	15	20	28
%silt	81	50	60	48	42
%clay	16	19	25	32	30
AASHTO	A-4	A-6	A-4	A-6	A-6
USCS	CL-ML	CL	CL	CL	CL
ψ_{opt} (kPa)	40	260	90	200	190

Note: w_L = liquid limit; w_P = plastic limit; PI = plasticity index; w_{opt} and γ_{dmax} = optimum water content and maximum dry unit weight (determined by the Standard Proctor compaction test, ASTM D698-12); G_s = specific gravity; AASHTO = American Association of State Highway and Transportation Officials soil classification system (AASHTO M145-91); USCS = Unified Soil Classification System (ASTM D2487-11); ψ_{opt} = approximate suction of the soil specimen at the w_{opt} (based on the measured soil-water characteristic curve (SWCC) of the five soils by using the pressure plate method, vapor equilibrium method, and WP4-T measurement as described in Section 4.4.3).

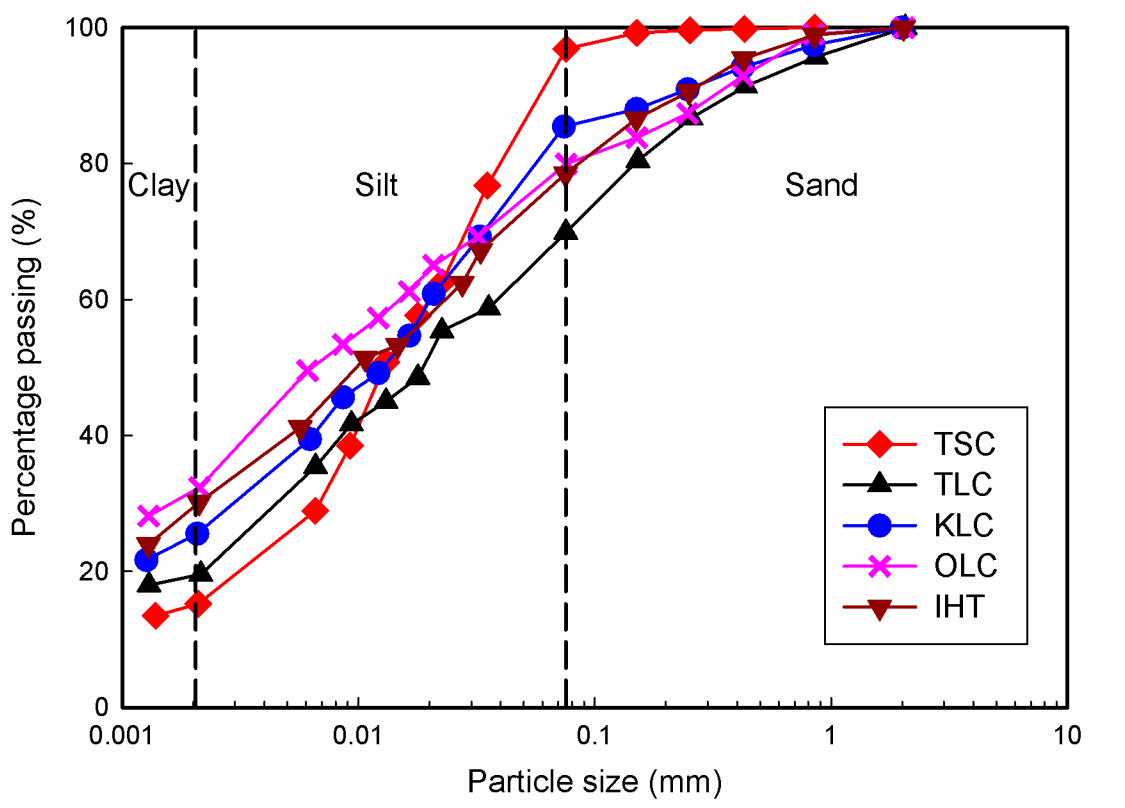

Figure 8.1 The gradation curves of the five soils

A pre-calculated amount of dry soil and water were mixed and statically compacted at the optimum water content and maximum dry density. The test specimens were compacted in five equal layers. Each layer was 20 mm high and the final soil specimen was 100 mm in height and 50 mm in diameter, as shown in **Figure 8.2**. In order to simulate the wetting process that in-situ subgrade soils typically undergo, the compacted specimens were wetted to different post-compaction water contents, ranging from the optimum water content to saturated water content conditions. During the wetting process, the soil specimens were covered with wet filter paper and sealed using cling wrap. The soil specimens were then stored in plastic containers (see **Figure 8.2**). The specimens were allowed to absorb water gradually from the wet filter paper until the predetermined water contents were achieved, by monitoring the amount of water absorbed by the specimens. These water contents are summarized in **Table 8.2**, together with the void ratios assuming constant volume conditions during the wetting process. In addition, the

degrees of saturation that were calculated from the volume-mass relationships of the five soils are summarized.

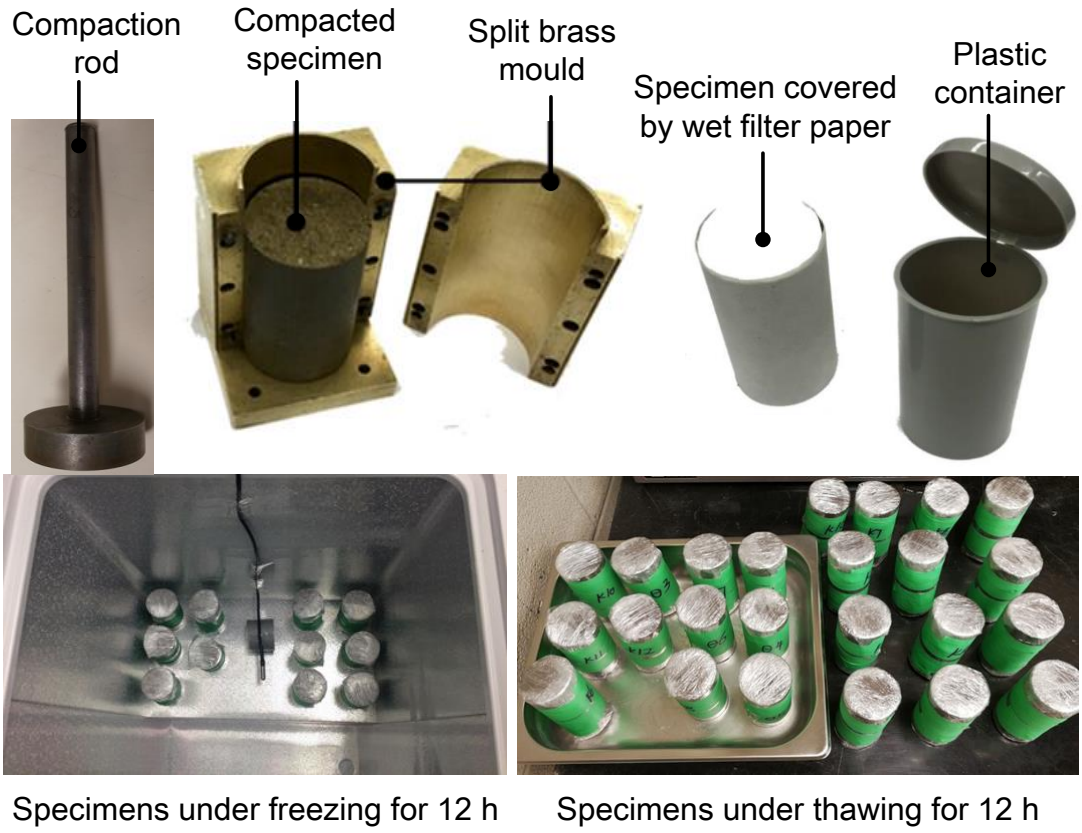

Figure 8.2 Compaction, wetting, and freezing-thawing of soil specimens

Table 8.2 Different post-compaction water contents of the five soils

Soil	Maximum dry unit weight (kN/m^3)	Void ratio	Post-compaction gravimetric water content (%)	Degree of saturation (%)
TSC	19.15	0.400	13.5[1]	90.5
			14.0	93.8
			14.6	97.5
			14.9[2]	100.0
TLC	19.62	0.371	12.3[1]	89.0
			12.8	93.2
			13.3	97.0
			13.8[2]	100.0

KLC	16.31	0.662	20.3[1]	83.2
			21.7	88.9
			23.1	94.6
			24.4[2]	100.0
OLC	16.16	0.702	23.0[1]	90.0
			23.8	93.2
			24.6	96.3
			25.5[2]	100.0
IHT	18.39	0.479	13.9[1]	79.0
			15.2	86.0
			16.4	93.0
			17.6[2]	100.0

Note: [1]Optimum water content (w_{opt}); [2]Saturated water content (w_{sat}).

The soil specimens with different post-compaction water contents were tightly sealed in cling wraps before they were subjected to different F-T cycles. The F-T cycles were imposed by repeatedly freezing the specimens in a freezer for 12 hours and thawing them under room temperature (around 23 °C) for 12 hours, under zero external stress and constant water content condition (see **Figure 8.2**). The freezing temperature was controlled at around -15 °C since several studies in the literature show that different freezing temperatures used for F-T cycles do not have significant influence on the measured soil properties (e.g., Liu et al., 2016; Zhou et al., 2018). The specimens were frozen and thawed three-dimensionally, which can be easily achieved in a laboratory environment. Ice lenses were not observed through three-dimensional and closed-system (i.e. constant water content) freezing. The M_R values were determined for various F-T cycles (e.g., 0, 1, 2, 3, 4, 6, 8, and 10) on the five soils at different post-compaction water content conditions. Several research studies suggest that the effect of F-T cycles is significant only in the first few cycles (e.g., Skaggs, 1992; Lee et al., 1995; Cui et al., 2017; Tang et al., 2018; Lu et al., 2019). For this reason, in the present study, 10 cycles were considered sufficient for characterizing the influence of F-T cycles on the five investigated soils. In total, over 150 specimens (each one of the specimens corresponds to a particular water content and F-T cycle condition) were prepared for the present experimental investigation.

8.4 Experimental procedures

The M_R of the five Canadian soils were experimentally determined using the GDS Entry Level Dynamic (ELDyn) triaxial testing system (see **Figure 8.3**). The test specimen is placed on the base pedestal and sealed with a rubber membrane and O-rings. A pneumatic regulator with air as fluid is used to apply the confining stress (σ_c) on the specimen. In addition, a pneumatic actuator is mounted on the loading frame with a rigid loading rod for applying the cyclic load. A 5 kN load cell with an accuracy of ±5 N (±2.5 kPa for specimen 50 mm in diameter) is mounted at the lower end of the loading rod inside the triaxial chamber to measure the force. An optical encoder that is embedded within the pneumatic actuator facilitates the measurement of the displacement of the loading rod, which is used in determining the axial deformation of the soil specimen. The ELDyn system has the capacity to detect the displacement of the soil specimen as low as 0.001 mm. The load cell and pneumatic actuator, along with the data acquisition systems, form a looped system to enable the application of the stress-controlled cyclic load. More details of this equipment are available in Han (2016).

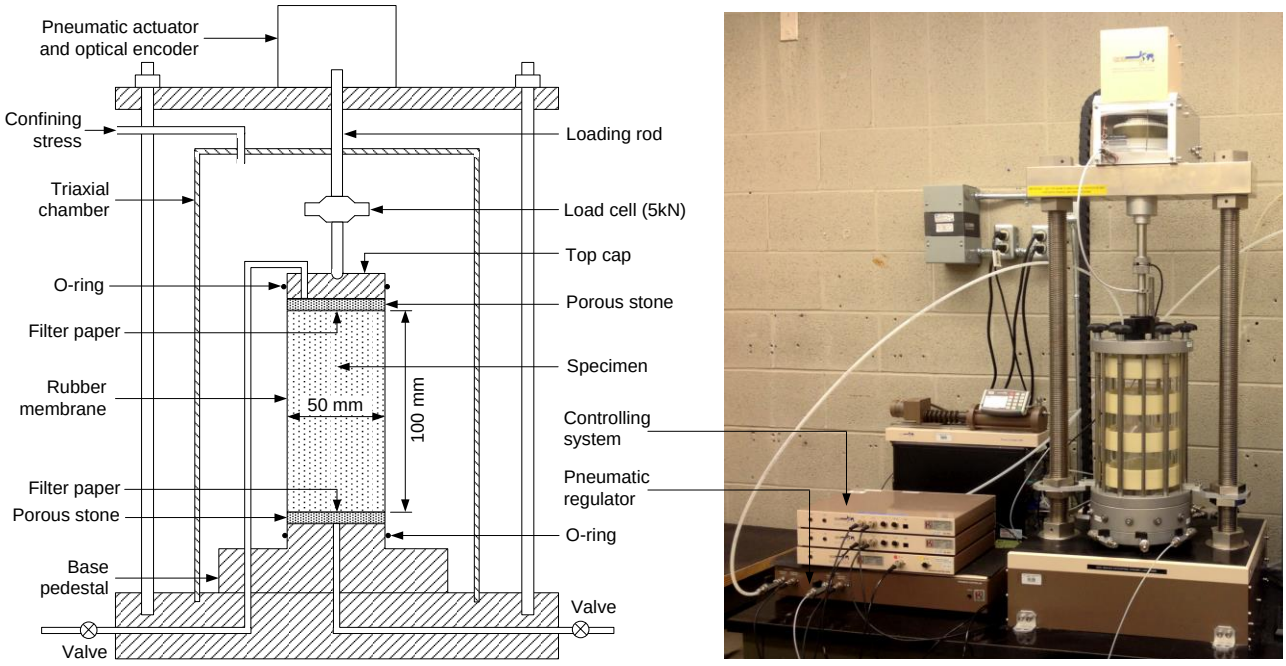

Figure 8.3 GDS Entry Level Dynamic (ELDyn) triaxial testing system used for testing (modified after Han, 2016)

The *Standard Method of Test for Determining the Resilient Modulus of Soils and Aggregate Materials* (AASHTO T307-99, 2007) was followed to measure the M_R of the five soils. The standard haversine load pulse in AASHTO T307-99 was modified to a sinusoidal form of cyclic load, which can be applied by the ELDyn system. **Figure 8.4** shows the applied sinusoidal form of load versus load duration, which is 1 sec for one loading cycle. There is a contact load (which is 10% of the maximum applied load during a loading cycle) acting on the specimen during the whole testing process. The maximum applied load is equal to $A*\sigma_d$, where A is the initial cross-sectional area of the soil specimen, and σ_d is the maximum deviator stress during a loading cycle. The cyclic load is 90% of the maximum applied load of a loading cycle. The M_R is defined as the cyclic stress (i.e. $0.9\sigma_d$) divided by the recovered axial strain. Different combinations of σ_c (e.g., 41.4 kPa, 27.6 kPa, and 13.8 kPa) and σ_d (e.g., 27.6 kPa, 41.4 kPa, 55.2 kPa, and 68.9 kPa) were applied on the specimen according to the loading sequences in AASHTO T307-99. As a result, the M_R of specimens under different stress levels were determined. The pre-conditioning loading (i.e. 500 to 1000 cycles) was applied on the specimen for minimizing the effects of initially imperfect contact between the top cap and the specimen. For each stress combination, 100 loading cycles were applied. The M_R was determined as the average values of the last five loading cycles under each stress combination.

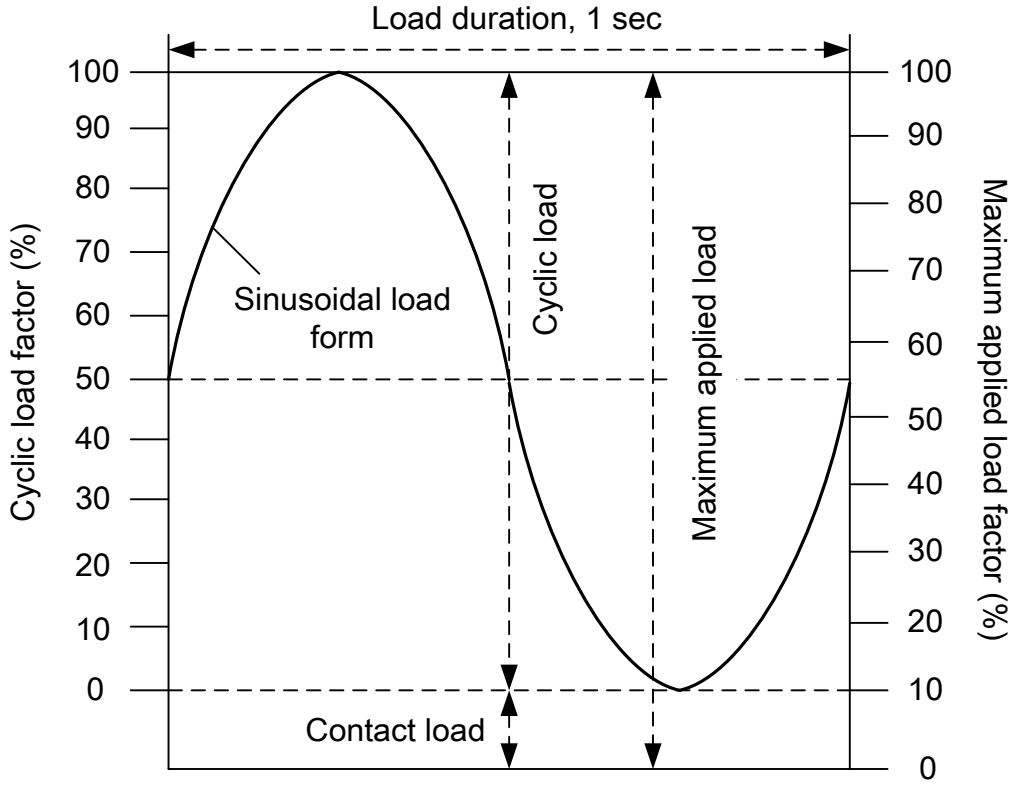

Figure 8.4 The sinusoidal load form used for resilient modulus test

8.5 Experimental results and analysis

8.5.1 Effect of freeze-thaw cycles

Figure 8.5 shows the variation of M_R with respect to F-T cycles under different stress levels for the OLC specimens. The behavior of the other four soils was also consistent with the observed behavior for OLC. **Figure 8.5**(a) shows the results of OLC specimens that were tested at the optimum water content. The measured M_R shows significant reduction within the first two F-T cycles. However, it shows negligible variation with further increase in the F-T cycles. A similar trend of variation is observed for M_R values determined for all the stress conditions investigated in the present study. For example, under the stress combination of 41.4 kPa and 68.9 kPa, the M_R of OLC was 62.2 MPa when the specimen was not subjected to any F-T cycles. The M_R decreased to 24.1 MPa after two F-T cycles, indicating a reduction greater than 60%. However, decrease in the M_R was minimal for further F-T cycles. The M_R decreased to around 20

MPa after ten F-T cycles, which was close to the M_R values after only two F-T cycles (see **Figure 8.5**(a)). In other words, the critical number of F-T cycles for OLC is 2. The critical number of F-T cycles for the other four soils; namely, TSC, TLC, KLC, and IHT were determined as 0, 1, 1, and 1, respectively based on the experimental results. The zero value for TSC means that the number of F-T cycles does not have any significant impact on its measured M_R values (see **Figure 8.7**(a)).

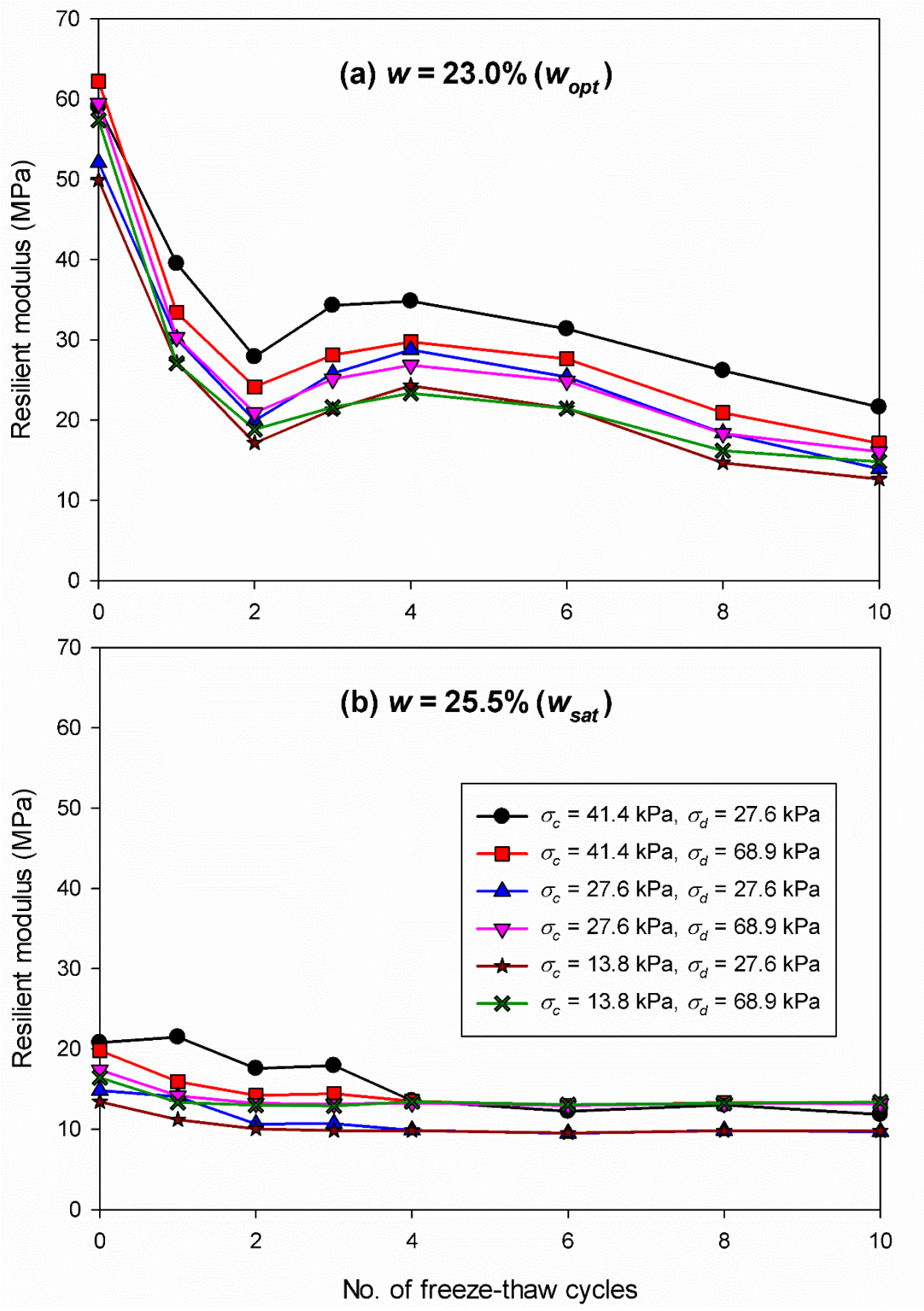

Figure 8.5 The effect of F-T cycle on the resilient modulus of OLC (a) at the optimum water content and (b) at the saturated water content

Table 8.3 summarizes reduction in the M_R of the five soils after the critical number of F-T cycles. These values were from specimens tested at their optimum water contents and under the stress level of σ_c = 41.4 kPa and σ_d = 68.9 kPa. It can be seen that the percentages of reduction in M_R of the five soils are different. An attempt was made to correlate the reduction values to soil physical properties such as the liquid limit (w_L), plastic limit (w_P), plasticity index (PI), and maximum dry density (γ_{dmax}) shown in **Table 8.1**. It was found that the best-fit linear relationship can be achieved between the percentage of reduction in M_R and PI of the five soils, with a high value of coefficient of determination (i.e. R^2 = 0.91) (as shown in **Figure 8.6**). Additionally, the values of percentage of reduction in M_R for the five soils at their optimum water contents and under different stress levels are summarized in **Table 8.4**, along with the fitting parameters (i.e. *a* and *b*) and R^2 values for the best-fit linear relationships. As can be seen, the percentage of reduction is strongly dependent on PI for most of the stress combinations (indicated by the high R^2 values), especially under large deviator stress and low confining stress.

Table 8.3 Reduction in resilient moduli of the five soils after the critical number of F-T cycles

Soil	M_R before F-T (MPa)	Critical number of F-T cycles	M_R after the critical number of F-T cycles (MPa)	Percentage of reduction in M_R after the critical number of F-T cycles (%)
TSC	35.9	0	35.9	0
TLC	62.2	1	42.5	31.7
KLC	40.1	1	31.0	22.7
OLC	62.2	2	24.1	61.3
IHT	43.6	1	28.0	35.8

Note: The soils were at their optimum water contents, and the M_R values were obtained at the stress level of σ_c = 41.4 kPa and σ_d = 68.9 kPa.

Table 8.4 Reduction in resilient moduli of the five soils under different stress levels

	Percentage of reduction in M_R after the critical number of F-T cycles (%)											
σ_c (kPa)	41.4				27.6				13.8			
σ_d (kPa)	27.6	41.4	55.2	68.9	27.6	41.4	55.2	68.9	27.6	41.4	55.2	68.9
TSC	0	0	0	0	0	0	0	0	0	0	0	0
TLC	40.9	43.8	31.5	31.7	14.7	17.9	23.2	28.4	22.5	24.1	25.4	30.0
KLC	24.8	27.6	25.3	22.7	27.0	28.0	26.7	24.2	34.0	33.5	31.4	28.0
OLC	52.7	56.4	59.1	61.3	61.8	63.8	64.6	64.8	65.7	67.4	67.6	67.2
IHT	/	/	21.1	35.8	12.9	29.8	34.4	36.8	32.3	33.0	34.9	37.0
Percentage of reduction in M_R after the critical number of F-T cycles (%) = a * PI + b												
a	2.25	2.39	2.26	2.66	2.39	2.72	2.80	2.85	2.69	2.77	2.84	2.87
b	-0.78	-0.35	-5.61	-8.60	-11.55	-11.82	-11.18	-10.75	-8.42	-8.90	-9.66	-9.53
R^2	0.74	0.73	0.71	0.91	0.64	0.86	0.91	0.93	0.81	0.83	0.87	0.90

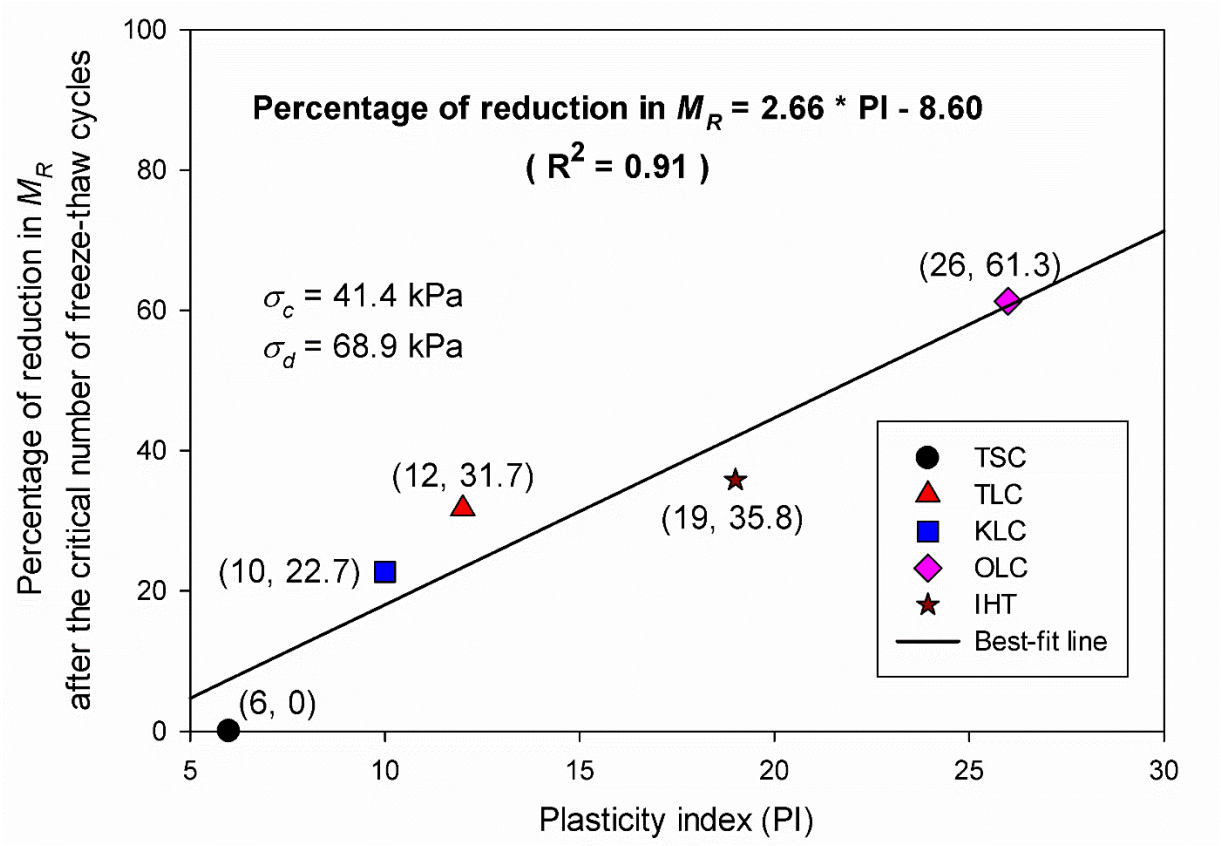

Figure 8.6 The linear relationship between the percentage of reduction in resilient modulus and PI

Figure 8.5(b) shows the influence of F-T cycles on the M_R of OLC specimens that were wetted to the saturated condition. The variation trends of the measured M_R are similar under different stress levels for the saturated specimens. However, the number of F-T cycles is found to have limited or no influence on the M_R values, which are typically in the range of 10 MPa to 20 MPa. In other words, the measured M_R values are relatively low for specimens with a water content that is close to saturated condition. Results from the present study suggest that when the specimens have high initial water content (or high degree of saturation), it is the water content rather than the number of F-T cycles which has the dominant influence on the magnitude of M_R.

The measured M_R values with F-T cycles at the stress level of σ_c = 41.4 kPa and σ_d = 68.9 kPa for the five soils at various water contents is shown in **Figure 8.7**. When the soil specimens were at their optimum water contents, the influence of F-T cycles on the M_R is significant for the first or second cycles for TLC, KLC, OLC, and IHT, except for TSC. However, when the soil specimens have higher water contents, the measured M_R values are typically much lower. In other words, when the water content is high, the influence of F-T cycles on the M_R values is negligible. For TSC, the F-T cycles do not show influence on its M_R. Such a behavior may be attributed to the high percentage of silty size particles and relatively low amount of clay particles (see **Table 8.1**). In other words, the effect of F-T cycles on the adhesion that bonds clay particles together is negligible in TSC.

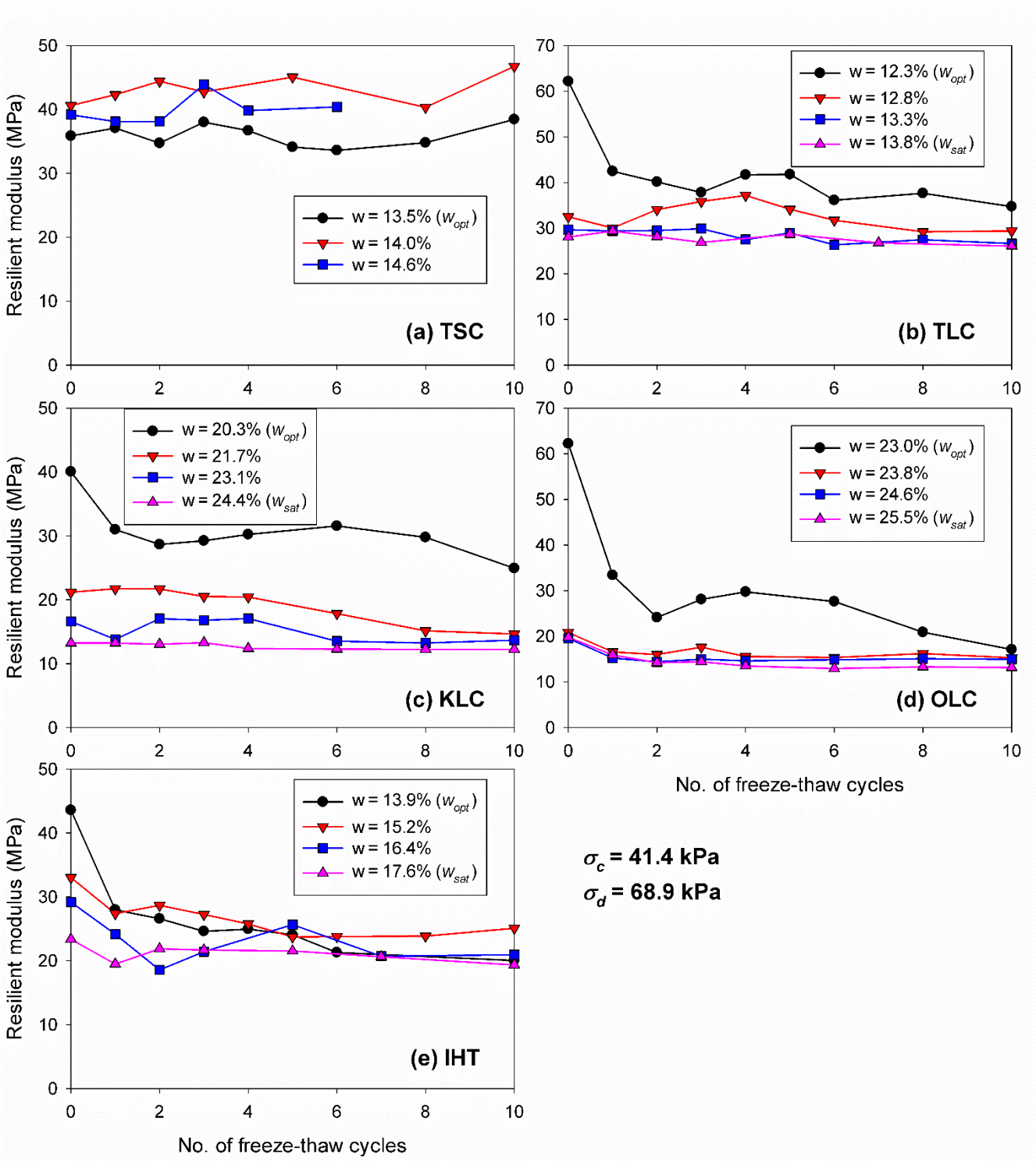

Figure 8.7 The effect of F-T cycles on the resilient moduli of (a) TSC, (b) TLC, (c) KLC, (d) OLC, and (e) IHT at various water contents (σc = 41.4 kPa, and σd = 68.9 kPa)

8.5.2 Effect of water content

Figure 8.8 summarizes the effect of water content on the M_R of the five soils subjected to different numbers of F-T cycles at a selected stress level (i.e., σ_c = 41.4 kPa, and σ_d = 68.9 kPa). It can be seen that for TSC (**Figure 8.8**(a)), water content does not have significant influence on its M_R, for all the F-T cycles. The M_R of TSC specimens at an initial water content of 14% is higher in comparison with those at the water contents of 13.5% and 14.6%. Such a behavior may predominantly be attributed to difference in the soil structure of the tested TSC specimens (due to wetting process). The M_R of saturated TSC specimen (i.e. at the water content of 14.9%, see **Table 8.2**) was not obtained since the compacted TSC specimen (i.e. at the optimum water content) could not absorb enough water for achieving fully saturated condition. This may be attributed to the influence of entrapped air bubbles.

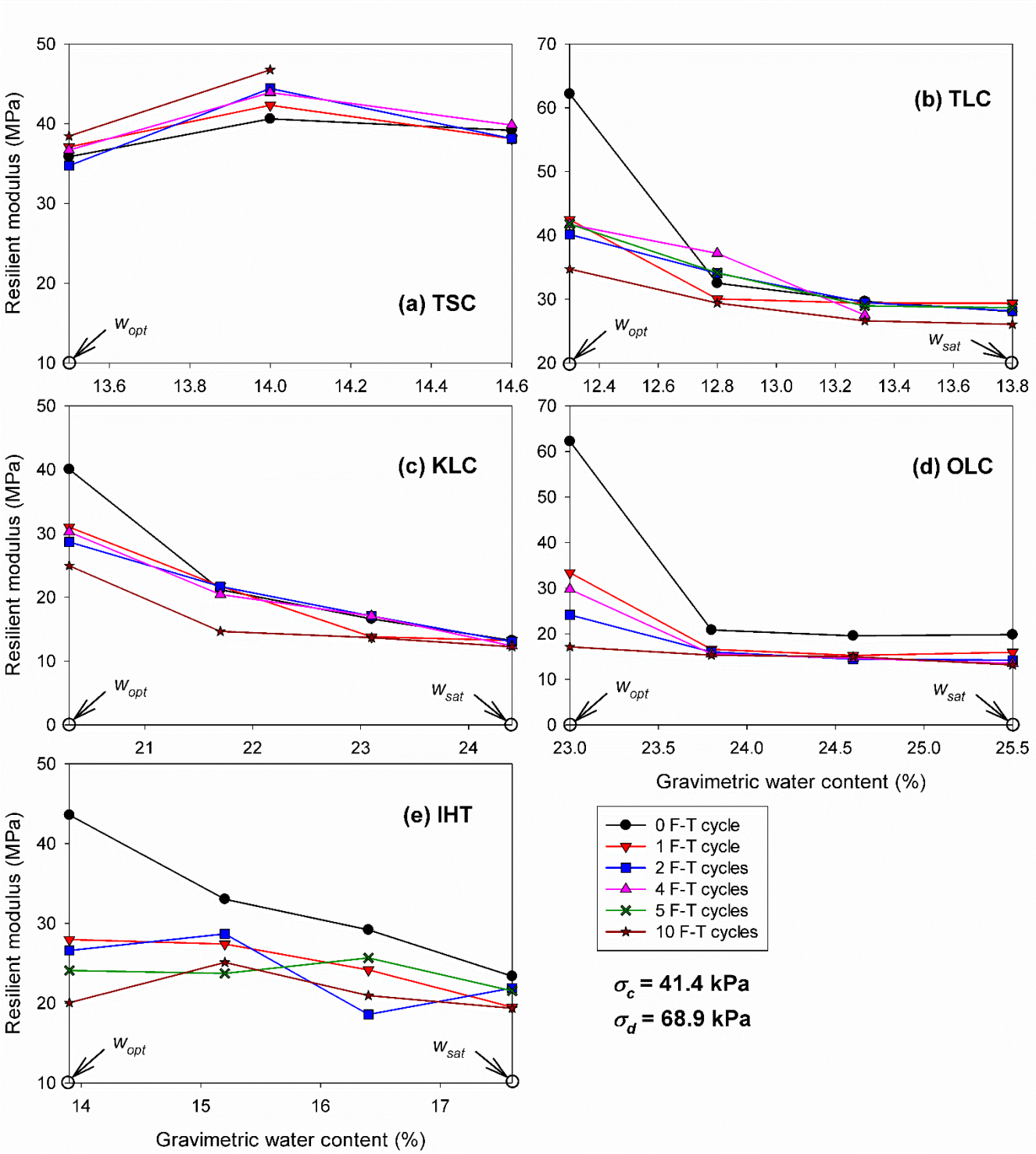

Figure 8.8 The effect of water content on the resilient moduli of (a) TSC, (b) TLC, (c) KLC, (d) OLC, and (e) IHT under different numbers of F-T cycles (σc = 41.4 kPa, and σd = 68.9 kPa)

The effects of water content on the M_R behavior of TLC, KLC, and IHT show similar trends, as summarized in **Figure 8.8**(b), (c), and (e). For the three soils, there is a gradual reduction in the M_R with an increase in the water content. Such a behavior is consistently observed for all the F-T cycles although the magnitudes of reduction under different numbers of F-T cycles are different. More specifically, the largest variation is observed for the specimens not subjected to any F-T cycles.

The M_R decreases when the water content increases from the optimum water content (i.e. 23.0%) to 23.8% for OLC specimens (see **Figure 8.8**(d)). This is true for all the F-T cycles except for the tenth F-T cycle; in other words, there is no influence of water content on the measured M_R for the tenth F-T cycle. In addition, the change of M_R is insignificant for all the F-T cycles from the water content value of 23.8% to the saturated water content (i.e. 25.5%) condition.

The effect of water content on the M_R under the other stress levels are similar to that shown in **Figure 8.8**. For example, the results obtained under the stress level of σ_c = 13.8 kPa and σ_d = 55.2 kPa are shown in **Figure 8.9**. The derived conclusions (i.e. from **Figure 8.8**) are also applicable for this stress level. It should be noted that the M_R of KLC specimen at the saturated condition was not obtained under this stress level (**Figure 8.9**(c)). The reason is that, for low value of confining stress (i.e. σ_c = 13.8 kPa or 27.6 kPa), the saturated KLC specimen deformed significantly under the applied cyclic load, resulting in unsuccessful measurement of its M_R. These results suggest that the confining stress influences the measured M_R. More detailed analyses are summarized in the following sections.

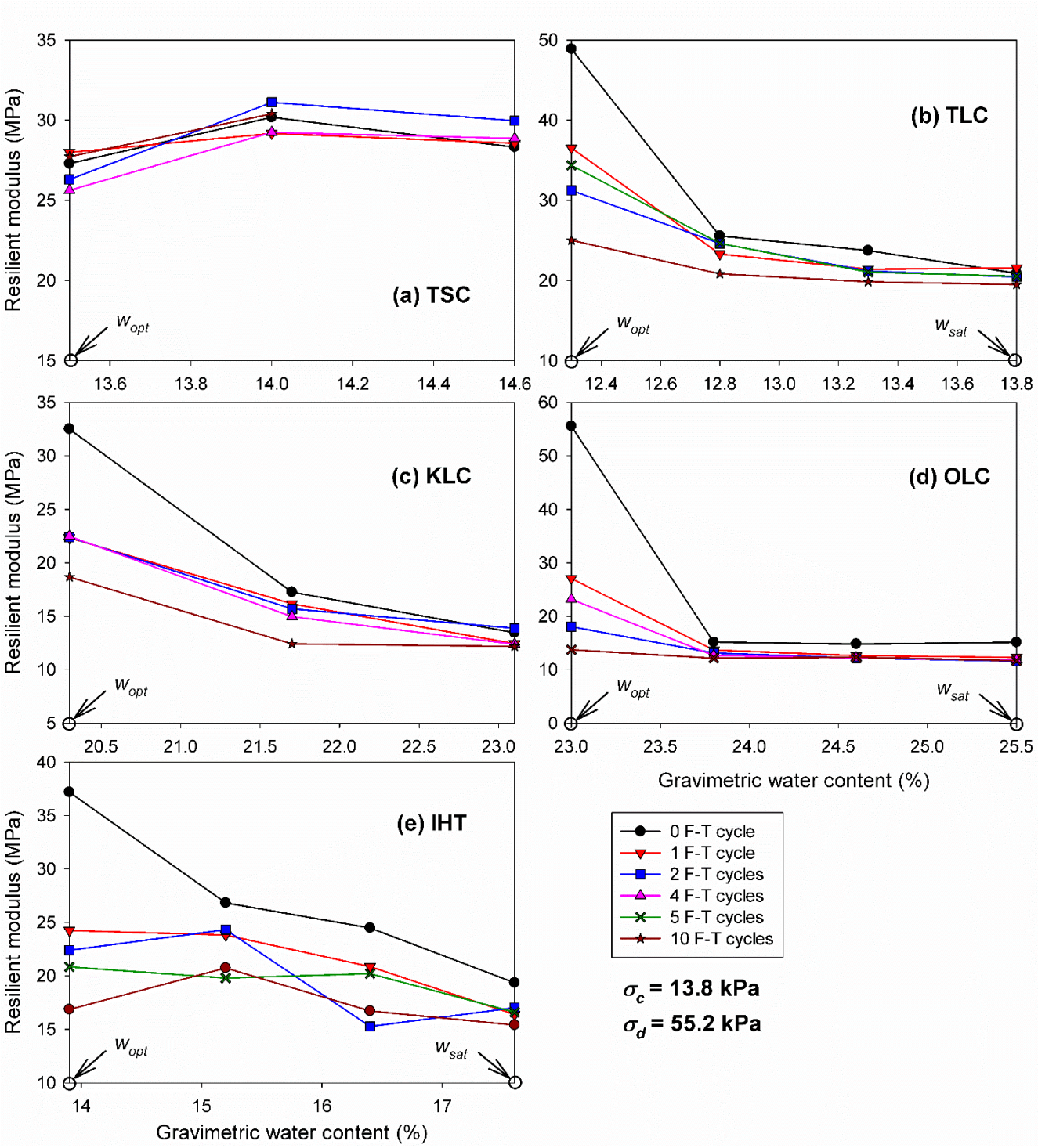

Figure 8.9 The effect of water content on the resilient moduli of (a) TSC, (b) TLC, (c) KLC, (d) OLC, and (e) IHT under different numbers of F-T cycles (σc = 13.8 kPa, and σd = 55.2 kPa)

8.5.3 Effect of stress levels

Figure 8.10 summarizes the three-dimensional surface plots to highlight the variation of M_R of the five soils versus the confining stress and deviator stress. For each soil, the experimental data of the specimens at the optimum water content and the highest water content at which the M_R test was performed are shown. The M_R values under zero F-T cycle are compared with those at the critical number of F-T cycles. Such a comparison provides valuable information about the measured M_R, which does not change significantly after the critical number of F-T cycles. For TLC, KLC, OLC, and IHT specimens tested at the optimum water content, the two surfaces at zero and critical number of F-T cycles are distinctly apart, suggesting that the M_R decreases significantly after the critical number of F-T cycles. However, the two surfaces for the TSC specimens tested at the optimum water content are close to each other (see **Figure 8.10**(a)). This is consistent with the previous results suggest that there is no impact of F-T cycles on the measured M_R of TSC (see **Figure 8.7**(a)). When the specimen has high water content (i.e. at or close to the saturated water content), there is no significant difference between the two surfaces. This indicates that the number of F-T cycles does not significantly influence the M_R of the five soils at high water contents.

The influence of confining stress and deviator stress on M_R is different for the five soils. The M_R of TSC specimen increases with an increase in the confining stress and deviator stress (**Figure 8.10** (a) and (b)). This is true for both the zero and one F-T cycles, and for both the optimum water content condition and when the water content is 14.6%. However, for TLC specimen tested at the optimum water content and zero F-T cycle, its M_R shows a peak area when the confining stress is large and the deviator stress is relatively small (e.g., σ_c = 41.4 kPa and σ_d = 27.6 kPa or 41.4 kPa). The M_R is not significantly influenced by the other combinations of confining and deviator stresses. For the TLC specimen tested at the critical number of F-T cycles, the M_R surface is relatively flat (**Figure 8.10**(c)). The influence of confining stress is more significant than that of deviator stress for the TLC specimens tested at the saturated condition (see **Figure 8.10**(d)).

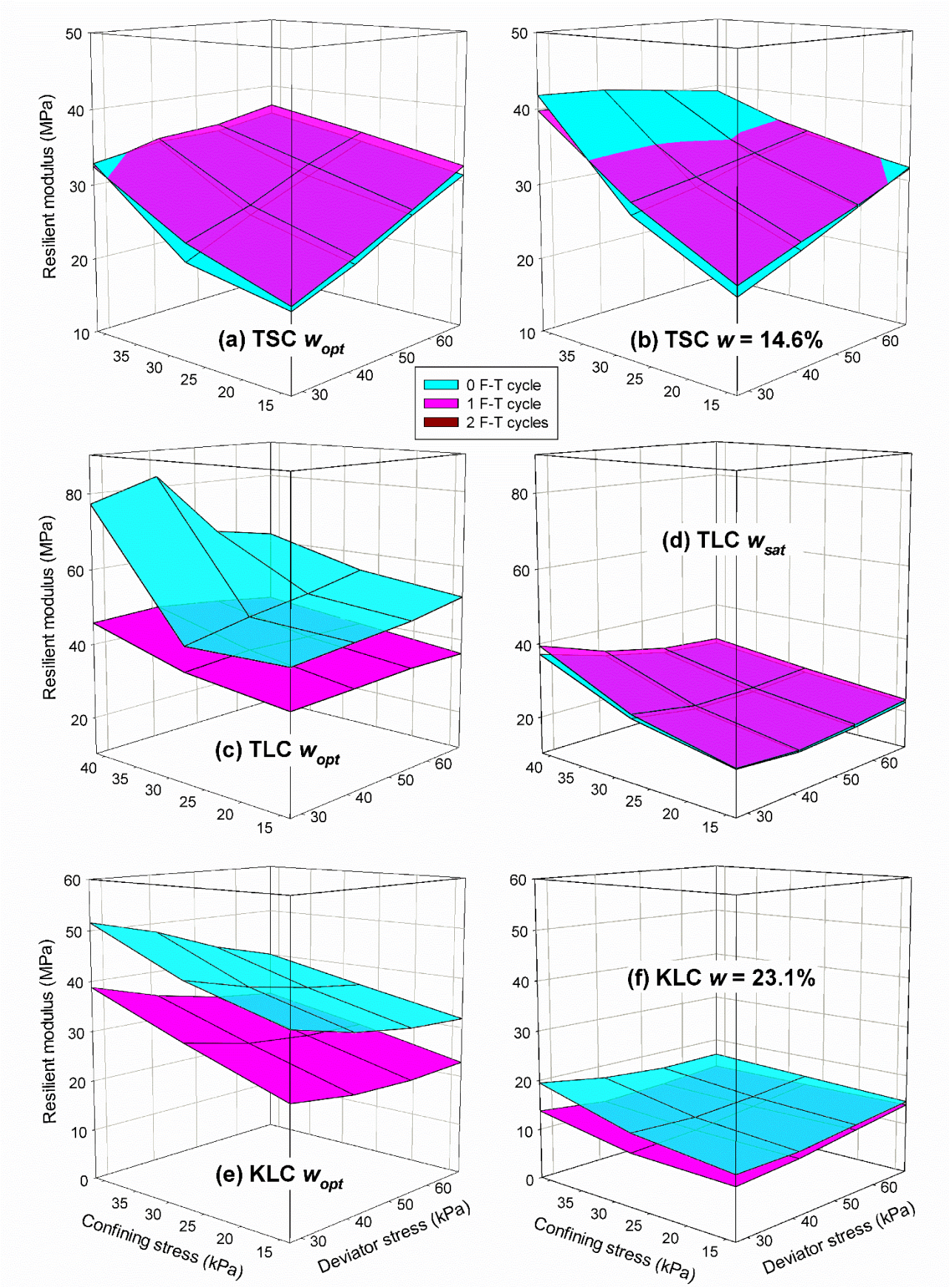

Figure 8.10 The effect of stress levels on the resilient moduli of (a) and (b) TSC, (c) and (d) TLC, (e) and (f) KLC, (g) and (h) OLC, (i) and (j) IHT

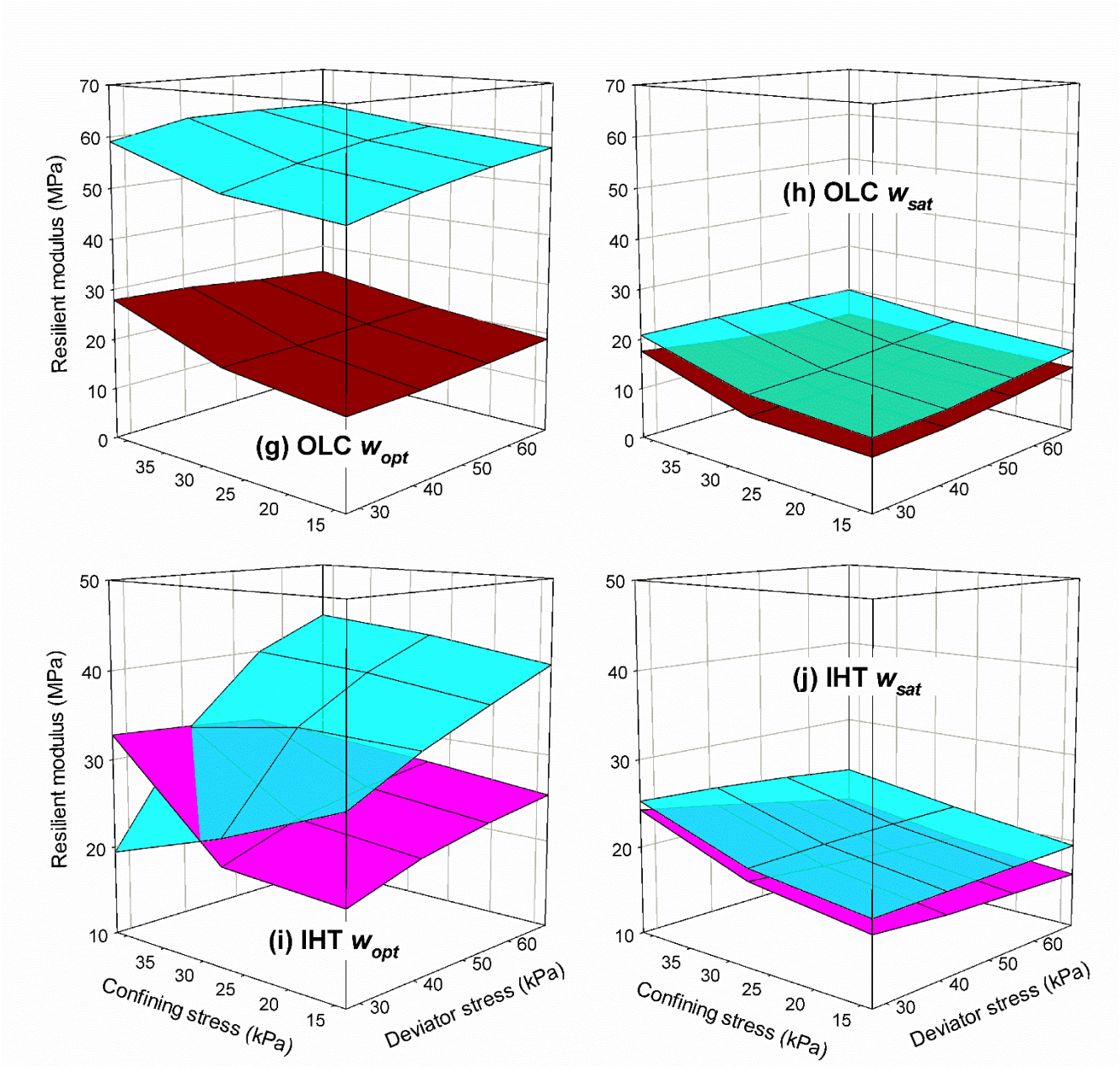

Figure 8.10 The effect of stress levels on the resilient moduli of (a) and (b) TSC, (c) and (d) TLC, (e) and (f) KLC, (g) and (h) OLC, (i) and (j) IHT (Cont'd)

The M_R increases with an increase in the confining stress and with a decrease in the deviator stress for KLC specimens tested at the optimum water content. This is true for both the zero and the critical number of F-T cycles (the two surfaces are parallel to each other), as can be seen from **Figure 8.10**(e). The M_R of KLC at a water content of 23.1% (see **Figure 8.10**(f)) is not

strongly dependent on stress levels. This is particularly true when the specimen was subjected to one F-T cycle, under which the M_R surface is approximately horizontal. The behavior of OLC is similar to that of KLC at the water content of 23.1%. In other words, when the OLC specimen is at its optimum water content, its M_R is slightly influenced by the confining stress and deviator stress, when the number of F-T cycles is zero or two (i.e. the critical number of F-T cycles of OLC). This observation is also applicable for OLC specimens tested at the saturated condition (**Figure 8.10**(h)).

The variation of the M_R of IHT with respect to the confining and deviator stresses however is complex. For example, from **Figure 8.10**(i) it can be seen that at the optimum water content and under zero F-T cycle, the M_R of IHT increases with an increase in the deviator stress. However, M_R increases and decreases with an increase in confining stress when the deviator stress is 68.9 kPa and 27.6 kPa, respectively. Under the critical number of F-T cycles, the M_R of IHT increases with an increase in confining stress, but it increases and decreases with an increase in the deviator stress when the confining stress is 13.8 kPa and 41.4 kPa, respectively. At the saturated condition (see **Figure 8.10**(j)), the M_R of IHT increases with an increase in confining stress and with a decrease in deviator stress, for both the zero and one F-T cycles.

8.6 Estimation of resilient modulus by an ANN model

8.6.1 Background of ANN model

The ANN is an adaptive information-processing technique, which allows the correlations between the input and output variables to be established through inter-connected neurons (Saha et al., 2018). The key advantage of an ANN model in comparison with the empirical and statistical methods is that it does not need any prior knowledge about the nature of the relationship between the input and output variables (Shahin et al., 2001). For example, regression analysis can only be successfully applied if prior knowledge of the nature of non-linearity exists. On the contrary, prior knowledge of the nature of non-linearity is not required for an ANN model. In an ANN model, the non-linearity can be taken into account and be modified easily by

changing the transfer function and network structure (e.g., the number of hidden layers and neurons in each layer) (Shahin et al., 2001).

The correlations developed by ANN model are shown as Eq. (8.1).

$$y_j = f(\sum w_{ji} x_i + b_j) \tag{8.1}$$

where x_i is the input variable; y_j is the output variable; w_{ji} is unknown weight factor; b_j is a bias term; and f is a transfer function.

Three sets of data (i.e. training, validation, and test datasets) are generally used in ANN modeling. The ANN model determines the weight factors and biases (i.e. w_{ji} and b_j) through training and validation processes. The training dataset is used to teach the network. Training continues as long as the network's performance continues improving on the validation dataset. The test dataset provides a completely independent measure of network accuracy. In the present study, the neural network toolbox of MATLAB software was used for establishing the ANN model for estimating the M_R of the five Canadian soils (as shown in the following section). The training algorithm used the Levenberg-Marquardt back propagation method to minimize the mean squared error (MSE) (low MSE indicates good performance of the ANN model). The gradient descent weight and bias function was employed as a learning algorithm to adjust the weight factors and biases.

The hyperbolic tangent sigmoid transfer function used in the present study is shown below, where I_i is input quantity.

$$f(I_i) = \text{tansig}(I_i) = \frac{2}{1+\exp(-2*I_i)} - 1, \qquad -1 \le f(I_i) \le 1 \tag{8.2}$$

The input and output variables are generally normalized before the ANN model is trained. The normalization equation used in the present study is expressed as,

$$\begin{aligned} x_i^{\mathrm{N}} &= (z_{\max} - z_{\min}) \times \frac{x_i - x_{\min}}{x_{\max} - x_{\min}} + z_{\min} \\ y_j^{\mathrm{N}} &= (z_{\max} - z_{\min}) \times \frac{y_j - y_{\min}}{y_{\max} - y_{\min}} + z_{\min} \end{aligned} \tag{8.3}$$

where x_i^{N} or y_j^{N} is the normalized input or output variable; $x_{\max}$ or $y_{\max}$ is the maximum value of

the input or output variables; x_{min} or y_{min} is the minimum value of the input or output variables; z_{min} and z_{max} is respectively the lower and higher boundary for the normalized input or output variable (z_{min} = -1, and z_{max} = 1). In other words, the normalization process converts the input or output variables to a range of [-1, 1].

8.6.2 Construction of the ANN model for the five Canadian soils and results

ANN simulation is an efficient way to incorporate various factors that influence the M_R of soils. A three-layered feed-forward back propagation ANN model was developed in the present study (as shown in **Figure 8.11**). It consists of an input layer, a hidden layer, and an output layer. The number of input and output neurons are determined by the parameters required for the modeling problem (Tutumluer and Meier, 1996). In the present study, the input layer consists of six neurons, one neuron for each of the independent variables that typically influence the M_R of subgrade soils. These variables include plasticity index (PI), maximum dry unit weight (γ_{dmax}), gravimetric water content (w), number of F-T cycles (No.), confining stress (σ_c), and deviator stress (σ_d). The output layer consists of only one neuron, i.e. resilient modulus (M_R). The input variables (i.e. PI, γ_{dmax}, w, No., σ_c, and σ_d) and output variable (i.e. M_R) were normalized by using Eq. (8.3) before the training process. In the present study, 1748 sets of M_R data for the five investigated soils are available. These data were based on different combinations of soil physical properties, water contents, stress levels, and number of F-T cycles. In addition, another 372 sets of M_R data measured on TSC, TLC, KLC, and OLC under various stress levels and water contents (considering both drying and wetting of the specimens after compaction) were collected from Vanapalli and Han (2017). In total, 2120 sets of data were used for developing and testing the ANN model. These data were automatically divided into training (70%), validation (15%), and test (15%) datasets in MATLAB.

For developing a sound ANN model, in addition to judiciously determining the number of neurons in the input and output layers, the number of hidden layers and the number of neurons in the hidden layers also have to be chosen. In the present study, the number of hidden layers was

set to one since one hidden layer is considered sufficient for developing a sound ANN model (e.g., Saha et al., 2018) and for keeping the developed ANN model simple. The proper number of neurons in the hidden layer was selected through a parametric study in order to achieve a reasonable ANN model, which can be used for the general application for the five Canadian soils. Six different ANN architectures (i.e. ANN 6-4-1 to ANN 6-9-1, which has 4, 5, 6, 7, 8, and 9 neurons in the hidden layer respectively) were compared to find the optimum number of neurons in the hidden layer.

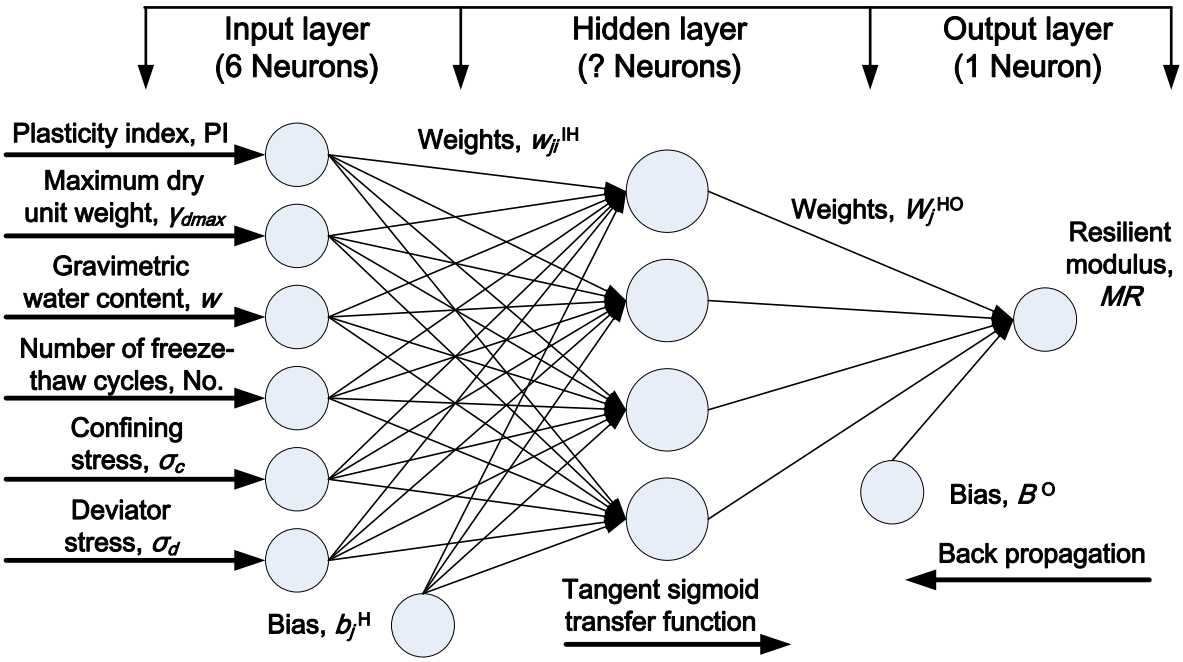

Figure 8.11 The three-layered feed-forward back propagation ANN model

The results on these ANN architectures such as the coefficient of determination (R^2) of different datasets (e.g., see **Figure 8.12**) and the MSE of the validation dataset are summarized in **Table 8.5**. It can be seen that when there are four neurons in the hidden layer (i.e. ANN 6-4-1), the R^2 values for the training, validation, and test dataset are 0.88, 0.90, and 0.88, respectively; and that for all the data is 0.88. This indicates that the M_R obtained through this ANN architecture is relatively close to the target (measured) M_R. The MSE of the validation dataset is

27.27. With an increase in the number of hidden neurons, the R^2 values typically increase and MSE of the validation dataset decreases. Good results were obtained through ANN 6-7-1. The R^2 values for the cases when the number of hidden neurons are 8 and 9 (i.e. ANN 6-8-1 and ANN 6-9-1) do not increase significantly compared to ANN 6-7-1, although MSE of the validation dataset shows some reduction. In order to avoid too many neurons in the hidden layer and keep the developed ANN model simple, the ANN 6-7-1 is chosen as the optimum network architecture for the estimation of M_R for the five investigated soils.

Table 8.5 Results for the six trained ANN models

	Training dataset, R^2	Validation dataset, R^2	Test dataset, R^2	All data, R^2	Validation dataset, MSE
ANN 6-4-1	0.88	0.90	0.88	0.88	27.27
ANN 6-5-1	0.89	0.91	0.90	0.90	24.47
ANN 6-6-1	0.89	0.92	0.89	0.89	22.21
ANN 6-7-1	0.90	0.93	0.92	0.90	20.35
ANN 6-8-1	0.90	0.92	0.92	0.91	19.69
ANN 6-9-1	0.92	0.92	0.92	0.92	17.35

Figure 8.12 summarizes the results for the ANN 6-7-1. The linear relationship between the ANN output (i.e. ANN model obtained M_R) and target output (i.e. measured M_R), and the R^2 for each dataset and for all data are shown. Most of the data are located along the 1:1 line, indicating that the ANN 6-7-1 can provide reasonably good estimation for the M_R of the five soils investigated in the present study. As discussed in the previous section, the test dataset provides a completely independent measure of network accuracy. The high R^2 value of 0.92 was achieved for the test dataset, which consists of 318 sets of data (i.e. 2120 * 15% = 318) that were not used for developing the ANN 6-7-1. The results suggest that the ANN 6-7-1 can provide reasonable estimation for the M_R of the five investigated Canadian soils under a variety of water contents, number of F-T cycles and stress levels.

The mathematical expression for the developed ANN 6-7-1 is shown below (Eq. (8.4)). **Table 8.6** summarizes its weight factors and biases. For using the developed ANN 6-7-1, the

initial inputs (i.e. PI, γ_{dmax}, w, No., σ_c, and σ_d) need to be normalized using Eq. (8.3). By incorporating the normalized inputs and the weight factors and biases into Eq. (8.4), the M_R of the five soils under various conditions can be calculated.

$$M_R{}^{\mathrm{N}} = \sum_{j=1}^{m} W_j^{\mathrm{HO}} * \mathrm{tansig}\left(\sum_{i=1}^{n} w_{ji}^{\mathrm{IH}} * x_i{}^{\mathrm{N}} + b_j^{\mathrm{H}}\right) + B^{\mathrm{O}} \tag{8.4a}$$

$$\begin{aligned} M_R &= (M_{R\max} - M_{R\min}) \times \frac{M_R{}^{\mathrm{N}} - z_{\min}}{z_{\max} - z_{\min}} + M_{R\min} \\ &= (128-8) \times \frac{M_R{}^{\mathrm{N}} - (-1)}{1-(-1)} + 8 = 60 \times M_R{}^{\mathrm{N}} + 68 \end{aligned} \tag{8.4b}$$

where, $M_R{}^{\mathrm{N}}$ is the normalized M_R obtained from the ANN model, w_{ji}^{IH} is the weight factor for the path from neuron i in the input layer to neuron j in the hidden layer; x_i^{N} is the normalized input variable; b_j^{H} is the bias for neuron j in the hidden layer; W_j^{HO} is the weight factor for the path from neuron j in the hidden layer to the neuron in the output layer (i.e. the single neuron M_R); B^{O} is the bias for the neuron in the output layer; n and m are the number of neurons in the input and hidden layers respectively, in the present study, n = 6 and m = 7; M_R is the estimated M_R by the ANN model (i.e. the de-normalized $M_R{}^{\mathrm{N}}$). The de-normalization equation (Eq. (8.4b)) is based on Eq. (8.3). In the present study, $M_{R\max}$ and $M_{R\min}$ (of the 2120 M_R values) are equal to 128 MPa and 8 MPa respectively.

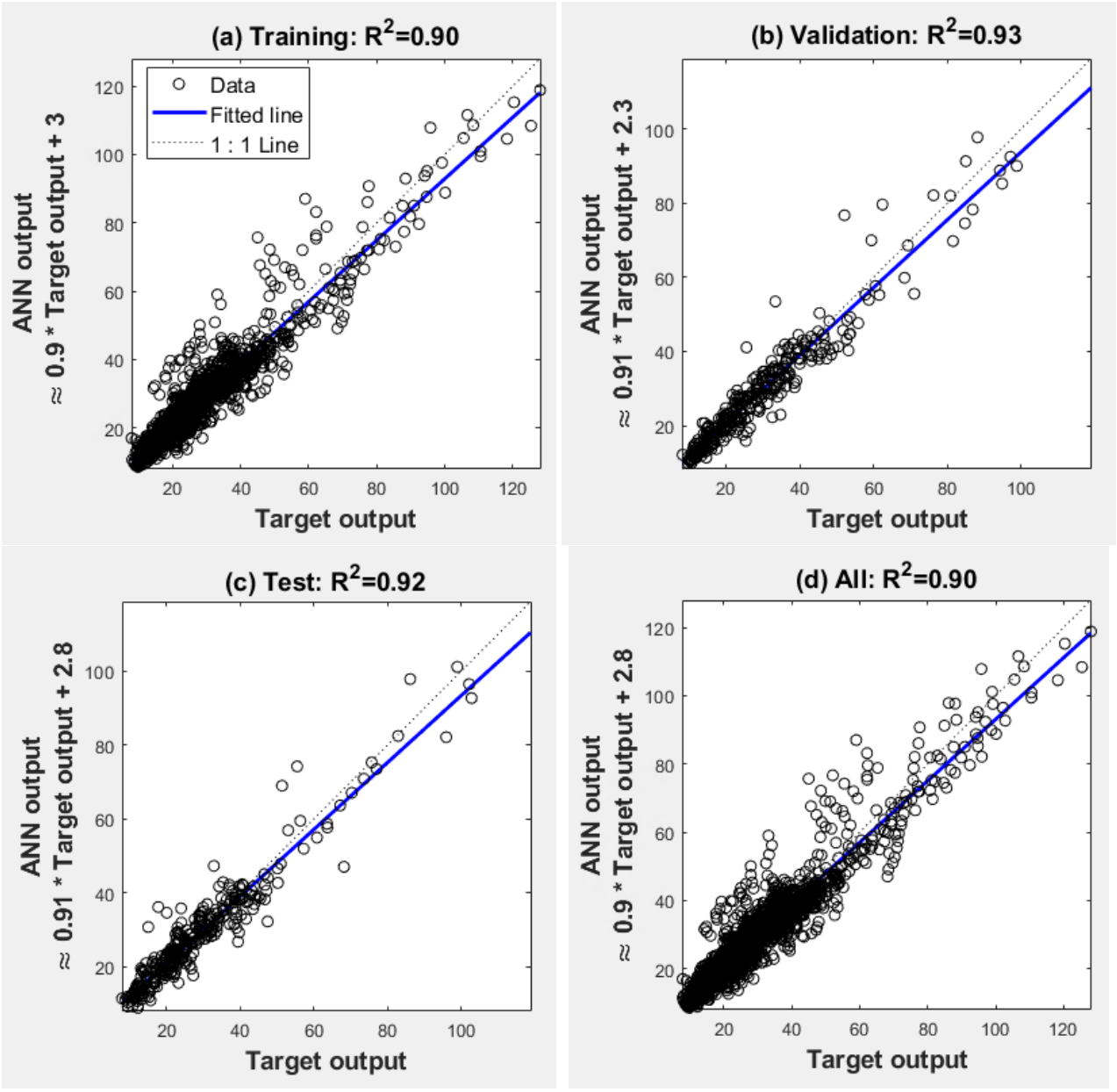

Figure 8.12 The results for ANN 6-7-1

Table 8.6 Weights and biases for the ANN 6-7-1

From the input layer to the hidden layer								
w_{ji}^{IH}	2.1996	-3.3817	-8.5388	-0.1639	-4.1615	-0.6179	b_j^H	-1.2678
	-0.0691	0.2057	-0.1282	-0.0185	0.7349	-0.3268		0.5969
	-7.4265	4.7010	-6.4106	-4.4007	0.0808	-0.0656		-5.9782
	-2.0040	1.9691	4.2567	3.1507	-0.0667	0.0441		4.0738
	0.1940	-0.1233	-0.6880	-0.0697	0.4158	-0.1041		0.0214
	-1.8386	1.9810	4.1023	3.0098	-0.0559	0.0449		4.1348
	-7.4754	1.0517	-2.0918	-0.0973	0.0141	-0.0192		-4.2881
From the hidden layer to the output layer								
W_j^{HO}		-0.0195	-0.1910	-1.2844	2.6729	0.3947	-4.1072	1.4110
B^O		0.7825						

8.7 Discussion

It is widely realized that when fine-grained soils are compacted on the dry side of the optimum water content, two families of pores (i.e. intra-aggregate pores (or micro-pores) and inter-aggregate pores (or macro-pores)) are formed in the soil structure. On the other hand, the soil structure appears more homogeneous with a single family of pores (i.e. intra-aggregate pores) when a fine-grained soil is compacted on the wet side of the optimum water content (Delage et al., 1996). The optimum water content therefore forms a transition and can appear with one or two families of pores (Leroueil and Hight, 2013).

In the present study, the five fine-grained soils were compacted at their optimum water contents to achieve their maximum dry density values. When they are subjected to three-dimensional freezing, water in large inter-aggregate pores near to the surface of the specimen freezes first and its volume increases by about 9%. At the same time, large cryogenic suction forms between the ice crystals and water phase that is adsorbed on soil particles' surfaces in these pores. These ice crystals grow at the expense of water in adjacent pores (e.g., in the smaller intra-aggregate pores and pores inside the specimen) which is drawn towards the ice through water films under the cryogenic suction gradient. The movement of water during freezing may cause development of the spatial network of channels (Hohmann-Porebska, 2002).

The ice crystals increase in size and therefore exert pressure on the surrounding soil particles and push them away from their original positions. As a result, these pores are enlarged, and the cohesion between soil particles is weakened. This is because the magnitude of cohesion is partially influenced by the space between soil particles (Wang et al., 2007). On the other hand, the large cryogenic suction (which can be considered equivalent to effective stress (e.g., Williams, 1967)) and the corresponding water migration cause desiccation and shrinkage of the soil specimen, which likely contribute to cracks. The bulk volume change, however, is mainly dependent on the degree of saturation of the specimen (e.g., Hamilton, 1966; Dagesse, 2010; Lu et al., 2019). The five investigated soils had relatively high initial degrees of saturation after compaction (see **Table 8.2**); therefore, it can be considered that the soil specimens experienced overall bulk volume increase, particles movement, loss of cohesion and formation of cracks during the freezing process.

During the thawing process, ice melts and soil volume decreases. Soil particles tend to move back but cannot completely recover to their original positions (i.e. irreversible plastic deformation occurs (Lu et al., 2019)). The cohesion between soil particles is also not able to recover fully. These characteristics along with the cracks that typically form during freezing weaken the soil structure. In addition, the initial weak interfaces between the adjacent compaction layers are likely weakened further by F-T cycling. The study by Bergan and Fredlund (1973) on remoulded Regina clay specimens suggested that there would be a significant drop in soil suction after F-T cycles. For the undisturbed specimens, a small but distinct suction reduction was observed after one F-T cycle. In other words, F-T cycles significantly altered soil suction even though the water content is constant before and after F-T cycles. The reduction in suction of a cohesive soil (with high fine fraction) that were subjected to three-dimensional closed-system F-T cycle was also observed by Ogawa et al. (1991) and Nishimura et al. (1994). Weimer (1972) measured the suction in compacted glacial till specimens after five F-T cycles; results from this study suggest that the reduction in suction was dramatic when specimens were compacted dry of the optimum water content. However, the reduction was

insignificant when specimens were compacted wet of the optimum water content. As a result, the M_R of TLC, KLC, OLC and IHT at their optimum water contents show dramatic reduction after 1, 1, 2 and 1 cycles of F-T, respectively, which are the critical numbers. Beyond the critical number of F-T cycles, the reduction in M_R values for these four soils is at a relatively lower rate and tends to level off. The only exception is TSC, its behavior may be attributed to the initial variation in the structure of the prepared TSC specimens.

When the soil specimen is subjected to wetting, water migrates from the wet filter paper (which was used to cover the top, bottom and side surfaces of the specimen as shown in **Figure 8.2**) to the specimen, due to suction gradient. The suction value in the soil specimen initially at the optimum water content is relatively high (see **Table 8.1**). On the contrary, the wet filter paper has a high amount of water and therefore has low or zero suction value. With the gradual migration of water towards the specimen, the original thin water films adsorbed on the soil particles' surfaces of the specimen become thicker, and the radii of curvature of the air-water menisci become larger, resulting in lower values of suction and more deformable soil structure. As a result, the pore spaces of the specimen enlarge as effective stress reduces (i.e. suction value is relatively low), and micro flow channels possibly form due to water migration. The M_R of the specimen reduces significantly due to wetting, which is destructive. This reduction in M_R could be approximated through conditioning the specimen with F-T cycles only (Skaggs, 1992). In addition, the reduction in suction values after F-T cycles is not significant due to the low initial suction values (higher water contents). This indicates that the number of F-T cycles does not have profound influence on the measured M_R under higher water contents.

For a specimen tested at a certain water content and under different stress levels, the variation of M_R with the number of F-T cycles presents similarities. This indicates that the stress level does not influence the M_R versus F-T cycle number relationships dramatically but influences the M_R magnitude (see **Figure 8.5**). From **Figure 8.10**, the effect of stress levels on the measured M_R is dependent on the initial water contents of the specimens and soil types. For the same soil tested under a specific water content, the influence of stress level is generally

straightforward. Fluctuation in the measured M_R values can be attributed to the possible variation in the water content at which the specimen was compacted (e.g., 0.2% lower or higher than the optimum water content may yield large differences in the pore structures of the compacted specimens) and the structure change during the wetting process. In spite of using elaborated equipment with experienced personnel, there were difficulties associated with accurately performing M_R tests, which may have also contributed to the fluctuation in the measured M_R values.

The in-situ subgrade soils are typically subjected to one-dimensional open-system F-T cycles. Ice lenses may form if the freezing and water conditions are favorable. Upon thawing, the melt water from ice is trapped in the thawed layer by the impermeable frozen layer below, resulting in high water content or even saturated condition in the upper portion of the subgrade soil. Additional water may be introduced by snowmelt and spring rainfall. These in-situ conditions were not simulated in the present study. However, the effect of increasing water content on the M_R was investigated through wetting the compacted soil specimens to different post-compaction water contents. The effect of different freezing-thawing methods (i.e. one-dimensional or three-dimensional) on the M_R is assumed not significant. Skaggs (1992) experimentally determined the M_R values of different soil specimens subjected to one-dimensional open-system F-T with water imbibition bottom to top. The results are similar to those in the present study, indicating that the conditioning methods used in this study is reasonably representative of the in-situ conditions. However, for achieving reliable results, experimental studies simulating the in-situ one-dimensional open-system F-T should be conducted.

A total of 2120 sets of M_R data of the five Canadian soils were used for developing an ANN model. Among them, 1484 sets of data were for training an ANN structure, and another 318 sets of data were for validating the trained ANN structure. After these two procedures, the optimum ANN model with one hidden layer and seven hidden neurons (i.e. ANN 6-7-1) was selected. The last 318 sets of data, which were not used for either training or validation, were

used for testing the developed ANN 6-7-1. The result of the test dataset confirms the ANN model's validity in estimating the M_R of the five Canadian soils subjected to different wetting and F-T conditions and to various stress levels. The proposed ANN model can provide reliable estimates of the M_R data for various conditions for pavement design when the five soils are used as subgrade soils. At this stage, however, the ANN 6-7-1 is not recommended for estimating the M_R of other soils since the M_R values of these new soils were not included to train and validate the ANN model (as pitfalls may exist when applying trained ANN models on new soils (Tutumluer and Meier, 1996)). As more data on the five investigated soils and other new soils become available, the ANN 6-7-1 can be further improved to make more estimations that are reliable.

8.8 Summary

The M_R is a key material property required for the rational design of pavement structures. In permafrost and seasonally frozen regions, temperature and moisture variations have significant influence on the M_R of subgrade soils. In the present study, the M_R of five Canadian subgrade soils considering the wetting and F-T conditions were measured and analyzed. The measured M_R values can provide valuable information for the rational design of pavement structures where the five soils are encountered. In addition, an ANN model (ANN 6-7-1) was developed and validated using the measured M_R values along with another 318 sets of M_R data considering the effect of wetting and drying, and stress levels. The proposed ANN model can be used for estimating the M_R of the five Canadian soils taking account of the influence of water content, number of F-T cycles and stress levels.

Several key findings from the present study are summarized as follows. The F-T cycle can be considered as weathering process, which results in weak soil structure due to reduction in suction, soil particles movement, loss of cohesion between particles, and formation of cracks / channels. The critical numbers of F-T cycles were determined as 1, 1, 2 and 1 for TLC, KLC, OLC and IHT at the optimum water content, respectively. No significant change in M_R after F-T

cycles was observed for TSC, possibly due to structure differences among tested TSC specimens. The percentage of reduction in M_R after the critical number of F-T cycles was strongly related to the plasticity index for soil specimens tested at the optimum water content. The wetting process results in the decrease in suction and enlargement of soil pore spaces. Consequently, relatively low M_R values were measured at high water contents, and the effect of F-T cycles for this scenario is insignificant. In addition, the effect of stress levels on the measured M_R was dependent on the initial water contents of the specimens and soil types.

8.9 References

AASHTO, 2007. Designation: T307-99: Standard method of test for determining the resilient modulus of soils and aggregate materials, American Association of State Highway and Transportation Officials, Washington, D.C.

AASHTO, 2012. Designation M145-91: Classification of soil and soil-aggregate mixtures for highway construction purpose. American Association of State Highway and Transportation Officials, Washington, D.C.

ARA, Inc., ERES Consultants Division. 2004. Guide for Mechanistic - Empirical Design of New and Rehabilitated Pavement Structures. Final report, NCHRP Project 1-37A. Transportation Research Board, Washington, D.C.

ASTM, 2011. Designation: D2487-11: Standard practice for classification of soils for engineering purposes (Unified Soil Classification System). American Society for Testing and Materials, West Conshohocken, PA.

ASTM, 2012. Designation: D698-12: Standard Test Methods for Laboratory Compaction Characteristics of Soil Using Standard Effort (12400 ft-lbf/ft^3 (600 kN-m/m^3)). American Society for Testing and Materials. West Conshohocken, PA.

Bergan, A.T., and Fredlund, D.G., 1973. Characterization of freeze-thaw effects on subgrade soils. Symp. on Frost Action of Roads, Organization for Economic Cooperation and Development, Oslo, Norway, pp. 119-143.

Caicedo, B., 2018. Geotechnics of Roads: Fundamentals. CRC Press, Boca Raton, Florida, USA.

Chamberlain, E.J. and Gow, A.J., 1979. Effect of freezing and thawing on the permeability and structure of soils. In Developments in Geotechnical Engineering, Vol. 26, pp. 73-92.

Cary, C.E., and Zapata, C.E. 2010. Enhanced model for resilient response of soils resulting from seasonal changes as implemented in mechanistic-empirical pavement design guide. Transportation Research Record: Journal of the Transportation Research Board, 2170: 36-44.

Cary, C.E. and Zapata, C.E., 2011. Resilient modulus for unsaturated unbound materials. Road Materials and Pavement Design, 12(3), pp.615-638.

Cui, H.H., Ma, Y., Liu, J.K. and Wang, Z.Y., 2017. Experimental study of the dynamic behavior of high-grade highway-subgrade soil in a seasonally frozen area. Sciences in Cold and Arid Regions, 9(3), pp.289-296.

Dagesse, D.F., 2010. Freezing-induced bulk soil volume changes. Canadian journal of soil science, 90(3), pp.389-401.

Delage, P., Audiguier, M., Cui, Y.J. and Howat, M.D., 1996. Microstructure of a compacted silt. Canadian Geotechnical Journal, 33(1), pp.150-158.

Duan, Z.H., Kou, S.C. and Poon, C.S., 2013. Using artificial neural networks for predicting the elastic modulus of recycled aggregate concrete. Construction and Building Materials, 44, pp.524-532.

Eigenbrod, K.D., 1996. Effects of cyclic freezing and thawing on volume changes and permeabilities of soft fine-gained soils. Canadian Geotechnical Journal, 33(4), pp.529-537.

Graham, J. and Au, V.C.S., 1985. Effects of freeze–thaw and softening on a natural clay at low stresses. Canadian Geotechnical Journal, 22(1), pp.69-78.

Hamilton, A.B., 1966. Freezing shrinkage in compacted clays. Canadian Geotechnical Journal, 3(1), pp.1-17.

Han, Z., 2016. Modelling Stiffness and Shear Strength of Compacted Subgrade Soils. Doctoral thesis, University of Ottawa, Ottawa, Canada.

Han, Z. and Vanapalli, S.K., 2016. State-of-the-Art: Prediction of resilient modulus of unsaturated subgrade soils. International Journal of Geomechanics, 16(4), p.04015104.

Han, Z., Vanapalli, S.K., Ren, J.P. and Zou, W.L., 2018. Characterizing cyclic and static moduli and strength of compacted pavement subgrade soils considering moisture variation. Soils and foundations, 58(5), pp.1187-1199.

Hohmann-Porebska, M., 2002. Microfabric effects in frozen clays in relation to geotechnical parameters. Applied clay science, 21(1-2), pp.77-87.

Ishikawa, T., Tokoro, T., Ito, K. and Miura, S., 2010. Testing methods for hydro-mechanical characteristics of unsaturated soils subjected to one-dimensional freeze-thaw action. Soils and Foundations, 50(3), pp.431-440.

Lee, W., Bohra, N.C., Altschaeffl, A.G. and White, T.D., 1995. Resilient modulus of cohesive soils and the effect of freeze–thaw. Canadian Geotechnical Journal, 32(4), pp.559-568.

Leroueil, S. and Hight, D.W., 2013, January. Compacted soils: From physics to hydraulic and mechanical behaviour. In Advances in Unsaturated Soils–Proceedings of the 1st Pan-American Conference on Unsaturated Soils, PanAmUNSAT (pp. 41-59).

Li, G., Wang, F., Ma, W., Fortier, R., Mu, Y., Mao, Y. and Hou, X., 2018. Variations in strength and deformation of compacted loess exposed to wetting-drying and freeze-thaw cycles. Cold Regions Science and Technology, 151, pp.159-167.

Liu, J., Chang, D. and Yu, Q., 2016. Influence of freeze-thaw cycles on mechanical properties of a silty sand. Engineering geology, 210, pp.23-32.

Lu, Y., Liu, S., Alonso, E., Wang, L., Xu, L. and Li, Z., 2019. Volume changes and mechanical degradation of a compacted expansive soil under freeze-thaw cycles. Cold Regions Science and Technology, 157, pp.206-214.

MTO, (Ministry of Transportation of Ontario). 2013. Pavement design and rehabilitation manual (Second Edition). Queen's Printer for Ontario, Canada.

Nishimura, T., Ogawa, S., and Fukuda, M., 1994. Effective stresses in unsaturated soils after freezing and thawing. Ground Freezing 94, Fremond (ed.), Rotterdam, pp.121-128.

Ogawa, S., Nishimura, T., and Fukuda, M., 1991. Influence of freezing and thawing on suction of unsaturated soils. Ground Freezing 91, Yu & Wang (ed.), Rotterdam, pp.71-76.

Othman, M.A., Benson, C.H., Chamberlain, E.J. and Zimmie, T.F., 1994. Laboratory testing to evaluate changes in hydraulic conductivity of compacted clays caused by freeze-thaw: state-of-the-art. In Hydraulic conductivity and waste contaminant transport in soil. ASTM International, 227-254.

Park, H.I., Kweon, G.C. and Lee, S.R., 2009. Prediction of resilient modulus of granular subgrade soils and subbase materials using artificial neural network. Road Materials and Pavement Design, 10(3), pp.647-665.

Qi, J., Ma, W. and Song, C., 2008. Influence of freeze–thaw on engineering properties of a silty soil. Cold regions science and technology, 53(3), pp.397-404.

Ren, J. and Vanapalli, S.K., 2018. Empirical model for predicting the resilient modulus of frozen unbound road materials using a hyperbolic function. Transportation Geotechnics, 17: 66-74.

Saha, S., Gu, F., Luo, X. and Lytton, R.L., 2018. Use of an Artificial Neural Network Approach for the Prediction of Resilient Modulus for Unbound Granular Material. Transportation Research Record, p.0361198118756881.

Shahin, M.A., Jaksa, M.B. and Maier, H.R., 2001. Artificial neural network applications in geotechnical engineering. Australian Geomechanics, 36(1), pp.49-62.

Skaggs, R.B., 1992. Effects of freeze-thaw and overload conditions on the resilient modulus of frost-susceptible soils. Master thesis, University of Wyoming, Laramie, USA.

Tang, L., Cong, S., Geng, L., Ling, X. and Gan, F., 2018. The effect of freeze-thaw cycling on the mechanical properties of expansive soils. Cold Regions Science and Technology, 145, pp.197-207.

Tutumluer, E. and Meier, R.W., 1996. Attempt at resilient modulus modeling using artificial neural networks. Transportation research record, 1540(1), pp.1-6.

Tutumluer, E. and Seyhan, U., 1998. Neural network modeling of anisotropic aggregate behavior from repeated load triaxial tests. Transportation Research Record: Journal of the Transportation Research Board, (1615), pp.86-93.

Vanapalli, S.K. and Han, Z., 2017. Characterization of the mechanistic-empirical pavement design guide input parameters for the resilient modulus of Ontario subgrade soils. Ministry of Transportation, Highway Standards Branch Report, HIIFP-000.

Wang, D.Y., Ma, W., Niu, Y.H., Chang, X.X. and Wen, Z., 2007. Effects of cyclic freezing and thawing on mechanical properties of Qinghai–Tibet clay. Cold regions science and technology, 48(1), pp.34-43.

Weimer, H.F., 1972. The strength, resilience, and frost durability characteristics of a lime-stabilized till. M.Sc. Thesis, University of Saskatchewan, Saskatoon, Canada.

Williams, P.J., 1967. The nature of freezing soil and its field behaviour. Norwegian Geotech Inst

Publ, 72, pp.91-119.
Xu, J., Ren, J., Wang, Z., Wang, S. and Yuan, J., 2018. Strength behaviors and meso-structural characters of loess after freeze-thaw. Cold Regions Science and Technology, 148, pp.104-120.
Yao, X., Qi, J. and Ma, W., 2009. Influence of freeze–thaw on the stored free energy in soils. Cold Regions Science and Technology, 56(2-3), pp.115-119.
Zaman, M., Solanki, P., Ebrahimi, A. and White, L., 2010. Neural network modeling of resilient modulus using routine subgrade soil properties. International Journal of Geomechanics, 10(1), pp.1-12.
Zhou, Z., Ma, W., Zhang, S., Mu, Y. and Li, G., 2018. Effect of freeze-thaw cycles in mechanical behaviors of frozen loess. Cold Regions Science and Technology, 146, pp.9-18.

Chapter 9 Summary and conclusions

9.1 Summary

In the permafrost and seasonally frozen regions, moisture and temperature are two key factors that influence the physical and mechanical behavior of soils. For example, the frost penetration in Ontario, Canada typically ranges between 1 to 4 m, depending on local climate. As a result, the subgrade and foundation soils in many areas in Ontario are subjected to moisture variation / migration, freezing / thawing, and F-T cycles. Due to the variations in moisture and temperature, soil in the permafrost and seasonally frozen regions can be in different states; saturated or unsaturated, frozen or thawed, or combinations of them. For this reason, it is important to design infrastructure taking account of the influence of these two parameters.

During the last two decades, the soil-water characteristic curve (SWCC) has been used as a key tool for the interpretation and prediction of soil behavior and for the rational design of infrastructure for unsaturated soils. More recently, several studies were undertaken and many are in progress to use the soil-freezing characteristic curve (SFCC) to predict or estimate frozen soils behavior and to facilitate the rational design of infrastructure in cold regions. However, sound understanding of the fundamental behavior of SFCC and frozen soils is required to achieve this goal. For this reason, in this thesis, the relationship between SWCC and SFCC, and the various forms of SFCC expressions were investigated. Extensive experimental investigations were undertaken to study the SWCC and SFCC of two soils from the Toronto region of Ontario (i.e. Toronto silty clay (TSC) and Toronto lean clay (TLC)). These studies are valuable for understanding the fundamental behavior of both the SWCC and SFCC. The focus of these studies was directed to understand the similarities and differences in the SWCC and SFCC behavior.

The soil resilient modulus (M_R) is a key material property used for the rational design of pavement structures based on the mechanistic-empirical methods. Environmental factors such as the variations in temperature and moisture have significant influence on the M_R of subgrade and

foundation soils. In this thesis, two novel yet simple models were proposed for the estimation of frozen M_R of various coarse- and fine-grained soils. These models facilitate pavement design in cold regions as well as the use of SFCC in pavement engineering by extending the mechanics of unsaturated soils. In addition, comprehensive experimental investigation on the M_R of five Canadian soils (i.e., TSC, TLC, Kincardine lean clay (KLC), Ottawa Leda clay (OLC), and Indian Head till (IHT)), considering the influences of moisture and temperature, was carried out with the aid of an advanced triaxial testing equipment. The soils, namely TSC, TLC, KLC, and OLC are from the most populated regions of Canada that are well connected with extensive roadways. The IHT is a typical glacial till that is a representative candidate of soils widely found in Alberta, Saskatchewan, and Manitoba provinces of Canada.

Major conclusions drawn from the studies undertaken in this thesis are summarized below.

(1) Critical evaluation on different expressions for the SFCC.

Many different expressions for the SFCC have been proposed in the literature. These expressions can be categorized into two groups. The first group is based on empirical relationships between unfrozen water content and subzero temperature. The second group is developed by exploiting the similarity between SFCC and SWCC, with the aid of the Clapeyron equation.

Four SFCC expressions; namely, the power relationship, exponential relationship, van Genuchten equation, and Fredlund and Xing equation were selected for providing comparisons between the measured and fitted unfrozen water contents for four different types of soils (i.e. Castor sandy loam, saline Lanzhou silt, Niagara silt, and Regina clay). The results of the study suggest that the exponential relationship and van Genuchten equation are more suitable for sandy soils. The power relationship provides reasonable fit for the SFCC of soils with different particle sizes; however, it is not suitable for saline silt. The Fredlund and Xing equation provides good fits for all the four soils, showing its flexibility for different soil types.

(2) Measurement and comparison of SFCC and SWCC for understanding the fundamental behavior of SFCC and its similarity to SWCC.

Both the SFCC and SWCC of TSC and TLC were measured. Different testing conditions are imposed to determine the freezing and thawing branches of SFCC of these two soils. Experimental results are critically interpreted to understand the fundamental behavior of the SFCC. The measured SFCC can be used for modeling soil properties such as the hydraulic conductivity, thermal conductivity, and stiffness, and for modeling the transport of water, heat and solute in frozen soils.

Many factors have a significant influence on the reliable measurement of SFCC, which include the sensors resolution and their stability, specific sensor calibration for each soil under investigation, thermodynamic equilibrium condition, and continuous soil structure changes that arise during the freezing / thawing processes.

The measured SFCC and SWCC of the two soils show significant differences, indicating their quantitative dissimilarity. Many reasons may contribute to the dissimilarity. For example, specimens structure variations during the compaction and saturation processes, and freezing / thawing processes, and cracks formation when sensors were inserted into the specimens. The performance and calibration of sensors would also significantly influence the comparison between SFCC and SWCC. In other words, the limitations associated with testing sensors prohibit a reliable characterization of the quantitative similarity between the two retention curves.

In addition, some fundamental differences may exist between drying / wetting and freezing / thawing processes. For example, the way ice replaces water in a frozen saturated soil is different in comparison with how air replaces water in an unfrozen unsaturated soil. The dominant wetting interactions that cause liquid films to coat soil particles in the unsaturated zone are different from those that cause premelted films to separate soil particles from pore ice. The existence of salinity further complicates the problem.

(3) Development of two novel models for the estimation of M_R of frozen soils that can be incorporated into the Mechanistic-Empirical Pavement Design Guide (i.e. MEPDG).

One of the novel models proposed is a semi-empirical model for estimating the M_R of frozen saturated soils with the aid of SFCC extending the mechanics of unsaturated soils. Seven saturated soils (including both coarse- and fine-grained soils) are used to validate this model. The results suggest that the model can be used to estimate the M_R of frozen saturated soils with a reasonable degree of accuracy. However, no relationships could be obtained for the model parameters (i.e. χ and δ) because of the limited data.

The second model proposed is an empirical hyperbolic model with two-constants (i.e. A and B) that is useful for best-fitting the relationship between M_R of frozen soils and subzero temperature. The model is validated using eighteen soils comprising of both coarse- and fine-grained soils that were tested under saturated / unsaturated conditions. It is found that the hyperbolic model can well predict the M_R of the eighteen soils that are in a state of frozen condition. The parameter A has significant influence on the prediction results and could be related to the unfrozen water content in the frozen soils. The parameter B was found to have a strong relationship with the initial M_R.

The two models are simple and promising for use in pavement engineering. For example, they can be incorporated into the MEPDG for reliably estimating the frozen M_R of pavement unbound soils taking account of the influence of subzero temperature. In comparison with the semi-empirical model, the hyperbolic model has wider application since it can be used for both saturated and unsaturated frozen soils. It would be a good practice to follow the standard AASHTO T307-99 for using the proposed models. More investigations on different types of soils would be useful for better understanding the strengths and limitations of the two models.

(4) Experimental investigation of the M_R of five Canadian soils under frozen condition.

The M_R of five Canadian soils (i.e., TSC, TLC, KLC, OLC, and IHT) considering wetting and freezing is experimentally determined with the aid of the GDS Entry Level Dynamic

(ELDyn) triaxial testing system. The wetting process simulates the increase in moisture content of in-situ subgrade soils after compaction and during their service life. The freezing process (and freeze-thaw cycles, see below) simulates the weathering process caused by temperature variation in cold regions. A freezing system with the cooling unit, thermal insulation, and modification to the triaxial testing system is established for accurately maintaining the desired testing temperatures within the soil specimens. The experimental results suggest that: (i) The effect of subzero temperature on the M_R of the five investigated soils is significant. The relationship curve between the frozen M_R and subzero temperature resembles hyperbola. (ii) For four of the five soils, the frozen M_R versus subzero temperature relationship of the saturated specimen typically has steeper slope than that at the optimum water content, for the temperature range of 0 to -5 °C. (iii) The effect of stress levels on the measured M_R is dependent on the types of soils, water contents of the specimens, and temperature. Lastly, (iv) Loading frequency does not show a significant influence on the measured frozen M_R.

The determination of frozen soils behavior such as the M_R is prone to fluctuations due to the difficulties associated with experimental investigations on frozen soils. For example, the accurate temperature control throughout the specimen is difficult; and the non-uniform distribution of unfrozen water and ice may contribute to the variation in frozen soils behavior. The large difference in the measured M_R between this study and other studies may be attributed to different soil types and water contents, different specimen preparation and freezing methods, and different loading forms, frequencies, and stress levels.

(5) Experimental investigation of the M_R of five Canadian soils subjected to wetting and freeze-thaw (F-T) cycles.

The M_R of the five Canadian soils (i.e., TSC, TLC, KLC, OLC, and IHT) considering wetting and F-T conditions are measured and analyzed. The soil specimens are compacted at their optimum moisture contents and then subjected to wetting and different numbers of F-T cycles. The measured M_R values can provide valuable information for the rational design of pavement structures where the five soils are encountered. An Artificial Neural Network (ANN)

model is developed and validated using the measured M_R values along with another 318 sets of M_R data considering the effect of wetting and drying, and stress levels. The proposed ANN model can be used for estimating the M_R of the five Canadian soils taking account of the influence of water content, number of F-T cycles and stress levels.

The F-T cycle can be considered as a weathering process that weakens the soil structure due to reduction in suction, soil particles movement, loss of cohesion between particles, and formation of cracks / channels. The critical numbers of F-T cycles are determined as 1, 1, 2, and 1 for TLC, KLC, OLC, and IHT at the optimum water content, respectively. No significant change in M_R after F-T cycles is observed for TSC, possibly due to structure variations among tested TSC specimens. The percentage of reduction in M_R after the critical number of F-T cycles is strongly related to the plasticity index for soil specimens tested at the optimum water content. The wetting process results in the decrease in suction and enlargement of soil pore spaces. Consequently, relatively low M_R values are measured at high water contents, and the effect of F-T cycles for this scenario is insignificant. In addition, the effect of stress levels on the measured M_R is dependent on the initial water contents of the specimens and soil types.

9.2 Suggestions for future research

Several suggestions for future research are summarized below.

(1) The reliable measurement of SFCC and use of SFCC in engineering practice.

The reliable measurement of SFCC is complex because of several difficulties associated with sensors accuracy and temperature control. The effect of volume change of soil specimen during the freezing and thawing processes on the measurement of SFCC should be considered in future investigations. For example, when ice lenses form in the soil mass, its SFCC may be significantly changed. Reliable methods (e.g., NMR and TDR) should be used to calibrate the frequency domain technique (e.g., the EC-5 sensor used in this thesis) measured unfrozen water content under frozen conditions. In addition, the effect of salinity on the SFCC should be studied.

The SFCC represents the variation in the amounts of unfrozen water and ice with respect to

subzero temperature. It is an essential tool for understanding the behavior of frozen soils. The SFCC has been used for the estimation of M_R of saturated frozen soils in this thesis. In future study, the use of SFCC can be extended to investigate the behavior of frozen soils such as the shear strength and frost heave characteristic, and the constitutive modelling of frozen soils behavior.

(2) Water migration and distribution of unfrozen water and ice during the freezing and thawing processes.

Water migration in the soil mass typically occurs when the soil is subjected to freezing and thawing. This is usually accompanied by frost heaving, soil desiccation, and formation of cracks and fissures. Therefore, the distribution of unfrozen water and ice is likely to be non-uniform due to freezing and thawing. The distribution of unfrozen water and ice (and therefore the soil structure) is influenced by many factors such as the initial soil structure prior to freezing and thawing, the rate and direction of freezing and thawing (e.g., one-dimensional freezing in the field or three-dimensional freezing in laboratory), and the availability of external water during freezing. The effects of the non-uniform distribution of unfrozen water and ice on the physical and mechanical behavior of frozen soils should be investigated.

(3) The effect of F-T cycles on soil structure and water retention characteristics.

The effect of F-T cycles on soil structure (e.g., pore size distribution, particle movement and breakage, and void ratio) can be investigated and reliably quantified through using advanced microscopic equipment, such as the scanning electron microscope (SEM) and X-ray computed tomography (CT). This can facilitate the reliable interpretation of the experimental results of frozen soils.

The F-T cycles may have significant influence on the water retention characteristics of soils due to changes in soil structure that were discussed earlier. The investigations on the effect of F-T cycles on the SWCC and SFCC are not widely recorded in the literature for interpreting soil behavior. Therefore, more studies are required to understand this topic, for example, soil suction variation due to F-T cycles.

Appendix A Discussion on "A new model for capturing void ratio-dependent unfrozen water characteristics curves"

The contents are from the manuscript of the publication:

Ren, J.P., and Vanapalli, S.K. 2018. Discussion on "A new model for capturing void ratio-dependent unfrozen water characteristics curves" by Q.Y. Mu, C.W.W. Ng, C. Zhou, G.G.D. Zhou, and H.J. Liao. Computers and Geotechnics, 103: 82-85.

DOI: 10.1016/j.compgeo.2018.07.017

The authors proposed a valuable void ratio-dependent unfrozen water characteristic curve (UWCC) model, which explicitly considers the effects of both capillarity and adsorption. The proposed model has been used to predict the UWCCs of silt at different initial void ratios and clay over a wide range of subzero temperatures. However, the discussers have some comments on the proposed model and the model parameters. In this discussion, these details are summarized.

The discussers would like to express their opinion that the determination of the maximum volumetric adsorbed water content (θ_{amax}) as the unfrozen volumetric water content at a temperature of -2 °C may not be rigorous. This is due to the reason that unfrozen water content at -2 °C may only be a representative value for the θ_{amax} for coarse-grained soils (as most of pore water freezes before -2 °C in coarse-grained soils). However, it may not be able to reasonably represent the θ_{amax} for fine-grained soils because they have a large amount of unfrozen water at relatively high subzero temperatures (e.g., –2 °C) (Patterson and Smith, 1981; Bronfenbrener and Bronfenbrener, 2012; Kurylyk and Watanabe, 2013). The typically large amount of unfrozen water in fine-grained soils is likely to be composed of both capillary and adsorbed water.

The authors suggest that "the freezing of absorbed water begins at approximately −2 °C with values of k ranging from 0.02 to 0.04. This is consistent with studies of unsaturated soils showing that the drying of absorbed water is initiated at a suction of 1500 kPa (equivalent to −2 °C calculated using Eq. (6))". It may be more appropriate if the temperature value of -2 °C is

replaced by -1.23 °C (as shown from the calculation summarized in the end of this Appendix). This is because from Figure 2 in the paper, the freezing of adsorbed water begins prior to −2 °C with values of k ranging from 0.02 to 0.04.

In addition, it is summarized by the authors that the parameter k is to be within a range from 0.02 to 0.04, which is mainly dominated by the soil specific surface area. However, according to Table 1 in the paper, the parameter k for silt and bentonite clay is 0.026 and 0.021, respectively. These two values are quite close for two different types of soils with significantly different values of specific surface area (e.g., 40 m^2/g for silt and 700 m^2/g for bentonite clay (Yoshikawa and Overduin, 2005)).

According to Figure 3 in the paper, Eq. (11) failed to well predict the unfrozen water content when the void ratio (e) is 0.58, especially when the subzero temperature is lower than −0.5 °C. This suggests that different model parameters should have been used for the specimen having a void ratio of 0.58, rather than directly using the model parameters that are derived from the three-dimensional best-fitting surface using the measured data of specimens with void ratios of 0.61 and 0.55 (i.e. the parameters summarized in Table 1 in the paper).

The authors summarized that "The void ratios of the three specimens were 0.61, 0.58, and 0.55". The discussers are not sure how these void ratio values were obtained from Azmatch et al. (2012) as there is no direct information related to the void ratios of the three specimens of Devon silt. These three specimens were prepared from slurry at a moisture content of 60% and consolidated under 50 kPa, 100 kPa, and 400 kPa, respectively.

On the other hand, according to Azmatch et al. (2012), the measured volumetric water content of the three Devon silt specimens (consolidated under 50 kPa, 100 kPa, and 400 kPa, respectively) at a suction value of 1 kPa are 0.387, 0.395, and 0.365, respectively. If these initial volumetric water content values are assumed to be equal to the porosity (n) of the specimen as they were measured at the saturated condition (i.e. suction value of 1 kPa), the void ratios ($e = n / (1 - n)$) of the three specimens can be calculated as 0.631, 0.653, and 0.575, respectively. These three calculated void ratio values are different from those summarized by the authors.

Furthermore, according to Azmatch (2013), the initial void ratio values of four Devon silt specimens prepared under identical initial conditions (i.e. prepared from slurry at a moisture content of 60%) and consolidated under 50 kPa, 100 kPa, 200 kPa, and 400 kPa were 0.795, 0.702, 0.623, and 0.583, respectively. These values are larger than the values provided by the authors.

In Eq. (11), the total amount of unfrozen water (θ) is equal to the sum of unfrozen capillary water (θ_{cw}) and unfrozen adsorbed water (θ_{aw}). The authors considered the influence of void ratio on the capillary water via using Eq. (8), which is modified from the Gallipoli et al. (2003) model. This was achieved by substituting the suction in unfrozen unsaturated soil with the cryogenic suction in frozen soil, which was obtained from subzero temperature through the Clapeyron equation (i.e. Eq. (6)). On the other hand, authors determined unfrozen adsorbed water (i.e. Eq. (10)) by directly using the subzero temperature (instead of cryogenic suction) to replace suction in unfrozen unsaturated soil using the Lu (2016) model. In other words, there is a difference in the treatment of suction in unfrozen unsaturated condition for the capillary and adsorbed water by the authors. The discussers suggest that it may be simpler and more straightforward to directly use the subzero temperature (rather than using the cryogenic suction obtained from the Clapeyron equation) as one of the independent variables (the other one is the void ratio) for calculating the amount of unfrozen capillary water using Eq. (9). By extending this philosophy, Eqs. (9) and (11) can be respectively modified as below,

$$\theta_{cw}=(\theta_s-\theta_{a\max})\{\frac{1}{1+[m_0 e^{m_1}(-T)]^{m_2}}\}^{m_3} \tag{A.1}$$

$$\theta=\theta_{cw}+\theta_{aw}=(\theta_s-\theta_{a\max})\{\frac{1}{1+[m_0 e^{m_1}(-T)]^{m_2}}\}^{m_3}+\theta_{a\max}\{1-[\exp(\frac{T-T_{\min}}{T})]^{k}\} \tag{A.2}$$

where, θ_s is the saturated volumetric water content, T is the subzero temperature (°C), T_{min} is the temperature at which all the pore water is frozen (= -259 °C, as determined by the Clapeyron equation with a suction value of 10^6 kPa), m_0, m_1, m_2, m_3, and k are model parameters. In the above equation, subzero temperature is directly taken as an independent variable for calculating

both the unfrozen capillary and adsorbed water contents.

Figure A.1 shows the effect of parameter m_1 on the freezing of capillary water using the modified capillary model suggested in this discussion (i.e. Eq. (A.1)). The parameters m_0, m_2, and m_3 are equal to 1500, 25, and 0.025, respectively. The values of θ_s, θ_{amax}, and e are equal to 41%, 10%, and 0.7, respectively. The value of m_1 ranges from 1 to 10. It can be seen that the freezing rate of capillary water decreases with an increase in the value of m_1. The unfrozen capillary water content under a given subzero temperature increases with an increase in m_1. These observations are consistent with those of the authors and provide credence for directly using subzero temperature as one of the independent variables for calculating unfrozen capillary water content.

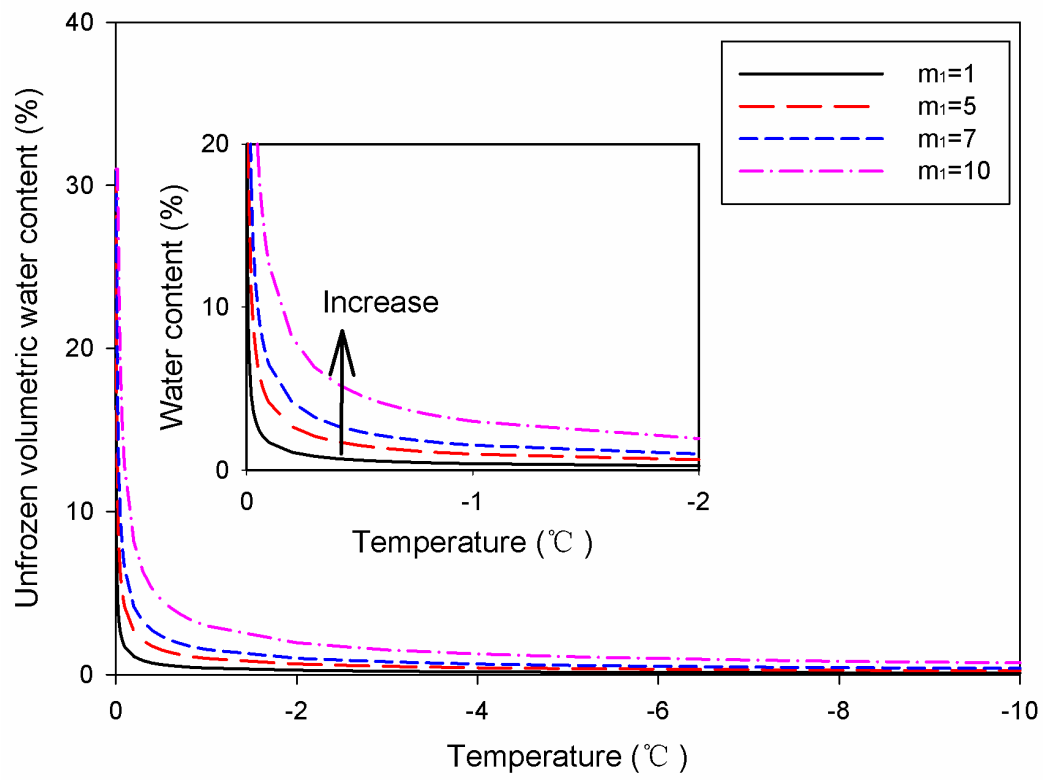

Figure A.1 Predicted freezing process of capillary water with different values of parameter m_1

The use of subzero temperature as an independent variable can be further supported by

employing a simplified form of the Clapeyron equation. Such a simplification can be achieved by taking x as T/273.15 and extending the assumption that $x \approx \ln(1+x)$ for relatively small values of x. Therefore, the temperature (-T) is equivalent to the cryogenic suction (s) as an independent variable, by including the constant (i.e. $r_w L_w$/273.15) into the fitting parameter m_0.

$$s = -r_w L_w \ln\frac{T + 273.15}{273.15} = -r_w L_w \ln(1 + \frac{T}{273.15}) = -r_w L_w \frac{T}{273.15} = -T\frac{r_w L_w}{273.15} \qquad \text{(A.3)}$$

The original and modified models proposed by the authors and discussers were respectively used to best-fit the measured unfrozen water content data of the Devon silt specimens with void ratios of 0.631 and 0.575. The input parameters and fitting results are summarized in Table A.1 of this discussion. The values of parameters for the two models are the same except for m_0. However, further close examination reveals that ratio of the two m_0 values (i.e. $5.282*10^5/435.7 = 1212$) is approximately equal to $r_w L_w$/273.15 (= 1000*333.7/273.15 = 1222), suggesting that the two models are equivalent. The high value of Adj. R^2 also suggests that the two models well fitted the measured data of the specimens with void ratios of 0.631 and 0.575.

Figure A.2 shows the comparison between the measured and calculated UWCCs of the three Devon silt specimens using the parameters summarized in Table A.1 of this discussion. Since the original and modified models have approximately the same characteristics, only the results calculated by the modified model are shown. From Figure A.2(a), it can be seen that the two models failed to well predict the UWCC of the specimen with void ratio of 0.653. Figure A.2(b) shows that the measured data of the specimen with void ratio of 0.653 are located above the 3D surface plot, which is calculated by using the parameters that were obtained by fitting the measured data of the specimens with void ratios of 0.631 and 0.575. Therefore, more future investigations are required to further improve the flexibility of the two models using the data of various other soils.

In spite of the modified model exhibiting similar characteristic behavior in comparison with the model proposed by the authors, the philosophy is different. The key advantage of the modified model is that it directly uses subzero temperature as an independent variable to

calculate both the unfrozen capillary and adsorbed water contents. This is straightforward and eliminates the prerequisite for employing the Clapeyron equation. In other words, the modified model does not require thermodynamic equilibrium condition between ice and water phases; hence, it is simple for interpreting frozen soils behavior.

Table A.1 Summary of parameters for original and modified models

	θ_s (%)	θ_{amax} (%)	m_0	m_1	m_2	m_3	k	Adj. R^2
Original model	38.7	16	435.7	22.75	1.750	0.5733	0.07	0.966
Modified model	38.7	16	$5.282*10^5$	22.73	1.751	0.5741	0.07	0.966

Finally, there were a few typographical errors in the paper that are summarized below:

(a). From Figure 2, θ_{amax} should be 15%, rather than 25%.

(b). In Figure 3, it should be written as Equation (11) rather than Equation (13). In addition, 'UWRC' should be 'UWCC'.

(c). In Table 1, the soil type of the first soil should be Silt rather than Clay.

(d). A negative sign in Eq. (9) is missing for achieving a positive value for cryogenic suction.

(e). Both the terms 'adsorbed' and 'absorbed' are found in the paper instead of just one term 'adsorbed'; this typographical error is confusing to the reader to clearly understand the details summarized in the paper.

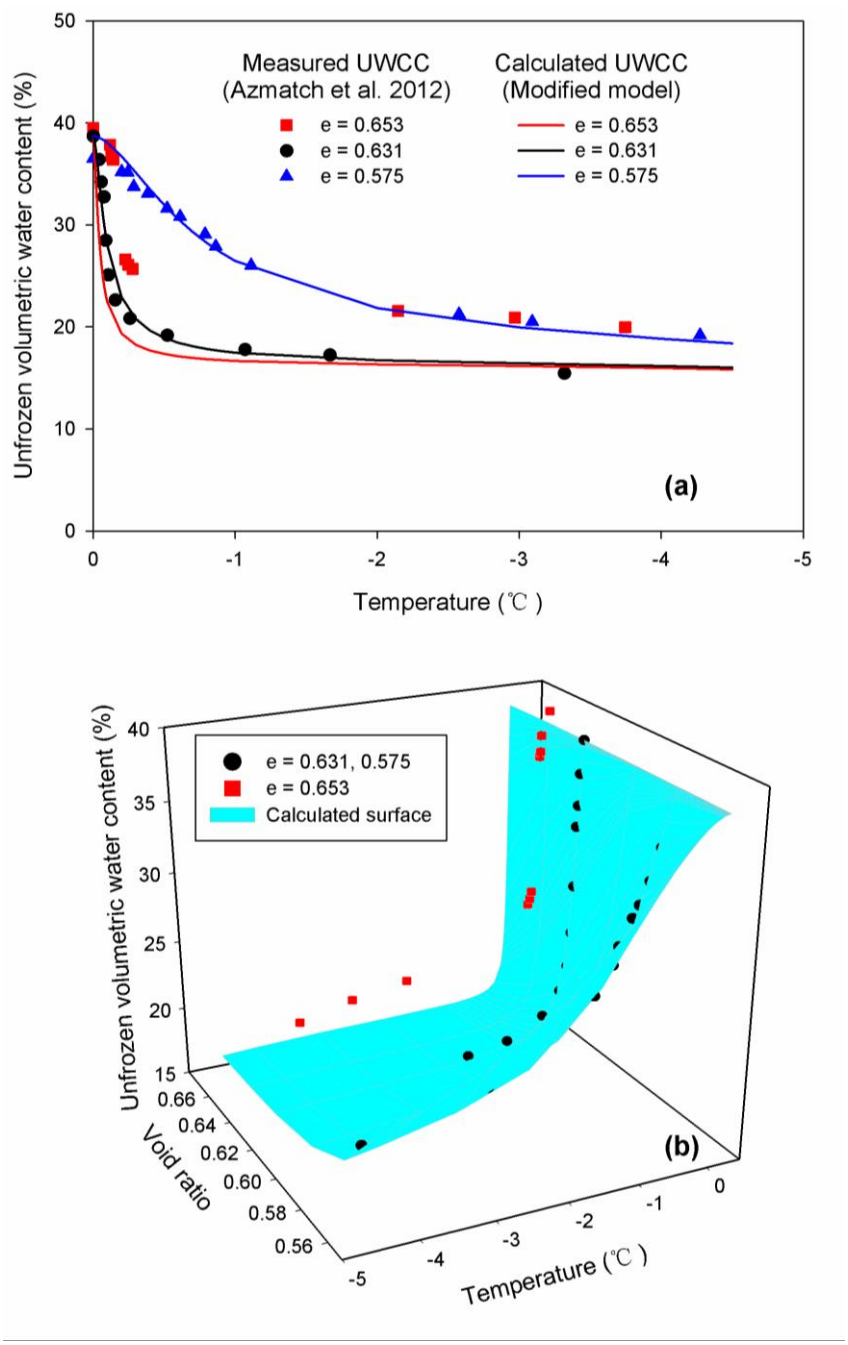

Figure A.2 (a) 2D and (b) 3D comparisons between the measured and calculated UWCCs of the three Devon silt specimens with different initial void ratios

Conversion of suction to temperature

Using Eq. (6), authors converted suction value of 1500 kPa to an equivalent temperature of -2 °C. However, this temperature value should be -1.23 °C as per the calculation summarized below. The Eq. (6) is shown as,

$$s = -r_w L_w \ln \frac{T + 273.15}{273.15}$$

where, s is the cryogenic suction (kPa), r_w is the water density (= 1000 kg/m^3), L_w is the latent heat of fusion of water (= 333.7 kJ/kg at 0 °C) which is assumed to be temperature-independent. From this information it should be,

$$1500\,(\text{kPa}) = -1000(\frac{\text{kg}}{\text{m}^3}) * 333.7(\frac{\text{kJ}}{\text{kg}}) * \ln \frac{T + 273.15}{273.15}$$

Since $1 \frac{\text{kg}}{\text{m}^3} \frac{\text{kJ}}{\text{kg}} = 1000 * \frac{\text{J}}{\text{m}} \frac{1}{\text{m}^2} = 1000 * \frac{\text{N}}{\text{m}^2} = 1\,\text{kPa}$, the relationship should be,

$$1.5 = -333.7 * \ln \frac{T + 273.15}{273.15}$$

Therefore, $T = 273.15 * \exp(-\frac{1.5}{333.7}) - 273.15 = -1.23\,°\text{C}$

References

Azmatch, T.F., 2013. Frost heave: New ice lens initiation condition and hydraulic conductivity prediction. PhD thesis, University of Alberta, Edmonton, Canada.

Azmatch, T.F., Sego, D.C., Arenson, L.U. and Biggar, K.W., 2012. Using soil freezing characteristic curve to estimate the hydraulic conductivity function of partially frozen soils. Cold Regions Science and Technology, 83, pp.103-109.

Bronfenbrener, L. and Bronfenbrener, R., 2012. A temperature behavior of frozen soils: Field experiments and numerical solution. Cold Regions Science and Technology, 79, pp.84-91.

Gallipoli, D., Wheeler, S.J. and Karstunen, M., 2003. Modelling the variation of degree of saturation in a deformable unsaturated soil. Géotechnique, 53(1), pp.105-112.

Kurylyk, B.L. and Watanabe, K., 2013. The mathematical representation of freezing and thawing processes in variably-saturated, non-deformable soils. Advances in Water Resources, 60, pp.160-177.

Lu, N., 2016. Generalized soil water retention equation for adsorption and capillarity. Journal of Geotechnical and Geoenvironmental Engineering, 142(10), p.04016051.

Patterson, D.E. and Smith, M.W., 1981. The measurement of unfrozen water content by time domain reflectometry: Results from laboratory tests. Canadian Geotechnical Journal, 18(1),

pp.131-144.
Yoshikawa, K. and Overduin, P.P., 2005. Comparing unfrozen water content measurements of frozen soil using recently developed commercial sensors. Cold Regions Science and Technology, 42(3), pp.250-256.